TURBIDITES OF THE CLORIDORME GROUP

SEDIMENTOLOGY OF SOME TURBIDITES AND RELATED ROCKS FROM THE CLORIDORME GROUP, ORDOVICIAN, QUEBEC

By

DAVID ROBERT BEEDEN, B.A.

A Thesis

Submitted to the School of Graduate Studies

in Partial Fulfilment of the Requirements

for the Degree

Master of Science

McMaster University

SEPTEMBER, 1983

© 1983, D.R. Beeden

MASTER OF SCIENCE (1983) McMASTER UNIVERSITY
(Geology) Hamilton, Ontario

TITLE: Sedimentology of some Turbidites and Related Rocks from the Cloridorme Group, Ordovician, Quebec

AUTHOR: David Robert Beeden, B.A.(Hons.)
(Cambridge University)

SUPERVISOR: Professor G.V. Middleton

NUMBER OF PAGES: xiii, 256

ABSTRACT

Sandstones and shales of the γ_4 Formation, Cloridorme Group (Middle Ordovician) are well-exposed on the northern coast of the Gaspé Peninsula, Quebec. The generally structureless, normally graded, medium to very coarse sandstones average 26 cm. in thickness and are interpreted as deposits of subcritical turbidity currents. Associated fine sandstones and siltstones were deposited from finer-grained turbidity currents which in some cases were the downcurrent equivalents of those which deposited coarse sandstones. Argillaceous sandstone layers containing clasts of siltstone and shale are the deposits of laminar debris flows.

Facies are organized into four unit types, the most important of which are sandstone packets and siltstone-shale interpacket units. Comparison of layer thickness trends in the actual section with those in a random section constructed from the same layer thickness population shows that the actual section is more ordered than expected under random processes. Layer thickness trends are superimposed on a smaller-scale alternation of thick and thin layers.

Sandstone packets are interpreted as depositional lobes of a submarine fan. Packets are characterized by mul-

tiple or single thickening-upward sequences, with a thinning-upward sequence at their top representing gradual lobe abandonment. A channel-fill about 10 m. thick occurs in one packet. It does not show a thinning-upward trend.

Interpacket units also show dominantly thickening-upward sequences and are interpreted as lobe-fringe facies. Switching of submarine fan channels results in changes in lobe position so that vertical sections are characterized by alternation of lobe and lobe-fringe facies (outer fan facies association).

Comparison of other parts of the Cloridorme Group with the γ_4 Formation allows their assignment to outer fan, fan-fringe and basin plain facies associations. Submarine fans grew along the axis of the longitudinal basin rather than perpendicular to its margin. Opposite palaeocurrents in different parts of the group suggest that two oppositely-directed fans were present. Sedimentation rate during Cloridorme Group deposition was approximately 420 m./m.y.

ACKNOWLEDGEMENTS

I would like to thank Dr. G.V. Middleton, my supervisor, for suggesting this project and for many valuable suggestions for improving the manuscript.

André Vallières of the Quebec Ministry of Energy and Resources added to our knowledge of the geology of the Lower St. Lawrence and Gaspé region on a field trip at the beginning of the study. Dr. John Riva (Laval University) identified the graptolite collections and showed me time-equivalent rocks to the Cloridorme Group near Quebec City. Dr. J.B. Southard (Massachusetts Institute of Technology) and Dr. I.C. Rust (University of Port Elizabeth) visited me in the field along with Dr. Middleton and provided stimulating discussion and encouragement. Dr. R.G. Walker (McMaster University) located data from sections measured in the Cloridorme by Barham Parkash, and discussed his own work in the area. Graduate students at McMaster, especially Rick Cheel, provided constructive criticism and practical help.

The following are also thanked for their assistance: Cynthia Millar of the Royal Ontario Museum, Toronto, for help and guidance with laboratory work; Jack Whorwood for photo-

graphic work and advice; and Linda Hillier for typing the final manuscript.

Financial support was provided through National Science and Engineering Research Council (Canada) grants to Dr. Middleton and a McMaster University scholarship to the author.

TABLE OF CONTENTS

ILLUSTRATIONS

LIST OF TABLES

CHAPTER 1

INTRODUCTION

Rationale

Dark-grey Argillite and interbedded Greywackes and Calcisiltites are superbly exposed on the wave-cut platform and in sea cliffs along the north shore of the Gaspé Peninsula, Quebec, between Cap des Rosiers and Marsoui (Fig. 1.1). These rocks were named the Cloridorme Formation by Enos (1965, p.22). The formation was divided into three sequences, each confined to one of three structural blocks. These sequences were named from east to west as α, β, and γ (Fig. 1.1) and were divided into a total of 14 members (α_{1-3}, β_{1-7}, γ_{1-4}). Stratigraphic relationships between members in different blocks were uncertain. The exposed thickness of the formation was estimated to be 7700 m. with an uncertainty factor of two (Enos, 1965, p.23).

The assemblage of sedimentary structures, including oriented sole marks, graded bedding, convolute lamination and cross-lamination suggested deposition by turbidity currents for most of the rocks (Enos, 1965, p.66). Correlation of beds over distances up to 7.5 km. enabled longitudinal changes in bed thickness and sedimentary structures to be examined. Lateral continuity of Greywacke and Calcisiltite beds is low; beds dis-

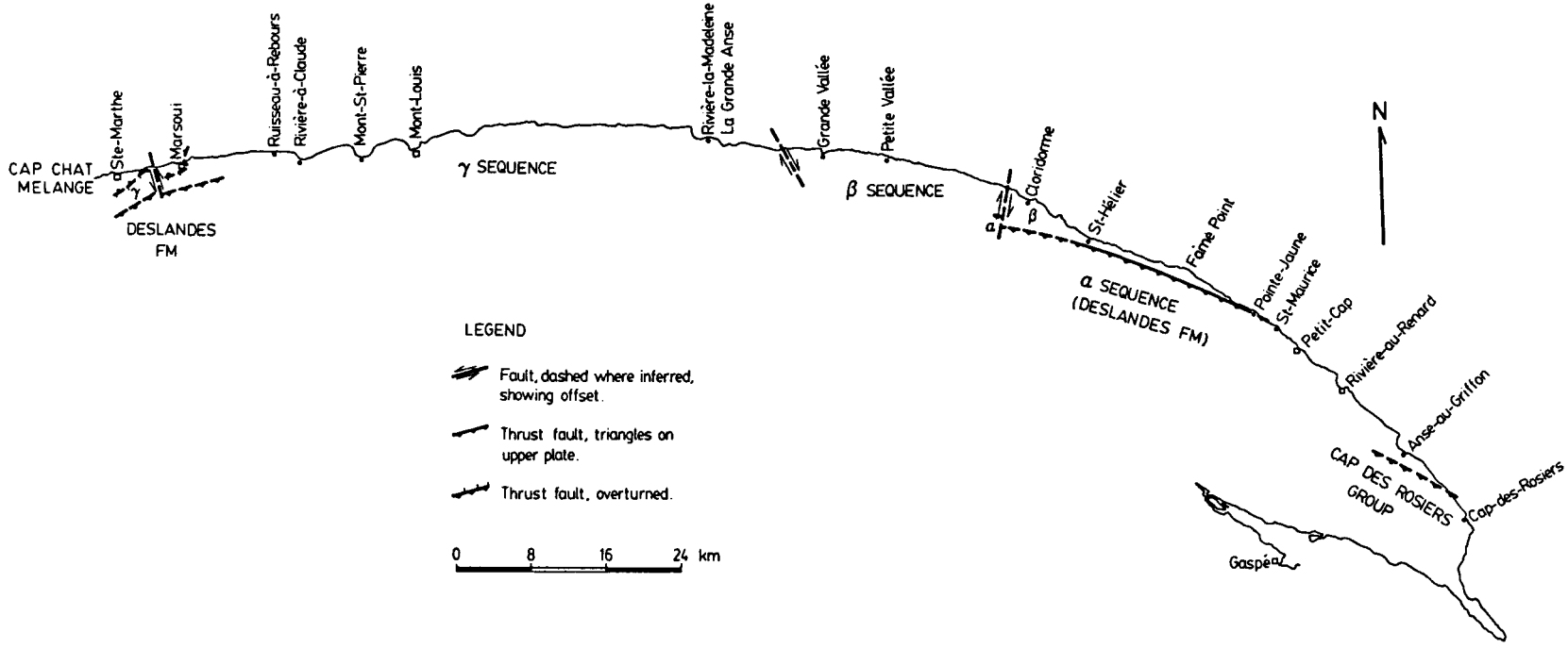

Figure 1.1: Map showing the three sequences of the Cloridorme Formation of Enos (1965). Place names mentioned in text are also shown. After Enos (1965, plate 1) and Biron (1973).

appear downcurrent at a rate of about 50% in 4 km. (Enos, 1969b).

Palaeocurrent directions in members α_1 through γ_2 are from east to west, and successively younger members are exposed in the downcurrent direction. Therefore, on the basin scale, Enos (1969b) envisaged filling of the longitudinal trough from the eastern end, with successively younger members deposited as imbricate wedges building out to the west. Enos (1965, p.76) also suggested the possibility of lateral supply, with turbidity currents turning and following the longitudinal slope of the basin. On a smaller scale, the dominant control on depositional pattern was thought to be localized subsidence caused by differential compaction of underlying sediments. Evidence for this was the fact that groups of beds thicken in nearly the same place when traced laterally. A pattern of imbrication was produced by deposition of beds as a series of wedges shingled one over the other with each successive current flowing down the slope built by deposits of the preceding current (Enos, 1965, p.92). Local thickness of an individual bed was strongly affected by topographic variations on the depositional surface. Downcurrent transitions from Greywacke and Calcisiltite beds to Argillite of similar thickness suggested some deposition of Argillite by turbidity currents.

Since Enos's study, the submarine fan facies model (Mutti and Ricci Lucchi, 1972; Walker and Mutti, 1973; Mutti, 1977; Walker, 1978) has been developed. A central feature of

the model is the presence of thickening-upward sequences of sandstone beds in depositional lobes and thinning-upward sequences in channels. The depositional pattern described by Enos as "deposition of beds as a series of wedges shingled one over the other" (above) is similar to that in progradational lobes of the submarine fan model, so we might expect to find thickening-upward sequences in such units. It seems logical, then, to re-examine this classic turbidite sequence to see whether such submarine fan models can be applied to it, or whether some other environmental interpretation is appropriate.

Area of Study

In order to reach conclusions on the applicability of a submarine fan model, detailed measurements (layer by layer) are required. This meant that only a small part of the formation could be examined in the time available. The γ_4 member, the westernmost member of the formation, was chosen for this detailed study (Fig. 1.2). The γ_4 member has the highest proportion of sandstone and siltstone lithologies (Greywacke, Calcareous Wacke and Calcisiltite) to lutite lithologies (Argillite, Dolomite and Limestone), according to Enos (1965, Table 2). It therefore seems the most likely member to show submarine fan features such as channels and depositional lobes, which typically have high or moderate sand/shale ratios. Another reason for looking at the γ_4 member is that it was one

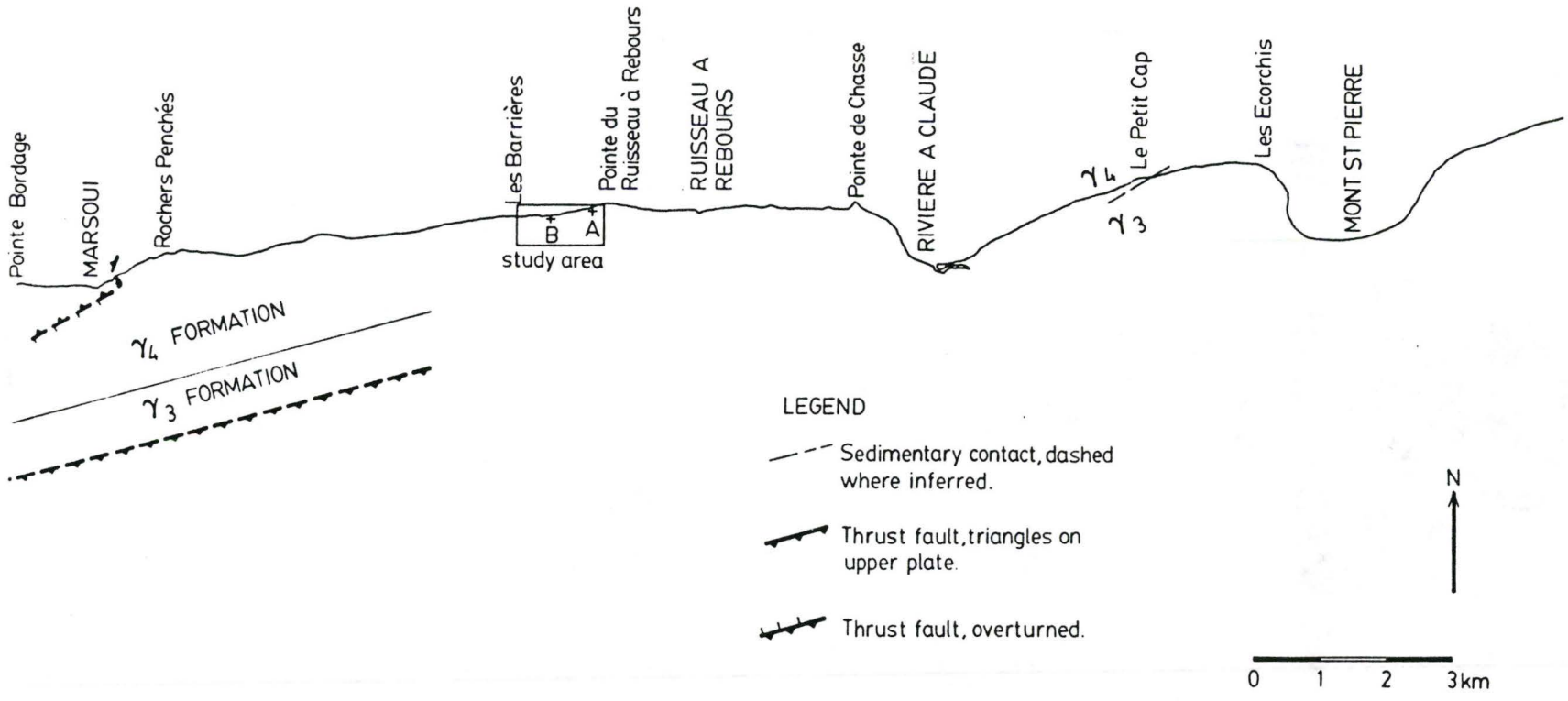

Figure 1.2: Location of study area. Reference points A and B refer to map in Appendix 2. Geology (simplified) taken from Biron (1973) and Enos (1965, plate 1).

of the least studied by Enos, who concentrated on the β sequence. The γ_4 member outcrops on the wave-cut platform and in roadcuts between Marsoui and Le Petit Cap, west of Mont St. Pierre.

Previous Work

Geologic work on the northern Gaspé Peninsula was begun by Logan (1846, 1863). Logan placed the structural discontinuity now known as Logan's Line south of the "Hudson River and Utica" rocks (Cloridorme Formation) rather than beneath the St. Lawrence (Fig. 1.3). Logan's interpretation has been revived by recent workers (Biron, 1973; St. Julien and Hubert, 1975). Geological mapping of the Gaspé Peninsula on a scale of 1:253,440 was carried out by Ells (1883), McGerrigle (1953), and McGerrigle and Skidmore (1967).

The study of Enos (1965, 1969a,b), which forms an essential background to this thesis, is described elsewhere. Walker (1969) studied the geometry of the ripple-drift cross-lamination in Calcisiltites at Petite Vallée. Parkash (1970) and Parkash and Middleton (1970) investigated downcurrent changes in sedimentary structures, textures and fabric in 8 Greywacke beds exposed over a distance of 2 miles (3 km.) at Grande Vallée. Parkash also measured detailed sections in the Cloridorme Formation. Some of his data were analyzed using the "ABC" index by Walker (1970). Bhattacharjee (1970) continued the studies of ripple-drift cross-lamination in the areas of St. Maurice,

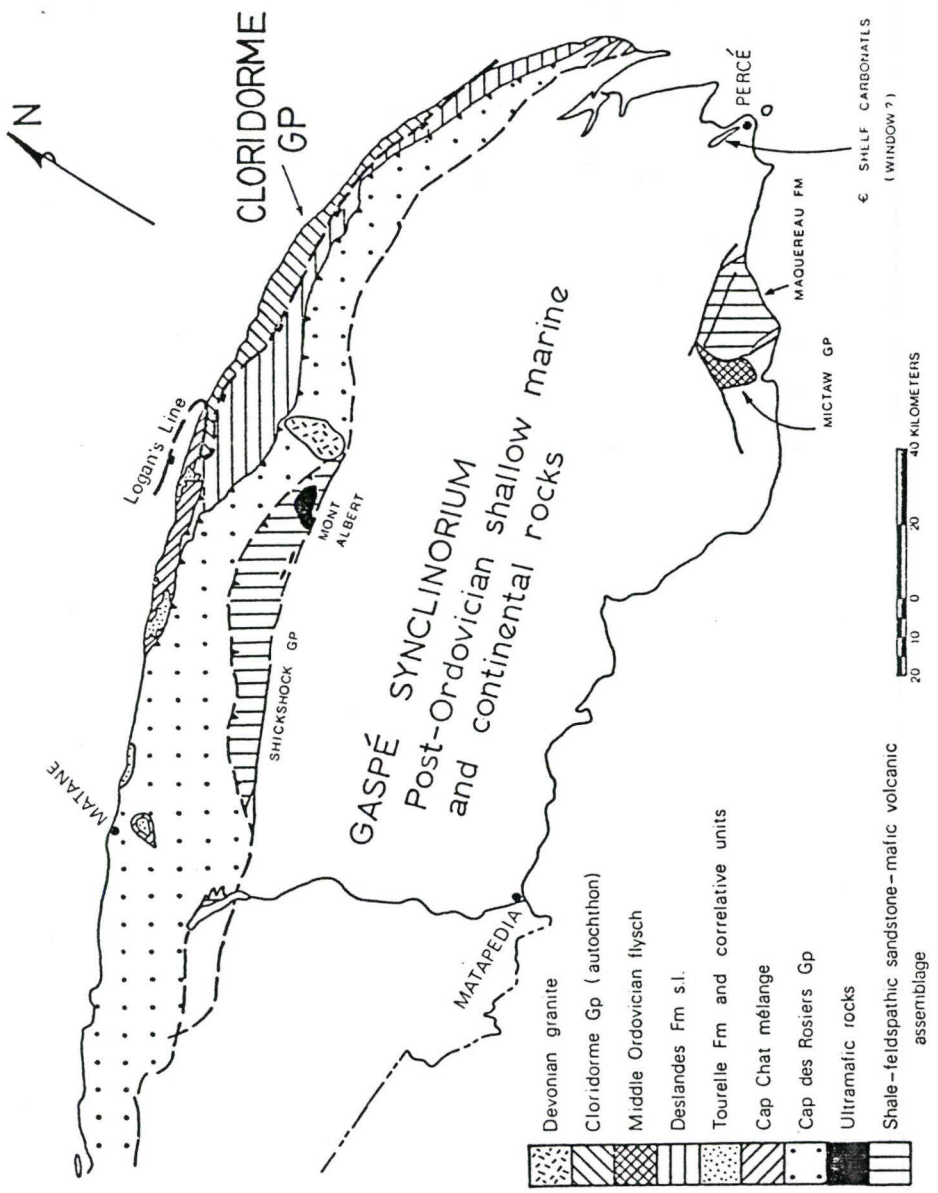

Figure 1.3: Regional geological map of the Gaspé Peninsula, modified from Hiscott, (1977, p.14).

Fame Point, Petite Vallée and Grande Vallée. Skipper (1970) studied the unusual Type 3 Greywackes (Enos, 1965, p.43) in the β_1 and β_2 members in the region of St. Hélier. The study included discovery of cross-stratification produced by migration of antidunes (Skipper, 1971); Markov chain analysis of the sequence of sedimentary structures (Doveton and Skipper, 1974); and depositional mechanics of these unusual turbidites, which could be correlated for distances up to 12 km. in the down-current direction (Skipper and Middleton, 1975). Pett and Walker (1971) studied the morphology of flute casts and its relationship with internal sedimentary structures in turbidites, taking most of their data from the Cloridorme Formation.

The β and γ sequences of the Cloridorme Formation were referred to as the Cloridorme Group by Biron (1971) with the members γ_1 to γ_4 elevated to formation status. The γ_3 and γ_4 members will be named the Mont. St. Pierre and Rochers Penchés Formations, respectively, in a forthcoming report of the Ministry of Energy and Resources, Quebec by S. Biron (pers. comm., 1981). The α_3 member is probably equivalent to the Deslandes Formation (Biron, 1972, 1973). The status of the β sequence in this new scheme is unknown to the present author.

Islam *et al*. (1982) studied the diagenesis and low-grade metamorphism of the Cambro-Ordovician flysch units of the Gaspé Peninsula, using illite crystallinity and maturation of organic matter in shales to estimate maximum temperatures

reached during burial. The Cloridorme Group falls within their anchizone, the zone of transition between diagenesis and true regional metamorphism (greenschist facies), corresponding to temperatures of 200-350°C. Regional patterns indicate that thermal maturation of the Cloridorme Group occurred as a result of tectonic burial by overlying nappe units.

Regional Setting and Structure

The Cloridorme Group lies on the northwestern margin of the Appalachian orogenic belt. The reconstructed Appalachian-Caledonian orogen has a combined length of about 10,000 km., stretching from Spitzbergen through Scandinavia and east Greenland, the British Isles, Newfoundland and continental North America as far south as southern Mexico (Williams, 1978).

The Quebec Appalachians may be divided into a series of tectonic domains from northwest to southeast. These are the autochthonous domain; the external domain, comprising an outer belt of thrust-imbricated structures and an inner belt of nappes emplaced by gravity sliding; and an internal domain, represented by metamorphosed and igneous rocks, part of which overlies a Grenville-like basement and another an oceanic crust. The northwestern limit of the gravity-emplaced nappes is known as Logan's Line (St. Julien and Hubert, 1975). In the northern Gaspé Peninsula, the external domain may be divided into four structural units in stacking sequence from base to top (Fig. 1.4).

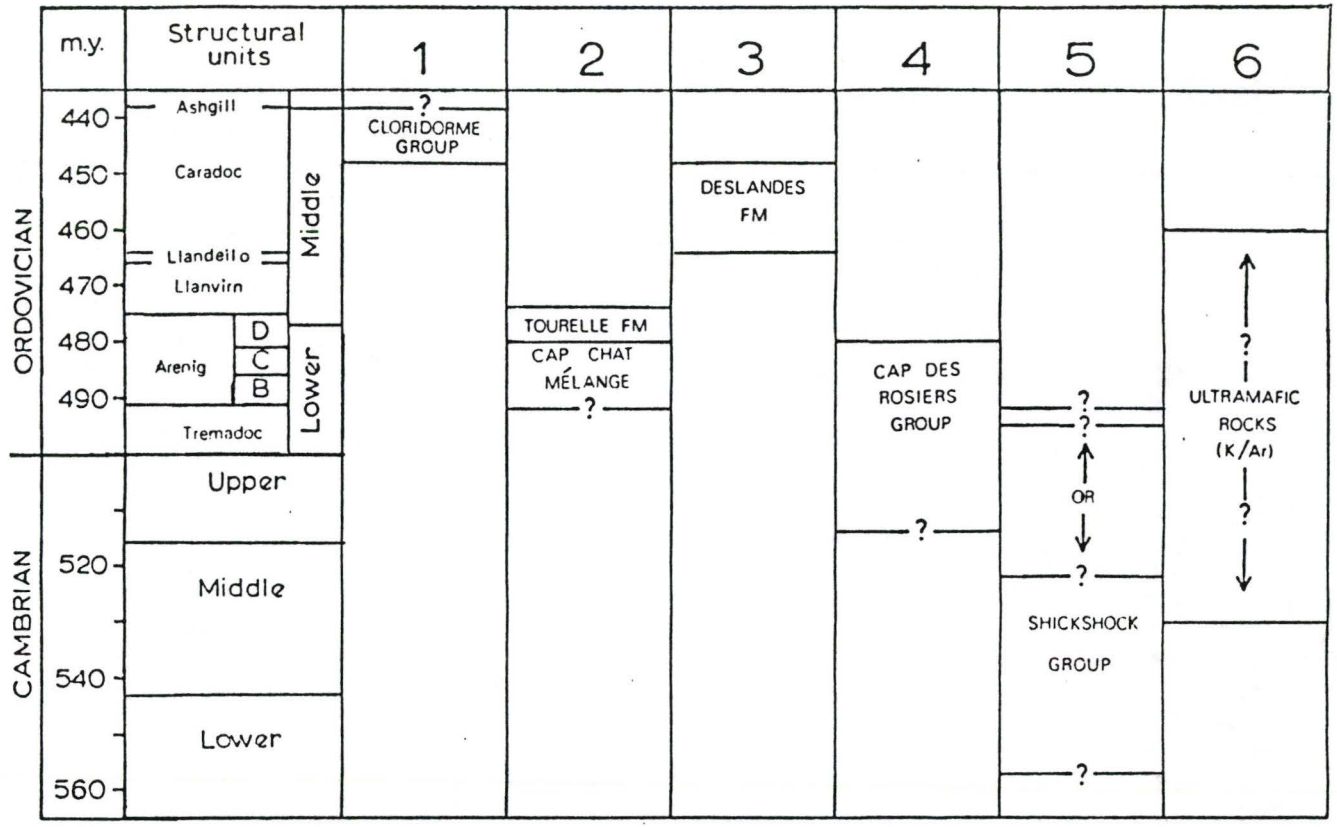

Figure 1.4: Stratigraphic table of various Cambrian and Ordovician stratigraphic units surrounding the study area. Unit 1 is para-autochthonous or autochthonous. Units 2 to 6 are thrust sheets in vertical stacking sequence from base to top. Unit 2 is the Cap Chat "mélange" zone, unit 3 is the Rivière Marsoui nappe, and unit 4 is the Rivière Ste-Anne nappe. Time scale for Llandeilo to Ashgill is taken from Carter et al. (1980). Figure modified from Hiscott (1977, p.15) and Biron (1974).

These are the Cloridorme Group, Cap Chat "mélange" zone, Rivière Marsoui nappe and Rivière Ste-Anne nappe (Biron, 1973). The nappes of the external domain may in turn be overthrust by the Shickshock Group and ultramafic rocks of the internal domain (St. Julien and Hubert, 1975). Further south, the internal domain is covered by post-Ordovician shallow marine and terrestrial sediments (Fig. 1.3).

Ultramafic rocks

Ultramafic rocks occur at Mont Albert and at Mount Serpentine in eastern Gaspé. These rocks form part of a discontinuous belt of ultramafic rocks and ophiolitic complexes through Quebec and western Newfoundland, many of which have been interpreted as obducted slices of oceanic crust (Church and Stevens, 1971; Laurent, 1975; Williams, 1975). The trend of the positive Bouguer gravity anomaly (Enos, 1965, Fig. 1) and of the aeromagnetic high (1:253,440 Aeromagnetic series, Geological Survey of Canada) runs along this belt in the Gaspé Peninsula, suggesting further ultramafic bodies may be present at depth.

Mont Albert consists of serpentinized peridotite with lenses of dunite, pyroxenite and chromite, with a primary foliation suggesting dip of sixty degrees to the south or southwest (St. Julien et al., 1972). It is surrounded by a metamorphic aureole 390-510 m. thick of granulite and amphibolite facies

which, along with similar aureoles beneath ophiolite complexes in western Newfoundland (Williams and Smyth, 1973), can probably be interpreted as the result of obduction of hot oceanic crust onto the ancient continental margin of North America (Hiscott, 1978).

Obduction of the ophiolite must have occurred at least as early as Late Arenig time (ca. 475 Ma), because ophiolite derived chromite is present in the Tourelle Formation (Hiscott, 1978). This age is in reasonable agreement with radiometric dates of 460-480 Ma for ophiolite obduction in western Newfoundland (Dallmeyer and Williams, 1975; Archibald and Farrar, 1976; Dallmeyer, 1977). Biotite and muscovite from the Mont Albert aureole give an emplacement age (K-Ar) of 495 ± 35 Ma (Neale et al., 1961). Younger dates have been obtained from hornblende (K-Ar) in amphibolite in the Shickshock Group (443 ± 18 Ma, Wanless et al., 1973) and in probable Shickshock equivalents associated with the Mount Serpentine ultramafics (437 ± 20 Ma, Wanless et al., 1971). These dates may reflect uplift during Middle Ordovician allochthony or perhaps uplift in late Ordovician or earliest Silurian, following emplacement of the allochthons (Wanless et al., 1973).

Shickshock Group

The Shickshock Group consists mainly of metavolcanic rocks (basalts, commonly pillowed where least metamorphosed)

which reach the albite-epidote-amphibolite facies of regional metamorphism. Metasediments (arkose and slate) also occur. The age of the group and its structural relationship with the Rivière Ste-Anne nappe is unclear (Biron, 1974). It could be a nappe overriding the Rivière Ste-Anne nappe, of Middle or Lower Cambrian age (St. Julien and Hubert, 1975). However, the work of Mattinson (1964), Ollerenshaw (1967) and Girard (1967) tends to indicate that the group interdigitates with the bordering Cap des Rosiers Group of the Rivière Ste-Anne nappe (St. Julien et al., 1972). In the former case, the group is considered to be part of the Cambrian shale-feldspathic sandstone assemblage which occurs throughout Quebec in the external domain (e.g. Cap Enragé Fm., Orignal Fm., St. Damase Fm., St. Roch Fm.) and as metamorphosed equivalents in the internal domain (Armagh Fm., Caldwell Group, Mansonville Fm.) (St. Julien and Hubert, 1975).

Rivière Ste-Anne nappe

The Rivière Ste-Anne nappe is made up of rocks of the Cap des Rosiers Group. The group has been divided into six formations, ranging in age from Upper Cambrian to Lower Ordovician (Upper Arenig) by Biron (1974). The dominant lithologies are red, green, or banded green and black shales and mudstones, siltstones (siliciclastic, calcareous and dolomitic), sandstones of sub-arkose to sub-greywacke composition, marly mudstones, ribbon limestone and continuous resistant bands of quartz arenite

and limestone conglomerate. This shale-limestone conglomerate assemblage occurs throughout the Quebec Appalachians, and is interpreted as a slope and base-of-slope accumulation (St. Julien and Hubert, 1975; Hiscott, 1977, p.18).

Rivière Marsoui nappe

The Rivière Marsoui nappe is made up entirely of rocks of the Deslandes Formation (Biron, 1972, 1974), of Nemagraptus gracilis and Diplograptus multidens zone age (Fig. 1.5). The formation consists of siltstone layers with occasional fine sand bases and thin calcisiltites. Its environment of deposition is not known.

Cap Chat "mélange" zone

This zone includes deformed and broken rocks of the Cap des Rosiers Group (the Cap Chat "mélange"), and the overlying Tourelle Formation. The Cap Chat "mélange" consists of banded green and black mudstones interbedded with dolomitic siltstones, ribbon limestones and a little limestone conglomerate (Biron, 1973). It is identical lithologically to the upper part of the Cap des Rosiers Group (Biron, 1974). The Tourelle Formation consists of thick greywacke beds up to 22 m. thick interbedded with siltstones, dolomitic siltstones and green, grey and red shales (Biron, 1973; Hiscott, 1977, p.29). The submarine slope on which the Cap des Rosiers Group was deposited initially re-

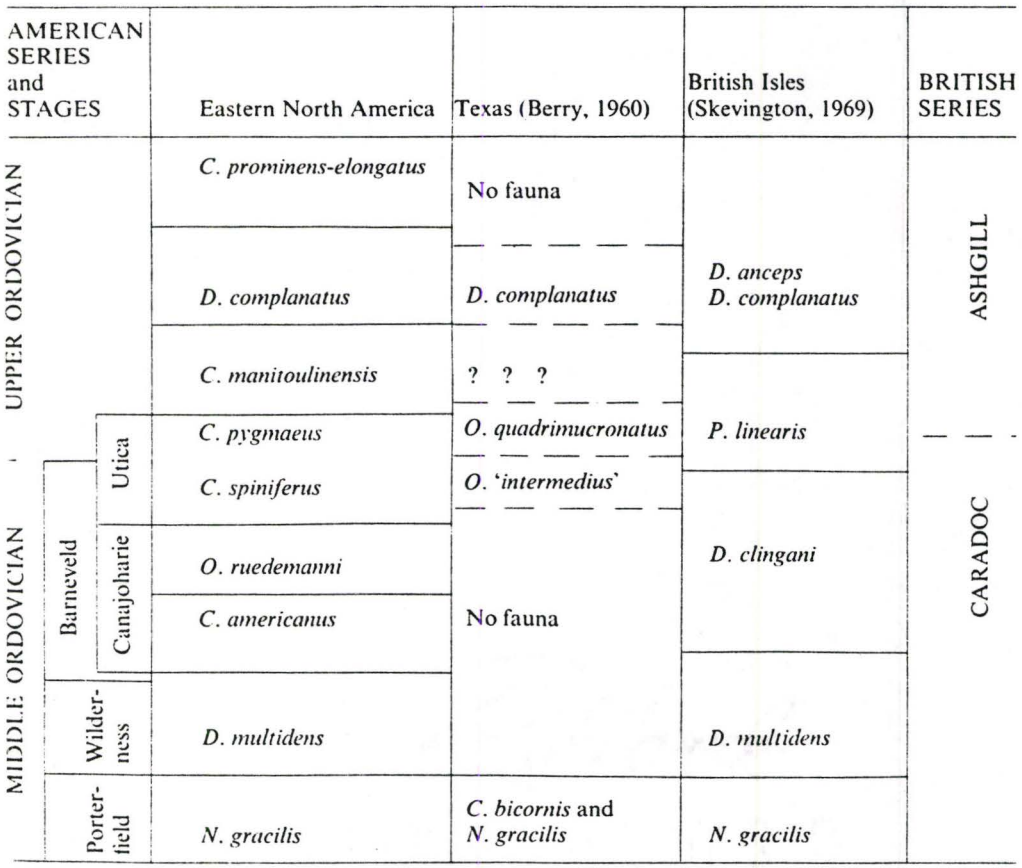

Figure 1.5: Middle and Upper Ordovician graptolite zones of eastern North America with a suggested correlation with those of Britain (from Riva, 1974).

ceived northerly-derived quartz clastics. Following a reversal of slope direction, carbonate detritus of southern origin was deposited. These sediments were cut by feeder channels of the overlying Tourelle submarine fans, which also received sediment from a southern source (Hiscott, 1977, p.431).

Deformation of this Lower Ordovician assemblage took place when it slid as a gravity nappe into the Middle Ordovician shale basin (site of Cloridorme Group deposition). The Cap des Rosiers Group lithologies were tightly folded and fragmented by nappe movement, while the stronger sandstone-dominated Tourelle Formation developed large folds overturned to the northwest. Only Cap des Rosiers Group and Tourelle Formation lithologies are present in the Cap Chat "mélange" and fragmentation is relatively minor, so it is best described as a broken formation and not a mélange (Hiscott, 1977, p.426). Debris shed from the advancing nappe formed on olistostrome which is exposed west of Marsoui (Hiscott, 1977, p.431).

Cloridorme Group

The Cloridorme Group appears to be autochthonous or para-autochthonous (Biron, 1974), though its northern boundary is not exposed so its relation with the platform sequence (St. Julien and Hubert, 1975) to the northwest of the Appalachian belt is unknown.

At Marsoui, the group is structurally overlain to the

west by burrowed green and grey silicified mudstones of the Cap Chat "mélange" (Fig. 1.6a). The final *in situ* beds of the Cloridorme Group are overturned thick Greywackes with fluid-escape structures (Fig. 1.6b). These beds are locally in fault contact with a zone of rounded Dolomite boulders in dark-grey Argillite (Fig. 1.6c). To the west, following the Dolomite boulder zone, or following the Greywackes directly, is a zone of highly cleaved dark-grey Argillite, separated by a fault. This Argillite is separated by another fault from Argillite containing large blocks of Greywacke (Fig. 1.6d) similar to that in the Cloridorme Group. This unit is overridden by the Cap Chat "mélange".

Graptolites belonging to the upper part of the *Climacograptus spiniferus* zone have been collected from the Argillite separating the *in situ* Cloridorme Group from the Cap Chat "mélange" (Riva, 1968). This deformed zone probably represents an Argillite-dominated part of the Cloridorme Group which was disturbed and faulted as the Cap Chat "mélange" zone nappe was thrust over it. No blocks were seen which could not have come from the Cloridorme Group, and so the zone appears to be unrelated to the olistostrome within the Cap Chat "mélange". The Dolomite boulder zone could be a minor olistostrome within the Cloridorme Group. Logan's Line is therefore placed immediately below the silicified mudstones of the Cap Chat "mélange" (St. Julien and Hubert, 1975).

At its eastern margin at Pointe-Jaune (Fig. 1.1), the

Figure 1.6a: Thrust fault contact (Logan's Line) between Cap Chat "mélange" (above 1 m. scale) and "argile-à-blocs" unit of Cloridorme Group (covered by seaweed). East of Marsoui wharf.

Figure 1.6b: Final overturned thick Greywackes of Cloridorme Group. Scale 1m.

Figure 1.6c: Dolomite boulders in Argillite adjacent to Greywackes in (b). Scale 1 m.

Figure 1.6d: Blocks of Cloridorme Greywacke in Argillite beneath Logan's Line, which is just left of this view. Scale 1 m.

group is thrust over by the α sequence of the Cloridorme Formation (Deslandes Formation?). The boundary between the central block (β sequence) and the western block (γ sequence) is a dextral strike-slip fault with an inferred displacement of 1700 m. at Le Grand Ruisseau, west of Grande Vallée (Enos, 1965, p.16-19).

Structurally, the western block is characterized by folds with broad, gently-dipping upright limbs and short, nearly vertical or overturned limbs. The folds resemble a flight of stairs descending to the north or northwest. In the γ_4 Formation, sharp north-plunging minor folds are superimposed upon this pattern. Folding occurred during the Taconic orogeny (Enos, 1965, p.19-21).

The contact between the γ_3 and γ_4 Formations is a conformable sedimentary contact and is marked by an abrupt upward transition from Calcisiltite of γ_3 to predominantly massive Greywacke of γ_4 at Le Petit Cap (Enos, 1965, p.60).

Age and Correlative Units

Extensive collections of graptolites were made by Enos in the Cloridorme Formation. These were identified by Berry (in Enos, 1965, p.62) as belonging to the zone of Orthograptus truncatus intermedius of the Ordovician section of west Texas (Berry, 1960), of late Wilderness and Trenton (equivalent of Canajoharie) age (Fig. 1.5). The entire formation was assigned to this zone and was considered correlative with the uppermost Normanskill and

overlying Canajoharie Formations of New York. Riva (1968) examined a number of collections from the Cloridorme Formation. He found Normanskill faunas (i.e. Nemagraptus gracilis zone) in the α sequence and younger Canajoharie and Lower Utica faunas in the β and γ sequences. The β and γ sequences were found to be partially time-equivalent, with the γ sequence younger than most of the β sequence. Graptolite collections made recently in the area of Grand Etang (St. Hélier) and Cloridorme in the β_1 and β_2 members are of Lorraine (Upper Ordovician) age (J. Riva, pers. comm., 1982). These members therefore appear to be of a younger age than the rest of the β sequence. The graptolite zonation of Berry (1960) appears not to be applicable to eastern North America because graptolite faunas in Texas belong to the Pacific faunal province and resemble those of Australia more than those of eastern North America, and because extensive gaps occur in the Texas succession (Riva, 1972).

The γ_4 Formation of the Cloridorme Group contains Lower Utica (Climacograptus spiniferus zone) fauna (Riva, 1968). Further graptolite collections made during this study and identified by John Riva (Appendix 1) belong to the lower or middle part of the C. spiniferus zone. The presence of C. typicalis and its predecessor C. "praetypicalis" in Collection 10, which contains the most specimens, suggests an age close to the middle of the zone (Riva, 1969, Fig. 2). The C. spiniferus zone corresponds to the upper Dicranograptus clingani zone of Britain which

is close to upper Caradoc (Riva, 1974). This is late Middle Ordovician of North America and mid Late Ordovician of Britain (Fisher, 1977). An attempt to extract a conodont fauna from the γ_4 Formation was unsuccessful (Appendix 1).

The Cloridorme Group forms part of an almost continuous belt of Cambro-Ordovician flysch along the western side of the Appalachian orogen from Newfoundland to SE Tennessee (Enos, 1969a). In Quebec, other rocks of the C. spiniferus zone occur in the area northeast of Quebec City, on the north shore of the St. Lawrence River. These are the Utica Shale, Beaupré Formation, Lotbinière Formation and "New Facies" (Belt et al., 1979). The Beaupré Formation and "New Facies" are interpreted as submarine fan deposits with a southeasterly or easterly source area. The "New Facies" appears to be similar sedimentologically to the Tourelle Formation and parts of the Cloridorme Group (Belt and Bussières, 1981). Utica Shale of this age also occurs in New York and elsewhere in Quebec. The Macasty Shale in the subsurface of the island of Anticosti to the north of the Gaspé Peninsula is partly of C. spiniferus zone age (Riva, 1968, 1969). The Mictaw Group at Port-Daniel on the southern coast of the Gaspé Peninsula (Fig. 1.3) may also be of this age (Ruedemann, 1947, p.74). Outside Quebec, parts of the Martinsburg Formation, stretching from New York to Virginia are also of this age, and include greywacke-shale sequences deposited by turbidity currents (McBride, 1962; Berry, 1971). In western Newfoundland, the Humber zone apparently

lacks rocks of this age (Williams, 1969; Whittington and Kindle, 1969; Kay, 1969; Bergström et al., 1974; Gonzalez-Bonorino, 1979; Williams, 1979). No deep-sea turbidites of this age exist in the equivalent to the Humber zone in the British Isles (Williams, 1978).

CHAPTER 2

FACIES DESCRIPTION, γ_4 FORMATION, CLORIDORME GROUP

Field Methods

Five months were spent in the field during the summers of 1980 and 1981. Three weeks of this were spent on a regional reconnaissance of the rocks along the coast between Quebec City and Anse au Griffon, near the easternmost point of the Gaspé Peninsula (Fig. 1.1). The remaining time was spent measuring detailed sections in the γ_4 Formation of the Cloridorme Group.

The area chosen for detailed study is located between Pointe de Ruisseau à Rebours (grid reference 842566, Canada 1:50,000 map sheet 22H/4 and 22H/5, Mont-Louis) and Les Barrières (828566), about 7 km. east of Marsoui (Fig. 1.2) along Route 132. This area was chosen because of the lack of structural complication and because good exposures are present on the wave-cut platform and in a recent roadcut. Strike of beds ranges from 029° to 058°, so that the beds made a high to moderate angle with the approximately east-west trending shoreline. Dip of beds ranges from 36°N to 58°N, thus thick stratigraphic sections can be measured in a relatively short distance. The section on the wave-cut platform is accessible at low tide. The roadcut section lies west of this, but correlation of key beds across

the road was a simple matter so that one continuous stratigraphic section was measured.

On the wave-cut platform, sections were measured perpendicular to strike, beginning at the roadside edge of the outcrop and continuing until near low-water mark, at which point section measurement returned to the roadside edge at the same stratigraphic level. Sections measured in this way were lettered with white paint at, or close to, the start of the section. A map with section locations is provided in Appendix 2.

With the exception of some units of multiply-interbedded thin Calcisiltites and Argillite, each sedimentary layer was measured and described in terms of thickness, grain size, reaction with dilute (2M) hydrochloric acid, grading, nature of contacts, sedimentary structures, lateral variation and lithologic type. A layer is defined as the deposit of a single sedimentary event, such as a turbidity current. A bed is a lithologically homogenous sedimentary unit, which may consist of one or more layers (Hiscott, 1980), or may form only part of a layer. Argillite beds were treated as layers, since their depositional relationship to underlying sandstones was unclear. Layers were measured if they were one centimetre or more in thickness, except in Argillite-dominated parts where thinner layers were sometimes recorded. Measurements were made to the nearest centimetre, or half centimetre for thin layers.

Grain size was taken as the maximum grain dimension

seen in a small area of the base (e.g. a 10 cm. length sample). Grain size was measured directly or with a hand lens (x10 magnification), or estimated visually for fine sand and smaller sizes. Grain size data were grouped into the classes of the Udden-Wentworth scale (Wentworth, 1922). Size of Argillite, Calcisiltite and other lithic clasts was recorded separately and not included in the grain size above. Reaction of a fresh surface with dilute hydrochloric acid was recorded on a scale of 0 to 3: 0-no reaction, 1-reacts when powdered, 2-reacts, 3-reacts strongly. Grading was described as normal, inverse to normal, inverse or absent. Absent includes all cases where grading was not observed. Additional comments were often made to describe the type of grading, but no pre-determined classification was used. Sedimentary structures were described and then summarized in terms of the Bouma (1962, p.49) sequence where this was appropriate. Lateral variation was recorded by noting changes which occurred on the outcrop scale, such as thickness variation due to an erosive base or eroded top. Palaeocurrent indicators were measured using a Silva compass/clinometer and protractor. Correction for tilt of beds was carried out in the field, assuming folding without significant plunge (Potter and Pettijohn, 1977, p.371). No fold axes were seen for measurement of fold plunge, though Enos (1965, Plate 1) recorded a minor fold plunge of 12°N in the area. Palaeocurrent indications were assigned a reliability of 1 (least reliable),

2, or 3 (most reliable), based on the quality and type of indication, and these reliabilities were used to calculate reliability-weighted means for each layer. Lithologic type was described according to the scheme of Enos (1965, p.23).

In the units of Calcisiltites and Argillite not measured in detail, the total thickness, the number of layers, the sandstone plus siltstone to shale ratio, and any palaeocurrent directions were recorded. A brief description of typical sedimentary structures in the Calcisiltites was also made.

Facies Classification

Since each lithology has an associated set of characteristics, such as sedimentary structures, the lithologies were also considered as facies. Using Enos's descriptions, it was fairly easy to fit most layers into one of these types. Problems of classification arose in a few cases of facies of transitional types and where layers, apparently resulting from a single depositional event, included more than one facies (e.g. a Greywacke 1-Calcisiltite 2 couplet). In the latter case, the layer was usually classified as belonging to the dominant facies within it, so that a thin Greywacke 1 or Calcareous Wacke overlain by a thick Calcisiltite 2 would be classified as a Calcisiltite 2. The good agreement between layer thickness means for each facies (Table 2.1) in this study and in that of Enos (1965, Table 3) suggests that the types were used in their original sense.

Facies are listed below, together with abbreviated forms. In order to distinguish facies names from lithological descriptions, facies names are capitalized: Argillite (ARG), Limestone (LST), Dolomite (DOL), Volcanic Ash (VA), Calcisiltite and Argillite (CSA), Calcisiltite 1 (CS1), Calcisiltite 2 (CS2), Calcareous Wacke (CW), Greywacke 1 (G1), Greywacke 2 (G2).

Greywacke 1 is identical to Type 1 Greywacke of Enos (1965, p.36) but the shorter notation is preferred, and similarly for the other numbered facies. The term "Greywacke" when used without a qualifying number indicates Greywacke 1 and/or Greywacke 2 facies and similarly for Calcisiltite. The additional facies CSA arose because some units of multiply-interbedded thin Calcisiltites and Argillite were not measured in detail. Facies CSA may contain Argillite, Calcisiltite 1, Calcisiltite 2, and rarely Calcareous Wacke. No examples of Enos's (1965, p.43 and 49) Type 3 Greywacke or Dolomitic Silty Argillite were identified in the measured sections.

Total thickness measured was 434 m., of which 425 m. was unique stratigraphy. This 425 m. is used for all calculations and descriptions of facies properties of the γ_4 Formation. Total number of layers or horizons (facies CSA) measured was 3581. Enos (1965, Table 2) estimated the thickness of the γ_4 Formation as 510 m., but this estimate seems low, considering that only a part of the formation was measured in this study. There was no time to measure the total thickness of the forma-

tion, but 1000 m. would seem a more plausible minimum thickness.

Table 2.1 shows the abundance of each facies within the γ_4 Formation. The succeeding lutite thickness is the thickness of the succeeding Argillite, Dolomite or Limestone bed. For example, in the case of a Greywacke 1 followed by Argillite followed by Dolomite, the thickness used would be that of the Argillite only. Figure 2.1 presents layer thickness histograms for each of the major facies. These histograms are plotted using a geometric scale, because it is generally observed that the frequency distribution of this variable is approximately log-normal (Ricci Lucchi, 1969). In Table 2.2, the major non-lutite facies are subdivided according to the divisions of the Bouma sequence that they show. Layers having Bouma divisions in no particular order (e.g. T_b, with T_c laterally) were taken as having the divisions in the usual order (i.e. T_{bc} in this example). Although reversals of the sequence (e.g. T_{cb}) were noticeable in the field, they comprise only a small percentage of layers. T_d and T_e divisions are bracketed in this analysis as T_d is difficult to distinguish from T_e in weathered or tectonized outcrops (Bouma, 1962, p.49) and they may be removed by erosion by the next influx of sediment.

Argillite

Argillite beds range in thickness from almost zero to 227 cm., with a mean of 10.3 cm. Argillite is by far the most

Table 2.1 Facies proportions and mean characteristics of the γ_4 Formation, Cloridorme Group

Facies	No. of layers (or horizons)	Percent of section	Thickness (cm.) $\bar{x}$	Thickness (cm.) s	Succeeding lutite $\bar{x}$	Succeeding lutite s
Argillite	1549	35.5	9.7	14.8		
Limestone	64	2.2	14.4	18.2		
Dolomite	66	2.5	13.1	8.6		
Volcanic Ash	3	0.0	1.7	1.3		
CSA	10	3.5	149.8	99.0		
Calcisiltite 1	826	6.2	3.2	3.3	8.1	10.2
Calcisiltite 2	197	5.0	10.8	10.4	5.8	11.7
Calcareous Wacke	227	6.9	12.8	10.4	8.9	20.0
Greywacke 1	546	33.9	26.3	28.2	9.2	17.8
Greywacke 2	93	4.2	19.2	16.1	6.4	7.0

$\bar{x}$ = mean thickness; s = standard deviation

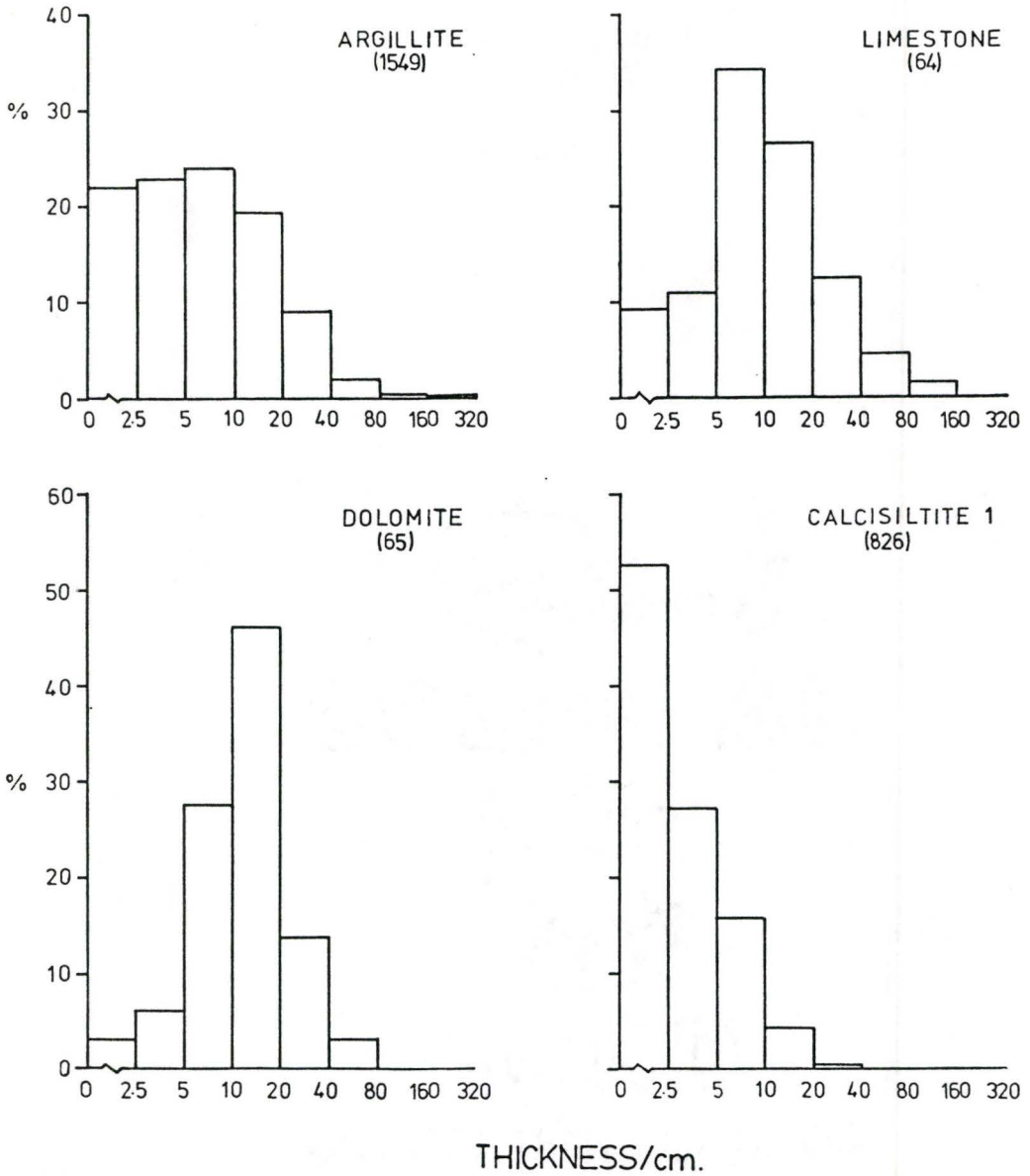

Figure 2.1: Layer thickness histograms for each facies. Number of layers measured is shown below facies name.

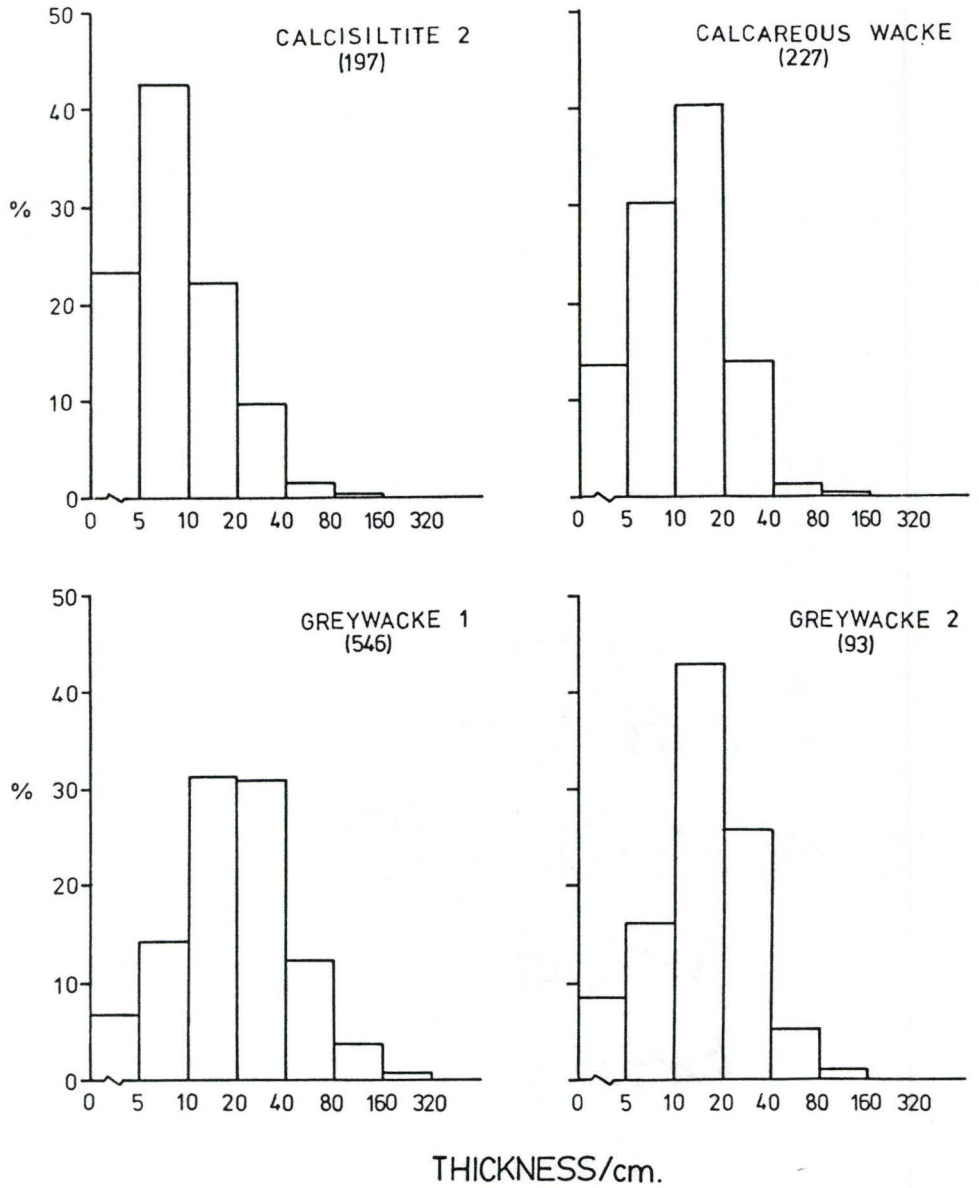

Figure 2.1 (continued): Note that thickness scale differs from previous page.

Table 2.2 Facies breakdown according to sequence of Bouma divisions

Bouma sequence	Greywacke 1	Greywacke 2	Facies % Calcareous Wacke	Calcisiltite 1	Calcisiltite 2
$T_{a(de)}$	60.6	74.2	8.1	0.6	1.0
$T_{ab(de)}$	10.3	8.6	2.2	-	-
$T_{abc(de)}$	5.0	3.2	3.1	-	0.5
$T_{ac(de)}$	20.5	14.0	14.8	0.6	3.6
$T_{b(de)}$	1.1	-	8.5	25.2	5.1
$T_{bc(de)}$	0.2	-	14.4	10.6	6.6
$T_{c(de)}$	0.6	-	44.8	58.9	82.1
$T_{d(e)}$	-	-	0.5	0.2	-
Reversals	1.8	-	3.6	3.9	1.0

important lutite material. Colour is generally dark grey, both fresh and weathered. Occasional black shale bands less than one centimetre in thickness were observed and these contained graptolites, often in abundance. Reaction with dilute HCl is variable (0-3), since there appears to be a continuous facies gradation from Argillite to dolomitic Argillite to Dolomite and similarly through calcareous Argillite to Limestone.

Most Argillite contains some proportion of silt, but the proportion is variable and hard to estimate. No graded layers were observed; vertical transitions from sandstone or siltstone layers are fairly sharp. Tops of Argillite beds are sharp except for gradational changes to some Limestone or Dolomite beds. No sedimentary structures were observed in the Argillite itself, but rare examples of parallel, alternating laminae of silt and Argillite about one millimetre thick were seen in fresh exposures. Small-scale loading was apparent between silt and Argillite laminae. Some of these silt laminae are irregular and may reach 4 mm. in thickness. One bed contained saucer-shaped cross-laminated sandstone lenses (e.g. 1.5 cm. x 16 cm.), which occurred at the same level but were isolated, or only connected by a thin layer(lenticular bedding). Argillite beds are uniform, with no obvious stratification, but horizontal parting is enhanced by weathering in the roadcut exposure. Thin calcite veins (a few millimetres in thickness), which may have slickensided surfaces, are sometimes present

along the bedding. Intersection of bedding and cleavage planes may produce sharp, angular fragments in weathered material. Flakes of mica can be seen on some broken surfaces.

Cross-sections of possible orthocone nautiloids were seen in one bed, but could not be extracted. Nautiloids collected by Enos were identified as belonging to the orders Endoceratida and Michelinoceratida (Enos, 1965, p.63). No bioturbation was seen in the Argillite, but some burrowing activity in the mud is suggested by the small hemispherical protrusions on the base of some Calcisiltite 1 layers which overly Argillite (Enos, 1965, p.26). Graptolites are quite common in certain beds and do not have any obvious preferred orientation. Some Argillite beds pass upcurrent into other facies, such as Greywacke 1 and 2 and Calcisiltite 2 (Fig. 2.2). Argillite is the least resistant to weathering of all facies and weathers to a rough surface on the wave-cut platform (Fig. 2.2d). Flatter surfaces are associated with more dolomitic Argillite. According to the classification of Potter *et al.* (1980, p.14), the Argillite facies would include clayshale and mudshale (variable proportion of silt), argillite, and rare slate (depending on the degree of metamorphism).

Enos (1965, p.25) examined Argillite clasts in Greywacke layers and found the dominant clay minerals to be chlorite and illite. The dark grey colour was accounted for by the presence of murky disseminated organic matter, together with less

Figure 2.2a,b: Lateral transition of Greywacke 2 to Argillite. Top photo was taken 2 m. SW (upcurrent) of bottom one. Lower layer of amalgamated bed is Calcisiltite 2. Scale 30 cm.

Figure 2.2c: Transition from Greywacke 2 (on left) to Argillite in downcurrent direction. Note very sharp boundary between them. Scale (1 m.) lies along bedding.

Figure 2.2d: Argillite dominated unit (Unit 6). Top is to left. Scale 1 m.

abundant disseminated pyrite. The former seems the most likely explanation since pyrite is not an important pigment (Potter et al., 1980, p.56).

Limestone

Argillaceous Limestone beds range in thickness from 1 to 120 cm., with a mean of 14.4 cm. Colour is black to dark grey when fresh but weathers to light grey. Reaction with dilute HCl is vigorous and this was the main criterion for distinguishing between Limestone and Argillite.

Grain size is clay; silty Limestones are rare, although many are underlain by very calcareous Calcisiltite 1 or Calcareous Wacke layers. The Calcareous Wacke layers commonly have wavy tops and the transition to Limestone always appears sharp. Calcisiltite 1 to Limestone contacts may be sharp or gradational. Some beds above Limestones are also highly calcareous. Limestone develops fissility on weathering in a similar way to Argillite. One thick Limestone bed had patches of sandy material within it, probably intruded in from the Greywacke 1 layer below. One Limestone bed contained graptolites. Limestones are more resistant to weathering than Argillite and form slight ribs above surrounding Argillite on the wave-cut platform (Fig. 2.3a).

Enos (1965, p.49) determined the composition as 84% calcite, 12% carbonaceous material, 2% chlorite and clay matrix, 1% silt-sized quartz and traces of pyrite, muscovite and dolo-

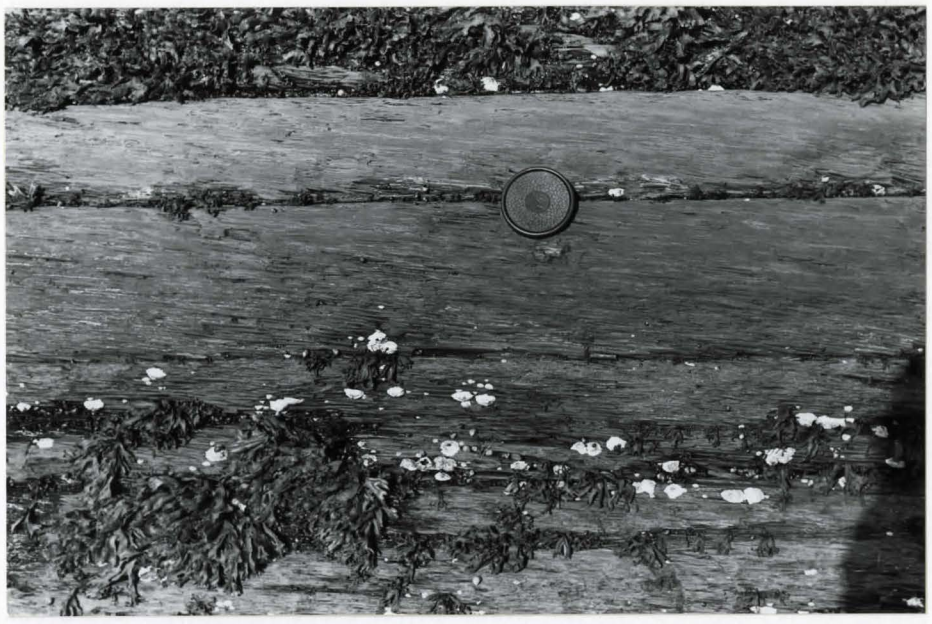

Figure 2.3a: Three beds of Limestone, standing out against less resistant Argillite. Scale: lens cap 6 cm. diameter.

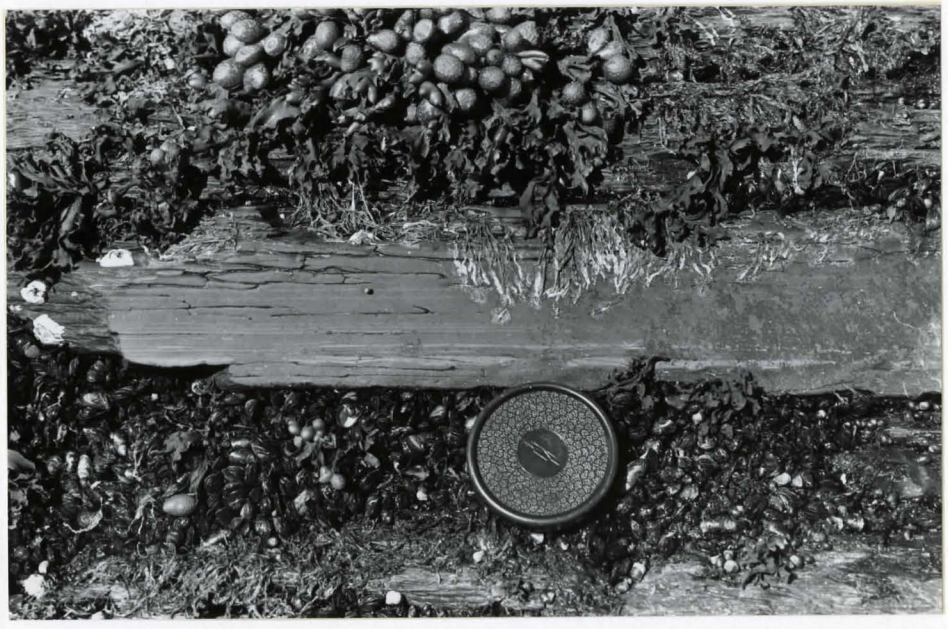

Figure 2.3b: Parallel silty lamination in Dolomite bed. Note small-scale loading of silty laminae into clay. Scale: lens cap 6 cm.

Figure 2.3c: Unusual wavy parallel silty lamination in Dolomite. Scale 20 cm.

Figure 2.3d: Typically parallel-sided Dolomite bed lies to right of 1 m. scale. Top is to left.

mite. Calcite grains were 0.003 to 0.02 mm. in diameter except for a few recrystallised grains 0.06 mm. in diameter. The Limestone is therefore a micrite by the classification of Folk (1959).

Dolomite

Dolomite beds range in thickness from 1 cm. to 52 cm., with a mean thickness of 13.1 cm. Dolomite is black when fresh but weathers to light grey-yellow on seawashed exposures and brown-orange in the roadcut. Fresh Dolomite reacts with dilute HCl only when powdered (1), but weathered material often reacts vigorously (3).

Some Dolomites are quite silty and many have fine parallel lamination, well seen on weathered surfaces (Fig. 2.3b,c), consisting of lighter coloured silt laminae (1-2 mm.) and darker clay laminae (1-5 mm.). Some laminae are wavy and occasional cross-laminated lenses are present. In many beds, laminae are variable in thickness, discontinuous or lensy. Small-scale loading at the silt-clay interface is the cause of this in some cases. Dolomite is well indurated and lacks the fissility of some Argillite; it breaks with a smooth fracture. Bases and tops of most beds are very flat, with occasional wavy or irregular tops. Most base and top surfaces are quite sharp, though some are gradational with Argillite.

Dolomite beds are very uniform in thickness on the outcrop scale (Fig. 2.3d). Enos (1965, p.47) was able to correlate

Dolomite beds in sections up to 6 miles (10 km.) apart. One 12 cm. Dolomite bed has an eroded upper contact with the overlying Greywacke 1 layer. Erosion was sufficient to remove almost the whole Dolomite bed at one point. The smooth nature of the contact suggests that the original mud may have been quite easy to erode. Dolomites are resistant to weathering and stick out as ribs against surrounding Argillite beds. Weathering produces very smooth, flat surfaces on Dolomite in contrast to the ragged appearance of Argillite. Dolomite lenses are rare in this section but common in other parts of the Cloridorme Group.

Enos (1965, p.48) found 93% of two Dolomites sampled was carbonate and 89% of the carbonate is dolomite as determined by X-ray diffraction. The samples also contained 4 and 7% organic matter, 0 and 2% argillaceous matrix and traces of pyrite and quartz. The dolomite grains were in the range 0.002 to 0.02 mm. except for a few recrystallised grains of 0.06 mm. size. The rock is thus a dolomitic micrite of Folk (1959).

Volcanic Ash

Three layers of Volcanic Ash, measuring 0.5 cm., 1.5 cm. and 3 cm. in thickness were observed. Colour is yellow-orange when weathered. Maximum grain size is 0.25 mm. No structures were seen, nor was grading detected. One layer (3 cm.) had a thin Argillite lens halfway through. Base and top surfaces are slightly uneven and sharp. The layers are less resistant to

weathering than Argillite and are thin, so they may easily be overlooked. It therefore seems likely that more layers are present in the section.

Enos (1965, p.51) was able to trace one Volcanic Ash layer over a distance of 1.9 miles (3.0 km.). He described the Volcanic Ash as being about half matrix, composed of nearly equal amounts of muscovite and clay, with small amounts of pyrite and chlorite. The muscovite flakes were 0.1 to 0.5 mm. in diameter, probably as a result of recrystallisation. The smaller clay flakes had properties indicative of montmorillonite. Broken, rounded or euhedral crystals of feldspar (An_{15}) were the only identifiable grains.

Calcisiltite 1

Calcisiltite 1 layers range in thickness from 1 mm. to 35 cm., with a mean of 3.2 cm. Colour is bluish-grey when fresh, weathering to brown-yellow. Reaction with dilute HCl is variable (1-3), though generally good (2).

Grain size of most layers is in the silt to fine sand range (98% of layers), with silt the most common (79%; see Fig. 2.4). Argillite clasts or lenses are extremely rare. Grading was absent in most layers; in any case it would be hard to detect in these thin layers and fine grain sizes.

The most common sequences of sedimentary structures in Calcisiltite 1 layers are cross-lamination only (41%), parallel

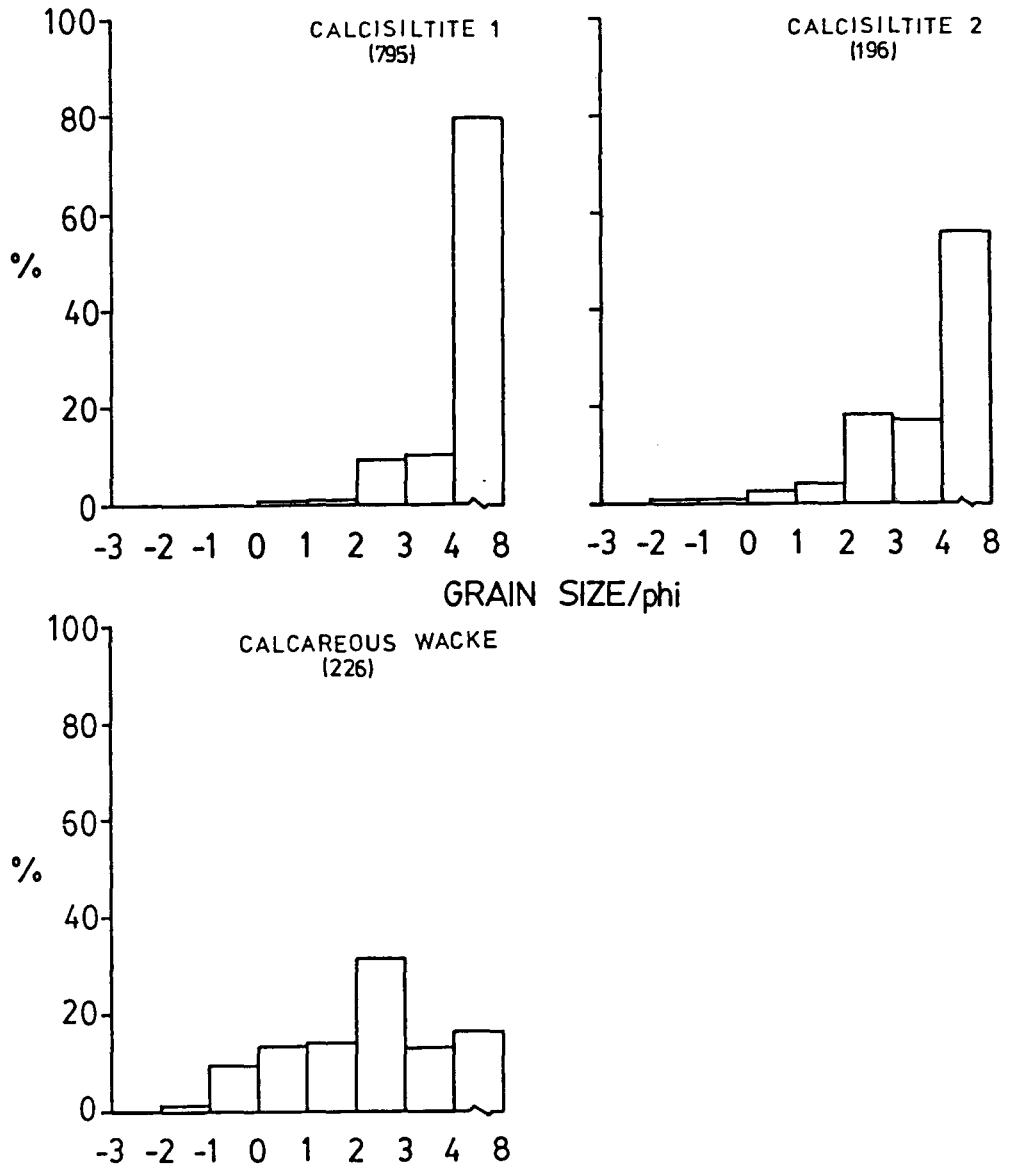

Figure 2.4: Maximum grain size in layers. Phi = $-\log_2 D$, where D is the grain size in millimetres. Percentage shown in each division is the percentage finer than the larger size (lower phi).

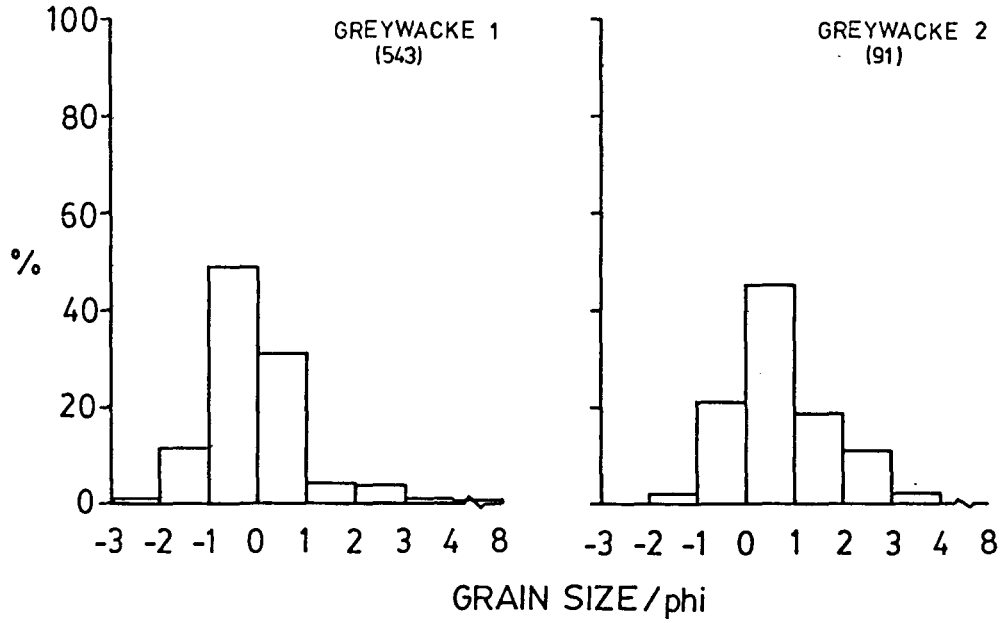

Figure 2.4 (continued)

lamination only (23%), cross-lamination and convolute lamination (10%), and parallel lamination followed by cross-lamination (8%). The sedimentary structure sequence was recorded for just under 60% of Calcisiltite 1 layers. In other layers the structures could not be determined, or were not recorded in order to save time.

Cross-lamination is commonly of climbing ripple-drift type, with stoss side laminae not preserved in most cases (Type A of Jopling and Walker, 1968; erosional-stoss of Ashley et al., 1982). Thin layers may have only a single set of ripples, without climb, and in this case the ripple form can often be seen clearly. Ripple wavelengths are very variable (Fig. 2.5a,b), in the range 25-110 cm. (corrected for obliquity of section to palaeocurrent direction), with amplitudes in the range of 0.5-3 cm. Ripple crests are sinuous in most cases, as seen by the curved intersections of ripple laminae with weathered surfaces (Fig. 2.5c). This feature has been named schrägschictungsbögen by Gürich (1933) and rib and furrow structure by Stokes (1953). In an extreme case, the crest-normal direction of a curved ripple lamina varied between 007° and 089°. Lamination is defined by alternations of light-coloured silt and darker, more clayey material, best seen on weathered surfaces. Laminae are 0.1 mm. to 1 mm. thick, with most of the dark laminae thicker than the light. There is a continuous range of structures from cross-lamination through slightly deformed or oversteepened cross-

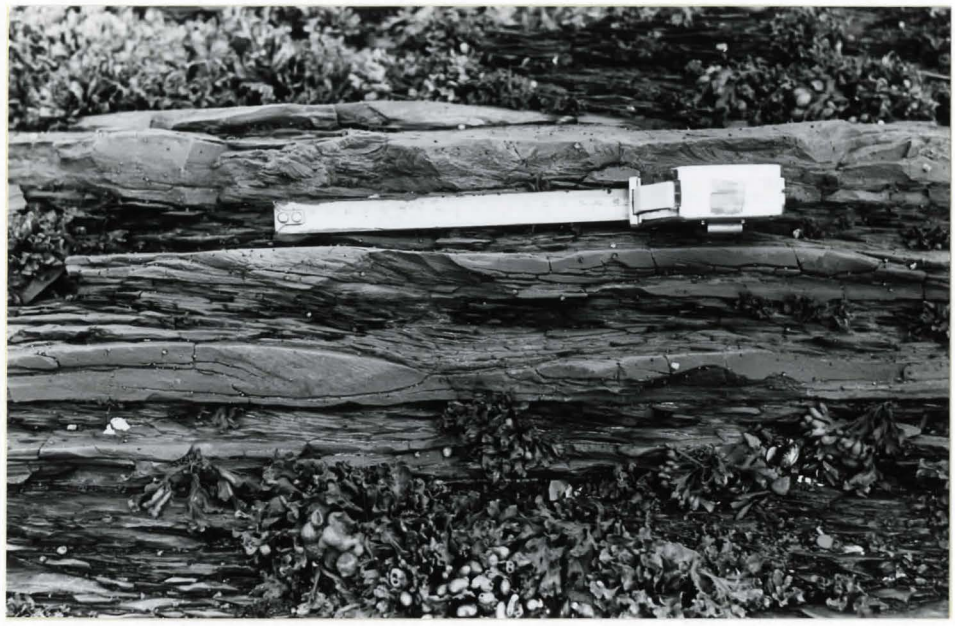

Figure 2.5a: Typical rippled Calcisiltite 1 layers. Scale 20 cm.

Figure 2.5b: Long wavelength (1 m.) ripples on Calcisiltite 1 layer beneath 30 cm. scale.

Figure 2.5c: Rib and furrow structure in Calcisiltite 1 division at the top of a Greywacke 2 layer. Current direction is to left, perpendicular to 30 cm. scale.

Figure 2.5d: Unit of interbedded Calcisiltite 1, Calcisiltite 2, and Argillite (Unit 16, an interpacket unit). Top is to left. Scale 1 m.

lamination to convolute lamination. Parallel lamination is made up of similar laminae to cross-lamination, and is taken to be the T_b division of the Bouma sequence.

Bases of most layers are irregular or uneven and tops are dominantly wavy. Both bases and tops are quite sharp. Flutes or grooves were seen on some soles, but few soles were exposed. Some soles have numerous small hemispherical protrusions, 2-5 mm. in diameter, filled with sand. These were interpreted as fillings of burrows in the underlying mud (Enos, 1965, p.26). Almost all palaeocurrent measurements in Calcisiltite 1 were made from rib and furrow structure, since tops of layers were much better exposed than soles. The top surface of one layer had the trace fossil Chondrites sp. (identified by M.J. Risk, McMaster University, 1981).

Rippled tops and consequent differential loading at the base gives many Calcisiltite 1 layers a lensy appearance (Fig. 2.5b), with marked local thickness variations. Calcisiltite 1 layers in two stratigraphically equivalent sections on the roadcut and wave-cut platform exposures could be correlated on layer thickness over a distance of 110 m. Of 80 such layers, only 2 disappeared downcurrent. Ten new layers appeared in the downcurrent (wave-cut platform) exposure, but this is probably due to the better exposure there. Most layers showed lateral thickness changes, with equal numbers increasing as decreasing. Calcisiltite 1 may occur as the upper part of Calcareous Wacke,

Greywacke 2 or Greywacke 1 layers. Calcisiltite 1 is more resistant to weathering than Argillite, but is less resistant than the other non-lutite facies, with the exception of some Greywacke 2 layers (Fig. 2.5d). Calcisiltite 1 facies is considered gradational with both Calcareous Wacke and Calcisiltite 2 facies. This means that layers exist which are borderline in character between Calcisiltite 1 and one of the other facies.

Enos (1965, p.29) found the carbonate content of Calcisiltite 1 varied between 45 and 82%. Other constituents were quartz, 7 to 30%; feldspar 1.5 to 8%; volcanic rock fragments, 0 to 2%; traces of mica, pyrite and heavy minerals; and argillaceous matrix, largely chlorite with some carbonaceous material. Carbonate grains were dominantly single crystals (0.005 to 0.08 mm.), probably recrystallised from microcrystalline mud particles of about the same size. One sample Enos analyzed consisted of 33% dolomite and 47% calcite; no textural distinction existed between the calcite and dolomite in thin section.

Calcisiltite 2

Calcisiltite 2 layers range in thickness from 1.5 to 83 cm., with a mean of 10.8 cm. Colour when fresh is blue-grey, the same as Calcisiltite 1. When weathered, the colour is brown-orange, or greenish-grey in the more argillaceous parts. Reaction with dilute HCl is variable (1-3), though generally good (2).

Grain size is dominantly in the silt to fine sand range (92% of layers), mostly silt (57%), and grading is not observed. The remainder of layers (8%) have medium or coarser sand at their bases and are normally graded (Fig. 2.4). These include layers with Calcareous Wacke or Greywacke 1 at their bases (Fig. 2.6a). Although most layers appear ungraded in the field (an observation also made by Enos, 1965, p.32), samples collected by Bhattacharjee (1970, p.70) from the base and top of layers in the β_1 and β_7 members suggest that normal grading is present. The mean size of the ten largest grains was recorded, using a binocular microscope, for each sample. Of 50 pairs of samples, 43 were finer at the top than at the base. The grain size differences are small (e.g. 0.05 mm. to 0.04 mm.) so it is understandable that grading is not seen in the field. Clasts of Argillite are absent in Calcisiltite 2.

The most common sequences of sedimentary structures in Calcisiltite 2 are shown in Fig. 2.7a. The next most common sequence is muddy parallel lamination only (2B), 5.1%. Climbing ripple-drift cross-lamination dominates this facies with both stoss and lee sides preserved in the majority of cases (Fig. 2.6a). Ripples commonly climb through the entire layer. An upward trend within a layer of increasing stoss side preservation is seen in several layers, so that the lower part of the layer will have lee sides only preserved (Fig. 2.6b: Type A or erosional-stoss), while the upper part will have complete preservation

Figure 2.6a: Thick Calcisiltite 2 bed in composite Greywacke 1-Calcisiltite 2 layer. Note that parallel lamination occurs both above and below climbing ripple division. Scale 30 cm.

Figure 2.6b: Type A (erosional-stoss) climbing ripples in Calcisiltite 2. Scale: lens cap 6 cm.

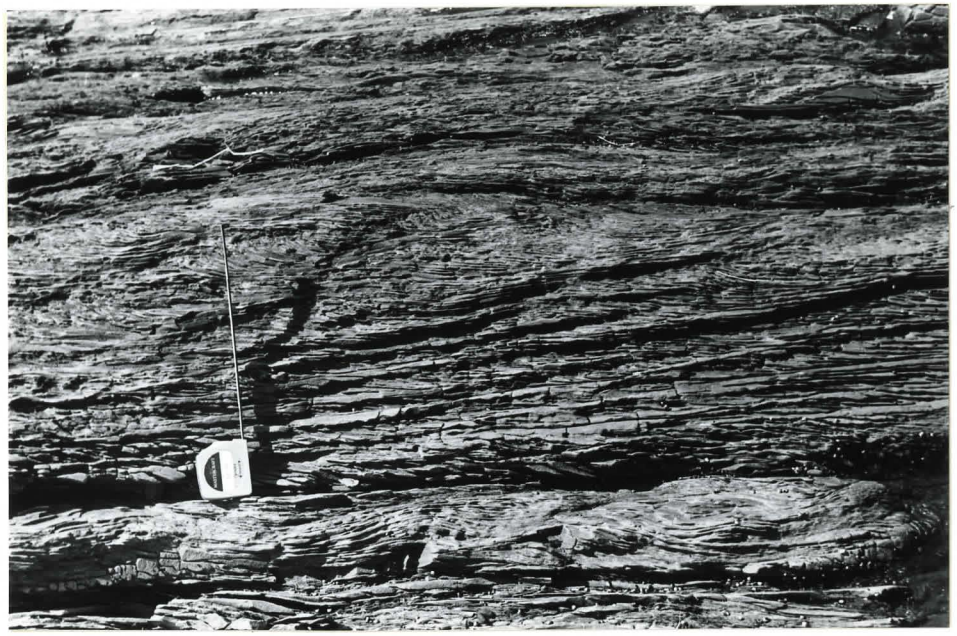

Figure 2.6c: False bedding in Calcisiltite 2. Ripple climb and palaeoflow are to the right. Scale 30 cm.

Figure 2.6d: Group of Calcisiltite 2 layers with broad thinning-upward trend (Unit 3, a Calcisiltite 2 packet). Top is to left. Scale 1 m.

Figure 2.7a-d: Sedimentary structure sequences

Most common sedimentary structure sequences for each of the major non-lutite facies are shown. In each diagram, numbers indicate the vertical sequence of internal divisions according to the following classification: 1-structureless division, 2A-parallel lamination, 2B-muddy parallel lamination, 3-ripple cross-lamination, and 4-convolute lamination. Numbers separated by slashes (/) indicate sedimentary structures with lateral and/or unordered vertical sequence. Percentage figure is the percentage of a facies accounted for by the sedimentary structure sequence. Figures shown represent at least 75% of layers of each facies. Percentage of normally graded layers (% N) for each sequence is also shown. Structure divisions and overlying lutite are shown with their relative thicknesses. Mean thicknesses and standard deviations for the layers, and for the overlying lutite layers, are shown. Grading pattern shown in diagram is stylized and not meant to indicate grading type. Most common types of base and top surfaces are shown. Types are irregular or uneven (e.g. Calcisiltite 2 bases), wavy (e.g. Calcisiltite 2 tops), and flat.

(a) CALCISILTITE 2

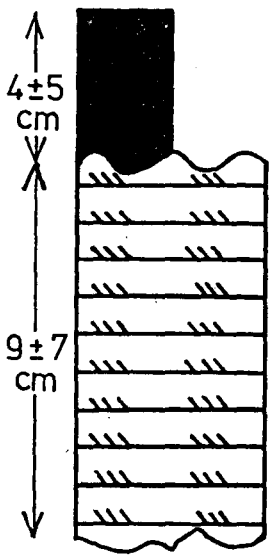

3
57·7%

4%N

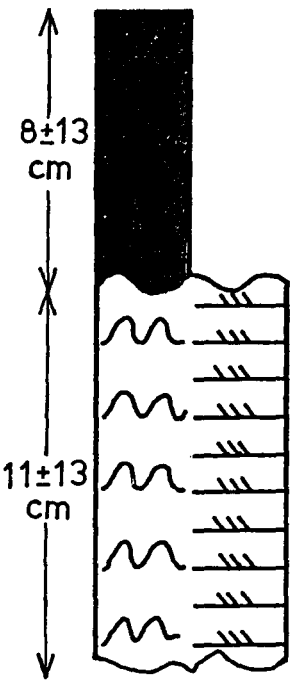

3/4
23·5%

7%N

(b) CALCAREOUS WACKE

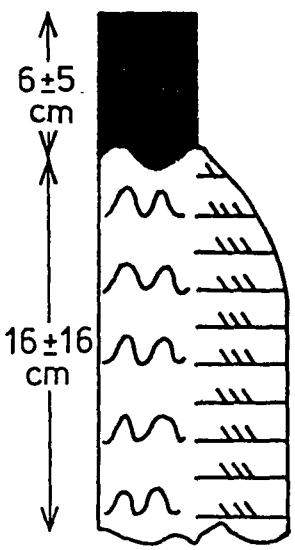

3/4
17·6%

51%N

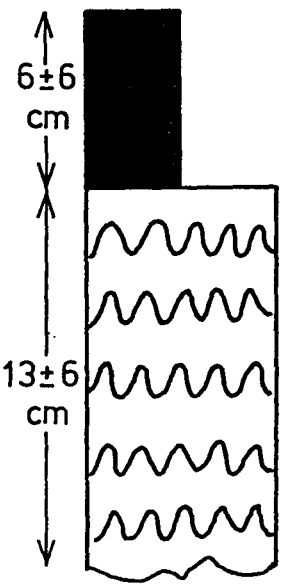

4
14·4%

33%N

(b) CALCAREOUS WACKE (contd.)

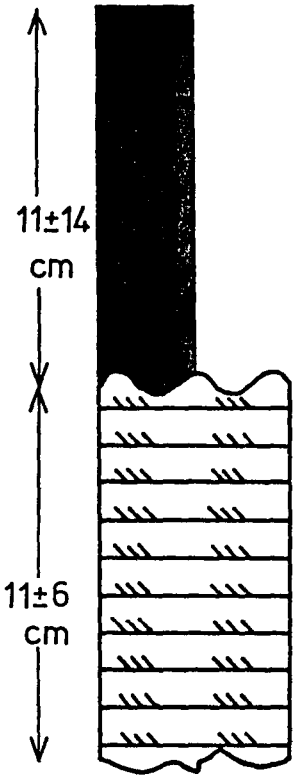

3

12·2%

20%N

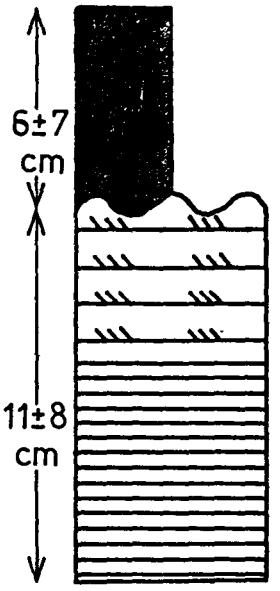

2A3

9·5%

38%N

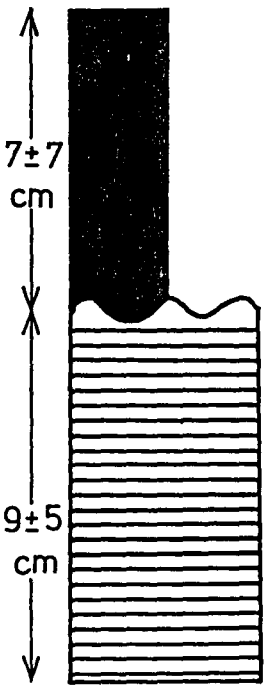

2A

8·6%

31%N

(b) CALCAREOUS WACKE (contd.)

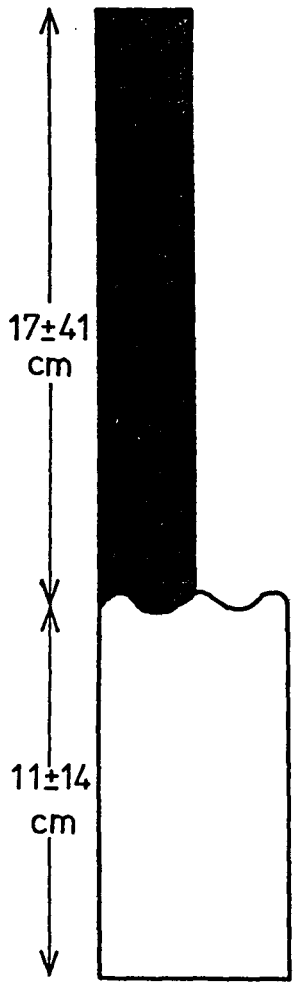

1

8·1%

41%N

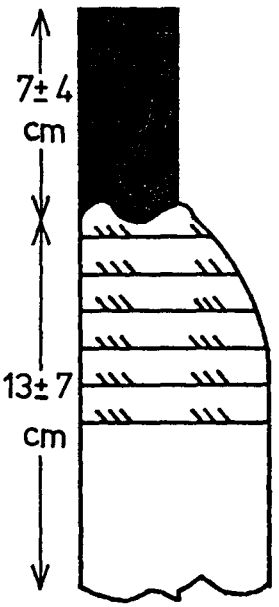

13

6·3%

92%N

(c) GREYWACKE 1

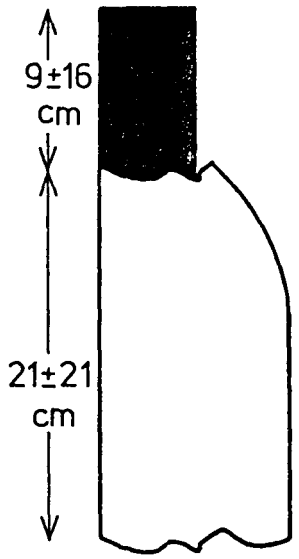

1
60·7%
69%N

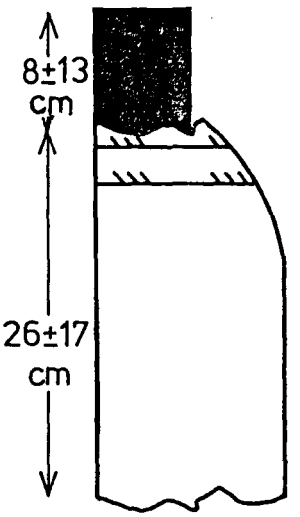

13
16·3%
78%N

(d) GREYWACKE 2

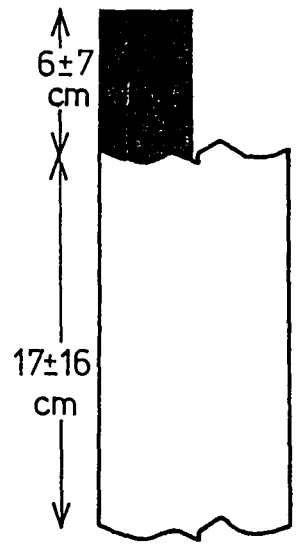

1
74·2%
29%N

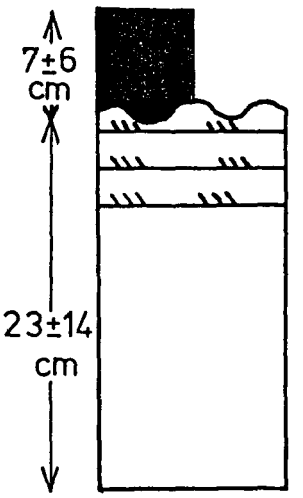

13
8·6%
25%N

(Type B of Allen, 1970; depositional-stoss of Ashley et al., 1982). Accumulation of fine material on lee faces, or occasionally on crests or in troughs, leads to the formation of a dark, less resistant band, dipping upcurrent at the angle of climb (0-27°). This feature is called false bedding (Fig. 2.6c). Angle of climb generally increases upward within a layer, or remains constant. In some layers the angle drops rapidly to zero near the top and passes into parallel lamination. Ripple wavelength is commonly in the 20-40 cm. range, with amplitudes of 1-5 cm. Trends of both increasing-upward amplitude and decreasing-upward amplitude (passing into parallel lamination) were seen. Crest shape is sinuous, as seen in curved rib and furrow structure on tops of beds. Crest-normal directions of 050° and 357° were obtained from one such curved lamina. Cross-laminae may show varying degrees of convolution, and in some cases this grossly exaggerates the ripple form.

Lamination is defined in a similar way to that in Calcisiltite 1. Some laminae are less resistant and weather out, giving a characteristic distinct splitting. Not all laminae weather out in this way so the scale of splitting is coarser than that of the lamination. In the more argillaceous upper parts of layers the lamination becomes a more definite alternation of silt and clay laminae on a 1-5 mm. scale. This type of lamination is the typical form of parallel lamination. Parallel lamination may occur both above and below cross-lamination (Fig. 2.6a). In

either case it is considered to be the T_b division of the Bouma sequence. Lateral transitions from cross-lamination to parallel lamination occur in the γ_4 Formation and are also seen in the β_7 member at Petite Vallée.

Bases of layers may be irregular or flat, with tops dominantly wavy. Basal contacts over Argillite are sharp; tops are fairly distinct unless the top of the layer is very argillaceous (e.g. muddy parallel lamination). Some Calcisiltite 2 layers have lower parts composed of Calcareous Wacke, Greywacke 1 or Greywacke 2. Transitions from Calcareous Wacke are gradational; those from Greywacke 1 are gradational, or separated by a thin (e.g. 2 cm.) argillaceous division; those from Greywacke 2 are sharp.

Palaeocurrent measurements on Calcisiltite 2 were mostly from rib and furrow structure. A few layers with Calcareous Wacke or Greywacke 1 bases had flutes or grooves. In three closely spaced layers which had both sole marks and rib and furrow structure, the current direction obtained from rib and furrow structure was rotated anti-clockwise from sole mark orientation by 40°, 52°, and 13°. Rib and furrow structure on the base of one layer agreed closely with sole marks, suggesting that this rotation of current direction occurred during deposition.

Most Calcisiltite 2 layers are constant in thickness on outcrop scale (Fig. 2.6d). One layer had a Calcareous Wacke

base which thinned and disappeared downcurrent. The total thickness of the layer remained constant, as the loss of the Calcareous Wacke was compensated for by an increase in thickness of Calcisiltite 2. Examples of Greywacke 1-Calcisiltite 2 couplets which passed into Calcisiltite 2 only downcurrent were also observed. One Calcisiltite 2 layer passes rapidly downcurrent into Argillite, with only a thin Calcisiltite 2 base remaining, but further on it reappears with an increased thickness. Enos (1965, p.30) found Calcisiltite 2 was the least persistent laterally of all lithologies, grading into Argillite with very rapid transitions in distances less than a mile (1.6 km.). Calcisiltite 2 is the most resistant to weathering of all facies and sticks out as prominent ribs, with notches eroded along the false bedding and parting. Because the weathering pattern brings out the structures which identify the facies, only one Calcisiltite 2 layer was identified in the fresh roadcut exposure. Calcisiltite 2 layers have almost certainly been recorded as Calcareous Wacke or Calcisiltite 1 there. Calcisiltite 2 facies is gradational with both Calcareous Wacke and Calcisiltite 1 facies.

Enos (1965, p.32) found Calcisiltite 2 had an average matrix content of 18.2%, rather higher than Calcisiltite 1. It also has more mica and less carbonate than Calcisiltite 1, but otherwise is similar in composition.

Calcareous Wacke

Calcareous Wacke layers range in thickness from 1 to 102 cm., with a mean of 12.8 cm. Colour is the same as Calcisiltite 1: bluish-grey when fresh, weathering to brown-yellow. Reaction with dilute HCl is variable (1-3), but generally good (2).

Grain size of Calcareous Wacke varies from silt up to a maximum of 2 mm. (Fig. 2.4). In many cases, the maximum size measured in a layer is only present in a thin division at the base (Fig. 2.8a), or in pockets in the base such as flutes. The median grain size class was coarse sand in the wave-cut platform exposure, but fine sand in the roadcut, perhaps reflecting the inclusion of some Calcisiltite 2 in the latter, as explained previously. However, mean layer thickness for this facies was identical in the two exposures. Rare layers have Argillite clasts up to 20 cm. in length; one layer contains a lens of Calcisiltite 50 cm. long, possibly a clast. Normal grading was observed in 45% of the layers. A few layers are graded throughout, but in most cases grading takes the form of a coarse base followed by fairly uniform fine sand or silt, or of a rapid transition to a finer Calcisiltite near the top. Grading is related to certain sedimentary structure sequences, as seen in Fig. 2.7b. In particular, the sequence 13 (also 13/4) is dominantly graded, while grading is commonly absent in layers with cross-lamination only (3).

Calcareous Wacke has the most variety of sedimentary

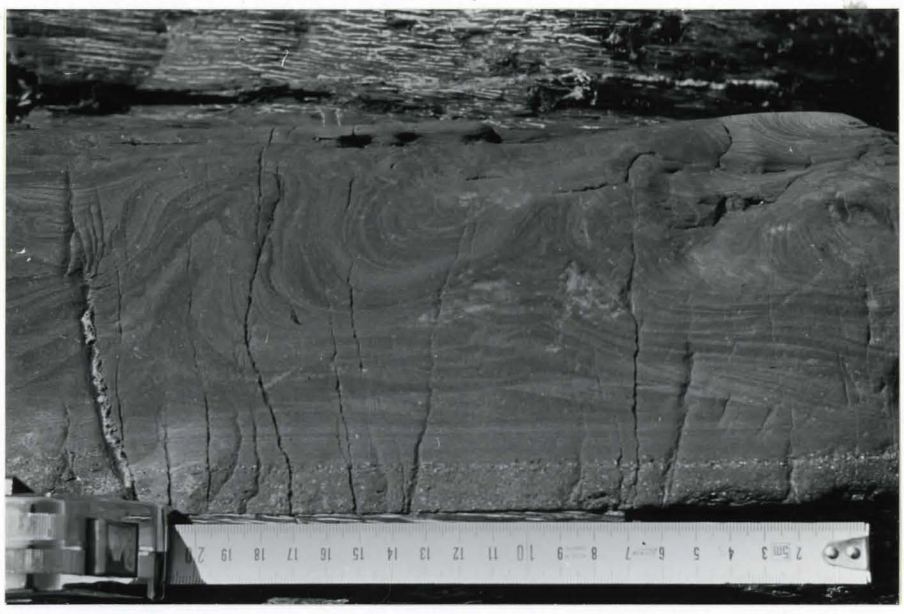

Figure 2.8a: Convolute and cross-laminated Calcareous Wacke layer, γ_4 Formation, west side of Rivière-à-Claude. Scale 20 cm.

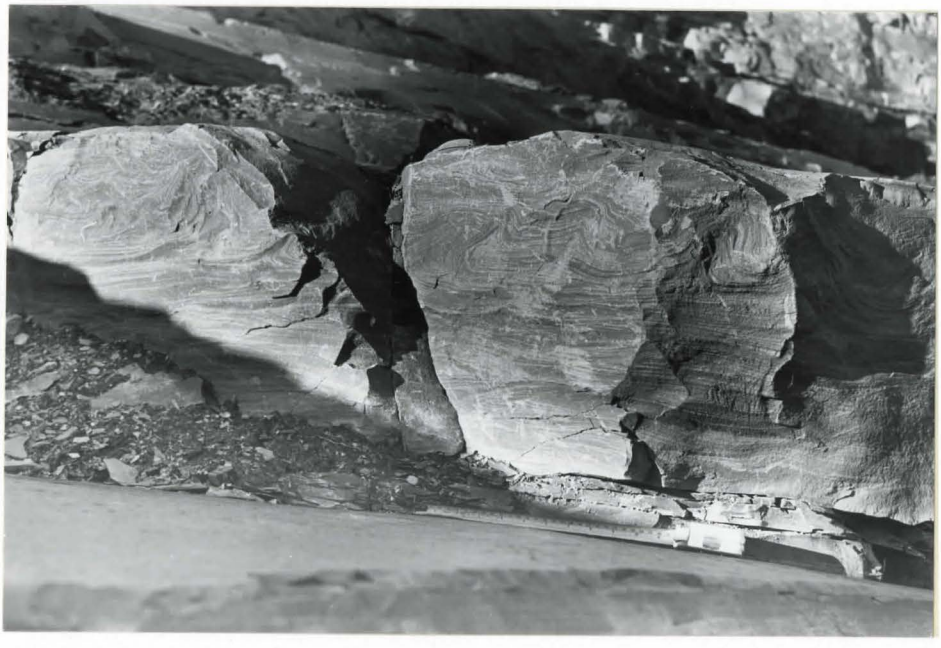

Figure 2.8b: Thick Calcareous Wacke layer showing typical cross-lamination and convolute lamination. Scale 30 cm.

Figure 2.8c: Parallel lamination in coarse-grained Calcareous Wacke. Scale 20 cm.

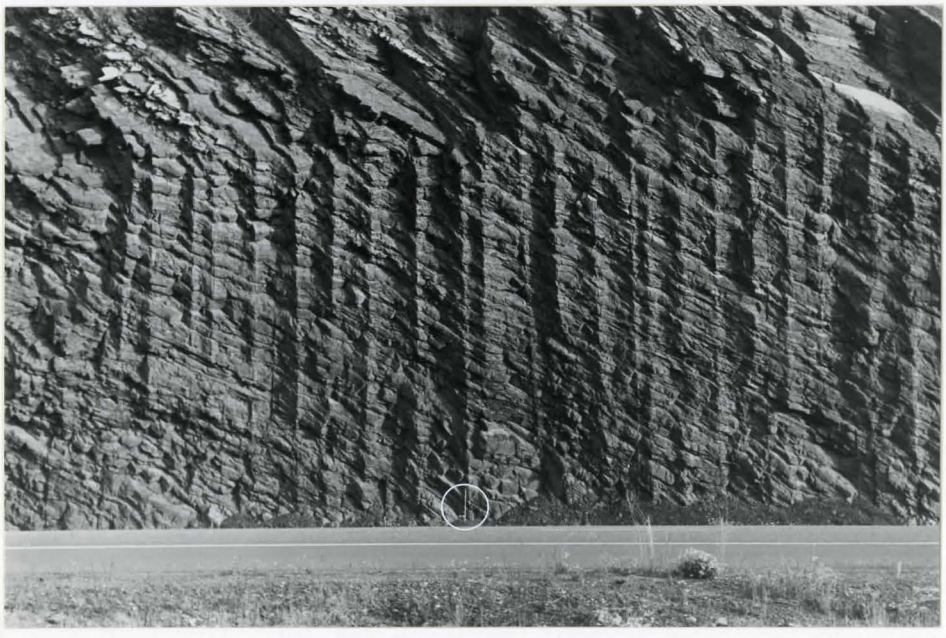

Figure 2.8d: Alternation of Calcareous Wacke and Argillite in roadcut section (Unit 23, a Calcareous Wacke packet). Vertical features are related to blasting; bedding dips to right. Scale 1 m.

structure sequence of all the facies (Fig. 2.7b). Many layers have upper parts of Calcisiltite 1 or 2 facies, with corresponding sedimentary structures. Within the Calcareous Wacke, ripple cross-lamination is commonly multi-set, sometimes climbing at low angles with preservation of lee-side laminae only in most cases (Type A or erosional-stoss). Other layers have only a single set of cross-lamination at the top. Cross-lamination commonly occurs in the fine sand to silt size material which makes up most of the layers, but it may also occur in coarse sand at the base. There is a complete range of structures from undeformed cross-lamination to extremely convoluted lamination (Fig. 2.8a,b). The most common sequence (3/4) has both convolute laminae and some cross-laminae which are essentially undeformed, either laterally or vertically within the layer (Fig. 2.7b). Where the variation is vertical, there is a tendency for the cross-laminae to be undeformed at the base and top of the layer, with convolute lamination in the middle. Convolute lamination sometimes has a regular separation of peaks ("wavelength") along a layer (Fig. 2.8a), and peaks may have a similar shape ("wave-form").

Parallel lamination takes two forms in different size material. The most common type is similar to that of Calcisiltite 1, with parallel to slightly wavy lamination consisting of an alternation of light-coloured silty laminae up to one millimetre thick with dark-coloured, more clayey laminae about one

millimetre thick. This is the usual form of convolute and cross-lamination also. In coarser material, the parallel lamination is very planar and consists of coarse sand laminae 1 to 5 mm. thick alternating with medium or fine sand laminae 3 mm. to 1 cm. thick (Fig. 2.8c).

Bases of layers may be flat, irregular or uneven and are sharp. Tops of most layers are wavy and sharp. Most palaeocurrent measurements were obtained from rib and furrow structure. Sole marks on the few exposed soles were mostly grooves with some flutes. In one layer with both grooves and rib and furrow structure, the direction obtained from the rib and furrow structure at the top of the layer was rotated 81° anti-clockwise from the sole marks, as in the Calcisiltite 2 layers in the same part of the section. Graptolite orientation in one layer agreed well with overall sole mark direction, and with parting lineation and Argillite clast orientation in nearby Greywacke 1 layers.

Most Calcareous Wacke layers show little thickness variation on the outcrop scale (Fig. 2.8d), unless involved in amalgamation with erosion. A few coarse sand layers do show marked lateral variation, with irregular thickness changes such as 20 cm. to 2 cm. over distances of 30 m. or so along strike. Vertical transitions of Calcareous Wacke to Calcisiltite 1 and 2 and lateral transitions to Calcisiltite 2 have already been described. Calcareous Wacke is more resistant to weathering than Calcisiltite 1, but less than Greywacke 1. Calcareous

Wacke facies is gradational with Greywacke 1, Calcisiltite 1 and Calcisiltite 2 facies.

Samples of Calcareous Wacke examined by Enos (1965, Table 1) averaged 31.9% carbonate with 10.6% argillaceous matrix. Major grain constituents, calculated as 100%, were quartz and quartzite (65%), unstable rock fragments (19%) and feldspar (16%). Carbonate size ranged from large sparry calcite crystals at the base of layers to fine single crystals and polycrystalline grains identical to those in the Calcisiltites. According to the classification of Pettijohn (1975, p.211), this rock is a lithic greywacke.

Greywacke 1

Greywacke 1 layers range in thickness from 0.5 cm. up to 240 cm., with a mean of 26.3 cm. (Fig. 2.9a). Amalgamated beds are up to 430 cm. thick (3 layers). Colour is dark grey when fresh, weathering to various grey-green and grey-brown colours. Reaction with dilute HCl is variable, but usually reaction occurs (2), or occurs when powdered(1).

Grain size is usually very coarse sand (49% of layers) or coarse sand (31%) (Fig. 2.4). Maximum size observed was 4 mm. Most Greywacke 1 layers contain clasts of Argillite. They vary in size from small chips of a few millimetres to clasts greater than a metre in length. In some layers, chips of green mudstone are present in addition to dark grey Argillite. Rare layers

Figure 2.9: Greywacke 1 facies

a) Typical Greywacke 1 layers, forming the upper part of a thickening-upward sequence. Scale 50 cm.

b) Composite Greywacke 1-Greywacke 2-Calcisiltite 1 layer. Note lensy form of Calcisiltite at top. Scale: lens cap 6 cm.

c) (next page) Thick set of cross-lamination filling scour in top of Greywacke 1 layer. Scale: lens cap 6 cm.

d) Linguoid ripples on top surface of Greywacke 1. Palaeoflow is to left. Scale 1 m.


A

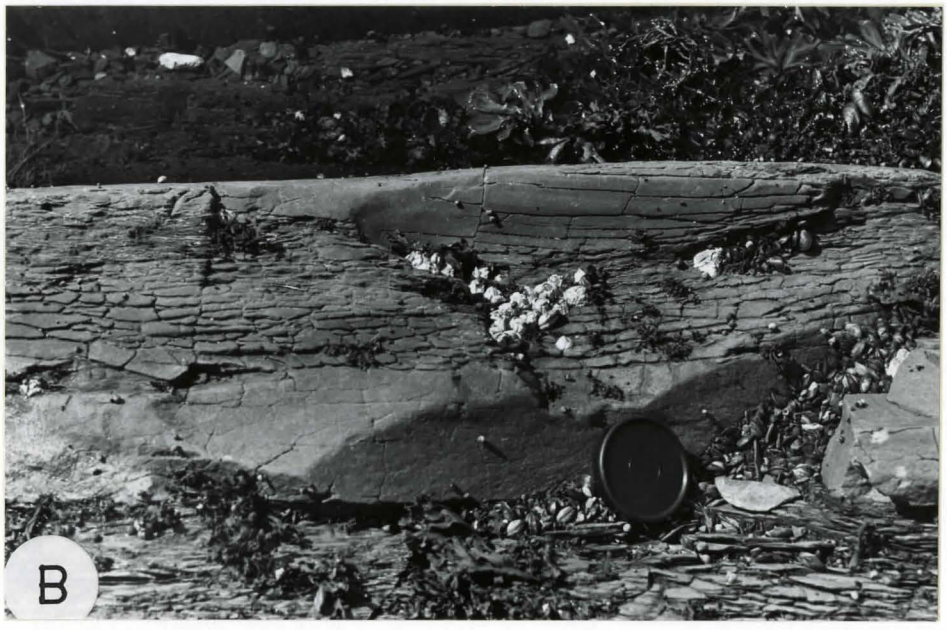
B

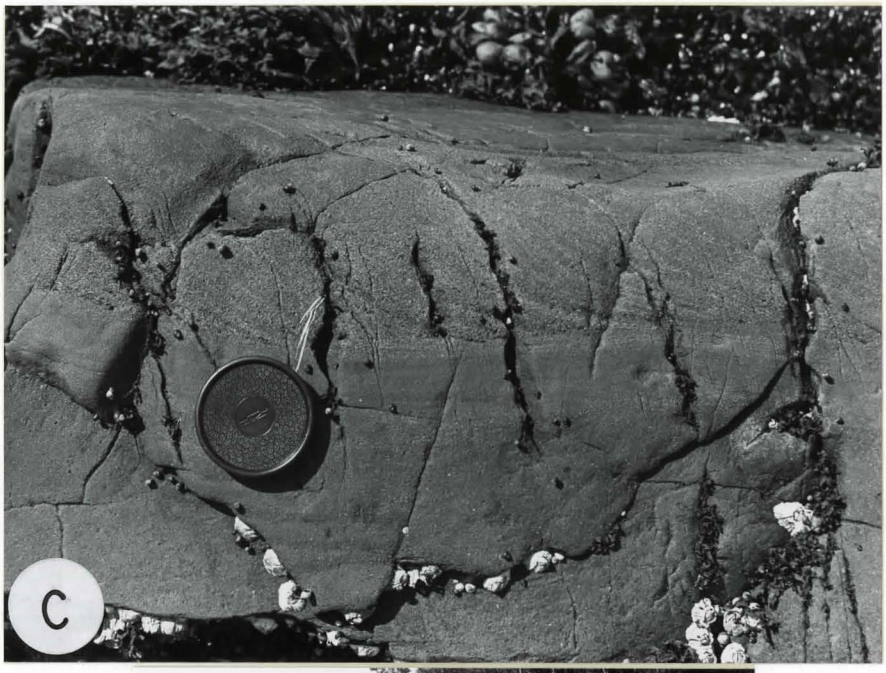
C

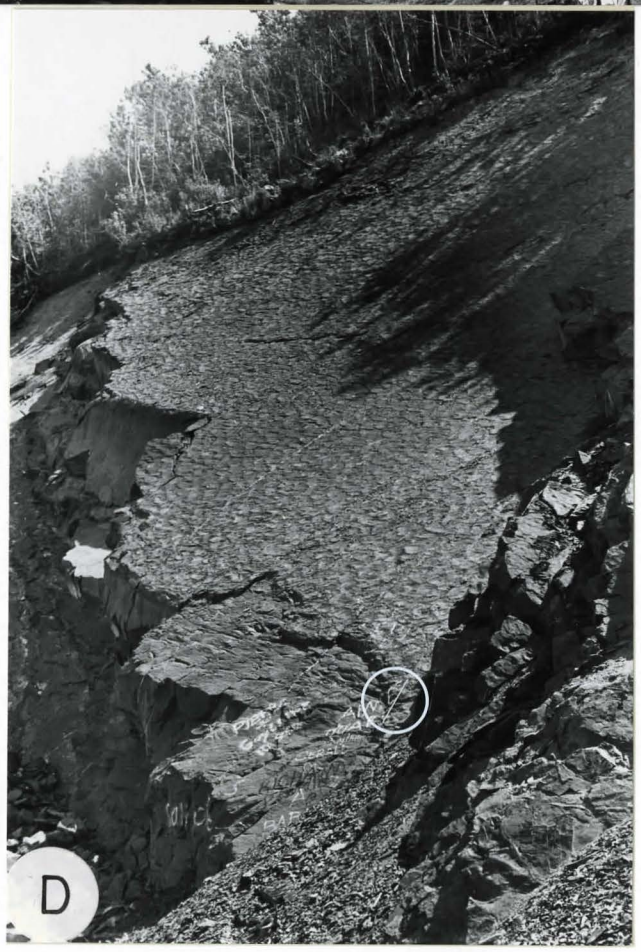
D

have imbricated Argillite chips, with long axes dipping upcurrent. Argillite clasts may occur anywhere in a layer, though the largest ones normally occur near the top of the layer. In some layers they occur as bands. Calcisiltite clasts are present in a few layers and can be up to 1.5 m. in length. Lamination is highly contorted in some of these clasts; in others it is undeformed. Normal grading is present in 71% of Greywacke 1 layers. A total of five layers had inverse to normal or inverse grading. Normal grading may be uniform or with most size change occurring in the transition from a coarse base or to a fine top. Change to a finer Calcisiltite at the top of the layer is common (Fig. 2.9b). Normal grading is generally absent in the lower part of layers 80 cm. or more in thickness. This lower part may be anything from 30% to 100% of the layer thickness. Two of these layers (out of 24) also have inverse grading in the basal 10 to 15 cm.

The structureless division only (1) is the most common sedimentary structure sequence for Greywacke 1 (Fig. 2.7c), followed by the structureless division overlain by cross-lamination (13). The third ranked type has the structureless division followed by parallel lamination (12A) and 79% of these layers are normally graded. These three types account for 85% of Greywacke 1 layers. Lamination may occur within Greywacke 1 material or within Calcisiltite material at the top of the layer. Sedimentary structures in the Calcisiltite tops are identical to those in layers of Calcisiltite facies.

In the Greywacke 1, cross-lamination may take the form of a single set at the top of the layer, or of a thicker multi-set division. Climbing ripples occur in a few layers, climbing at low angle (e.g. 5°), with only lee sides preserved or with lee-side only preservation passing up into complete preservation. Lateral change from multi-set cross-lamination to parallel lamination was seen in one layer. Two normally graded layers in one part of the section had multiple sequences of parallel lamination and cross-lamination with abrupt grain size decreases between some divisions. Ripple laminae are generally fine, one millimetre or less in thickness, and show up as brown-orange laminae in weathered material. Thicker laminae may occur in coarser grain sizes. One unusual layer had a set of cross-lamination up to 14 cm. thick, apparently filling a scour or depression in the layer below (Fig. 2.9c). Maximum grain size was 1.5 mm. and lamination consisted of an alternation of darker, muddier laminae with lighter, cleaner laminae on a scale of several millimetres. Coarse grains were present in both types of lamina. The few top surfaces of rippled layers which were well exposed had linguoid ripple crests (Fig. 2.9d), with extreme variation of crest-normal direction within a set from 354° to 073°. One top had straight-crested ripples with a wavelength of 32 cm., though only one wavelength could be seen. Convolute lamination is present in 6% of layers, and in most cases occurs as a thin division at the top of the layer.

Parallel lamination in the Greywacke 1 takes a variety of forms. The most common type is a fine parallel or sometimes slightly wavy lamination on a 1 to 2 mm. scale, generally occurring as a division only a few centimetres thick at the top of the layer in fine sand to silt size material (Fig. 2.10a). In a few layers these laminae are separated by laminae or bands of Argillite. Most of this fine lamination was put into the T_b division of the Bouma sequence, since it does not have a division of cross-lamination beneath it and it occurs in sand. Fine parallel lamination of silt and clay visible in a few layers was classified as the Bouma T_d division. Coarse parallel lamination or stratification is rare, but is well developed in a few layers (Fig. 2.10b). Coarse bands, typically 1 to 2 cm. thick, alternate with finer, thinner laminae (0.3 to 1 cm.). No evidence of grading within the bands was seen.

Fluid-escape structures (Fig. 2.10c) were observed in 4.2% of Greywacke 1 layers. Such layers have a mean thickness of 51 cm., nearly twice the mean of all Greywacke 1 layers (26 cm.). Structures show up as lighter coloured pillars or patches, suggesting that dark, fine material has been removed from them. They are commonly 1mm. to 1 cm. wide and a few centimetres long as seen in two dimensions. Maximum length observed was 60 cm. They may be irregular, vertical or inclined (usually dipping upcurrent), and are more abundant in the upper parts of layers. Structures occur only in the T_a division of the Bouma sequence,

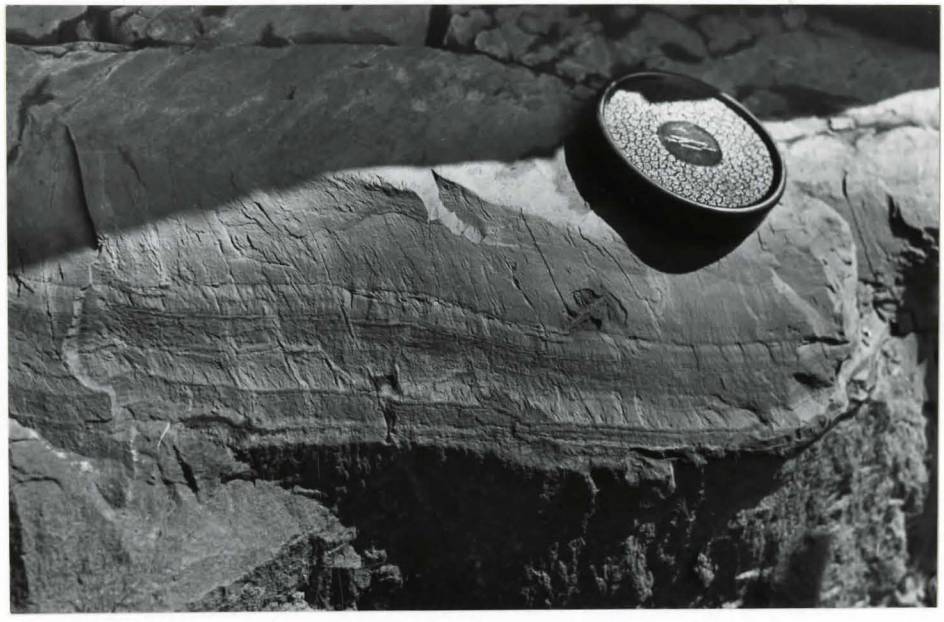

Figure 2.10a: Fine parallel lamination at top of Greywacke 1 layer. Scale: lens cap 6 cm.

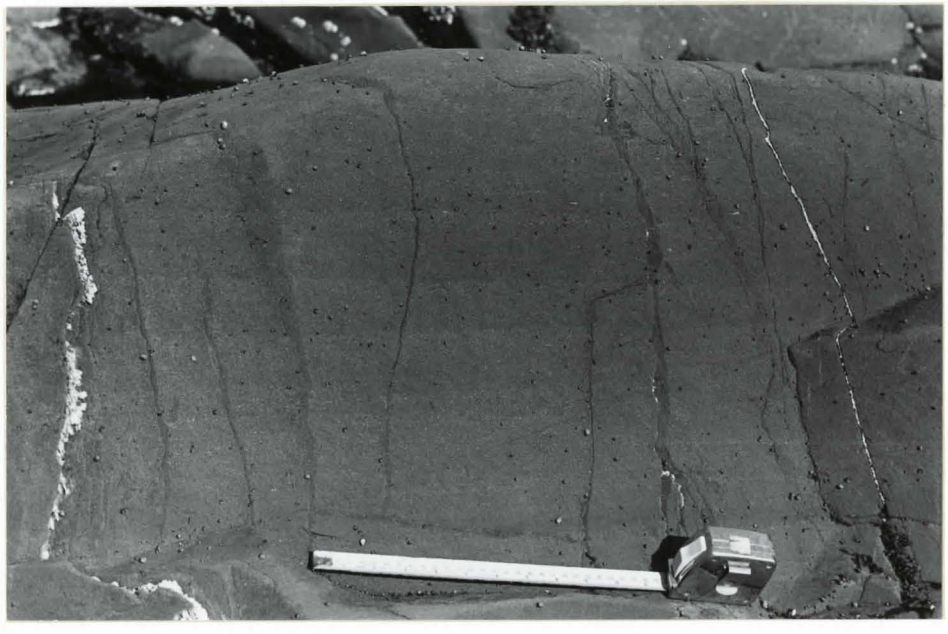

Figure 2.10b: Parallel stratification in thick Greywacke 1 layer. Scale 30 cm.

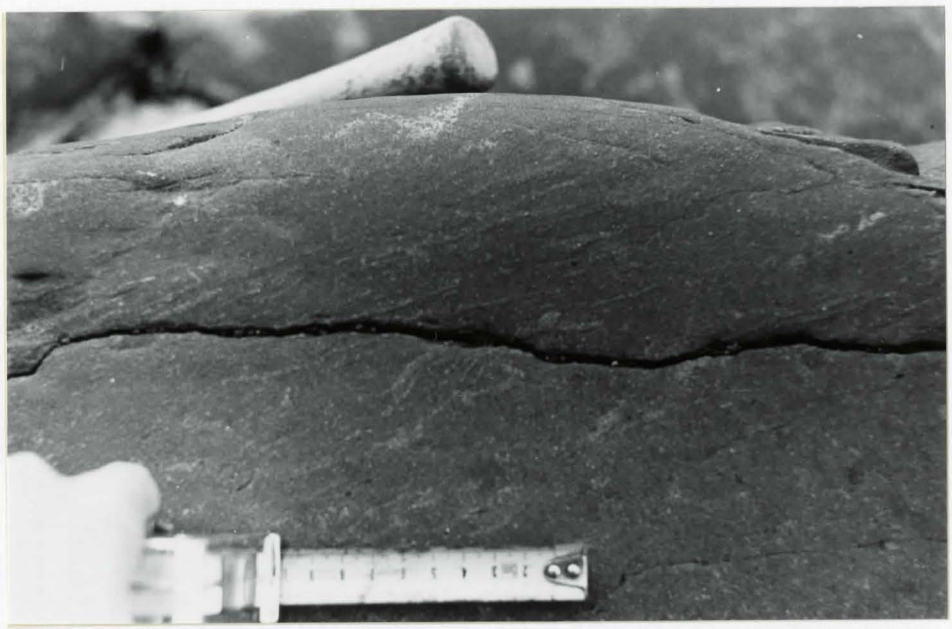

Figure 2.10c: Fluid-escape structures in Greywacke 1 at low angle to bedding, which is horizontal in this view. Scale: 10 cm.

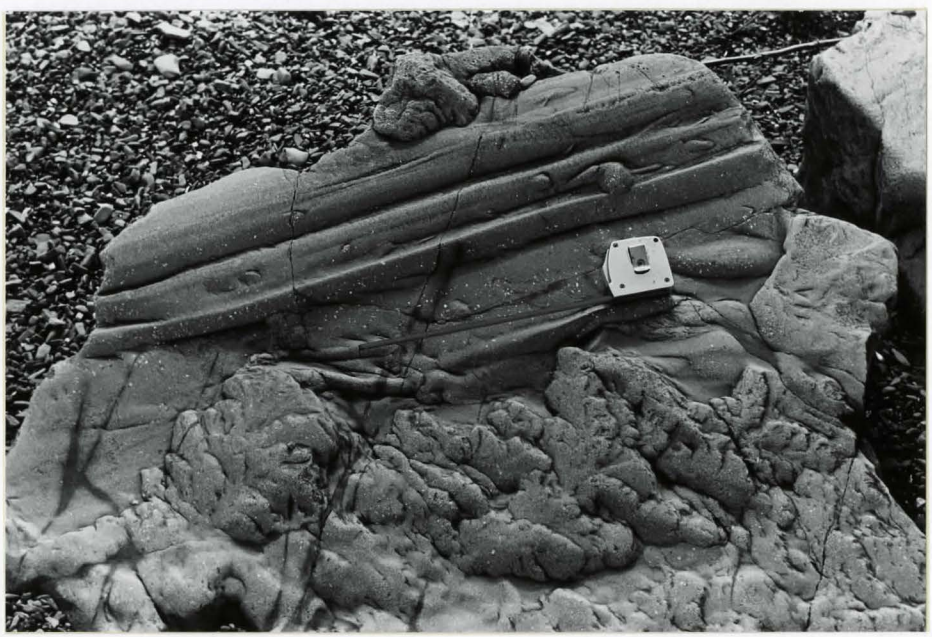

Figure 2.10d: Grooves and load casts (bottom of photo) on sole of Greywacke 1 block. Scale 30 cm.

with the exception of one layer where they continued into the lower part of the T_b division. They are not restricted to layers with any particular sedimentary structure sequence, however. They correspond to Type B pillars of Lowe (1975), except for one possible example of Type D stress pillars (also called sheet structures by Laird, 1970). Fluid-escape structures do not cross layer boundaries; in one case, structures were truncated upwards at an amalgamation surface.

Basal contacts of Greywacke 1 layers with lutite are irregular or uneven (including loaded) in the majority of cases (63%) and are very sharp. Tops may be irregular or uneven (39%), flat (39%) or wavy (17%) and most are quite distinct. Amalgamated contacts with other Greywacke 1 layers or other non-lutite facies are dominantly irregular or uneven (79% of bases and 69% of tops). Amalgamation surfaces are not always easy to see. They may be observed because of one or more of the following: colour change, grain size change, the presence of a thin lens or wisp of Argillite, and splitting of the bed by an Argillite layer laterally.

Palaeocurrent indicators in Greywacke 1 layers were rib and furrow structure, grooves, flutes, parting lineation and Argillite clast orientation. Rib and furrow structure may occur in the Greywacke 1 or in a Calcisiltite 1 or 2 division forming the upper part of the depositional unit. Of the sole marks, grooves are the most common. One sole had flutes, with grooves

cutting the flutes obliquely. Soles may also have load casts, which will obliterate oriented sole marks (Fig. 2.10d). Palaeocurrent measurements from grooves, flutes, parting lineation and Argillite clast orientation agree closely in the same part of the section. Rib and furrow structure tends to be rotated anticlockwise from sole marks in neighbouring layers. Two layers with both sole marks and rib and furrow structure did not show a consistent rotation, however.

The majority of Greywacke 1 layers show lateral thickness changes on the outcrop scale, as a result of erosional bases, eroded tops, irregular (depositional?) top surfaces, or loading. Erosional scours at the base range in size from centimetre-scale irregularities to shallow channeling of 60 cm. depth. Greywacke 1 layers may have upper parts similar to Greywacke 2, as well as Calcisiltite tops (Fig. 2.9b). Downcurrent transitions to Greywacke 2 and Calcisiltite 2 also occur. One layer thinned markedly downcurrent and its upper part was replaced by thin layers of Calcisiltite 1 and Greywacke 1 interbedded with Argillite.

A few examples of clastic injection structures (Morris, 1971) were seen. Rare thin dykes (e.g. 1 cm.) lead upwards into Argillite from Greywacke 1 layers, and may extend as far as the next Greywacke 1 layer (e.g. 30 cm.). At least two sills were seen. One was seen to transgress through an Argillite-dominated unit about one metre thick and then continue conformably above it. The second terminated abruptly in the downcurrent direction,

thinning from 79 cm. to zero over a distance of 1 to 2 m. (Fig. 4.4c). It had fluid-escape pillars in its upper part; flat, sharp basal and upper contacts; and was ungraded very coarse sand. Other sills may have been present, but without rapid terminations, transgression, or presence of feeder dykes, they would not be distinguished from depositional Greywacke 1 layers.

Fossils found in Greywacke 1 layers were graptolites, brachiopod and coral fragments, and crinoid ossicles. Greywacke 1 layers are relatively resistant to weathering, second only to Calcisiltite 2. Greywacke 1 facies is gradational with both Greywacke 2 and Calcareous Wacke.

Enos (1965, p.40 and Table 1) studied 12 samples of Greywacke 1 which contained an average 16.7% fine-grained carbonate and 17.2% argillaceous matrix. Some proportion of the clay matrix was diagenetic in origin, as shown by ghosts of grain outlines or twinning. Coarse detrital grains, calculated as 100%, consisted of quartz, 60%; rock fragments, 25%; feldspar (almost all plagioclase), 10%; mica, 2%; and small amounts of fragmented fossils, authigenic pyrite, and detrital heavy minerals including chromite. The rock may be classified as a lithic greywacke of Pettijohn (1975, p.211).

Greywacke 2

Greywacke 2 layers range in thickness from 1.5 cm. to 105 cm., with a mean of 19.2 cm. Colour is dark grey, both fresh

and weathered. Reaction with dilute HCl is variable (1-3), though generally good (2).

Grain size is commonly coarse sand (45% of layers), very coarse sand (21%), or medium sand (19%). Maximum size observed was 3 mm. The grain size is therefore a little finer than that of Greywacke 1. Many layers contain clasts of Argillite or Calcisiltite. Argillite clasts range in size from small chips up to a maximum of 160 cm. by 10 cm. Calcisiltite clasts are commonly in the 20 to 50 cm. size range, with a maximum of 75 cm. Many of them have deformed lamination (Fig. 2.11a). Both types of clast may occur throughout the layer, though they are more common and more abundant at the top. In some cases, the increase in proportion of clasts upwards in a layer culminates in a coherent division of Calcisiltite or Argillite at the top. Clasts of Calcareous Wacke and Greywacke 1 were much less common. The largest clast observed was a 4.5 m. by 30 cm. piece of bedded material consisting of Argillite, Calcisiltite and Calcareous Wacke (Fig. 2.11b). Boundaries between clasts and matrix may be vague, particularly with Argillite, suggesting some mixing has occurred. Grading of the maximum size is absent in most Greywacke 2 layers (62%). However, many layers become more argillaceous upwards, with decreasing numbers of coarse grains (content grading of McBride, 1962).

The structureless division only is the most important sedimentary structure sequence (Fig. 2.7d). Most other sequences

Figure 2.11: Greywacke 2 facies

a) Contorted clasts of Calcisiltite in Greywacke 2 layer. Scale 30 cm.

b) Large (4.5 m x 30 cm.) clast of bedded Calcisiltite, Calcareous Wacke and Argillite within a thick (105 cm.) Greywacke 2 layer. Clast is in centre of photo with Greywacke 2 material above (left) and below. Scale: hammer handle 40 cm.

c) (next page) Typical Greywacke 2 layer. Layer is slightly more resistant to erosion than underlying Argillite at bottom of photo. Scale 30 cm.

d) Thick Greywacke 2 layer within thin-bedded unit of Calcisiltite 1 and Argillite (interpacket unit - Unit 12). Scale 1m.


A

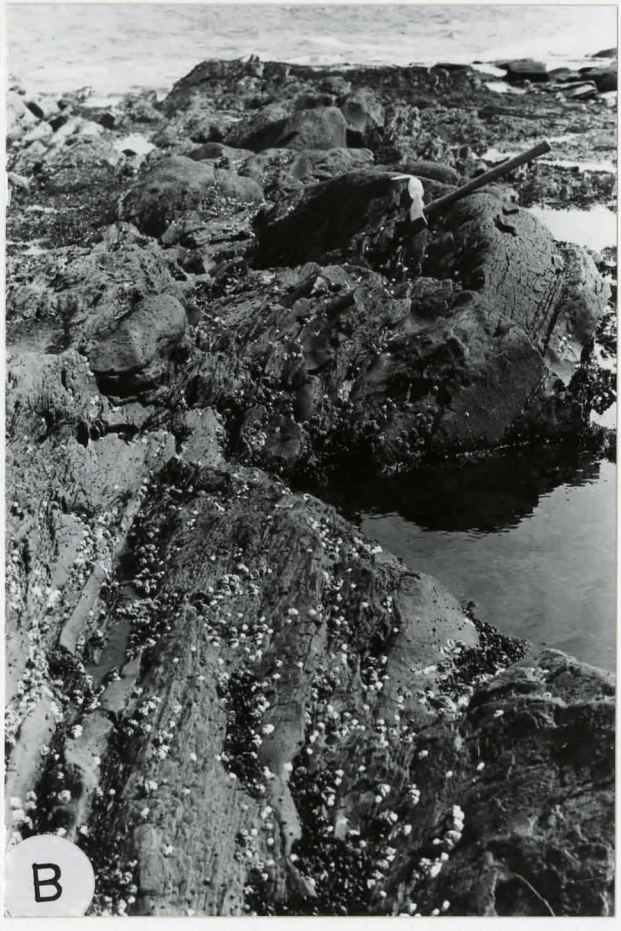
B

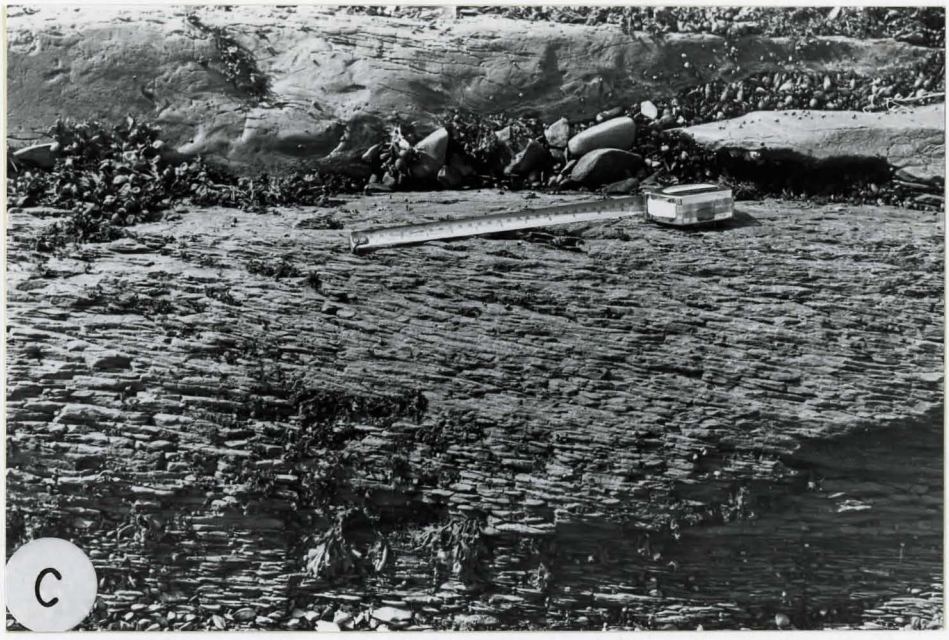
C


D

result from layers having an upper part of Calcisiltite 1 or 2, with typical sedimentary structures, considered to have been deposited along with the Greywacke 2. The exceptions to this are three layers which appear to have cross-lamination in Greywacke 2 material, and one layer with muddy parallel to wavy lamination. Bases and tops of layers are mostly irregular or uneven, though cross-laminated Calcisiltite tops are wavy and parallel laminated ones flat. Bases are sharp and most tops are fairly distinct. Even though the top of a Greywacke 2 layer may be very argillaceous, the boundary between material having coarse grains and that without (Argillite) is clear. Soles of Greywacke 2 layers were never exposed, since Greywacke 2 is not much more resistant to weathering than Argillite and appears as relatively recessive layers (Fig. 2.11c,d). Palaeocurrent direction was measured from rib and furrow structure in Greywacke 2 or Calcisiltite 1 or 2 in a few layers. Layers commonly show lateral thickness variations, but only rarely pass into Argillite on outcrop scale (Fig. 2.2). Greywacke 2 facies is gradational with Greywacke 1 facies.

Enos (1965, p.42 and Table 1) found 5 samples of Greywacke 2 averaged 48.4% argillaceous matrix with 7.6% fine-grained carbonate, a much higher matrix content than Greywacke 1. The mineralogy of the coarse detrital grains differed little from Greywacke 1. The main constituents were quartz, 62%; rock fragments, 20%; and feldspar (largely plagioclase), 13%. This composition is a lithic greywacke of Pettijohn (1975, p.211).

CHAPTER 3

FACIES INTERPRETATION 1: DEPOSITIONAL MECHANICS

Greywacke 1

Grading and fabric

Evidence for turbidity current deposition of most Cloridorme facies has already been discussed (p.1). In Greywacke 1 facies, grading appears to be distribution grading in most cases, suggesting deposition from low-concentration turbidity currents (Middleton and Hampton, 1973). Thicker layers which are partly ungraded were probably deposited from high-concentration turbidity currents. Rare inverse grading may indicate movement as a grain flow just before final deposition. Type B fluid-escape pillars are formed at high rates of fluid escape (Lowe, 1975). High rates of fluid escape may be a consequence of trapping of water as a result of rapid deposition from a high-concentration turbidity current.

Grain fabric and grading data from the β_7 member of the Cloridorme Formation are consistent with deposition from low-concentration turbidity currents (Parkash and Middleton, 1970),

though these authors suggest formation of a quick bed to produce the structureless division. In experimental studies, quick bed formation is characteristic of deposition from high-concentration turbidity currents (Middleton, 1967). Upcurrent angles of grain imbrication are generally less than 20° (Parkash and Middleton, 1970) and so do not fall within the 20°-35° range characteristic of grain flow deposits (Taira, 1976).

This evidence suggests that Greywacke 1 layers were deposited from turbidity currents of various concentrations. Working with this hypothesis, an attempt will be made to get some quantitative ideas on conditions of deposition.

Turbidity current modelling

1) Theory

Settling velocity of single spherical quartz grains in still water (w_o) may be obtained from standard graphs (e.g. Blatt et al., 1980, p.65). In a concentrated dispersion, hindered settling occurs and true settling velocity (w) is related to w_o and to the volume concentration C by the following expression (Richardson and Zaki, 1954)

$$w/w_o = (1 - C)^n \qquad (3.1)$$

where n has the value 2.4 for values of the Reynolds number $Re'_o = w_o D/\nu$ greater than 500. D is the grain diameter and ν the kinematic viscosity. For $1 < Re'_o < 500$,

$$n = 4.4(Re'_o)^{-0.1} \text{ for wide flows.} \qquad (3.2)$$

The effective viscosity in the presence of suspended sediment is related to the clear water viscosity and C (Roscoe, 1953).

$$\nu_e = \frac{(\nu\rho)\text{water}}{\rho}(1-1.35C)^{-2.5} \qquad (3.3)$$

A limiting criterion for turbulent suspension is that shear velocity $u_* = w$ (Middleton and Southard, 1977, p.6.27). For flows with a considerable amount of sediment in suspension, $\overline{U}$, the vertically averaged mean velocity, is related to u_* by the following expression (Einstein and Chien, 1955, p.33)

$$\frac{\overline{U}}{u_*} = 17.66 + \frac{1}{\kappa}\ln\left(\frac{d}{96.5k_s}\right) \qquad (3.4)$$

where κ is von Karmann's constant, d is the depth of flow and k_s is the equivalent sand roughness of the bed. For a turbidity current, the equation only applies up to the depth of the velocity maximum in the flow (Hiscott and Middleton, 1979).

The densiometric Froude number (Fr) is given by

$$Fr = \frac{\overline{U}}{\sqrt{\frac{\Delta\rho}{\rho} gd}} \qquad (3.5)$$

where ρ is the density of the flow and $\Delta\rho$ the density difference between the flow and the overlying water (Middleton and Southard, 1977, p.8.9). A Froude number of 1 defines the boundary between supercritical (Fr > 1) and subcritical flow (Fr < 1). Slope may be calculated from shear velocity (Hiscott and Middleton, 1979).

$$S = \frac{u_*^2\rho}{gd\ \Delta\rho} \qquad (3.6)$$

2) Application

Estimation of settling velocity and viscosity requires knowledge of water temperature. This is taken as 10°C, because the

palaeolatitude of the area was 15°S (Bambach et al., 1980). The Caradoc corresponds to a polytaxic phase of Fischer and Arthur (1977), marked by lack of polar ice-caps and therefore lowered temperature contrast between ocean surface and bottom waters (Leggett et al., 1981). The viscosity of water at 10°C is 0.01307 poise (C.G.S. units are used here to aid comparison with other workers' results). Effective viscosity is 0.01471 poise for a flow density of 1.1 g cm^{-3} and 0.02033 poise for 1.3 g cm^{-3} (see below).

Densities of natural sandy turbidity currents probably range from 1.05 g cm^{-3} to 1.3 g cm^{-3} (Komar, 1977) and values of 1.1 and 1.3 are used in calculations for Table 3.1. Absence of significant channeling in the Cloridorme Group (P. Enos, pers. comm., 1981; and this study) suggests that flows were more or less unconfined. On leaving channel mouths flows would spread out and become thinner. This might be partly counterbalanced if flows went through a hydraulic jump on leaving the channel, leading to thickening of the flow and velocity reduction. Flow thicknesses (d) used are 2.5 m. and 10 m. An inferred distributary channel in the γ_4 Formation has a depth of at least 10 m. (Chapter 4). For Froude numbers close to 1 expected for turbidity currents, the velocity maximum will occur at a depth of approximately 0.67 d above the bed (Middleton, 1966). A multiplier of 0.67 was therefore inserted in Equation 3.4.

Estimation of the equivalent sand roughness, k_s, used in Equation 3.4

is difficult. In Einstein and Chien's (1955) experiments, a layer of sand was glued to the bottom of the flume, and flow conditions were arranged so that no significant deposition occurred on the bed. With this arrangement, k_s is equal to some measure of the grain size of the sand used. Einstein and Chien (1955, p.28) found this value was somewhat larger than D_{65} (65 weight percent of the sediment is finer than D_{65}). For flow over a movable bed, as in the case of a turbidity current, k_s will be some multiple of the maximum grain size. Van Rijn (1982) showed that there is a large variation in the value of k_s/D_{90} for plane bed conditions, and suggested an average value of $3D_{90}$ for k_s. The bedform beneath a Greywacke 1 turbidity current at the start of deposition would most likely be antidunes or plane bed. Flow resistance is similar for antidunes (without breaking waves) and plane bed in flume experiments (Simons et al., 1965). Flow resistance is higher in the case of antidunes with breaking waves. Fortunately, the mean velocity ($\bar{U}$) is not very sensitive to changes in k_s because k_s occurs within a logarithmic expression in Equation 3.4. The value $k_s = 3D_{90}$ is therefore used as the best approximation available. D_{90} is probably close to the maximum size (D) measured in the field.

Von Karmann's constant, κ, is reduced by the presence of suspended sediment. Einstein and Chien (1955, Fig. 15) present data in which κ varies from 0.17 up to 0.4 for river and flume studies. Use of their graph requires knowledge of the grain

Table 3.1 Turbidity current modelling

ρ (g cm^{-3})	d(m)	u_* (cm s^{-1})	$\bar{U}$ (cm s^{-1})	Fr	S	Re	f_o
2 mm. grains		w_o=27.1 cm s^{-1}					
	2.5		511	3.42	0.0244		0.0167
1.1		23.3				951	
	10		640	2.14	0.0061*		0.0106
	2.5		366	1.54	0.0049*		0.0167
1.3		16.7				493	
	10		459	0.96	0.0012		0.0106
1 mm. grains		w_o=14.4 cm s^{-1}					
	2.5		299	2.00	0.0066*		0.0131
1.1		12.1				247	
	10		367	1.23	0.0016*		0.0088
	2.5		205	0.86	0.0012		0.0131
1.3		8.3				122	
	10		251	0.53	0.0003		0.0088
0.5 mm. grains		w_o=6.7 cm s^{-1}					
	2.5		151	1.01	0.00135*		0.0106
1.1		5.49				56.0	
	10		181	0.61	0.00034		0.0074
	2.5		97	0.41	0.00022		0.0106
1.3		3.54				26.1	
	10		117	0.25	0.00006		0.0074

*Slopes comparable with outer parts of modern submarine fans

size distribution within the flow, which is not known for Cloridorme turbidity currents. A value of 0.25 for κ is used, following Hiscott and Middleton (1979). Results are presented in Table 3.1 for suspension of 2 mm., 1 mm., and 0.5 mm. quartz grains. These sizes cover the range of maximum size for most Greywacke 1 layers (Fig. 2.4).

3) Discussion of results

One noteworthy feature of the results is the low values of the Reynolds number ($Re = u_* k_s / \nu_e$) for suspension of 0.5 mm. grains. Einstein and Chien (1955) do not indicate for what range of Reynolds number Equation 3.4 is valid, but their experiments were carried out with high velocity, supercritical flows. The equivalent clear-water flow equation (Yalin, 1972, p.35) is strictly only valid for rough turbulent conditions ($Re \geq 70$). For values of Reynolds number between 5 and 70, there is only a small error when $\overline{U}$ is many times u_*, as it is in this case. If Equation 3.4 follows a similar relation with Reynolds number, then errors are probably small.

In Chapter 4 it is suggested that the depositional environment of the γ_4 Formation was on the outer part of a submarine fan. Slopes on the outer parts of modern submarine fans commonly fall in the range 0.002 to 0.006 (e.g. Nelson et al., 1970; Nelson and Kulm, 1973; Bouma and Treadwell, 1975; Wilde et al., 1978). If slopes during Cloridorme deposition were similar, choice of possible turbidity currents in Table 3.1 is

limited to those marked with an asterisk. All of these have a Froude number greater than one and so are supercritical. Since some Greywacke 1 layers have cross-lamination or parallel lamination in their upper parts, suggesting deposition from subcritical flow, this result requires some explanation. Transition from supercritical to subcritical flow takes place by means of a hydraulic jump, an abrupt thickening and slowing of the flow, accompanied by a density reduction (Komar, 1971). Either a hydraulic jump must have migrated upstream over the bed before deposition of the parallel and cross-lamination, or else parameters calculated in Table 3.1 do not represent conditions at the start of deposition, and deposition took place entirely from a subcritical flow.

Properties of subaqueous hydraulic jumps are not well known (Komar, 1971). Komar estimated that for the average canyon-fan system, a hydraulic jump would occur at the break in slope at the canyon mouth (slope of 0.05 goes to 0.005). Substantial migration of the hydraulic jump away from this position was not predicted, though no consideration was given to the waning phase of the turbidity current. Passage of a hydraulic jump might be marked by evidence of erosion, such as a scoured surface, because of the additional turbulence generated during the jump. This surface might be difficult to distinguish from an amalgamation surface between two layers representing separate turbidity currents. Little or no increase in

grain size would be expected above an erosional surface created by a hydraulic jump, because coarser material will already have been deposited during the supercritical flow phase.

Johnson (1966) pointed out that there will be a lag effect for reaction of a turbidity current to changes in slope, due to the time taken for sediment to fall out from suspension once conditions are right, and to the time taken for the velocity to adjust to the changed slope. This distance was estimated as 25 km. in the case he discussed. Turbidity current characteristics in Table 3.1 may therefore represent conditions some distance upstream from the actual site of deposition. It is possible that turbidity currents had already gone through a hydraulic jump, perhaps at a distributary channel mouth, before they reached the outcrop area. Turbulence generated during the hydraulic jump will aid in suspension of sediment, and this may increase the lag effect further.

Alternatively, the theory used may simply be wrong. Extrapolation of Einstein and Chien's laboratory results to natural turbidity currents is certainly hazardous, but such extrapolations are inevitable if turbidity current flow is ever to be understood. Could estimates of one or more parameters be grossly inaccurate? The value of k_s is uncertain, but increasing k_s from 3D to 10D will only reduce the Froude number from 2.14 to 1.76 in line 2 of Table 3.1, for example. Friction factors ($f_o = 8S/Fr^2$) shown are for friction at the

base of the flow only, because of the use of the thickness of the flow up to the maximum velocity in Equation 3.4. These values result from the assumption that k_s is equal to 3D, and depend only on the ratio of k_s to flow depth (i.e. relative roughness). Increasing the depth of the turbidity currents will result in lower Froude numbers. However, for a turbidity current of density 1.1 g cm^{-3} carrying 2 mm. grains to be sub-critical (Fr = 0.99) a flow depth of 80 m. is required. This depth seems incompatible with unchannelized turbidity current flow originating from a shallow distributary channel (10 m.?). It is difficult to see how other parameters could be radically different from estimated values.

Assuming that the theory can be relied upon, the explanation of high Froude numbers by the lag effect is preferred, because there is little evidence for the passage of a hydraulic jump. Amalgamation surfaces generally have a large grain size contrast, though it is possible that surfaces without this contrast could have been overlooked. Without the passage of a hydraulic jump, deposition must have been entirely from sub-critical flow. Initial deposition occurred rapidly, producing a coarse, structureless division. As deposition of a layer proceeded, the overlying turbidity current became thinner, less dense, and carried progressively smaller grains. This resulted in a graded layer, and reduced deposition rates permitted the development of traction structures in the upper part of the

layer. Layers with only the structureless division are interbedded with those having parallel or cross-lamination in their upper parts. Depositional slopes for interbedded layers are assumed to be similar, and maximum grain sizes are also similar, so it follows that structureless layers must also have been deposited from subcritical flows in most cases.

Support of large clasts

While turbulent suspension is quite capable of supporting all sand-size grains in Greywacke 1 layers, it is unlikely to have supported clasts of Calcisiltite which can be one metre or more in length. Argillite clasts are very common, and perhaps were of sufficiently low density that they could be supported by buoyancy and turbulence alone. Two possibilities for movement of the Calcisiltite clasts are considered. Clasts are most likely to have been supported by buoyancy and matrix strength (debris flow) or to have been rolled along the bed beneath a turbidity current.

Consideration of the debris flow possibility requires knowledge of the original matrix content of the flows. Greywacke 1 layers now contain an average of 17.2% argillaceous matrix, partly of diagenetic origin, and 16.7% fine-grained carbonate (Enos, 1965, Table 1). Arguments for and against the presence of primary matrix in sandstones of the Tourelle Formation have been discussed in detail by Hiscott (1977, p.340).

Similar arguments discussed below suggest that Greywacke 1 layers contain approximately 12-14% primary matrix.

Fluid-escape features are seen because they lack dark matrix relative to the surrounding rock, suggesting removal of primary matrix by fluids escaping immediately after deposition. Formation of fluid-escape pillars rather than dish structure is favoured by the presence of abundant primary matrix (Hiscott, 1977, p.228). Petrographic data presented by Enos (1965, Table 1) are averages, which makes interpretation difficult. However, comparison of the β_7 and γ_2 members shows no inverse relationship between argillaceous matrix content and unstable rock fragments plus feldspar. This suggests that the additional argillaceous matrix in γ_2 samples does not come from decomposition of unstable rock fragments or feldspar. Argillaceous matrix plus fine-grained carbonate percentages are similar, suggesting total percentage of fine-grained material was the same, and that the variation results from a change in ratio between the two types. Enos (1965, p.40) suggested that Greywacke 1 differed petrographically from Calcareous Wacke in that its higher matrix content prevented recrystallisation of fine-grained carbonate to the sparry calcite cement characteristic of Calcareous Wacke. If sparry calcite cement formed early in diagenesis, this suggests that Greywacke 1 layers must have contained more primary matrix than the Calcareous Wacke average of 10.6%. Possible primary matrix contents therefore range from

greater than 10.6% to less than 17.2%, with 12-14% considered the likely range.

Hiscott (1977, p.267) showed that the similar Tourelle Formation sandstones required only 4-7 volume percent matrix to move as debris flows and support sand. It therefore seems likely that most Greywacke 1 layers had sufficient matrix to have moved as debris flows. Calculations on two Greywacke 1 layers are presented in Table 3.2 (p.102). Methods of calculation are discussed in the section on Greywacke 2. Considerable uncertainty exists because the fine-grained carbonate, which is ignored, may have contributed substantially to matrix strength. Conditions shown seem unrealistic: clasts are supported almost entirely by buoyancy as strengths are very low. Strengths of subaerial debris flows are on the order of 10^4 dyne cm^{-2} (Johnson, 1970, p.489) or 1000 times greater than values shown for Greywacke 1 layers in Table 3.2. If some Greywacke 1 layers did move as debris flows, they probably contained greater than average proportions of argillaceous matrix, or else fine-grained carbonate contributed to matrix strength.

Rolling of clasts on the bed may be considered using Shields' criterion for initiation of movement (Blatt *et al.*, 1980, p.102). It should be noted that Shields' criterion strictly only applies to movement of well-sorted sediment, so results will be approximate. Shields' β will have the value 0.06 so that

$$\tau_c = 0.06(\rho_s - \rho)gD \qquad (3.7)$$

where τ_c is the shear stress required for movement and ρ_s is the density of the clast (1.9 g cm^{-3} for Calcisiltite - see section on Greywacke 2). If the clast is rolled along the bed with its long axis transverse to flow, its thickness may be taken as the value of D. Critical values of $u_* \left(=\sqrt{\frac{\tau_c}{\rho}}\right)$ for layer Y29a are 20.7 cm s^{-1} for a flow density of 1.1 g cm^{-3}, or 16.5 cm s^{-1} for a density of 1.3 g cm^{-3}. These values are a little less than those for suspension of 2 mm. grains (Table 3.1), and so are compatible with the 1½ mm. maximum size for quartz grains in this layer. Rolling of large clasts may not proceed for very long, since the clast will stop if it deviates substantially from the long axis transverse to flow position. It is possible that clasts are ripped up from the layer below by the head of the turbidity current and then rolled a short distance by the rest of the flow. In the case of layer Y29a, the underlying layer is a 6 cm. Calcisiltite. If this layer thickened laterally, it could have provided the 10 cm. thick clast. Rolling therefore seems a much more plausible mechanism for this particular clast than transport in a debris flow.

It seems likely that some clasts were rolled beneath turbidity currents and others carried by debris flows. Rolling cannot explain the tendency for clasts to occur in the middle or at the top of layers. In general, clasts carried by debris flows would be found towards the tops of the layers, because

of dispersive pressure effects during flow. If debris flows were laminar, clasts would be relatively undeformed. Rolled clasts would occur at the base of layers and would be highly deformed if they were unlithified at the time of movement. Rolling can occur beneath a debris flow as well as a turbidity current (Lowe, 1979). Movement of some Greywacke 1 flows as debris flows is consistent with the downcurrent change to Greywacke 2 (interpreted as debris flow deposits) within a layer noted by Enos (see section on Greywacke 2), and with the fact that some layers have an upper part identical to Greywacke 2 (Fig. 2.9b).

Interpretation of sedimentary structures

Coarse, parallel stratification (Fig. 2.10b) was only observed in three layers. Although bands are not noticeably inverse graded, they are tentatively interpreted as due to deposition by freezing of successive flowing grain layers (grain flows) beneath a turbidity current (Sanders, 1965; Hiscott and Middleton, 1979). The more common coarse to fine parallel lamination in sand or silt-sized material (Fig. 2.10a) is interpreted as having been produced under upper flow regime plane bed conditions. Fine silt-clay lamination (Bouma T_d division) may be similar to that interpreted as resulting from burst-sweep cycles within the viscous sublayer of fine-grained, dilute turbidity currents (Hesse and Chough, 1980). The origin of the

alternation of sand and clay laminae at the top of some layers may relate to reworking of the top of the layer by the tail of the turbidity current, or by a separate fine-grained turbidity current.

An interesting feature of the γ_4 Formation is the difference between palaeocurrents obtained from sole marks and those obtained from rib and furrow structure and rippled tops. Ripple direction modes are commonly rotated about 45° anticlockwise from sole marks. This trend occurs in all facies (Fig. 4.5). Such bimodal palaeocurrent directions have been used as the main evidence for reworking of sediments by bottom currents in the ancient record (Anketell and Lovell, 1976). Climbing ripple cross-lamination, which occurs in some Greywacke 1 layers and in their Calcisiltite tops, implies considerable rates of sediment fallout from suspension, in addition to traction. Such rates of deposition are unlikely to have occurred from bottom currents as they are presently understood (Stow and Lovell, 1979). Parkash (1969, p.177) studied graptolite and grain orientation through Greywacke 1 layers and found that they showed a gradual change from bottom to top from parallel to sole marks to deviation of as much as 90°. Gradual change would not be expected for bottom current reworking; directions should be bimodal. The enclosed nature of the area of deposition (Bambach et al., 1980) would not favour strong bottom currents. The high global sea level and poor ocean circulation during the

Caradoc (Leggett et al., 1981) also argues against the existence of strong bottom currents (Shanmugam and Moiola, 1982). For these reasons, an explanation of the palaeocurrent divergence in terms of fan geometry is suggested (Chapter 5).

Absence of the Bouma T_b division between the T_a and T_c divisions in most layers with cross-lamination (Table 2.2) suggests either that the upper flow regime plane bed was never the stable bed phase during deposition or, more likely, that sedimentation was too rapid for plane lamination to develop. Linguoid ripple crests (Fig. 2.9d) found on the few top surfaces are typical of slow deposition under unidirectional flow (Harms et al., 1975, p.56), as would occur beneath the tail of a turbidity current.

Greywacke 2

Greywacke 2 layers are interpreted as having been deposited from debris flows. Their high percentage of argillaceous matrix, poorly developed grading and the presence of large matrix-supported clasts of Calcisiltite and Argillite constitute the main evidence for this mechanism.

Theory of debris flow

The consequences of this hypothesis may be examined using the various equations governing the behaviour of such flows. For a subaqueous debris flow the shear stress acting at the bed is due entirely to the downslope component of the submerged weight of the debris. In order for the flow to move, this shear stress must exceed the yield strength, k, of the debris. When the debris flow just comes to rest, the shear stress at the base will be equal to the yield strength of the debris (Johnson, 1970, p.488-9). Therefore

$$k = \Delta\rho \; g \; T \sin\alpha \qquad (3.8)$$

where T is the thickness of the flow and α is the slope angle. Johnson (1970, p.487) was also able to calculate the yield strength from the size of clasts supported by the flow.

$$k \approx \frac{h}{4} (\rho_s - \rho N) g \qquad (3.9)$$

where h and ρ_s are the thickness and density of the clast, and N is the fraction of the clast volume submerged in the flow. This equation was derived for the case of clasts which partly

protrude from the top of the flow. For clasts supported within the flow, the equation should be approximately true with the parameter N set at 1. Hampton (1972) presented data for the strengths of kaolinite and montmorillonite slurries against weight percentage of water.

Support of material in a debris flow is by matrix strength and buoyancy. Buoyancy is particularly important when the density difference between clasts and fluid is low (Hampton, 1979). For a clast of a particular size, the effective density of the fluid is due to the mass of all material smaller than the clast. Thus sand-size grains in the flow contribute to the buoyant support of larger clasts. Addition of up to 95 volume percent poorly-sorted debris or 50 volume percent single-sized clasts does not increase the strength of the flow above that of the clay-water slurry. Therefore dense debris flows carrying large amounts of material are able to move on low slopes (Rodine and Johnson, 1976).

Application of theory

In order to make calculations using Equations 3.8 and 3.9, various parameters must be estimated. There is considerable uncertainty in many of these and any conclusions must be treated as speculative. Argillite clasts were probably of low density, as suggested by partial mixing between clasts and matrix, and may have floated in the Greywacke 2 flow. Calcisiltite

and Calcareous Wacke clasts were probably supported by both matrix strength and buoyancy. Density of Calcisiltite clasts is estimated as 1.9 g cm^{-3}, because this is the density of modern resedimented calcisiltite sampled 26 m. beneath the Gulf of Mexico floor by the Deep Sea Drilling Project (Beall and Fischer, 1969). Although this calcisiltite is rather different in composition, it is probably the best estimate that can be made. Density of Calcareous Wacke may have been a little higher and is estimated as 2.1 g cm^{-3}.

Strengths of kaolinite and montmorillonite slurries for the same water content are very different (Hampton, 1972). The composition of clay in Greywacke 2 layers is mostly illite with some chlorite (Enos, 1965, p.42). The original composition of the clay is unknown. Tectonic burial of the Cloridorme Group certainly caused the rocks to be heated above the temperature when smectite clays would normally be converted to illite (Blatt et al., 1980; Islam et al., 1982), although montmorillonite is still preserved in Volcanic Ash layers (Enos, 1965, p.51). Many modern clays are mixtures of two or more clay minerals (Berger, 1974). The palaeolatitude of the northern Gaspé area during the Middle Ordovician was approximately 15°S (Bambach et al., 1980) This suggests that tropical weathering was taking place in the source area, producing kaolinite. The position of the area adjacent to the North American continent (Laurentia) suggests an input of continent-derived illite, while the volcanic

input may have produced some montmorillonite. The clay may therefore have been a mixture of kaolinite, illite and montmorillonite. The strength data for kaolinite-ocean water slurries will be used in calculations. The possibility that a small percentage of the clay matrix results from breakdown of unstable rock fragments will be ignored as will the presence of a small percentage of carbonate mud which might contribute to matrix strength.

Five Greywacke 2 layers were selected which contained clasts of known dimensions (Table 3.2). A trial and error method of calculation was employed using Equations 3.8 and 3.9 together with the strength data of Hampton (1972). 1) A value for the slope was guessed and a value k_1 calculated using Equation 3.8. Since the shear stress depends on the density difference between the flow and water, the rock density (approximately 2.55 g cm^{-3}) and layer thickness may be used. The original flow thickness is not required. 2) The value k_1 was used to calculate a value for the density of the flow, ρ, using Equation 3.9. 3) This flow density was used to calculate the weight percent water in the clay-water slurry, assuming an average Greywacke 2 composition of 48.4% clay matrix (Enos, 1965, Table 1) with density 2.5 g cm^{-3}. 4) A second value of the strength, k_2, was obtained from the graph of Hampton (1972) using the weight percentage of water.

Different values of slope were tried until the best fit

Table 3.2 Strength and slope estimates for debris flows

Layer number	T(cm)	L(cm)	S	k_1 (dyne cm^{-2})	ρ ($g\ cm^{-3}$)	Wt. % Water	k_2	$\bar{U}_c$ ($cm\ s^{-1}$)
R299	49	15	0.010	745	1.70	50.3	760	662
S58	28	6	0.010	426	1.61	56.0	390	514
U193*	101	10	0.006	921	1.72	48.5	825	732
Y28	15	7	0.020	456	1.63	54.4	480	529
C1468*	53	15	0.010	806	1.68	51.3	740	693
R21(Gl)	14	9	0.002	43	1.88	70.0	45	151
Y29a(Gl)*	12.5	10	0.002	38	1.88	69.8	45	142

U193 clast is Calcareous Wacke; others are Calcisiltite. Layer R299 and clast can be seen in Fig. 2.11a.
*Layers with clasts near base

between values of k_1 and k_2 was obtained. Finally, the mean velocity at which the flow would become turbulent was calculated using the Hampton number criterion (Hiscott and Middleton, 1979). Similar calculations using the montmorillonite slurry strength data give strength and slope values which are roughly twice those in Table 3.2. Two of the layers considered had clasts close to the base. There was no evidence that these clasts were locally eroded pieces of the layer below. The clasts may have been partly supported during flow by dispersive pressure (Bagnold, 1956). When the flow stopped, they may have sunk to the base of the flow because matrix strength and buoyancy alone were insufficient to support them. Alternatively, clasts may have been rolled along the bed at the base of the debris flow (Lowe, 1979). Strength and slope estimates for these layers are therefore maximum values.

Discussion of results

Values of $\bar{U}_c \left(=\sqrt{\frac{1000k_1}{\rho}}\right)$ for turbulence are very high and it seems unlikely that flows were turbulent. Despite this there is other evidence suggesting flows were turbulent. Enos (1965, p.41) noted that "flutes are much less abundant" than in Greywacke 1 layers, which suggests that flutes were present on some soles, indicating turbulence. Also, many layers have a division at the base containing more coarse grains than the rest of the layer. This is similar to the pattern interpreted

by Lowe (1982, his Fig. 13c) as due to deposition from a turbulent cohesive flow (debris flow). The base of the layer is deposited by suspension sedimentation from a turbulent debris flow and is followed by deposition of the upper part of the layer by cohesive freezing of a laminar debris flow. This mechanism, together with the upward increasing abundance of floating shale clasts of various sizes, could explain the frequently observed content grading. However, Greywacke 2 debris flows with the strengths shown in Table 3.2 would have been competent to support all the sand grains found in the layers. Sheared kaolinite-ocean water slurries with 60 weight percent water can support 2.56 mm. quartz grains (Hampton, 1975), so the 1 to 2 mm. size quartz grains generally found in Greywacke 2 layers could have been supported. Traction structures in the upper part of a few Greywacke 2 layers may be due to reworking of the top of the debris flow deposit by associated low-concentration turbidity currents (Hampton, 1972). Deposition from such turbidity currents would account for the divisions of Calcisiltite at the top of some layers.

Slopes estimated for debris flows (Table 3.2) are somewhat higher than those on the outer parts of modern submarine fans (0.002 to 0.006). The model used for debris flow calculations assumes that the strength is uniform throughout the flow. It is quite possible that this is not the case, and that movement occurs by shearing along relatively weak zones in the flow separated by rigid plugs. In this case, clasts could be sup-

ported in strong rigid plug areas while flow occurred on low slopes by movement along weak shear planes or zones. Embley (1976) found modern debris flow deposits off the Spanish Saharan continental slope which had apparently moved on slopes as low as 0.1° (0.0017). The high slopes in Table 3.2 may therefore result from the inadequacy of the model used.

A difficult feature to account for in terms of depositional mechanics is the observation of Enos (1965, p.98-99) of a downcurrent passage from Greywacke 1 to Greywacke 2 to Argillite within layers. Downcurrent transition from a turbulent turbidity current to a laminar debris flow upon lowering of slope has been suggested by Middleton and Southard (1977, p.8.18). This could account for the downcurrent change from Greywacke 1 (turbidity current deposit) to Greywacke 2 (debris flow deposit) within a layer. Passage from Greywacke 2 to Argillite is marked by abrupt disappearance of coarse grains, or gradual fining over a few metres (Enos, 1965, p.99). A few such transitions were observed in this study (Fig. 2.2). In one case (Fig. 2.2a,b), the Greywacke 2 passed abruptly into Argillite with thin silt layers. In another example (Fig. 2.2c) the transition is sharp and appears to be the lateral margin of a shallow channel, suggesting that Argillite was eroded by the flow which deposited the Greywacke 2 layer. In general, Argillite layers downcurrent of Greywacke 2 were probably deposited from a fine-grained turbidity current related to the Greywacke 2 debris flow (see sec-

tion on Argillite).

Facies relationships (Chapter 4) suggest that some Greywacke 2 layers are not lateral equivalents of Greywacke 1. These occur as isolated thick layers with abundant clasts in units of thin-bedded Calcisiltite and Argillite (Fig. 2.11d), whereas most Greywacke 1 layers occur in groups as thick-bedded packets. All Greywacke 2 layers in Table 3.2 except for C1468 fall into the isolated category.

Calcareous Wacke

Calcareous Wacke layers are interpreted as turbidity current deposits. They differ from Greywacke 1 in having lower matrix content and more common traction structures. Presence of traction structures implies slower rates of deposition than for the mostly structureless Greywacke 1 layers. Abundant flutes on soles (Enos, 1965, p.33) suggest extensive scouring of the underlying mud by the head of the turbidity current, prior to deposition of the layer. Extensive scour and slow deposition are predicted for turbidity currents close to auto-suspension (Bagnold, 1962), which may have travelled greater distances from their source than those which deposited Grey-wacke 1 layers (Middleton and Hampton, 1973). The lateral per-sistence (Enos, 1965, p.33) and thinner layers (Figs. 2.1, 3.1) of Calcareous Wacke relative to Greywacke 1 are in accord with this hypothesis.

An alternative explanation for the low matrix content is that fines have been removed by reworking by bottom currents or non-depositing turbidity currents. This explanation is par-ticularly attractive for coarse, parallel and cross-laminated layers showing marked lateral thickness variation. These show many of the characteristics of sandy contourites (Stow and Lovell, 1979). Arguments against bottom current reworking have already been discussed in the section on Greywacke 1. While reworking is a possibility for these uncommon coarse layers,

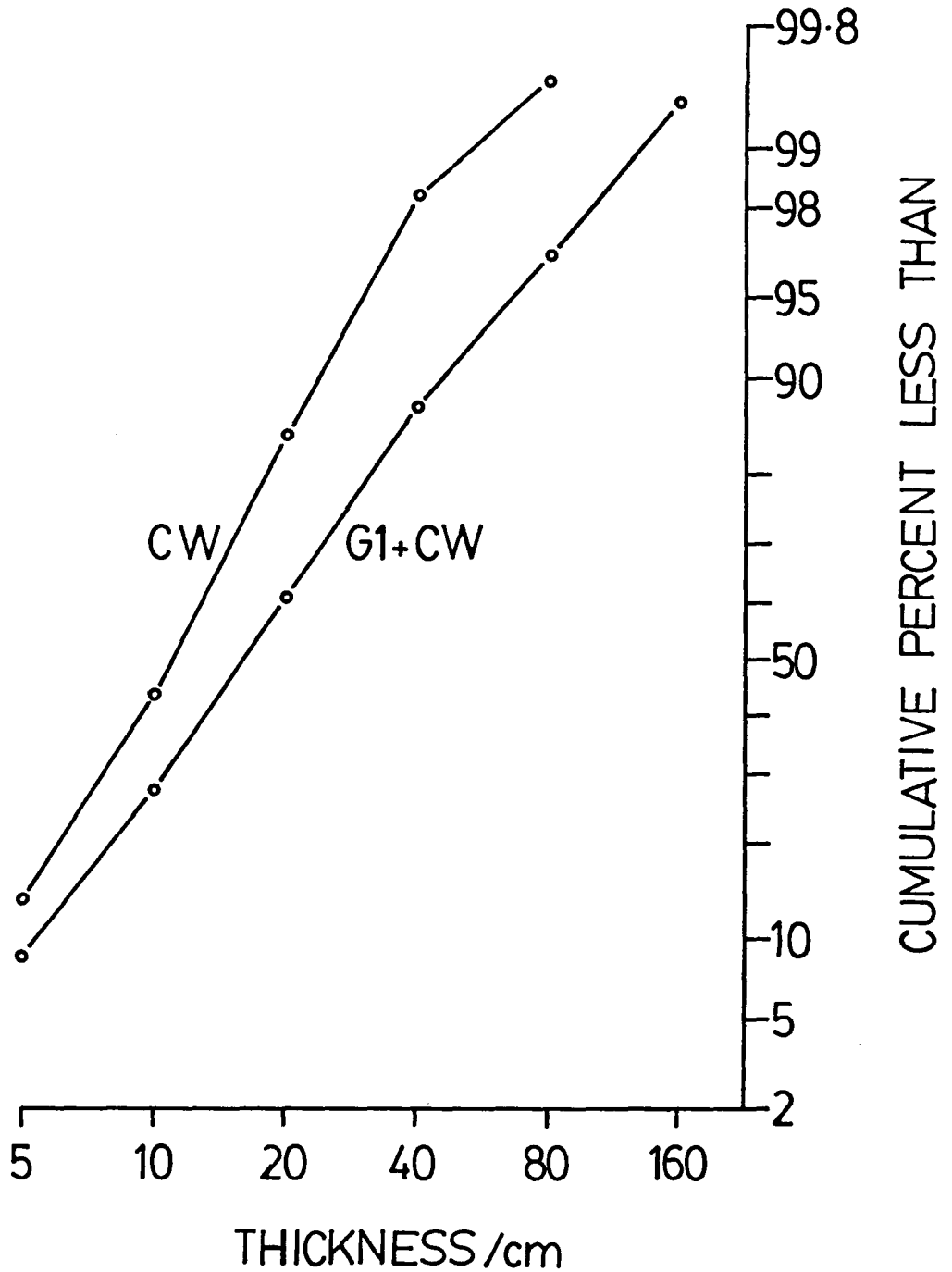

Figure 3.1: Cumulative layer thickness distribution of Calcareous Wacke (227 layers) and of Calcareous Wacke and Greywacke 1 combined (773 layers), plotted on log-probability paper.

turbidity current deposition alone is the most likely origin for the vast majority of Calcareous Wackes. No transitions from Greywacke 1 to Calcareous Wacke are observed, but layer thickness plots which combine the two facies show a roughly log-normal distribution (Fig. 3.1). Such a distribution suggests all layers were deposited by the same mechanism, or by a continuum of mechanisms (Hiscott and Middleton, 1979). The layer thickness plot for Calcareous Wacke layers alone shows a break in slope at a thickness of 40 cm., reflecting the rarity of layers thicker than this value.

All parallel lamination in Calcareous Wacke layers is thought to have been produced under upper flow regime plane bed conditions. Convolute lamination is thought to result from the liquefaction of the lower part of layers by escaping pore waters (Lowe, 1975). Normal grading results in a layer of upward-decreasing permeability, favouring trapping of water. Better packing of grains towards the top of the layer because of slower deposition may produce a reversed density gradient. The finer, more cohesive upper part of the layer resists liquefaction and partially sinks into the less dense, liquefied lower part of the layer, producing convolute lamination (Anketell et al., 1970). The relationship between normal grading and convolute lamination is not seen in the summary of sedimentary structure sequences (Fig. 2.7b), perhaps because grading is hard to recognize in convoluted layers, or is partly destroyed by

liquefaction. Wavelength of convolution may reflect original ripple wavelength (Lowe, 1975), though in Calcareous Wackes the 10-15 cm. wavelength of convolutions (Fig. 2.8a) is somewhat less than ripple wavelengths seen in undeformed Calcisiltite layers (20 cm. or more). The common downcurrent fold asymmetry probably results from fluid drag by the tail of the current, or the effect of gravity, or both. Convolution appears to have taken place immediately after deposition. In cases where undeformed cross-lamination overlies convolute lamination in a layer, convolution may have occurred before deposition of the upper cross-laminated part of the layer.

Calcisiltite 2

Calcisiltite 2 layers are interpreted as turbidity current deposits. Their characteristic climbing ripple cross-lamination has previously been discussed in detail by Walker (1969) and Bhattacharjee (1970).

The commonly observed upward increase in stoss side preservation and angle of climb within a layer result from an increase in the ratio of aggradation rate to ripple migration rate (Allen, 1971; Ashley et al., 1982). Slight grading through layers suggests competence, and therefore velocity, were decreasing during deposition. The trend of upward-increasing amplitude of ripples can be explained by the increasing aggradation/ripple migration ratio, together with the increased co-

hesiveness of finer material which allows formation of steeper sided ripples (Bhattacharjee, 1970, p.126). Upward passage from climbing ripples to parallel lamination by decreasing angle of climb and amplitude results from a decrease in the aggradation/ripple migration ratio.

Parallel lamination is thought to have been deposited under upper flow regime plane bed conditions. It is not necessary for upper flow regime plane bed conditions to occur at higher flow velocities than ripples, as they do in flume experiments at equilibrium (no net deposition or erosion), because Calcisiltite 2 layers were deposited at high rates of sedimentation and were certainly not at equilibrium. In flume experiments with well-sorted quartz (median size 0.15 mm.), climbing ripple sequences about 20 cm. thick that most closely resemble natural sequences were deposited in 1.5 to 3 hours at flow velocities of 15-40 cm s^{-1} (Ashley et al., 1982). In one experimental run, an abrupt upward transition from climbing ripples to parallel lamination was produced under increasing flow velocity. In Calcisiltite 2, where the transition presumably occurred under decreasing flow velocity, climbing ripples pass gradually upward into parallel lamination (Fig. 2.6a). Equivalence of parallel lamination found above and below cross-lamination is shown by their similar character and by the fact that they join together when lateral transition from cross-lamination to parallel lamination occurs.

False bedding is produced by current sorting of fines onto the lee faces of ripples. This occurs because current velocity is greatest over stoss slopes, and fines are removed from there and preferentially deposited on the more protected lee face (Enos, 1965, p.31). Ripple wavelengths up to 84 cm. have been reported in Calcisiltite 2 (Bhattacharjee, 1970, p.68). Long wavelength ripples have been produced in flume experiments under high viscosity flows of sugar solution. Similar effects might be produced by the high viscosity resulting from presence of suspended sediment in a turbidity current (J.B. Southard et al., 1980; and pers. comm., 1981). Convolute lamination occurs in some layers, and preferential water escape through the more permeable ripple crests (Lowe, 1975) results in exaggeration of ripple form.

Rotation of palaeocurrent directions obtained from rib and furrow structure from those of sole marks on the same layer was not observed by Walker (1969) or Bhattacharjee (1970, p.149), who found good parallelism between the two. Change in current direction is thought to have occurred during deposition of the layer (p.59). Bhattacharjee observed opposite palaeocurrent directions in adjacent layers in a few cases, and interpreted this as deposition from two sources on a very low slope. Walker (1969) was able to trace a ripple lamina over 38 ripples in one layer, and concluded that the depositional surface dipped downstream at a slope of 0.01 relative to the base of the layer.

This slope might be sufficiently local that effects on a turbidity current would be unimportant. However, it is difficult to see how such a depositional surface could have been maintained. The surface could not have prograded fast enough to keep pace with the turbidity current velocity, so sediment would have to be deposited downstream of the surface. This would lead to a reduction in slope of the depositional surface.

Rapid fallout of fine sediment from suspension implies a sudden reduction in flow velocity. This could be caused by a sudden reduction in slope (Walker, 1969), such as might occur by spilling of a turbidity current from the end or sides of a channel. Poor lateral continuity of Calcisiltite 2 (Enos, 1965, p.30) would be expected in this case. The current would not be competent to support its silt and fine sand load on the lowered slope, and all such material would be deposited over a short distance. Lateral transitions from Calcisiltite 2 to Argillite with little change in thickness suggest that the Argillite was deposited by the same turbidity current as the Calcisiltite 2.

Calcisiltite 1

Calcisiltite 1 layers are interpreted as turbidity current deposits. Preservation of possible burrows on the base of some layers suggests deposition took place without erosion of the underlying mud. Flutes and grooves indicate erosion did take place in other cases, probably beneath the head of the

current. The thin-bedded character of Calcisiltite 1 may reflect the small size of the flows, the low concentration of sediment in the flows, or alternatively it may mean that the turbidity currents were close to autosuspension, so that little material was deposited at any point. If the latter is true, the difference between Calcisiltite 1 and the thicker-bedded Calcisiltite 2 (whose composition and grain size are similar) may result from a more gradual lowering of slope experienced by flows which deposited Calcisiltite 1, compared to a rapid lowering of slope for Calcisiltite 2 flows. In this theory, initially similar flows would deposit a thin, extensive Calcisiltite 1 layer on a gradually decreasing slope, and a thick, low continuity Calcisiltite 2 layer on a rapidly lowered slope.

Climbing ripple cross-lamination is generally Type A in Calcisiltite 1, indicating lower aggradation rate/ripple migration rate ratio than the Type B characteristic of Calcisiltite 2. Following from the above reasoning, this is most likely to be due to lower aggradation rates. Ripple wavelengths range from 25 to 110 cm., suggesting a wide range of flow viscosities. Long wavelengths in some layers suggest deposition was from flows of relatively high viscosity and concentration (J.B. Southard et al., 1980; and pers. comm., 1981), even though the layer thickness is low. This could indicate that some currents carried much silt and fine sand at conditions close to autosuspension, or that they carried considerable concentrations of

clay which was deposited above and beyond the Calcisiltite 1 layer.

Volcanic Ash

Volcanic Ash layers must have been deposited by direct pelagic sedimentation. Any resedimentation mechanism would dilute the volcanic material with normal terrigenous sediment, and would not account for the uniformity of layers over long distances.

Dolomite and Limestone

Dolomite and Limestone beds and concretions in the Cloridorme Group have been studied in detail by Islam (1981). They are believed to be diagenetically formed. Dolomite concretions consist of ferroan dolomite, and show a decrease in total carbon, carbonate carbon, organic carbon and carbonate from the core to the periphery of each concretion (Islam, 1981, p.120). Carbon isotope evidence indicates that decay of organic matter by microbial oxidation and methane production may be responsible for the carbonate in the concretions. Oxygen isotopes suggest that concretions began to develop just below the sediment-water interface and continued to grow at greater depth with sedimentation (Islam, 1981, p.130). Conditions favouring bed or concretion development are not known, but processes of formation were probably similar.

Parallel laminae in Dolomite could be thin silt turbidites whose visibility is enhanced in Dolomite relative to normal Argillite, in which such laminae are rarely seen. Rare cross-laminated lenses in these laminae indicate current action, either by bottom currents or turbidity currents.

Argillite

Lack of sedimentary structures in the Argillite makes interpretation of its transport and deposition difficult. Argument centres around whether Argillite was deposited by turbidity currents or by hemipelagic processes, where deposition occurs by quiet settling of material through the water column.

Lateral change from Calcisiltite 2 to Argillite within a layer without thickness change suggests turbidity current deposition of some Argillite (Enos, 1965, p.99). Similar transitions from Greywacke 2 suggest Argillite deposition from fine-grained turbidity currents associated with Greywacke 2 debris flows. Thin black shale bands with abundant unoriented graptolites are probably pelagic in origin. Enos (1965, p.100) computed linear regressions of Argillite thickness against distance and coarser clastic facies thickness against distance to determine the thickness of Argillite at the point downcurrent where extrapolated coarser clastic thickness would be zero. On this basis, he estimated that a mean of 56% of Argillite was of turbidity current origin. This is probably a minimum figure,

since Argillite would have been deposited from turbidity currents beyond the termination of sandstone layers. Evidence from the Black Shell turbidite on the Hatteras abyssal plain (Elmore et al., 1979) shows that lutite and sand fractions deposited from the same turbidity current have different areal thickness distributions, making this kind of extrapolation dubious.

Turbidite Argillite could have been deposited from the same flow that deposited the underlying sand layer, from a separate fine-grained turbidity current associated with the sandy turbidity current, or from an unrelated fine-grained turbidity current. Most vertical transitions from Greywackes, Calcareous Wackes and Calcisiltites to Argillite are distinct, because of the grain size break between layers. This is a common situation in turbidites, and need not imply that contacts represent a break in deposition (Piper, 1978). Fine-grained turbidity currents proposed by Stow and Bowen (1980) have concentrations of 2.5 g l^{-1}, thicknesses of several hundred metres, and deposit mud at velocities of 9-16 cm s^{-1}. These flows may occur on their own or be associated with "classical" turbidity currents. If turbidity currents which deposited Argillite were anything like this, they are clearly not the same as the turbidity currents suggested for deposition of Greywacke 1 and other facies. Most probably, thick fine-grained dilute turbidity currents are generated along with the

sandy turbidity currents. Some material will be added to them during flow from sediment lost at the upper boundary of the sandy turbidity current. If most Argillite is of turbidity current origin, as seems likely, some thick layers were probably deposited from several fine-grained turbidity currents without associated sandy turbidity currents. Silt laminated units may have been deposited by a single fine-grained turbidity current (graded laminated units of Stow and Bowen, 1980) and need not require a series of flows. Movement of a fine-grained turbidity current above a sandy turbidity current should be considered in modelling of the latter. The usual assumption is that the overlying water is static and clear.

Flow Evolution

Attempts are often made to explain different turbidite facies as representing deposition from a single flow during various stages of its evolution (e.g. Nelson and Kulm, 1973). These explanations seem rather unlikely. A debris flow cannot be deposited as a "proximal exotic" facies and simultaneously evolve into a sandy turbidity current. It either stops and deposits or it accelerates and evolves into something else; it cannot do both. In the Cloridorme Group, the variety of facies and their lateral relationships make such a single flow explanation impossible. However, some facies do appear to be related, and a number of trends in flow evolution can be suggested.

One of these trends is the downcurrent change from Greywacke 1 to Greywacke 2 to Argillite. This was documented by Enos (1965, p.99) and has been interpreted here as a downcurrent change from turbidity current to debris flow deposition, with Argillite deposited from a fine-grained, dilute turbidity current associated with the sandy flow.

The tendency for Greywacke 1 and Calcisiltite 2 layers to occur in packets with similar layer thickness means and sand/shale ratios (Table 4.7), plus the existence of packets containing layers of both facies and Greywacke 1-Calcisiltite 2 couplets, suggests that these facies are related. Transitions from Greywacke 1 to Calcisiltite 2 and from Calcisiltite 2 to Argillite along strike also occur. A trend from Greywacke 1 to Calcisiltite 2 to Argillite is therefore suggested. This may represent a lateral trend from the centre to the edges of a turbidity current path in contrast to the downcurrent Greywacke 1-Greywacke 2 trend. Deposition of Calcisiltite 2 could occur on a lower slope at the edge of the depositional area, or could be related to frictional slowing of the turbidity current at its lateral margins. Most probably, both of these factors would be important.

Some Greywacke and Calcareous Wacke layers have a division of Calcisiltite 1 at their top, which raises the possibility that Calcisiltite 1 layers may be deposited downcurrent from the termination of Greywacke and Calcareous Wacke layers.

Enos (1965, p.26) inferred such a relationship between Calcareous Wacke and Calcisiltite 1 but apparently did not observe transitions from Greywacke to Calcisiltite 1. Interpretation of facies associations (Chapter 4) suggests that thin-bedded Calcisiltite 1-dominated units (interpacket units) are the downcurrent and lateral equivalents of Greywacke 1 packets. This implies that at least some Calcisiltite 1 layers are related to Greywacke 1 layers. Association of Calcareous Wacke and Calcisiltite 1 layers in the section also suggests that some Calcisiltite 1 layers are downcurrent equivalents of Calcareous Wacke. It has already been suggested that Calcareous Wackes were deposited from turbidity currents closer to autosuspension than those which deposited Greywacke 1. The cause of the difference between the two types of flow is not known for certain; it presumably relates to some factor such as the site or cause of flow initiation, its composition, or the distance travelled before reaching the outcrop area. Petrographically, Calcareous Wacke and Greywacke 1 differ in that Calcareous Wacke has more carbonate and less argillaceous matrix than Greywacke 1 (Enos, 1965, Table 1). Total percentage of all original fine-grained material (argillaceous matrix plus carbonate) is also higher for Calcareous Wackes. Enos (1965, p.82) suggested that fine-grained carbonate might give different properties to the turbidity currents than terrigenous clay. Either this or the

higher overall content of fine material might be a factor in causing different turbidity current behaviour. Evolution of Greywacke 1-type and Calcareous Wacke-type turbidity currents through deposition may have led to eventually similar fine-grained flows from which Calcisiltite 1 layers were deposited.

Not all examples of all facies will fall into one of the trends described above. Some flows probably deposit layers of a single facies only, and other trends may be possible.

CHAPTER 4

FACIES INTERPRETATION 2: DEPOSITIONAL ENVIRONMENT

Facies Sequence

Facies do not occur randomly through the section, but show varying degrees of organization. The most striking feature of facies organization, which can easily be seen in the field, is the alternation of thicker-bedded units of high sand/shale ratio with thinner-bedded units of low sand/shale ratio (Fig. 4.1). The term sand/shale ratio is used here for the thickness ratio of non-lutite facies (G1, G2, CW, CS2, CS1) to lutite facies (ARG, LST, DOL, VA). Thicker-bedded units are referred to as packets, following Hiscott (1977, p.104).

Most packets consist dominantly of Greywacke 1 interbedded with Argillite (Fig. 4.1), but packets with Calcisiltite 2 (Fig. 2.6d) or with Calcareous Wacke instead of Greywacke 1 also occur. Calcareous Wacke packets (Fig. 2.8d) are less well-defined than those of Greywacke 1 or Calcisiltite 2. Inter-packet units (Figs. 2.2d, 2.5d and 2.11d) consist dominantly of Argillite, with variable proportions of the other facies, of which Calcisiltite 1 is the most important. Packets range in

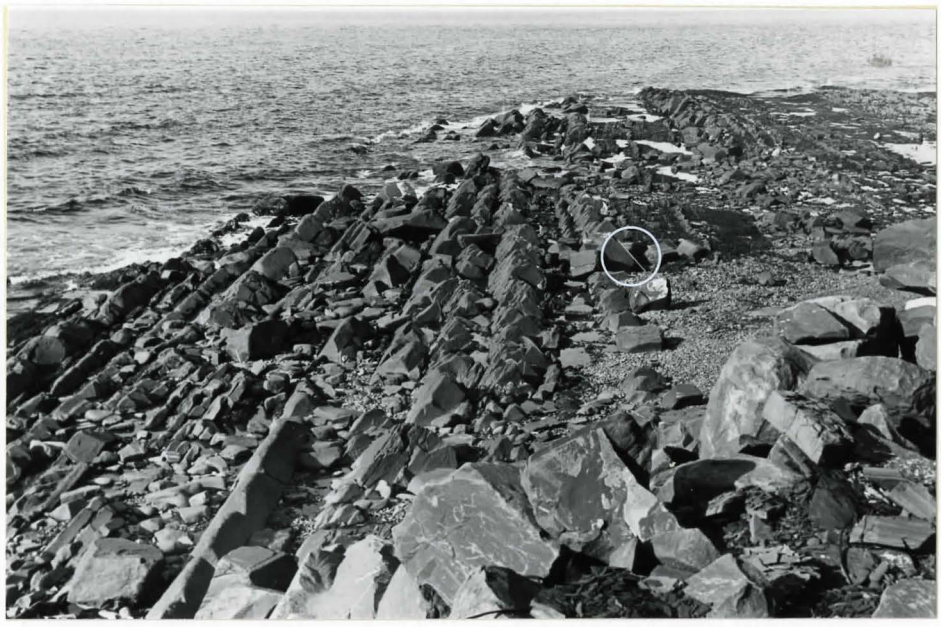

Figure 4.1a: Greywacke 1 packet (unit 7) showing thickening-upward sequence (far right of photo) from underlying interpacket unit. Top is to left. Scale 1 m.

Figure 4.1b: Photo taken to left of (a) showing the top of the same Greywacke 1 packet with thinning-upward sequence into overlying interpacket unit. Scale 1 m.

thickness from 3.0 m. to at least 45 m. (packet terminated by fault at end of section). Interpacket units range from 2.4 m. to 37 m. The lower boundary of the thickness range results from the fact that intervals thinner than this were not regarded as sufficiently significant to merit unit status, rather than from any real lower limit. Facies proportions based on totals from all examples of each of the four unit types (Greywacke 1 packets, Calcareous Wacke packets, Calcisiltite 2 packets and interpacket units) are shown in Fig. 4.2. Facies proportions for Greywacke 1 packets and interpacket units are presented separately for the wave-cut platform and roadcut exposures, because of the difficulty in recognizing Calcisiltite 2 facies in the roadcut. Calcareous Wacke packets only occur in the roadcut and Calcisiltite 2 packets only occur on the wave-cut platform. Total section thickness is divided among the unit types as follows: Greywacke 1 packets, 53%; interpacket units, 35%; Calcareous Wacke packets, 9%; and Calcisiltite 2 packets, 3%. Although there is some variability between different units of the same type, the four unit types are easily distinguished.

Markov Chain Analysis

Facies sequence may be analyzed in terms of a Markov process, in which facies are regarded as states. Probability of an upward transition to a particular state depends only on the nature of the previous state or states. In this analysis,

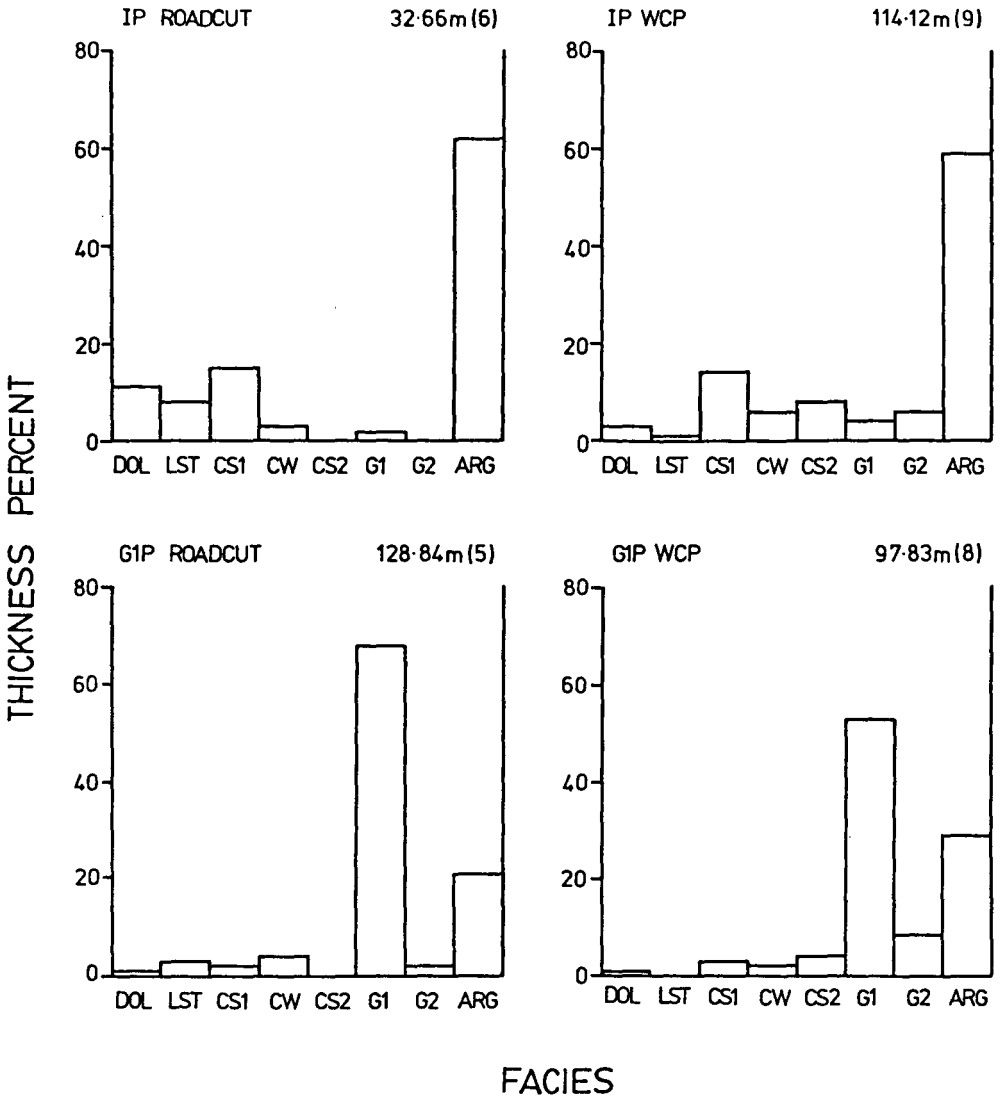

Figure 4.2: Facies thickness proportions for the various unit types. IP-interpacket units, G1P-Greywacke 1 packets, CS2P-Calcisiltite 2 packets, CWP-Calcareous Wacke packets, WCP-Wave-cut platform section. The heading for each histogram gives unit type, section, and total thickness followed by the number of units in brackets.

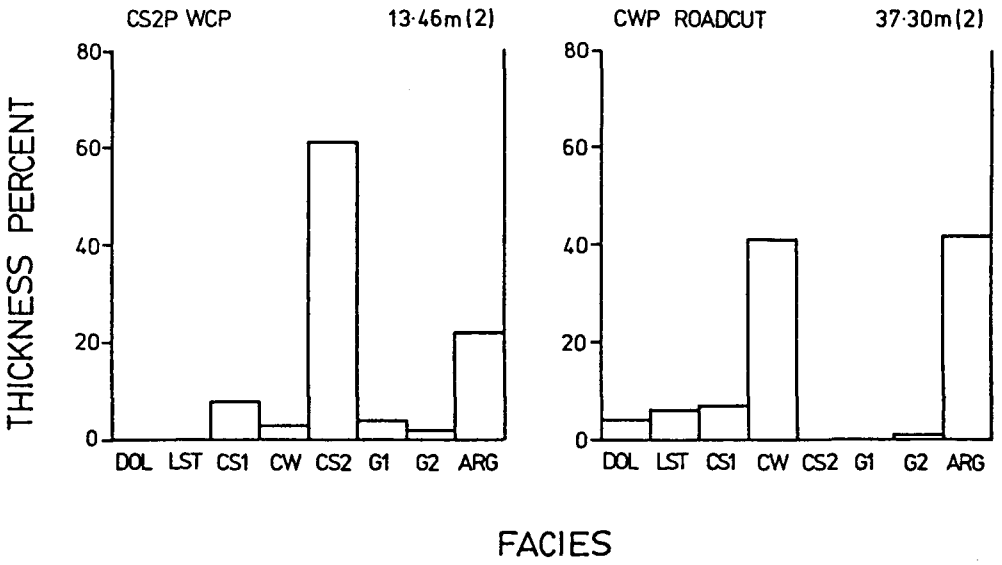

Figure 4.2 (continued)

a first-order Markov process will be considered, where the probability depends only on the nature of the immediately preceding state.

Some adjustment of the facies types previously described is required to get useful results. The regular alternation between sandstone or siltstone layers and Argillite is obvious and requires no analysis to "prove" its existence. Use of the existing sequence of facies in a Markov analysis might yield only the result that the probability of the sandstone or siltstone to Argillite transition, and vice versa, is high. For this reason, a new facies Thick Shale (TKSH) was defined. Thick Shale intervals have a thickness of 50 cm. or more of Argillite plus Dolomite, Limestone and Volcanic Ash which lacks layers one centimetre or more in thickness of other facies. In an attempt to allow for different thicknesses of Argillite deposited along with the underlying sandstone or siltstone layer, an amount equal to half the underlying layer thickness was subtracted from the Argillite before comparing its thickness with 50 cm. Argillite layers which were too thin to be counted as Thick Shales were then ignored in the analysis.

Techniques for Markov chain analysis have recently been discussed by Carr (1982) and his method is used here. Methods of Markov chain analysis involve some type of comparison between the matrix of observed transition frequencies and a matrix of transition frequencies predicted from a random model. Matrices

which contain pre-defined (structural) zeros cannot result from a simple independent random process (Schwarzacher, 1975, p.116). Since transitions between the same facies were prohibited, matrices for γ_4 facies transitions contain structural zeros along the leading diagonal (Table 4.1). A log-linear model of quasi-independence (Bishop et al., 1975, p.178) may be used to compute expected cell values for a matrix with structural zeros. If comparison of observed and expected frequencies indicates deviation from the quasi-independent model, a stepwise procedure (Brown, 1974) can be used to identify cells which contribute most to the departure from the model. If results of such an analysis are to be meaningful, the data must have the property of stationarity. Stationarity means that transition probabilities are constant through time and space (Harbaugh and Bonham-Carter, 1970, p.122).

Computation was performed using the program BMDP 4F (Brown, 1981), which replaces the program BMDP 2F used by Carr (1982). Preferred facies transitions were selected using the maximum absolute standardized deviate at each step (see below). After identification of a preferred transition, this cell is treated as a structural zero and the expected value matrix is refit using a log-linear model of quasi-independence. Stepwise selection of deviant cells ends when the probability for the likelihood ratio chi-square value (G^2) for comparison of observed and expected matrices exceeds 0.1. This procedure gives

similar results to the program BMDP 2F with the Pearson chi-square statistic (χ^2) as the criterion for cell selection used by Carr (1982). Test statistics are defined as follows for observed cell frequencies a_{ij} and expected cell frequencies e_{ij}, where the subscript "ij" refers to the cell in row i and column j.

$$\text{Standardized deviate} = \frac{\left| a_{ij} - e_{ij} \right|}{(e_{ij})^{\frac{1}{2}}}$$

$$G^2 = 2 \Sigma\Sigma\, a_{ij}\, \ell n\, (a_{ij} / e_{ij})$$

$$\chi^2 = \Sigma\Sigma\, (a_{ij} - e_{ij})^2 / e_{ij}$$

where the summations are over all cells.

Results are presented in Table 4.1 and show tables of observed frequencies (1), expected frequencies (2) and expected frequencies after stepwise removal of deviant cells (4). Values of G^2 and corresponding probability are shown after each cell deletion (3). All transitions selected occur more frequently than expected. If the probability for G^2 already exceeds the specified probability of 0.1, stepwise cell deletion is not performed and the probability value (P-value) is given (e.g. Table 4.1b). The number of facies types in the data subsets varies because all facies do not occur in all unit types. A single Calcisiltite 2 layer in the roadcut section was treated as Calcisiltite 1.

Non-stationarity is a serious problem in analyzing the γ_4 data. Transition probabilities differ for the wave-cut plat-

Table 4.1a-g: Markov chain analysis

Output from program BMDP 4F (Brown, 1981) for Markov chain analysis of the entire section (Table 4.1a, facing page) and of the various unit types (Table 4.1b-g, following pages). Numbered tables in Table 4.1a are referred to in text.

(a) All section

```
**********
* TABLE PARAGRAPH  1 *
**********

*****  OBSERVED FREQUENCY TABLE  1
ASTERISK INDICATES MISSING VALUE
BELOW                                  ABOVE
            G1        G2        CW        CS1       CS2       TKSH      TOTAL
G1           0 *      31        22        88        26        11 I      178
G2          35         0 *      1         25        10         0 I       71
CW          19         3         0 *      84        13         4 I      123
CS1         89        24        86         0 *      45        11 I      255
CS2         22        12        13        46         0 *       2 I       95
TKSH        13         1         1        12         1         0 *       28
TOTAL      178        71       123       255        95        28 I      750

        TOTAL OF THE OBSERVED FREQUENCY TABLE IS     750
              SUMMED OVER    30  CELLS WITHOUT STRUCTURAL ZEROS

*****  INITIAL FITTED VALUES --ZEROS INDICATE STRUCTURAL ZEROS  -- TABLE  1
ASTERISK INDICATES MISSING VALUE
BELOW                                  ABOVE
            G1        G2        CW        CS1       CS2       TKSH
G1           0 *       1         1         1         1         1
G2           1         0 *       1         1         1         1
CW           1         1         0 *       1         1         1
CS1          1         1         1         0 *       1         1
CS2          1         1         1         1         0 *       1
TKSH         1         1         1         1         1         0 *

****************
*   MODEL  1   *
****************

MODEL                                  D.F.  LIKELIHOOD-RATIO CHI-SQUARE  PROB   PEARSON CHI-SQUARE  PROB
A,B.                                    19        99.72          .0000        97.56          .0000

*****  EXPECTED VALUES USING ABOVE MODEL
ASTERISK INDICATES MISSING VALUE
BELOW                                  ABOVE
            G1        G2        CW        CS1       CS2       TKSH      TOTAL
G1          50.3 *    16.9      31.4      100.0     23.3       6.3 I    228.3
G2          16.9       5.7 *    10.6       33.6      7.8       2.1 I     76.7
CW          31.4      10.6      19.6 *     62.5     14.6       4.0 I    142.6
CS1        100.0      33.6      62.5      198.7 *   46.3      12.6 I    453.7
CS2         23.3       7.8      14.6       46.3     10.8 *     2.9 I    105.8
TKSH         8.3       2.1       4.0       12.6      2.9        .8 *     28.8
TOTAL      228.3      76.7     142.6      453.7     105.8      28.8 I   1035.9

***** CRITERION TO SELECT CELLS IS MAXIMUM STANDARDIZED DEVIATE = (OBS. - EXP.) /SQRT(EXP.).

                                       MAXIMUM      FOUND IN CELL
STEP   CHISQUARE   D.F.    PROB       DEVIATION    BELOW     ABOVE
  0      99.72      19    .00000                  4.403     G2        G1
                                                  3.759     G1        G2
  1      74.53      18    .00000
                                                  3.364     TKSH      G1
  2      56.46      17    .00000
                                                  2.841     CS2       G2
  3      44.75      16    .00015
                                                  2.553     G1        TKSH
  4      36.71      15    .00140
                                                  2.489     G2        CS2
  5      29.75      14    .00825
                                                  2.306     G1        CS2
  6      23.66      13    .03445
  7      16.18      12    .18302

P-VALUE EXCEEDS SPECIFIED PROBABILITY LEVEL. STEPPING STOPS.

*****  EXPECTED VALUES USING ABOVE MODEL
ASTERISK INDICATES MISSING VALUE
BELOW                                  ABOVE
            G1        G2        CW        CS1       CS2       TKSH
G1           0.0 *     0.0 *    21.2       88.8      0.0 *     0.0 *
G2           0.0 *     0.0 *     4.9       20.4      0.0 *      .7
CW          22.2       5.3       0.0 *     61.6     11.1       2.8
CS1         93.1      22.1      81.6        0.0 *   46.5      11.7
CS2         14.6       0.0 *    12.8       53.7      0.0 *     1.8
TKSH         0.0 *      .7       2.5       10.4      1.4       0.0 *
```

① ② ③ ④

(b) Greywacke 1 packets, wave-cut platform section

```
**************************
* TABLE PARAGRAPH   1  *
**************************

*****  OBSERVED FREQUENCY TABLE  1

ASTERISK INDICATES MISSING VALUE

BELOW                                   ABOVE
------                                  ------
              G1          G2          CW          CS1         CS2         TKSH        TOTAL
-------------------------------------------------------------------------------------------
G1             0 *        16           3          32          18           5 I        74
G2            23           0 *         1           7           5           0 I        36
CW             2           2           0 *         4           0           0 I         8
CS1           27          10           1           0 *         4           0 I        42
CS2           18           6           1           2           0 *         0 I        27
TKSH           1           1           0           1           0           0 *I        3
-------------------------------------------------------------------------------------------
TOTAL         71          35           6          46          27           5 I       190

        TOTAL OF THE OBSERVED FREQUENCY TABLE IS     190
              SUMMED OVER   30  CELLS WITHOUT STRUCTURAL ZEROS

*****  INITIAL FITTED VALUES --ZEROS INDICATE STRUCTURAL ZEROS  -- TABLE  1

ASTERISK INDICATES MISSING VALUE

BELOW                                   ABOVE
------                                  ------
              G1          G2          CW          CS1         CS2         TKSH
-------------------------------------------------------------------------------
G1             0 *         1           1           1           1           1
G2             1           0 *         1           1           1           1
CW             1           1           0 *         1           1           1
CS1            1           1           1           0 *         1           1
CS2            1           1           1           1           0 *         1
TKSH           1           1           1           1           1           0 *

****************
*   MODEL  1   *
****************

                                                  LIKELIHOOD-RATIO              PEARSON
   MODEL                                  D.F.    CHI-SQUARE      PROB        CHI-SQUARE      PROB
   -----                                  ----    ----------      ----        ----------      ----
   A,B.                                    19       22.48        .2613          19.71        .4124

*****  EXPECTED VALUES USING ABOVE MODEL

ASTERISK INDICATES MISSING VALUE

BELOW                                   ABOVE
------                                  ------
              G1          G2          CW          CS1         CS2         TKSH        TOTAL
-------------------------------------------------------------------------------------------
G1          81.8 *      21.9         3.3         30.0        16.1         2.7 I      155.8
G2          22.0         5.9 *       .9           8.1         4.3         .7 I        41.9
CW           4.3         1.1         .2 *         1.6         .8          .1 I         8.2
CS1         27.3         7.3        1.1          10.0 *       5.4         .9 I        52.0
CS2         15.8         4.2         .6           5.8         3.1 *       .5 I        30.1
TKSH         1.6          .4         .1           .6          .3          .1 *         3.1
-------------------------------------------------------------------------------------------
TOTAL      152.8        40.9        6.2         56.0        30.1         5.1 I      291.0

******  STEPWISE CELL DELETION IS NOT PERFORMED.   P-VALUE OF MODEL FIT (    .2613)
```

(c) Greywacke 1 packets, roadcut section

```
**************************
* TABLE PARAGRAPH   1   *
**************************

*****  OBSERVED FREQUENCY TABLE  1

ASTERISK INDICATES MISSING VALUE

BELOW                                  ABOVE

              G1        G2        CW        CS1       TKSH      TOTAL
 G1            0 *      12        16        40         3 I       71
 G2           11         0 *       0         3         0 I       14
 CW           14         1         0 *       5         1 I       21
 CS1          39         1         4         0 *       4 I       48
 TKSH          4         0         0         2         0 *       6
 TOTAL        68        14        20        50         8 I      160

          TOTAL OF THE OBSERVED FREQUENCY TABLE IS     160
                SUMMED OVER    20   CELLS WITHOUT STRUCTURAL ZEROS

*****  INITIAL FITTED VALUES --ZEROS INDICATE STRUCTURAL ZEROS  -- TABLE  1

ASTERISK INDICATES MISSING VALUE

BELOW                        ABOVE

              G1        G2        CW        CS1       TKSH
 G1            0 *       1         1         1         1
 G2            1         0 *       1         1         1
 CW            1         1         0 *       1         1
 CS1           1         1         1         0 *       1
 TKSH          1         1         1         1         0 *

*****************
*   MODEL  1    *
*****************

                                                  LIKELIHOOD-RATIO              PEARSON
 MODEL                                  D.F.   CHI-SQUARE      PROB   CHI-SQUARE      PROB
 A,B,                                    11       11.37       .4130        9.93       .5364

*****  EXPECTED VALUES USING ABOVE MODEL

ASTERISK INDICATES MISSING VALUE

BELOW                                  ABOVE

              G1        G2        CW        CS1       TKSH      TOTAL
 G1        136.5 *     9.5       14.4      41.3       5.4 I     207.5
 G2          9.7        .7 *      1.0       2.9        .4 I      14.7
 CW         14.8       1.1        1.6 *     4.5        .6 I      22.6
 CS1        39.4       2.8        4.2      11.9 *     1.6 I      59.9
 TKSH        4.1        .3         .4       1.2        .2 *       6.2
 TOTAL     204.5      14.7       21.6      62.0       8.2 I     310.8

******  STEPWISE CELL DELETION IS NOT PERFORMED.   P-VALUE OF MODEL FIT (    .4130)
```

(d) Interpacket units, wave-cut platform section

```
*************************
* TABLE PARAGRAPH   1   *
*************************

*****  OBSERVED FREQUENCY TABLE  1

ASTERISK INDICATES MISSING VALUE

BELOW                                   ABOVE
                G1          G2          CW          CS1         CS2         TKSH        TOTAL
G1              0 *         3           1           19          5           1 I         29
G2              1           0 *         0           13          4           0 I         18
CW              2           1           0 *         23          12          2 I         40
CS1             21          10          30          0 *         37          4 I         102
CS2             2           5           11          38          0 *         1 I         57
TKSH            5           0           0           4           1           0 *         10
TOTAL           31          19          42          97          59          8 I         256

          TOTAL OF THE OBSERVED FREQUENCY TABLE IS     256
                SUMMED OVER    30  CELLS WITHOUT STRUCTURAL ZEROS

*****  INITIAL FITTED VALUES --ZEROS INDICATE STRUCTURAL ZEROS  -- TABLE  1

ASTERISK INDICATES MISSING VALUE

BELOW                                   ABOVE
                G1          G2          CW          CS1         CS2         TKSH
G1              0 *         1           1           1           1           1
G2              1           0 *         1           1           1           1
CW              1           1           0 *         1           1           1
CS1             1           1           1           0 *         1           1
CS2             1           1           1           1           0 *         1
TKSH            1           1           1           1           1           0 *

****************
*   MODEL  1   *
****************

                                                    LIKELIHOOD-RATIO            PEARSON
MODEL                                       D.F.    CHI-SQUARE      PROB        CHI-SQUARE      PROB
A,B.                                        19      34.92           .0143       40.42           .0029

*****  EXPECTED VALUES USING ABOVE MODEL

ASTERISK INDICATES MISSING VALUE

BELOW                                   ABOVE
                G1          G2          CW          CS1         CS2         TKSH        TOTAL
G1              2.6 *       1.6         3.7         17.5        5.6         .6 I        31.6
G2              1.6         .9 *        2.2         10.5        3.3         .4 I        18.9
CW              3.8         2.2         5.3 *       25.1        8.0         .9 I        45.3
CS1             19.0        11.3        26.8        126.3 *     40.3        4.6 I       228.3
CS2             5.8         3.4         8.1         38.3        12.2 *      1.4 I       69.2
TKSH            .9          .5          1.2         5.6         1.8         .2 *        10.2
TOTAL           33.6        19.9        47.3        223.3       71.2        8.2 I       403.6

***** CRITERION TO SELECT CELLS IS MAXIMUM STANDARDIZED DEVIATE = (OBS. - EXP.) /SQRT(EXP.).

                                        MAXIMUM         FOUND IN CELL
STEP    CHISQUARE   D.F.    PROB        DEVIATION   BELOW       ABOVE
  0       34.92     19      .01426
                                          4.499     TKSH        G1
  1       22.49     18      .21097

P-VALUE EXCEEDS SPECIFIED PROBABILITY LEVEL. STEPPING STOPS.

*****  EXPECTED VALUES USING ABOVE MODEL

ASTERISK INDICATES MISSING VALUE

BELOW                                   ABOVE
                G1          G2          CW          CS1         CS2         TKSH
G1              0.0 *       1.5         3.6         17.8        5.4         .6
G2              1.3         0.0 *       2.2         10.8        3.3         .4
CW              3.2         2.2         0.0 *       25.8        7.9         .9
CS1             16.7        11.6        27.6        0.0 *       41.4        4.7
CS2             4.8         3.4         8.0         39.4        0.0 *       1.4
TKSH            0.0 *       .3          .6          3.1         1.0         0.0 *
```

(e) Interpacket units, roadcut section

```
**************************
* TABLE PARAGRAPH   1  *
**************************

*****  OBSERVED FREQUENCY TABLE  1
ASTERISK INDICATES MISSING VALUE
BELOW                    ABOVE
                G1        CW        CS1       TKSH      TOTAL
G1              0 *       0          1         1 I        2
CW              0         0 *       10         1 I       11
CS1             1        13         0 *       3 I        17
TKSH            4         0         3         0 *        7
TOTAL           5        13        14         5 I        37

        TOTAL OF THE OBSERVED FREQUENCY TABLE IS      37
              SUMMED OVER   12  CELLS WITHOUT STRUCTURAL ZEROS

*****  INITIAL FITTED VALUES --ZEROS INDICATE STRUCTURAL ZEROS  -- TABLE  1
ASTERISK INDICATES MISSING VALUE
BELOW                    ABOVE
                G1        CW        CS1       TKSH
G1              0 *       1         1         1
CW              1         0 *       1         1
CS1             1         1         0 *       1
TKSH            1         1         1         0 *

****************
*   MODEL  1   *
****************

                                                  LIKELIHOOD-RATIO          PEARSON
   MODEL                                  D.F.  CHI-SQUARE    PROB    CHI-SQUARE    PROB
   A,B.                                      5      21.04     .0008       28.48     .0000

*****  EXPECTED VALUES USING ABOVE MODEL
ASTERISK INDICATES MISSING VALUE
BELOW                    ABOVE
                G1        CW        CS1       TKSH      TOTAL
G1              .2 *      .6        1.2       .2 I       2.2
CW             1.2        4.0 *     8.4      1.3 I      15.0
CS1            3.2       10.4      21.9 *    3.5 I      38.9
TKSH            .6        2.0       4.3       .7 *       7.7
TOTAL          5.2       17.0      35.9       5.7 I      63.8

***** CRITERION TO SELECT CELLS IS MAXIMUM STANDARDIZED DEVIATE = (OBS. - EXP.) /SQRT(EXP.).

                                    MAXIMUM          FOUND IN CELL
STEP   CHISQUARE   D.F.    PROB    DEVIATION    BELOW       ABOVE
  0      21.04      5    .00080       4.273     TKSH        G1
  1       5.44      4    .24479

P-VALUE EXCEEDS SPECIFIED PROBABILITY LEVEL. STEPPING STOPS.

*****  EXPECTED VALUES USING ABOVE MODEL
ASTERISK INDICATES MISSING VALUE
BELOW                    ABOVE
                G1        CW        CS1       TKSH
G1              0.0 *      .4       1.5        .1
CW              .2        0.0 *    10.0        .8
CS1             .8       12.1       0.0 *     4.1
TKSH            0.0 *      .6       2.4       0.0 *
```

(f) Calcareous Wacke packets

```
**************************
* TABLE PARAGRAPH   1   *
**************************

*****  OBSERVED FREQUENCY TABLE  1

ASTERISK INDICATES MISSING VALUE

BELOW                                  ABOVE

              G1        G2        CW        CS1       TKSH      TOTAL
-------------------------------------------------------------------------
G1             0 *       0         0         1         0 I       1
G2             0         0 *       0         2         0 I       2
CW             1         0         0 *      39         0 I      40
CS1            1         2        38         0 *       1 I      42
TKSH           0         0         1         0         0 *       1
-------------------------------------------------------------------------
TOTAL          2         2        39        42         1 I      86

          TOTAL OF THE OBSERVED FREQUENCY TABLE IS      86
                SUMMED OVER    20  CELLS WITHOUT STRUCTURAL ZEROS

*****  INITIAL FITTED VALUES --ZEROS INDICATE STRUCTURAL ZEROS  -- TABLE  1

ASTERISK INDICATES MISSING VALUE

BELOW                        ABOVE

              G1        G2        CW        CS1       TKSH
-------------------------------------------------------------
G1             0 *       1         1         1         1
G2             1         0 *       1         1         1
CW             1         1         0 *       1         1
CS1            1         1         1         0 *       1
TKSH           1         1         1         1         0 *

*****************
*   MODEL  1    *
*****************

                                                LIKELIHOOD-RATIO          PEARSON
    MODEL                              D.F.   CHI-SQUARE      PROB   CHI-SQUARE      PROB
    -----                              ----   ----------      ----   ----------      ----
    A,B,                                 11         6.96     .8020         5.73     .8911

*****  EXPECTED VALUES USING ABOVE MODEL

ASTERISK INDICATES MISSING VALUE

BELOW                                  ABOVE

              G1        G2        CW        CS1       TKSH      TOTAL
-------------------------------------------------------------------------
G1            .0 *      .0        .3        .7        .0 I      1.0
G2            .0        .0 *      .5       1.5        .0 I      2.0
CW            .5        .5      13.5 *     38.7       .3 I     53.5
CS1          1.5       1.5      38.3    110.1 *      .7 I    152.1
TKSH          .0        .0       .3        .7        .0 *      1.0
-------------------------------------------------------------------------
TOTAL        2.0       2.0      52.8     151.7       1.0 I    209.6

******  STEPWISE CELL DELETION IS NOT PERFORMED.   P-VALUE OF MODEL FIT (   .8020)
```

(g) Calcisiltite 2 packets

```
        ************************
        * TABLE PARAGRAPH   1  *
        ************************

***** OBSERVED FREQUENCY TABLE  1
ASTERISK INDICATES MISSING VALUE
BELOW                            ABOVE
                G1        G2        CW        CS1       CS2     TOTAL
------------------------------------------------------------------------
G1              0 *       0         1         0         2 I        3
G2              0         0 *       0         0         1 I        1
CW              0         0         0 *       1         1 I        2
CS1             2         0         0         0 *       5 I        7
CS2             1         1         1         8         0 *       11
------------------------------------------------------------I-----------
TOTAL           3         1         2         9         9 I       24

        TOTAL OF THE OBSERVED FREQUENCY TABLE IS        24
              SUMMED OVER   20  CELLS WITHOUT STRUCTURAL ZEROS

***** INITIAL FITTED VALUES --ZEROS INDICATE STRUCTURAL ZEROS  -- TABLE  1
ASTERISK INDICATES MISSING VALUE
BELOW                  ABOVE
                G1        G2        CW        CS1       CS2
------------------------------------------------------------
G1              0 *       1         1         1         1
G2              1         0 *       1         1         1
CW              1         1         0 *       1         1
CS1             1         1         1         0 *       1
CS2             1         1         1         1         0 *

****************
*   MODEL  1   *
****************
                                              LIKELIHOOD-RATIO              PEARSON
   MODEL                               D.F.  CHI-SQUARE   PROB         CHI-SQUARE     PROB
   -----                               ----  ----------   ----         ----------     ----
   A,B.                                 11       9.58     .5686            9.95       .5350

***** EXPECTED VALUES USING ABOVE MODEL
ASTERISK INDICATES MISSING VALUE

BELOW                            ABOVE
                G1        G2        CW        CS1       CS2     TOTAL
------------------------------------------------------------------------
G1             .3 *      .1        .2        .9        1.8 I      3.3
G2             .1        .0 *      .1        .3         .6 I      1.0
CW             .2        .1        .1 *      .6        1.2 I      2.1
CS1            .8        .2        .5       2.9 *      5.5 I      9.9
CS2           2.0        .6       1.3       7.1       13.6 *     24.6
------------------------------------------------------------I-----------
TOTAL         3.3       1.0       2.1      11.9       22.6 I     40.9
****** STEPWISE CELL DELETION IS NOT PERFORMED.   P-VALUE OF MODEL FIT (    .5686)
```

form and roadcut exposures because of the difficulty of recognizing Calcisiltite 2 in the latter. The organization of the sequence into units of different types also suggests non-stationarity. Initially, analysis was performed for the entire section, and a number of "preferred" facies transitions were identified (Table 4.1a). However, when the data were divided by unit type and exposure (Table 4.1b-g), only one preferred transition (Thick Shale to Greywacke 1 in interpacket units) was identified. Other transitions identified using the data for the entire section therefore arise from the non-stationarity of the system. They are only geologically meaningful in that they reflect associations of facies which occur in the different unit types.

It should be pointed out that the 6 data subsets (Table 4.1b-g) do not satisfy the criterion suggested by Brown (1981) for a chi-square distribution. He suggested that the expected frequency of any cell should not be less than 1 and that no more than 20% of cells should have frequencies less than 5. The consequence of this is that probability values are only approximate. This is not a serious problem as none of the probabilities are close to the cut-off value of 0.1.

The preferred facies transition from Thick Shale to Greywacke 1 appears to be related, at least in the roadcut section, to the transition from interpacket units to Greywacke 1 packets. The Thick Shale is the last facies in the interpacket

unit and the overlying Greywacke 1 is the first in the Greywacke 1 packet. Three out of four interpacket Thick Shale to Greywacke 1 transitions occur in this position in the roadcut section, while only one out of five do so in the wave-cut platform section, although another one is very close to the start of a packet.

Layer Thickness Trends

Layer thickness trends are important because of their central role in submarine fan facies models (Walker and Mutti, 1973; Ricci Lucchi, 1975; Mutti and Ricci Lucchi, 1975; Walker, 1978), in which thinning-upward sequences are associated with channel-fills and thickening-upward sequences with depositional lobes. Definition of such sequences has been subjective. Hiscott (1981) showed that "convincing" sequences can be produced by random draws from actual layer thickness populations, and concluded that sequences recognized subjectively by Ghibaudo (1980) could have been produced by random processes. Objective tests are difficult to apply to layer thickness analysis, because it is hard to integrate geological judgement into a mathematical test. Subjectively, we would be quite happy to dismiss a few thin siltstone layers within an otherwise well-ordered thickening-upward sequence as having come from a different source, and we would probably be correct in doing so. But it is hard to justify such adjustments in a supposedly objective

mathematical test, especially if all layers form part of the same log-normal layer thickness distribution.

Both thickening- and thinning-upward sequences, some of which form symmetric cycles, were recognized during section measurement. These were thin (maximum 3 m.) and consisted of only a few layers (maximum of 8), even allowing some deviation from a perfect trend. Much of the section lacked any consistent trend. Sequences can only be defined on the basis of detailed layer measurement; thick beds marking the base or top of trends seen on casual outcrop examination may be amalgamated (Fig. 4.4a).

Ricci Lucchi (1975) found sequences were between 2 and 70 m. thick in two formations in the Northern Apennines. In order to discover whether thicker, more general trends like these exist in the section, layer thickness for all non-lutite layers was plotted against layer number for the entire section. A new set of sequences was identified using this plot, which is shown in Fig. 4.3a and Appendix 3 (redrawn at a smaller scale). Care was taken to avoid picking sequences defined only by thick and thin layers at the base and top of the sequence. The method used to do this was to cover the points representing the top and bottom layers of the proposed sequence with sheets of paper and see if there was still a trend. The minimum acceptable length of a sequence was 5 layers, in which case there must be a consistent trend without reversals. The section was examined several times to make sure criteria for sequence selection were

Figure 4.3: Comparison of actual section with random draw, unit 29

Coarse layer thickness plots for unit 29. Layer thickness trends are shown, together with their thickness in metres. Layers more than 180 cm. thick are plotted as 180 cm. thick.

(a) Layer thickness plot for the actual section (opposite page).

(b) Layer thickness plot for a section produced by random superposition of the layers in unit 29 (next page).

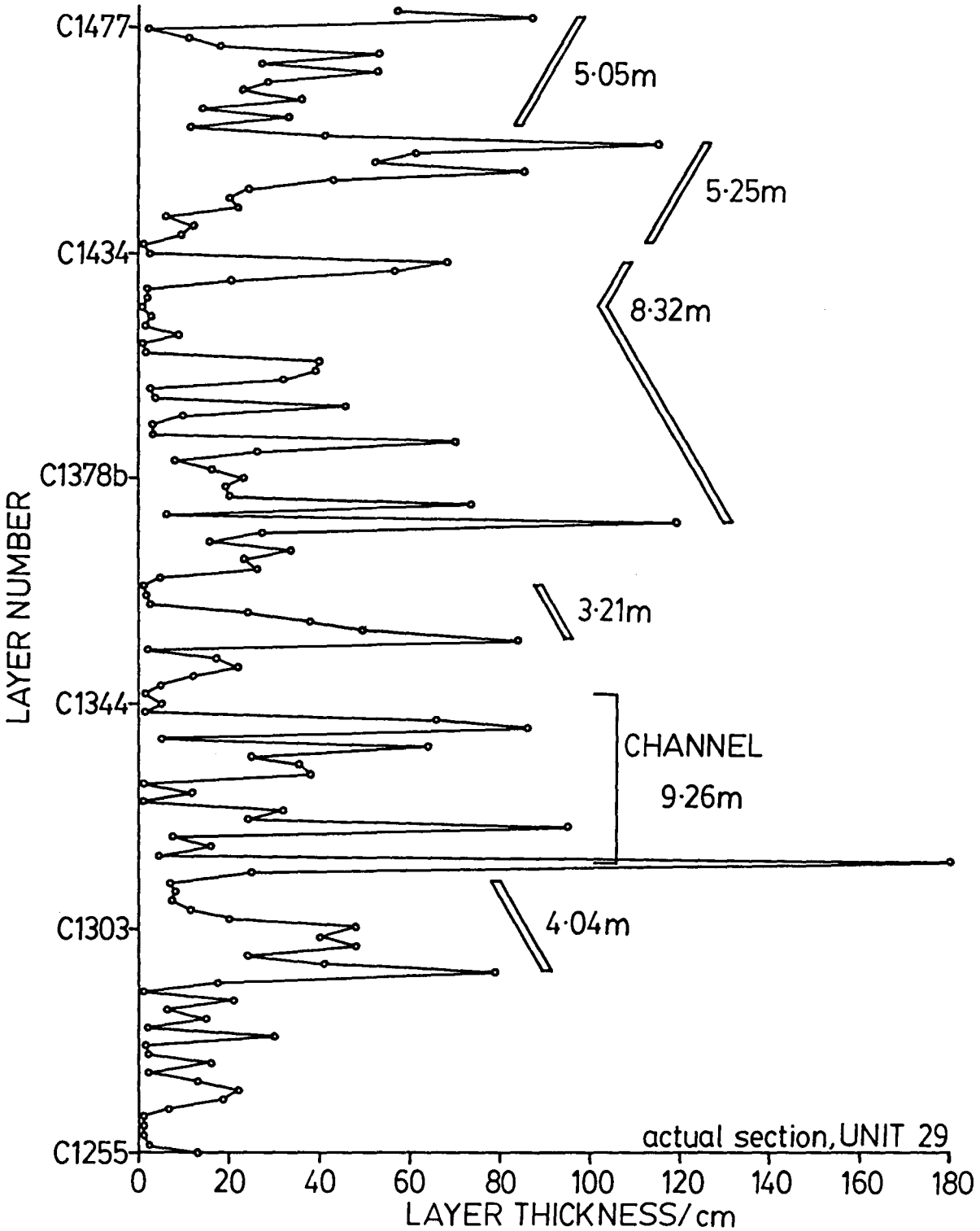
C1477
C1434
C1378b
C1344
C1303
C1255
LAYER NUMBER
5·05m
5·25m
8·32m
3·21m
CHANNEL
9·26m
4·04m
actual section, UNIT 29
0
20
40
60
80
100
120
140
160
180
LAYER THICKNESS/cm

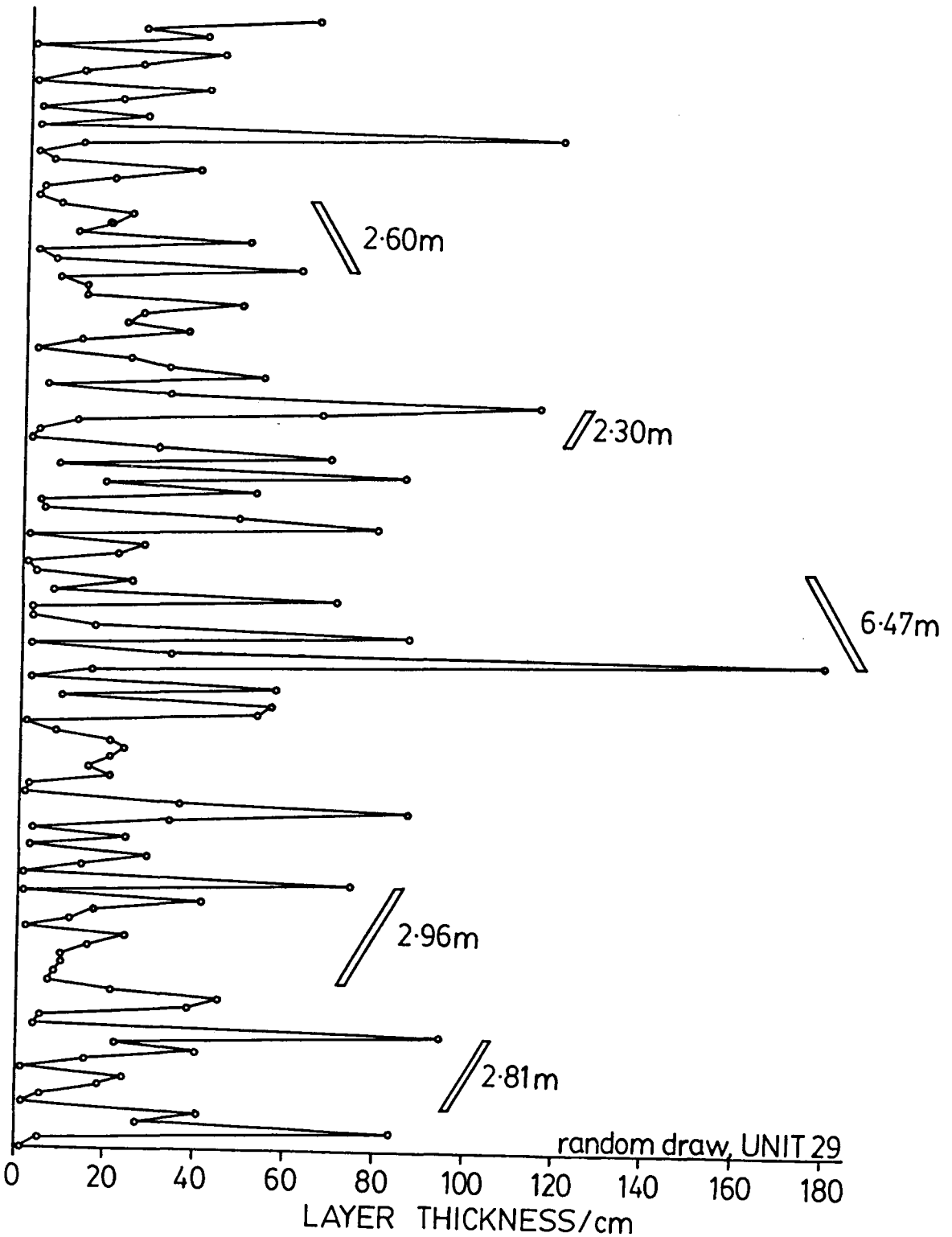
2·60m
2·30m
6·47m
2·96m
2·81m
random draw, UNIT 29
0
20
40
60
80
100
120
140
160
180
LAYER THICKNESS/cm

applied uniformly throughout the section. The section was examined from bottom to top and top to bottom to eliminate any bias from this cause. Within thin-bedded units it was found useful to plot layer thicknesses at a larger scale in order to pick out sequences. Ideally, when searching for sequences within units, layers should be plotted at a scale inversely proportional to the mean layer thickness for the unit. This eliminates the bias towards finding sequences in thick-bedded units. Since lutite thicknesses do not appear on layer thickness plots, graphic section logs were consulted to check that sequences did not contain unreasonable thicknesses of lutite, particularly between thick layers.

Sequences identified by this method were not always related to sequences seen during section measurement, but in the majority of cases they were. The old sequences were often combined or expanded into larger scale sequences identified by the new method. Examples of sequences are shown in Fig. 4.4. Statistics summarizing the sequences are shown in Table 4.2. Some sequences included parts of more than one unit; these were classified as belonging to the unit type which contained the majority of their layers. Most sequences occur in Greywacke 1 packets (Table 4.2a). Sequences are thicker than those observed directly in the field, but still fall at the low end of the 2-70 m. range found by Ricci Lucchi (1975). Sequences are thicker in Greywacke 1 and Calcisiltite 2 packets than in Calcareous Wacke

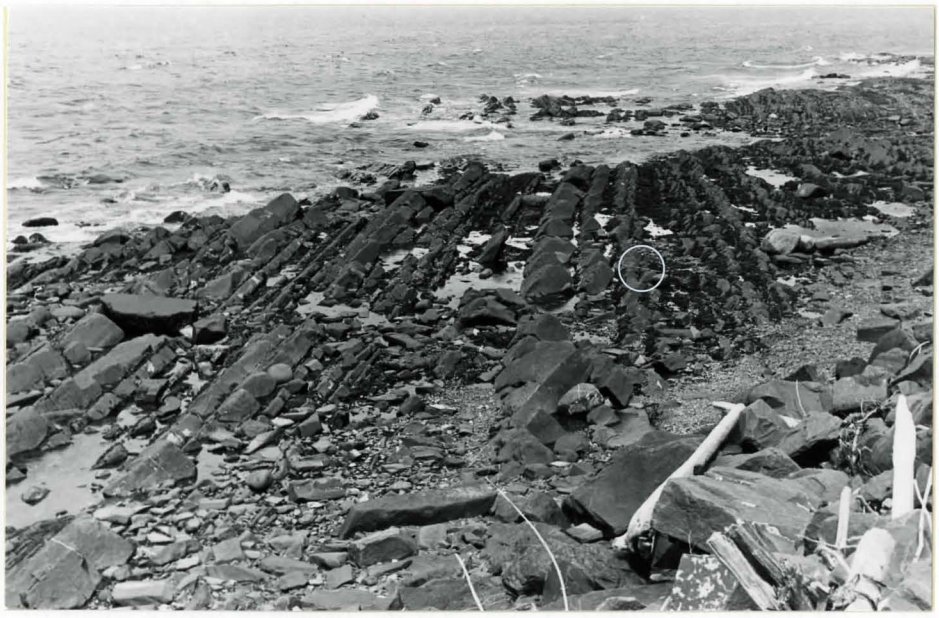

Figure 4.4a: Greywacke 1 packet (unit 5) showing gradational boundary with underlying interpacket unit (to right) and three stacked thickening-upward sequences. Final sequence extends one bed further than it appears because thickest bed is amalgamated. Scale 1 m.

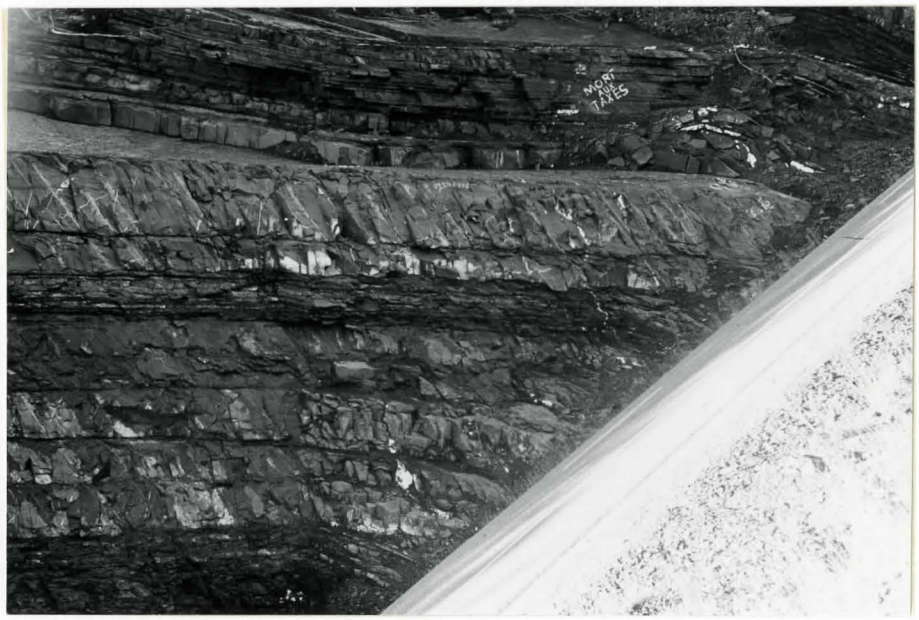

Figure 4.4b: Thinning-upward sequence from thickest bed to top of photo. Thick beds in lower part of photo form the core of a symmetric cycle (not visible). Unit 27, a Greywacke 1 packet. Scale: thickest bed is 3.1 m. thick (2 amalgamated layers).

Figure 4.4c: Thick bed in centre of photo is a sandstone sill which terminates just before waterline. Above (to left of) sill is the lower part of a Greywacke 1 packet (unit 11) which does not show layer thickness trends. Scale 1 m.

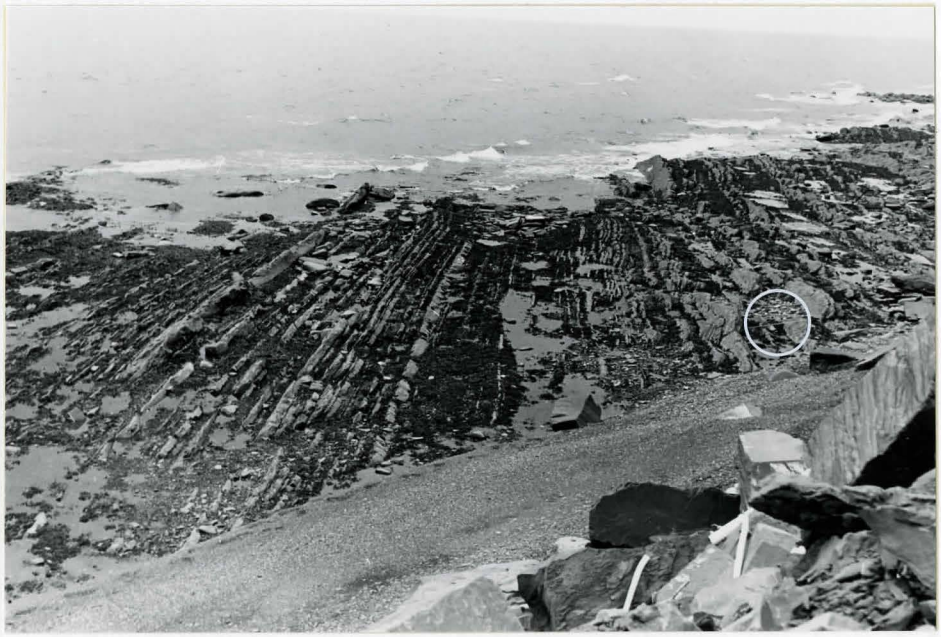

Figure 4.4d: Interpacket unit (unit 6) showing thickening-upward sequence just left of centre (1.4 m. thick). A thinning-upward sequence forming the upper part of a symmetric cycle can be seen to the left of the 1 m. scale.

Table 4.2 Layer thickness trends

(a) Summary of sequences

Unit type	Sequence type	No. of sequences	Mean thickness (m)	Mean no. of layers	Mean sand/ shale ratio
G1P	TK	18	3.26	10.1	3.10
G1P	TN	10	3.43	10.2	3.74
G1P	SYM(TK-TN)	7	5.82	21.0	4.50
G1P	SYM(TN-TK)	1	8.32	30.0	6.77
IP	TK	10	1.00	7.2	0.98
IP	TN	3	1.97	9.7	1.27
IP	SYM(TK-TN)	2	2.49	19.0	0.82
CS2P	TN	2	3.51	16.5	5.15
CWP	TK	1	1.62	9.0	0.73
CWP	TN	1	1.43	6.0	2.76

Unit types: G1P-Greywacke 1 packets, IP-interpacket units, CS2P-Calcisiltite 2 packets, CWP-Calcareous Wacke packets.

Sequence types: TK-thickening-upward sequence, TN-thinning-upward sequence, SYM-symmetric sequence.

Table 4.2 (cont'd.)

(b) Percentage of sequence types in Greywacke 1 packets and interpacket units

Sequence type	% by thickness GlP	% by thickness IP	% by no. of layers GlP	% by no. of layers IP
TK	41.4	47.9	39.5	51.8
TN	24.1	28.3	22.1	20.9
SYM(TK-TN)	28.7	23.9	31.9	27.3
SYM(TN-TK)	5.9	-	6.5	-
if symmetric sequences divided				
TK	56.0	54.2	61.4	70.5
TN	44.0	45.8	38.6	29.5

(c) Percentage of total thickness of units represented by sequences

Unit type	% thickness	% no. of layers
GlP	60.6	55.8
IP	20.4	20.4
CS2P	49.2	45.2
CWP	6.5	7.1

packets and interpacket units. This appears to be due to the thicker-bedded nature of the former, because there is little difference in mean number of layers forming sequences in the four unit types. Percentages of the sequence types are similar in Greywacke 1 packets and interpacket units, with thickening-upward sequences more common than thinning-upward (Table 4.2b). Symmetric sequences in which a thinning-upward sequence follows a thickening-upward sequence are more common than the reverse combination. Table 4.2c shows that sequences form a much smaller part of interpacket units and Calcareous Wacke packets than of Greywacke 1 or Calcisiltite 2 packets. The thickness of sequences which include more than one unit type was divided between the unit types for this calculation. Parts of the section not measured in detail were not included.

To test whether the sequences discussed above differed from those that would be produced by random superposition of layers, the method of Hiscott (1981) was applied to unit 29 (a thick Greywacke 1 packet) and to unit 2 (an interpacket unit). For each unit, layer numbers were drawn successively from a "hat" containing all remaining layer numbers in the unit. The alternation of sandstone or siltstone with lutite was preserved by considering a sandstone or siltstone layer and the overlying lutite layer as a single layer. Artificial sections were thus produced containing all the layers in the actual units, but with their order completely randomized. Coarse layer thickness plots

were drawn exactly as for the real section and the plots examined for sequences in the same manner as before (Fig. 4.3b, Appendix 3).

Sequences for the actual and random sections are described in Table 4.3a. The thickest sequence in the random section for unit 29 (6.47 m.) includes two Thick Shale horizons. This sequence would not have been acceptable in the actual section, but because the significance of Thick Shale horizons in the random section is unclear, it was included. Percentage thickness of sequences in the random sections (Table 4.3b) differs for Greywacke 1 packets and interpacket units because of the different layer thickness distributions within these units. The percentage thickness of the actual sections made up of sequences is greater than that for the random sections. The total number of layers involved in sequences is also greater for the actual sections. This strongly suggests that the actual sections are more ordered than would be expected under random processes. The percentage thickness made up of sequences for unit 29 is close to the percentage for all Greywacke 1 packets (Table 4.2c). Unit 29 is therefore similar to other Greywacke 1 packets in degree of ordering andit may be concluded that other Greywacke 1 packets are also more ordered than expected under random processes. Identical arguments can be made for interpacket units. Although no comparisons with random sections were made, it seems reasonable to assume that sequences in Calcisil-

Table 4.3 Comparison of actual section with random draws

(a) Sequences in actual and random sections

Sequence type	Thickness(m)	No. of layers	Sand/shale ratio
	Actual section, unit 29 (GlP)		
TN	4.04	11	4.81
TN	3.21	7	1.67
SYM(TN-TK)	8.32	30	6.77
TK	5.25	12	6.09
TK	5.05	13	3.65
	Random draw, unit 29		
TK	2.81	9	3.88
TK	2.96	12	2.91
TN	6.47	12	1.99
TK	2.30	5	5.87
TN	2.60	9	2.28
	Actual section, unit 2 (IP)		
TK	1.81	8	0.59
TK	0.47	6	0.34
SYM(TK-TN)	1.16	13	0.88
TN	1.67	10	1.23
	Random draw, unit 2		
TK	1.29	10	0.83
TN	0.74	5	0.36

Table 4.3 (cont'd.)

(b) Percentage thickness of units represented by sequences

Section	% by thickness	% by no. of layers
Actual unit 29	57.7	57.0
Random unit 29	38.2	36.7
Actual unit 2	28.2	25.3
Random unit 2	11.2	10.3

tite 2 packets are significant, while those in Calcareous Wacke packets are probably the result of random processes (Table 4.2c).

Another approach to the problem of layer thickness trends is the up and down test (Nederlof, 1959). Each layer is given a sign, positive or negative, depending on whether it is thicker or thinner than the layer below. Layers which are the same thickness as the layer below are ignored. This produces runs of positive signs (thickening-up) or negative signs (thinning-up) of various lengths. A simple formula predicts the number of runs of each length if thickening- or thinning-upward at each step have equal probabilities:

$$k_m = \frac{(n - m - 1)!\, n_i!\, (n - n_i + 1)!}{n!\, (n_i - m)!\, (n - n_i - 1)!},$$

where n is the number of layers, m is the length of the run and n_i is the number of transitions of a particular type (i.e. positive or negative). If thickening- or thinning-upward trends (or both) are strongly developed, we expect there to be more long runs and fewer short runs than expected under a random model.

Results of this test for unit 29 and for unit 28, which includes a Calcareous Wacke packet (28b) and an inter-packet unit (28a), are shown in Table 4.4a and b. It can be seen immediately that both units have more short runs and fewer long runs than expected. Thus, on the scale of individual layers, the section is not characterized by thickening- or thinning-upward sequences, but by a tendency for thinner layers

Table 4.4 Up and down test

Length of run	Number of tk-up sequences Actual	Predicted	Number of tn-up sequences Actual	Predicted
(a) Unit 29				
1	26	16.1	24	15.4
2	9	7.9	12	7.9
3	4	3.8	3	4.0
4	1	1.8	0	2.0
5	0	0.9	0	1.0
6	0	0.4	1	0.5
(b) Unit 28				
1	20	12.1	18	11.6
2	10	6.0	13	5.9
3	2	2.9	1	2.9
4	0	1.4	0	1.5
(c) Unit 29 (sequences only)				
1	12	9.2	12	8.4
2	5	4.4	5	4.3
3	2	2.1	2	2.2
4	1	1.0	0	1.1
5	0	0.5	0	0.5
6	0	0.2	1	0.3

and thicker layers to alternate. The same result is obtained even if only layers which form part of the previously identified sequences are considered, although the approach to the predicted values is much closer in this case (Table 4.4c).

In summary, sequences can be identified subjectively in the section, and these are probably similar to those identified by other workers (e.g. Ricci Lucchi, 1975; Ghibaudo, 1980). Both thickening-upward and thinning-upward sequences occur in sandstone packets which are not channelized on the outcrop scale (up to 100 m. along strike). The best evidence for the existence of these sequences is that they are more common in the actual section than in a random section with the same layer thickness population. Sequences occur against a background of layer by layer alternation of thicker and thinner layers, as shown by the up and down test. Even a perfect alternation of thicker and thinner layers (i.e. with runs of length 1 only) can have a larger scale layer thickness trend if the magnitude of variations in one direction is greater (e.g. if layer thickness increases are always by 2 cm. and layer thickness decreases are always by 1 cm.).

Palaeocurrents

Palaeocurrent data for each facies are presented in the form of equal area rose diagrams in Fig. 4.5. Data from sole marks and rib and furrow structure are shown separately. All

Figure 4.5a,b: Equal area rose diagrams of palaeocurrent data

Numbers in centre circles are summed reliabilities (see p.26) of readings for each facies. Area of a sector is proportional to summed reliability within the sector. Sole mark plot (b) includes data from parting lineation and oriented shale flakes or graptolites. Sole mark data are treated as non-directional because they include some non-directional elements. Sole mark plots are at the same scale as rib and furrow plots within any 180° semi-circle.

(a) RIB AND FURROW STRUCTURE

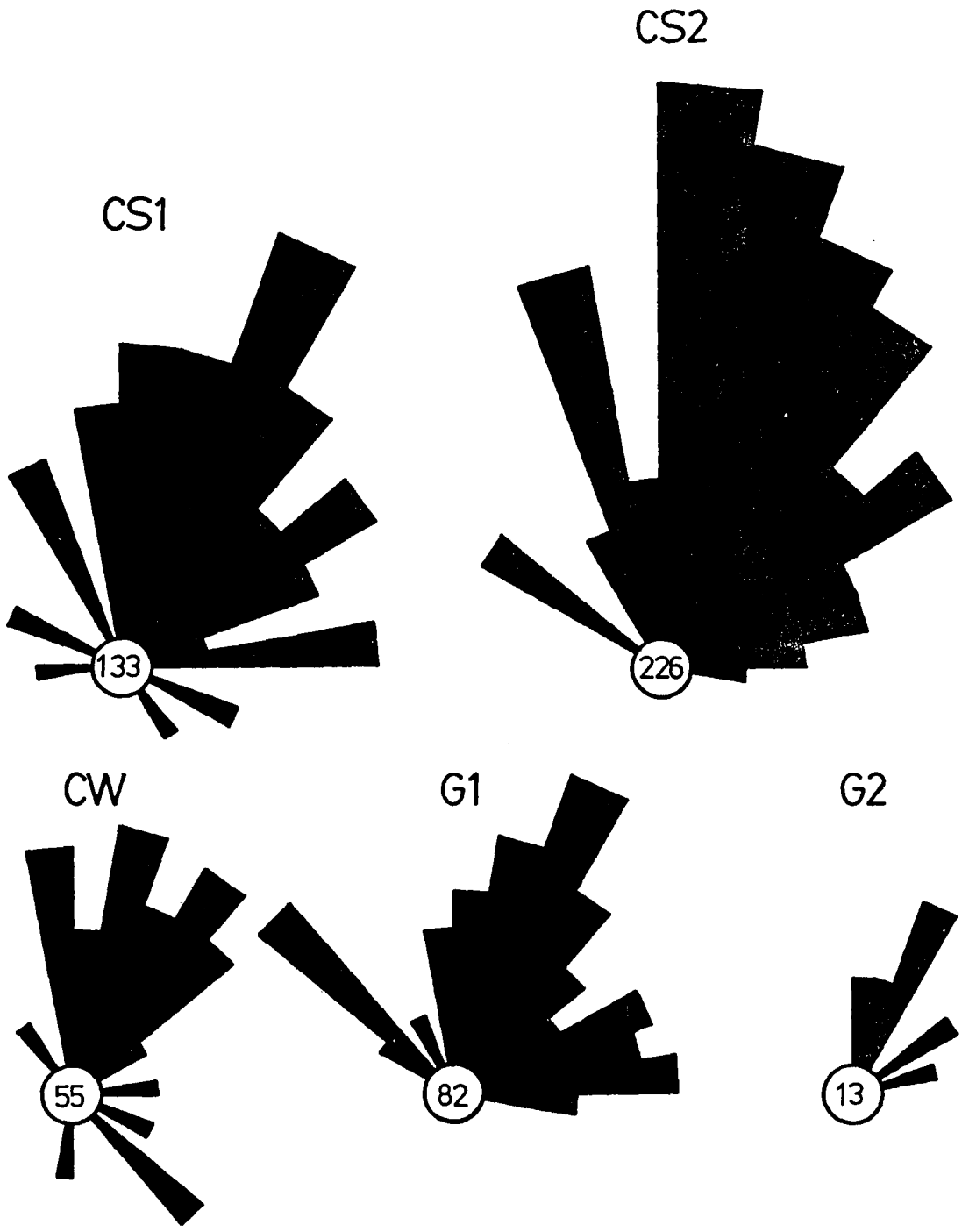

(b) SOLE MARKS

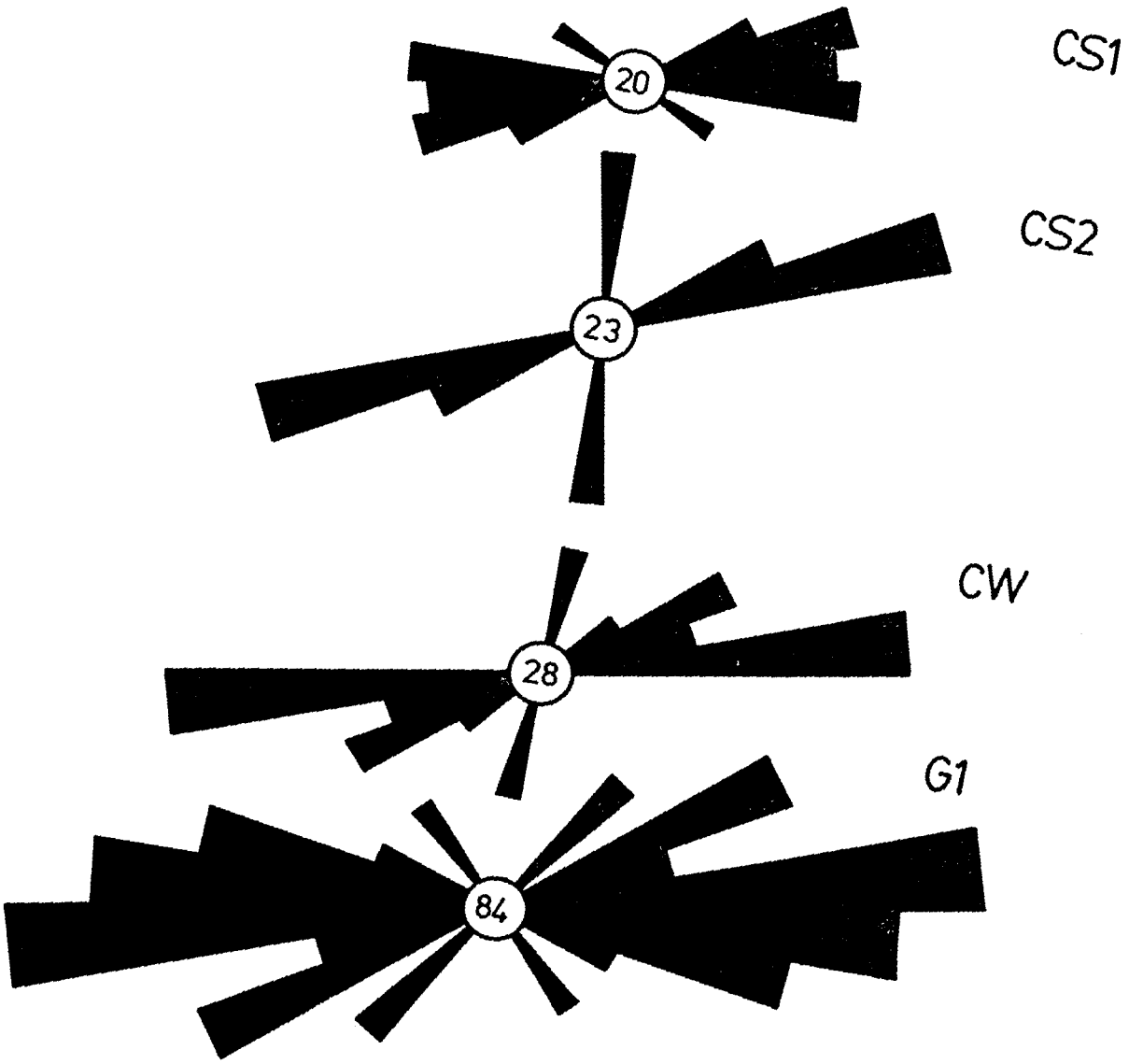

sole marks are treated as non-directional because the data includes some non-directional elements. Directed sole marks show that the direction of flow was towards the ENE, without exception. Parting lineation and oriented shale flakes and graptolites found in some Greywacke 1 and Calcareous Wacke layers agree with sole mark orientation and have therefore been included in the sole mark data.

The most notable feature of the palaeocurrent data is the anti-clockwise rotation of directions obtained from rib and furrow structure from those of sole marks by various amounts, averaging 47°. This occurs in all facies. Sole mark directions commonly fall in the range 050° to 100°. Spread of directions from rib and furrow structure is greater, reflecting the greater variability in orientation of ripple foresets than sole marks. Facies show very similar palaeocurrent patterns. Rib and furrow structure in Calcisiltite 2 shows a more northerly direction than other facies. This direction also appears as a secondary mode on the sole mark plot. This reflects the local palaeocurrent direction in the single packet from which most Calcisiltite 2 palaeocurrents were taken. Rib and furrow structures on Greywacke 1, Greywacke 2 and Calcisiltite 1 layers show a secondary mode in a direction close to the sole mark mode.

Analysis of stratigraphic variation in palaeocurrent direction requires separate treatment of rib and furrow structure and sole marks, in order to compare like with like.

Palaeocurrent means and associated parameters have been calculated for each unit (Table 4.5). Reliabilities have not been used in these calculations; all readings were given equal magnitude. Palaeocurrent means remain fairly constant throughout the section, with the exception of units 23 and 25 where rib and furrow structure is rotated clockwise from sole marks, instead of the usual anti-clockwise rotation. Sole mark directions in these units are within the normal range. In most units, the parameter L, the vector magnitude as a percentage of the maximum possible vector magnitude, is greater than the value of L for the whole section. This is because the value of L for the whole section is reduced by the variability through the section. However, values of L within units are not consistently greater than for similar lengths of the section which include more than one unit. This suggests that, in general, any variation in palaeocurrent direction occurs continuously through the section, rather than being associated with the unit organization. Similarly, it could not be shown that groups of layers forming thickening- or thinning-upward sequences had more uniform palaeocurrent directions than groups of layers lacking thickness trends. Analysis of palaeocurrent variation within units and sequences is hampered by the small number of these with many measurements. Results for sequences in which three or more layers had palaeocurrent indicators are shown in Table 4.6.

Table 4.5 Palaeocurrent means for units

Unit	Unit type	Rib and furrow $\bar{\theta}^{o}$	L	N	Sole marks etc. $\bar{\theta}^{o}$	L	N
1	GlP	357	98.99	5			
2	IP	022	85.95	47	059*	98.42	4
3	CS2P	006	91.56	92	039	85.04	11
4	IP	023	90.38	47			
5	GlP	028	83.76	42	077*	99.30	4
6	IP	037	89.65	65	066	98.68	4
7	GlP	350	94.09	6	065*	98.90	2
8	IP	033	96.84	5			
9c	GlP	060	89.76	3	080*	99.62	2
10	IP	032	99.14	2			
11	GlP	018	93.45	4	092	99.27	3
12	IP	043	93.61	5	110	-	1
13	GlP	033	92.57	11	077	99.87	4
14	IP	002	99.98	2			
15	GlP	027	93.54	15	072*	98.63	2
16	IP	057	78.23	10			
17	CS2P	037	89.91	12	089	98.65	3
18	IP	024	68.64	37	071*	99.83	6
19	GlP	026	38.19	19	073	87.82	20
20	IP	332	-	1			
21	GlP				030	-	1
23	CWP	145	89.90	5	051	89.46	4
24	IP	051	99.86	2	077*	99.68	5
25	GlP	144	-	1	073*	-	1
27	GlP	024	96.34	3	083	95.61	14
28b	CWP	083	-	1			
29	GlP				071*	99.03	2
All section		024	81.35	440	071	92.21	97

$\bar{\theta}$ - vector mean of all measurements in unit
L - vector magnitude as percentage
N - number of measurements
* - orientation only
Palaeocurrent means are also shown graphically in Appendix 3.

Table 4.6 Palaeocurrents in sequences

Unit	Type of sequence	Thickness (m)	Type of PC	No. of layers with PCs	$\bar{\theta}^{o}$	L	N
2	SYM(TK-TN)	1.16	RF	5	038	90.82	13
3	TN	5.14	RF	11	002	94.40	39
3	TN	1.88	RF	6	000	86.55	22
5	TK	4.37	RF	9	015	95.10	19
5	SYM(TK-TN)	3.01	RF	4	052	87.62	6
6	TK	1.40	RF	5	030	98.67	7
9c	SYM(TK-TN)	2.84	RF	3	060	89.76	3
13	SYM(TK-TN)	8.56	RF	5	023	96.63	8
15	SYM(TK-TN)	5.52	RF	3	036	95.52	4
19	TN	4.89	RF	3	312	86.94	9
19	TN	2.83	SOLE	3	085	98.86	10

RF - Rib and furrow structure
PC - palaeocurrent
Refer to Table 4.5 for explanation of other symbols and for unit types

Mutti-Ricci Lucchi Facies

In order to aid interpretation in terms of submarine fan facies models, the section was classified according to the facies scheme of Mutti and Ricci Lucchi (1975) and Mutti (1979). Most of the section consists of facies C and D, with facies C being dominant in Greywacke 1 packets and facies D most common in the other unit types.

A few difficulties were encountered in applying their facies scheme, mostly related to layer thickness. The thickness range given for facies C is 50-300 cm. (Mutti and Ricci Lucchi, 1975). In the γ_4 section, many layers classified as facies C on the basis of other criteria (e.g. sedimentary structures, sand/shale ratio) are thinner than this. Greywacke 2 layers containing clasts were classified as facies A_2 and many of these were also thinner than the 0.5 - 15 m. thickness given for this facies. Some γ_4 layers have a Bouma T_{ac} sequence with a thick unit of climbing ripple cross-lamination forming the T_c division. This fits neither the C_1 facies (T_{ac} with thin cross-laminated division) nor the C_2 facies (T_{abc} with thick laminated divisions). Such layers were classified as facies C_2.

The main facies occurring in each unit, along with sand/shale ratio and layer thickness means are shown in Table 4.7. Greywacke 1 packets contain C_1 facies with some C_2 and smaller proportions of D_{1-3}, A_2 and B_1 facies. Interpacket units have D_2, with some D_1 and D_3 and smaller proportions of C_{1-2}, A_2 and

Table 4.7 Unit characteristics

Unit no.	Unit type	Thickness (m)	No. of ss layers	$\bar{x}$(ss) (cm.)	$\bar{x}$(l) (cm.)	Sand/ shale ratio	Main M-RL facies
1	GlP	17.88	74	18.5	5.7	3.28	C_1
2	IP	18.13	146	5.1	7.3	0.70	$D_2(D_1)$
3	CS2P	8.48	47	15.4	2.7	5.78	$D_1(C_2)$
4	IP	25.72	199	4.9	8.0	0.62	$D_2(D_1)$
5	GlP	20.45	93	16.3	5.7	2.85	$C_1(C_2D_1D_2)$
6	IP	37.35	(192)	(6.9)	(8.8)	0.71	$D_2D_1(D_3)$
7	GlP	15.02	54	19.5	8.4	2.33	C_1
8	IP	4.92	(8)	(5.7)	(34.3)	0.12	D_3D_2
9a	GlP	4.73	15	13.5	18.0	0.75	C_1
9b	IP	4.43	(10)	(13.6)	(20.9)	0.53	$D_2D_3A_2$
9c	GlP	2.99	13	19.1	3.9	4.92	C_1
10	IP	3.04	14	3.2	18.5	0.17	D_3D_2
11	GlP	9.99	40	15.0	10.0	1.49	C_1
12	IP	8.44	(39)	(8.4)	(8.0)	0.76	D_2
13	GlP	13.94	50	19.7	8.2	2.42	$C_1(B_1)$
14	IP	3.79	13	7.1	20.5	0.32	$D_2C_1D_3$
15	GlP	12.83	55	15.8	7.6	2.09	$D_1C_1(D_2C_2)$
16	IP	8.29	(14)	(7.5)	(27.3)	0.30	$D_2(C_1D_3)$
17	CS2P	4.98	26	12.4	6.8	1.82	D_1
18	IP	8.03	72	4.8	6.4	0.76	D_1D_2
19	GlP	17.47	74	15.2	8.4	1.81	C_1
20	IP	2.39	16	3.3	11.6	0.28	D_2D_3
21	GlP	11.99	37	21.9	10.5	2.08	C_1
22	IP	4.24	8	2.2	45.2	0.04	D_3D_2
23	CWP	20.30	118	8.2	9.0	0.92	D_1D_2
24	IP	11.00	64	2.6	14.6	0.18	D_2
25	GlP	19.15	63	22.0	8.4	2.63	$C_1(C_2)$
26	IP	4.06	4	12.4	71.3	0.14	$D_3(C_1)$
27	GlP	35.04	96	31.1	5.4	5.72	$C_1C_2(D_1)$
28a	IP	2.94	6	2.0	46.9	0.04	$D_3(D_2)$
28b	CWP	17.00	94	9.0	9.1	0.98	$D_1D_2C_1(C_2)$
29	GlP	44.87	128	25.9	9.1	2.83	$C_1(C_2)$
29*	GlP	9.26	21	33.8	10.3	3.30	C_1C_2

ss - sandstone and siltstone
$\underline{l}$ - lutite
$\bar{x}$ - mean layer thickness
M-RL - Mutti-Ricci Lucchi
* - channel only
Bracketed facies are of secondary importance. Bracketed numbers refer to part of the unit measured in detail only.

G. Facies E was the only one not represented, though examples of A_1, B_2 and F are extremely rare and their classification is tentative.

Depositional Environment

Introduction

It is not intended here to prove that the γ_4 Formation was deposited on a submarine fan. This would require demonstration of the presence of all (or most) parts of a submarine fan, together with proof that they are laterally equivalent. It would also require a definition of a submarine fan, and the means to apply this definition when working in ancient sediments. However, it is hoped to show that observed facies and facies associations can be assigned to various submarine fan environments by comparison with descriptions of similar facies which have been interpreted as submarine fan deposits by other workers (Mutti and Ricci Lucchi, 1975; Mutti, 1977, 1979; Ricci Lucchi and Valmori, 1980). Arguments will also be presented against other environments in which turbidites are commonly deposited.

Environmental interpretation uses all evidence discussed in Chapters 2 to 4, especially Mutti-Ricci Lucchi facies, sand/shale ratios, mean layer thicknesses, layer thickness trends and the presence or absence of channeling. Interpretation was done on a unit by unit basis, but since nearly all units of the same

type were assigned to the same environment, discussion may be generalized to the four unit types.

Interpretation of unit types

1) Greywacke 1 packets

Greywacke 1 packets are thought to have been deposited in a depositional lobe environment. They have non-channelized, gradational boundaries with underlying interpacket units. In some cases there is a thickening-upward sequence from the interpacket unit into the Greywacke 1 packet (Fig. 4.1a, Fig. 4.4a). Similarly, the upper boundary of the Greywacke 1 packet may be marked by a thinning-upward sequence into the overlying interpacket unit (Fig. 4.1b). Within the Greywacke 1 packets, thickening-upward sequences are more common than thinning-upward sequences, indicating the generally progradational nature of the lobe deposition. Sand/shale ratios for individual units range from 0.75 to 5.72 (Table 4.7) with a mean of 2.71, somewhat lower than means of 3.30 to 28.20 for turbidite formations of the Northern Apennines (Mutti and Ricci Lucchi, 1975). Greywacke 1 packets range in thickness from 3 to 45 m., compared with the 2 - 90 m. range given by Mutti and Ricci Lucchi (1975) for lobe sandstone bodies. The dominant facies is C_1 with some C_2, which is also consistent with a lobe environment.

The only exception to the interpretation of Greywacke 1 packets as depositional lobes occurs in unit 29. Part of this

unit is interpreted as a channel-fill, with depositional lobe deposits above and below it. The channel-fill is not characterized by a well-developed thinning-upward sequence (Fig. 4.3a). The channel base has a relief of at least 60 cm. and downcutting of this magnitude also occurs between amalgamated layers within it. Lateral wedging of layers can be seen on the outcrop scale (Fig. 4.6). The channel-fill terminates with a Thick Shale horizon which is followed by more regular-bedded Greywacke 1 layers interpreted as lobe deposits. The channel-fill sequence is 9.26 m. thick where measured, suggesting a maximum exposed channel depth of about 10 m. Facies within the channel-fill are similar to those in lobes, with C_1 and C_2 dominant. Facies C_2 and D_2 were not observed in channel-fills of the Hecho Group (Mutti and Ricci Lucchi, 1975), but both are present in this example.

2) Calcisiltite 2 packets

Calcisiltite 2 packets are also interpreted as lobe deposits. The two Calcisiltite 2 packets are similar in terms of sand/shale ratio, mean layer thickness and total thickness to Greywacke 1 packets, and both types of packet have gradational, non-channelized boundaries with interpacket units. They differ in terms of Mutti-Ricci Lucchi facies in that Calcisiltite 2 packets are characterized by D_1 facies in contrast to the C_1 of Greywacke 1 packets. Packets of intermediate type exist (e.g. unit 15) which include substantial proportions of both facies

Figure 4.6: Channel-fill sequence, unit 29

Channel-fill extends from erosive base of thick, amalgamated bed to shaly horizon near top of photo. Note lateral wedging of layers within the sequence. Top is towards centre of thesis. Scale: rucksack is 40 cm. high.

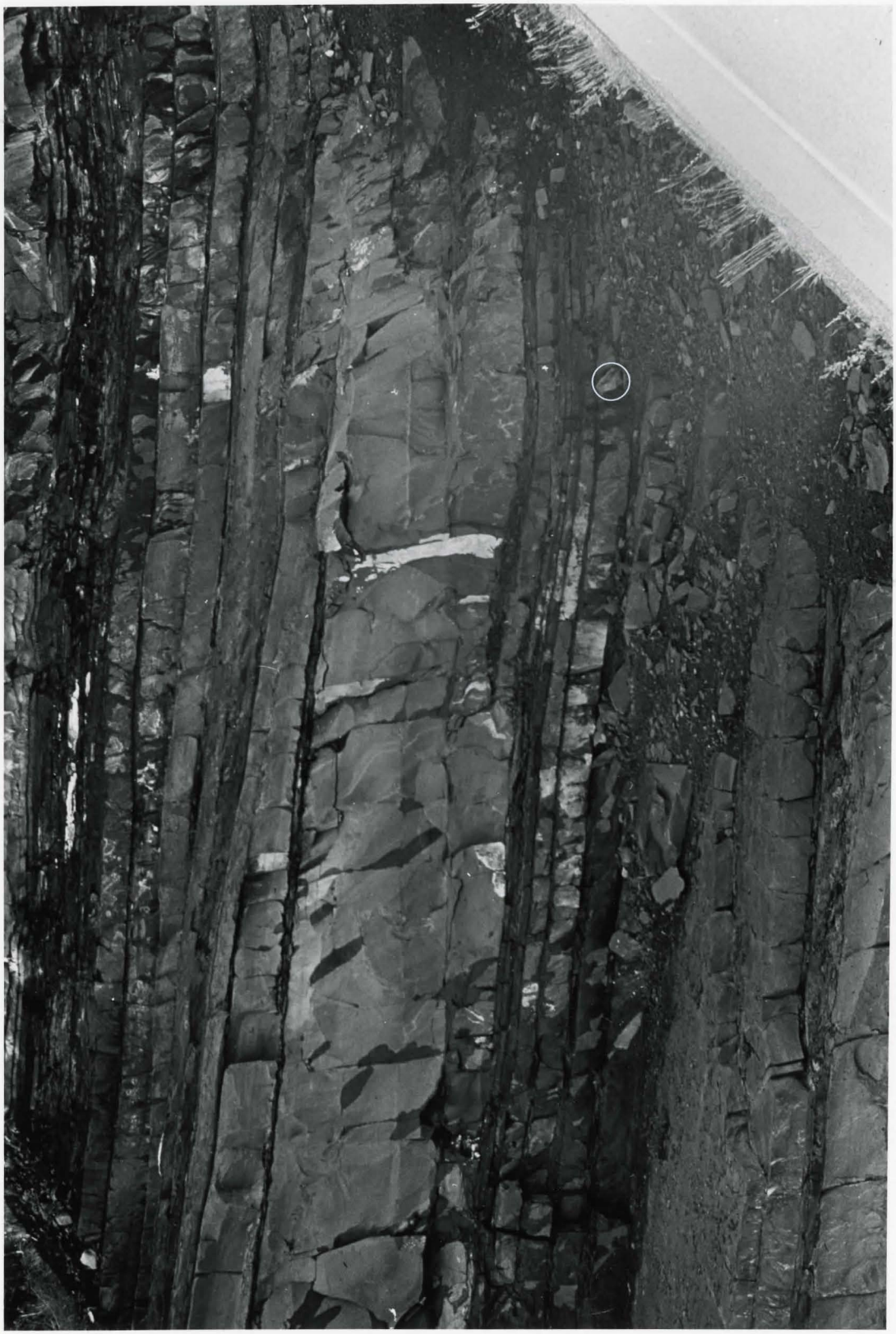

C_1 and D_1, suggesting a gradation between the two packet types. It was suggested earlier (p.119) that Calcisiltite 2 layers were deposited at the lateral margins of turbidity current paths. If this is the case, Calcisiltite 2 packets could represent the lateral margins of lobes.

Thinning-upward sequences, which occur within one of the Calcisiltite 2 packets (Fig. 2.6d), do not fit the lobe model. Calcisiltite 2 packets differ from channel-margin facies (Mutti, 1977) because they do not show dip of beds towards a channel axis or minor channeling. Furthermore, they are thicker-bedded and are not associated with channel-fill deposits.

3) Interpacket units

Interpacket units are interpreted as lobe-fringe deposits. Sand/shale ratios range from 0.04 to 0.76 and mean sandstone-siltstone layer thickness is in the range 2.0 to 7.1 cm., except for the anomalous unit 26 (see below). Mutti-Ricci Lucchi facies are mostly D_2, with some D_1 and D_3. These data are consistent with both interchannel and lobe-fringe environments (Mutti, 1977), and distinction between the two alternatives in isolation is difficult. The presence of shallow, broad channels filled by a single T_{b-e} or T_{a-e} layer may be diagnostic of interchannel facies (Mutti, 1977). Such channels were not observed in interpacket units. Interpretation as lobe-fringe deposits rather than as interchannel deposits depends largely on their vertical association with the Greywacke 1 packet lobes.

The dominance of thickening-upward sequences over thinning-upward sequences in both interpacket units and Greywacke 1 packets (Table 4.2b) suggests a lateral association between them as well.

Unit 26 consists of two Thick Shale horizons separated by a group of four Greywacke 1, facies C_1 layers. It contains no facies D_{1-2} layers and so differs markedly from the typical interpacket unit. Interpretation is uncertain, but with Greywacke 1 packets above and below it, lobe-fringe still seems the most likely environment.

4) Calcareous Wacke packets

Calcareous Wacke packets are also interpreted as lobe-fringe deposits. Sand/shale ratios are 0.92 and 0.98, with mean sandstone-siltstone layer thicknesses of 8.2 cm. and 9.0 cm. for the two examples. Mutti-Ricci Lucchi facies are mostly D_1, D_2 and C_1. Sand/shale ratio and facies are therefore consistent with a lobe-fringe environment (Mutti, 1977), but layer thickness is higher than that in lobe-fringe deposits of Hecho Group (0.37 cm. to 5.3 cm.).

General environmental interpretation

The depositional environment is therefore characterized by an alternation of lobe and lobe-fringe environments, with a single example of a shallow channel. This alternation presumably results from lobe switching due to changes in channel posi-

tion. Change in channel position by avulsion results in establishment of a new lobe in a different position and abandonment of the old lobe, which then receives only thin-bedded lobe-fringe sediments. Later, further changes in channel position result in re-establishment of lobe deposition in the area (Walker, 1978; Normark et al., 1979; Hiscott, 1980). The section can therefore be referred to the depositional and progradational system of a submarine fan (Mutti, 1979). In the model of Mutti and Ricci Lucchi (1975) this is equivalent to the outer fan, while in the models of Walker (1978) and Normark (1978) it is equivalent to the lower mid-fan.

If the channel is part of the distributary system (Mutti, 1979), it suggests a close association between distributary channels and depositional lobes, rather than their separation by a zone of bypassing as in the facies model for high-efficiency fans (Mutti, 1979). Although there is no evidence for the existence of a zone of bypassing, the fan is still thought to be a relatively high-efficiency type because of the low sand/shale ratios, abundance of facies D turbidites and the presence of well-developed depositional lobes surrounded by lobe-fringe deposits. These are all characteristic of high-efficiency fans (Mutti, 1979; Ghibaudo, 1981). There should be a spectrum of intermediate fan types between the low-efficiency and high-efficiency models, depending on variations in the sand/shale ratio of sediment supplied to the fan (Ghibaudo, 1980, 1981).

Lobe deposition

A distinction has recently been drawn between progradational and aggradational lobe deposition (Ricci Lucchi and Valmori, 1980; Hiscott, 1981; Ghibaudo, 1981). The presence of multiple or single thickening-upward sequences and gradational bases in most Greywacke 1 packets suggests that they are of the progradational type. Symmetric sequences in which a thickening-upward sequence is followed by thinning-upward seem to represent gradual abandonment of a progradational lobe, passing up into lobe-fringe sediments. Markov analysis of the sequence of Mutti-Ricci Lucchi facies within Greywacke 1 packets was carried out using the method discussed earlier in this chapter. No preferred transitions were found (Table 4.8). This suggests that there is a strong random element in lobe deposition which masks the tendency for more "proximal" facies to occur upwards within the prograding lobe (Walker and Mutti, 1973).

Enos (1965, p.92) described progradational deposition in the β_7 member as follows: "The picture that emerges is one akin to the outbuilding of a delta by a series of wedges shingled one over the other with each successive current flowing down the slope built by the deposition of the preceding current". Although this pattern applies to the groups of layers he describes, most of his longitudinal sections of groups of layers show complex patterns. Enos (1965, p.95) found that local subsidence was a more important control on deposition than thick-

Table 4.8: Markov chain analysis of lobes

Markov chain analysis of the sequence of Mutti-Ricci Lucchi facies in Greywacke 1 packet lobes (channel-fill is excluded). Explanation of tables is given in Table 4.1 and in the section on Markov chain analysis.

****
* TABLE PARAGRAPH 1 *
****

***** OBSERVED FREQUENCY TABLE 1

ASTERISK INDICATES MISSING VALUE

BELOW / ABOVE

	A1	A2	B1	B2	C1	C2	D1	D2	D3	F	TOTAL
A1	0 *	0	0	0	1	0	0	0	0	0	1
A2	0	0 *	0	0	9	1	2	2	0	0	14
B1	0	0	0 *	0	3	0	1	2	0	0	6
B2	0	1	0	0 *	0	0	1	0	0	0	2
C1	0	7	4	2	0 *	35	43	37	5	0	133
C2	0	2	2	0	26	0 *	12	9	1	0	52
D1	1	1	0	0	45	12	0 *	6	1	0	66
D2	0	5	0	0	37	6	6	0 *	1	1	56
D3	0	0	0	0	5	0	0	2	0 *	0	7
F	0	0	0	0	1	0	0	0	0	0 *	1
TOTAL	1	16	6	2	127	54	65	58	8	1	338

TOTAL OF THE OBSERVED FREQUENCY TABLE IS 338
SUMMED OVER 90 CELLS WITHOUT STRUCTURAL ZEROS

***** INITIAL FITTED VALUES --ZEROS INDICATE STRUCTURAL ZEROS -- TABLE 1

ASTERISK INDICATES MISSING VALUE

BELOW / ABOVE

	A1	A2	B1	B2	C1	C2	D1	D2	D3	F
A1	0 *	1	1	1	1	1	1	1	1	1
A2	1	0 *	1	1	1	1	1	1	1	1
B1	1	1	0 *	1	1	1	1	1	1	1
B2	1	1	1	0 *	1	1	1	1	1	1
C1	1	1	1	1	0 *	1	1	1	1	1
C2	1	1	1	1	1	0 *	1	1	1	1
D1	1	1	1	1	1	1	0 *	1	1	1
D2	1	1	1	1	1	1	1	0 *	1	1
D3	1	1	1	1	1	1	1	1	0 *	1
F	1	1	1	1	1	1	1	1	1	0 *

****
* MODEL 1 *
****

MODEL	D.F.	LIKELIHOOD-RATIO CHI-SQUARE	LIKELIHOOD-RATIO PROB	PEARSON CHI-SQUARE	PEARSON PROB	ITER.
A,B.	71	48.30	.9821	58.70	.8513	10

***** EXPECTED VALUES USING ABOVE MODEL

ASTERISK INDICATES MISSING VALUE

BELOW / ABOVE

	A1	A2	B1	B2	C1	C2	D1	D2	D3	F	TOTAL
A1	.0 *	.0	.0	.0	.5	.1	.1	.1	.0	.0	1.0
A2	.0	.5 *	.2	.1	7.9	1.7	2.1	1.8	.2	.0	14.5
B1	.0	.2	.1 *	.0	3.3	.7	.9	.8	.1	.0	6.1
B2	.0	.1	.0	.0 *	1.1	.2	.3	.3	.0	.0	2.0
C1	.6	9.2	3.4	1.1	161.4 *	34.0	42.6	37.0	4.5	.6	294.4
C2	.1	1.8	.7	.2	32.2	6.8 *	8.5	7.4	.9	.1	58.8
D1	.1	2.4	.9	.3	42.3	8.9	11.2 *	9.7	1.2	.1	77.2
D2	.1	2.0	.7	.2	35.1	7.4	9.3	8.0 *	1.0	.1	64.0
D3	.0	.2	.1	.0	3.9	.8	1.0	.9	.1 *	.0	7.1
F	.0	.0	.0	.0	.5	.1	.1	.1	.0	.0 *	1.0
TOTAL	1.0	16.5	6.1	2.0	288.4	60.8	76.2	66.0	8.1	1.0	526.0

****** STEPWISE CELL DELETION IS NOT PERFORMED. P-VALUE OF MODEL FIT (.9821) IS GREATER THAN CRITERION PROB (.1000)

ness of the previously deposited layer, because layers tend to thicken in the same place rather than compensate for thickness variations in the underlying layer.

The thickest packets at the top of the section (units 27 and 29) show more complex layer thickness trends (Figs. 4.3a and 4.4b), and lobe portions of these may have been aggradational. Aggradational growth may be typical of the more proximal parts of lobes (Ricci Lucchi and Valmori, 1980). This is in agreement with the presence of a channel in unit 29, suggesting that the upper Greywacke 1 packets are in a relatively proximal lobe position. Large-scale progradation of the submarine fan, indicated by an upward increase in thickness of Greywacke 1 packets through most of the section also suggests that the upper units are the most proximal (Fig. 4.7).

The question of the degree of topographic expression of the depositional lobe area is extremely important when comparing ancient sediments with modern submarine fans. In the case of the γ_4 Formation, knowledge of lobe topography is crucial to understanding of the deposition of Calcisiltite 2 packets at the lobe margin. Mutti (1979) has suggested that the depositional lobe area in high-efficiency fans may be represented by a submarine plain in modern fans, explaining the apparent absence or rarity of such fans at the present day (Normark, 1980; Normark and Hess, 1980; Ghibaudo, 1981). This is a surprising statement, since lobe switching, progradation and aggradation

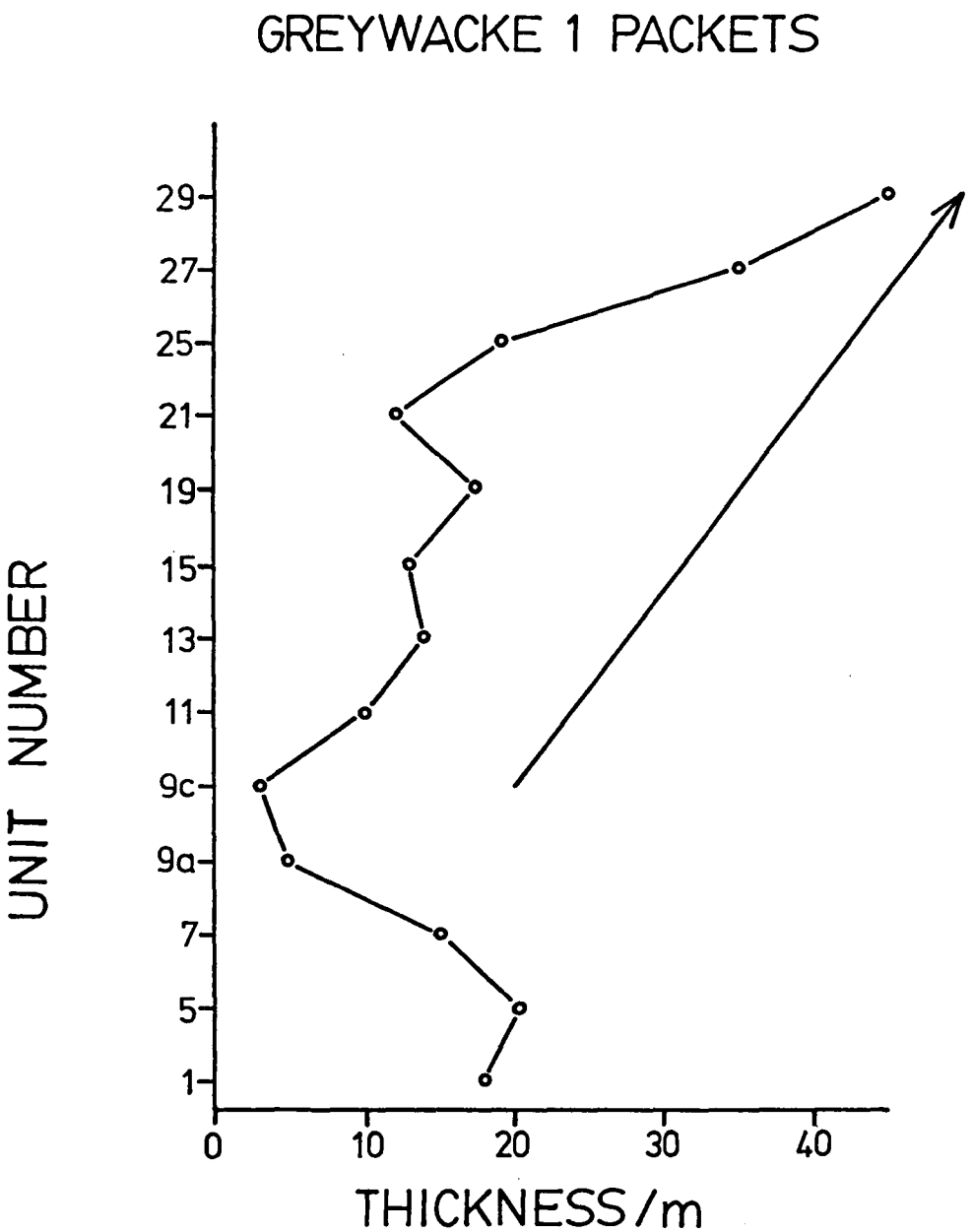

Figure 4.7: Plot of Greywacke 1 packet thickness against unit number, showing the upward increase in thickness of packets within the section.

are all related to topographic expression of the lobe. Perhaps the problem is simply the difficulty of resolving the subdued lobe topography in modern environments with existing techniques.

Size of depositional lobes

No long-distance correlations of layers or packets were possible in the γ_4 Formation, so the size of depositional lobes is not known. Correlations of individual layers were made by Enos (1969b) in part of the β_7 member where similar non-channelized packets occur. Although individual layers are discontinuous, all three packets can be traced across the five sections, a distance of 3.0 km. in the downcurrent direction (Enos, 1965, plate 5). These results were confirmed by Parkash (1969, Fig. 1.4). In Parkash's figure the sections are extended upwards and his correlation shows a Calcisiltite 2 packet which thins dramatically over the 3.0 km. interval. Rapid thinning is consistent with the hypothesis that Calcisiltite 2 packets represent the lateral margins of depositional lobes. The strike of Parkash's section is almost exactly parallel to the mean palaeocurrent in the area, but palaeocurrent variability is sufficient that a lateral termination rather than a downcurrent termination of a packet could be seen. These correlations suggest that sandstone lobes have a minimum downcurrent extent of 3 km.

In the lower part of the β_7 member, Enos (1965, p.86)

was able to correlate units 10 - 50 m. thick defined by laterally continuous marker beds of Dolomite and Limestone. This allowed correlation of Greywacke units and Calcisiltite units (Enos, 1969a), which are probably similar to the Greywacke 1 packets and interpacket units defined in this study. Of the six Greywacke units, three have more or less wedged out after the 10.5 km. distance and three are continuous over this distance. This provides further evidence that the continuity of packets is much greater than that of individual layers.

Continuity of depositional lobes and their individual layers in other ancient turbidite formations appears to be very variable. Correlations based on widely-spaced outcrops or well-logs must be treated with caution. Extrapolation of thickness gradients to estimate lobe sizes is a very dubious procedure because there is no reason why lobes should thin in a linear way. Ricci Lucchi and Valmori (1980) believe that the discontinuity of layers in the Cloridorme Group is anomalous, but their comparison is mostly with basin plain turbidites, which should be much more continuous than submarine fan turbidites. They were able to correlate sandstone lobes over distances from 24 - 57 km. in the Marnoso-Arenacea. Some component layers wedge out within 10 km. while others are continuous through all the measured sections. Most of these continuous layers are "mega-turbidites" more than one metre thick, and so are not comparable with the thinner layers correlated by Enos. Mutti *et al*. (1978)

traced sandstone lobes and most individual layers over an area of 16 km^2 in the Laga Formation. Correlated distances were 2 km. in the downcurrent direction and 4.5 km. (in some cases up to 8 km.) perpendicular to current direction. Again, layers which can be correlated across the whole area are thick sandstones one metre or more in thickness; thinner layers are more discontinuous. Sandstone lobes in the Laga Formation can also be correlated over distances of 11.5 km. and perhaps as much as 30 km. downcurrent on the basis of SP-resistivity logs (Casnedi et al., 1978). In the San Salvatore sandstone (Mutti, 1975), most lobe sandstone bodies undergo rapid thinning followed by total disappearance over distances of 2 to 5 km. downcurrent. These three examples are all from the Northern Apennines, Italy. Hirayama and Nakajima (1977) traced individual turbidite layers for 30 km. downcurrent in the Otadai Formation of Japan. Since turbidite layers die out upcurrent and have thinned considerably by the most downcurrent outcrop, this distance is probably close to their total extent. The turbidites are thought to represent the channelized suprafan to smooth outer suprafan (Normark, 1970) of a submarine fan deposited in a trench-slope basin.

Comparison of continuity in these turbidite formations is difficult because the upcurrent and downcurrent terminations of a sandstone body are not usually seen, and so lengths are minimum values and are a function of outcrop length as much as actual length. However, continuity of Cloridorme sandstone

bodies is not radically different from that of other formations. The only way in which the Cloridorme Group is anomalous is that individual layers are discontinuous relative to some other formations (Ricci Lucchi and Valmori, 1980). This seems to be partly a result of comparisons of continuity between layers of different thicknesses. Thin layers in the Laga Formation are not continuous over the outcrop area even though thick (1 m. plus) layers are (Mutti et al., 1978). On the other hand, in the Otadai Formation layers of similar thickness to those in the Cloridorme Group are much more continuous.

Lobe-fringe deposition

The absence of packets composed dominantly of Greywacke 2, which might be predicted to occur downcurrent of Greywacke 1 packets (p.105), suggests that not all Greywacke 1 layers pass downcurrent into Greywacke 2. The alternation of the Greywacke 1 packet depositional lobes with interpacket unit lobe-fringe sediments suggests that the downcurrent and lateral transtion to Calcisiltite 1 is more important. Thick Greywacke 2 layers with abundant clasts which occur in interpacket units are thought to be debris flows originating from slumping of lobe-fringe sediments, and are not downcurrent equivalents of Greywacke 1. No slump scars were observed, but a local source is suggested by the facies types (Argillite, Calcisiltite, Calcareous Wacke) of clasts found in the layers. Greywacke 2

layers are similar to slurried and chaotic beds described by other workers. Slurries in fan-fringe deposits have been attributed to current erosion on top of lobes (Mutti et al., 1978; Ricci Lucchi and Valmori, 1980). Hiscott (1977, p.132) found slurry sandstones were associated with channel abandonment. Pickering (1981) found chaotic beds at the base of proximal lobes, and these were interpreted as due to erosion of fan-fringe sediments by the first lobe-building flows. None of these explanations appear to fit the thick Greywacke 2 layers of the γ_4 Formation.

Calcareous Wacke packets are thicker-bedded units associated with interpacket lobe-fringe units. They are thought to be deposits of turbidity currents which were closer to autosuspension than those which deposited Greywacke 1 layers (p.107). These currents may have bypassed depositional lobes and only begun to deposit sediment as relatively thin, continuous layers in lobe-fringe regions. Calcisiltite 1 layers in the lobe-fringe area were probably deposited by both Calcareous Wacke-type and Greywacke 1-type turbidity currents which had already dropped all sediment coarser than fine sand (p.121).

Alternative models

Could turbidites of the γ_4 Formation have been deposited in an environment other than a submarine fan? The main non-fan environments of siliciclastic turbidite deposition are

basin plains of various types (Rupke, 1978), and deep-sea channels (Nelson and Kulm, 1973). A further possibility is that sediment was supplied from a number of different sources or from a line source similar to those in carbonate slope systems (McIlreath and James, 1979), rather than from a point source as in the submarine canyon-fan model.

Characteristics of basin plain sediments include long-distance continuity of layers, lack of abrupt vertical or lateral changes in facies, and absence of distinct thinning- and thickening-upward sequences (Mutti and Ricci Lucchi, 1975; Rupke, 1978; Ricci Lucchi and Valmori, 1980). Individual layers in a possible ancient trench basin plain have been traced for 115 km. by Hesse (1974). Basin plain sediments may display palaeocurrent directions with divergences up to 180° as a result of sediment dispersal from opposite sources (Mutti and Ricci Lucchi, 1975). None of these characteristics apply to the γ_4 Formation, though palaeocurrent reversals between adjacent beds do occur in other parts of the Cloridorme Group (γ_3 and β_7 units: Enos, 1969b; Bhattacharjee, 1970, p.149).

Continuity of layers deposited in deep-sea channels also seems to be high. Turbidite sand layers in the Cascadia Channel (NE Pacific) can be traced for at least 170 km. downchannel (Griggs et al., 1969). Sands and gravel are restricted to the channel in the Northwest Atlantic Mid-Ocean Channel (NAMOC); levee deposits are finely (1 mm.) laminated silts and clays

(Chough and Hesse, 1976). The NAMOC has a meandering channel and thalweg, with evidence of point bars and lateral accretion surfaces analogous to those in fluvial channels. The channel position appears to be controlled by oceanic basement features and is stabilized by high levees which are present along almost its entire length. In deep-sea channel deposits, sands should be restricted to a relatively narrow linear zone, surrounded by large volumes of clay and thin silts. Grain size contrast between channel and non-channel deposits will be much greater than between submarine fan depositional lobes and lobe-fringe sediments. Frequent vertical alternation between thick- and thin-bedded facies is unlikely because of channel stability.

If turbidity currents were supplied from various geographically distinct sources, packets might represent successive deposits from the same source. Palaeoflow must have been controlled by the basin shape rather than by source area, because of the relative uniformity of mean sole mark direction between packets (Table 4.5). Layer thickness trends within packets could be produced by mechanisms such as progradation as in submarine fan turbidites, or by control of size of flows at the source. A difficult problem with this model is the cause of a shifting source of siliciclastic detritus. Switching of fluvial delta lobes or complexes is one possibility, but it seems unlikely that this would be reflected so clearly in packet-interpacket alternation in a depositional area distant from

the source. Delta switching rates for the Mississippi (Frazier, 1967) are much too high to account for packets in the γ_4 Formation, based on the sedimentation rate calculated in Chapter 5.

There appears to be no siliciclastic equivalent of the carbonate-type line source of sediment. A line source could not explain the packet organization unless packets were produced by regional changes such as tectonic events or sea level variations. Production of multiple thickening-upward sequences within packets by source area events seems unlikely. Packet organization and sequences are much more likely to have been produced by processes acting within the depositional area itself. If carbonate production was occurring on the adjacent shelf during Cloridorme deposition, as is suggested in Chapter 5, it is possible that some Calcisiltite 1 layers could have been supplied to the basin independently of the main sand dispersal systems.

Facies and facies relationships in the γ_4 Formation and in the β_7 member studied by Enos (1965) are therefore different from those observed and predicted for non-fan turbidite environments, particularly in relation to continuity of layers, packet organization and layer thickness trends.

CHAPTER 5

PALAEOGEOGRAPHY DURING CLORIDORME GROUP DEPOSITION

Source Area

The source area of the Cloridorme Group sediments has been discussed in detail by Enos (1965, p.73). Provenance of sandstones of the Tourelle Formation, which are very similar in composition to those in the Cloridorme Group, has been worked out in great detail by Hiscott (1978).

The most useful indicator of provenance in the Cloridorme Group is the presence of chromite and serpentine. These indicate that an ophiolite was exposed in the source area and this is identified with the Mont-Albert and Mount Serpentine ultramafic rocks to the south and their eroded equivalents. Chromite is not present in ultramafic rocks of the Canadian Shield to the north (Enos, 1965, p.74). Three samples taken from the γ_4 Formation did not contain chromite or serpentine, and were rich in quartz (Enos, 1965, p.61). It seems that ophiolites may not have been exposed in the source area during γ_4 deposition, but the close similarity with other Cloridorme rocks suggests that the γ_4 was also derived from a southerly source.

The maturity of the heavy mineral assemblage, plus the presence of sandstone or siltstone rock fragments suggests that erosion of pre-existing sedimentary rocks provided some of the Cloridorme material (Enos, 1965, p.79). Volcanic rock fragments are rather silica-rich, although some may be as mafic as Andesite (Enos, 1965, p.75). Feldspar grains are virtually all plagioclase, which has the composition of oligoclase where identification is possible. Volcanic material may have been supplied from erosion of the upper Tetagouche Group calc-alkaline volcanics of northern New Brunswick (Enos, 1965, p.79). If volcanism was occurring in the Tetagouche area during Cloridorme deposition, as is suggested by the presence of Caradocian graptolites in slates interbedded with the volcanics (Ruitenberg et al., 1977), it could have provided the Volcanic Ash layers in the Cloridorme Group as well. Fine-grained carbonate was probably supplied as calcareous ooze from a carbonate shelf surrounding the source land (Enos, 1965, p.81).

The source area for the Cloridorme Group therefore lay to the south of the outcrop area. It consisted of a land area which included sedimentary rocks, a large ophiolite (Hiscott, 1978) and a volcanic arc. An adjacent shelf was an area of carbonate production, and may have been cut by submarine canyons connected directly to fluvial deltas, which allowed funneling of terrigenous material into the basin (Enos, 1965, p.81; Hiscott, 1977, p.446). Some mixing between river-derived sand

and shallow marine material must have occurred to account for the rare shallow marine fossils and the fine-grained carbonate. Shallow marine fossils are not found in Tourelle sandstones, and carbonate is less abundant with only 2% of siltstones being calcisiltites (Hiscott, 1977, p.36) compared with almost 100% in the Cloridorme.

Depositional Environments, Cloridorme Group

Interpretation of depositional environments of ancient turbidites should ideally be done on the basis of detailed sedimentological section measurement and study of lateral and downcurrent variation in facies. Detailed study of the γ_4 Formation has led to its interpretation as the depositional lobe system of a submarine fan. Considerable information is available on the characteristics of other parts of the Cloridorme Group, and it seems worthwhile to consider whether these can be tentatively assigned to submarine fan environments. It should be noted that the β_1 and β_2 members at Grand Etang (St. Hélier) and Cloridorme discussed below appear to be of a younger age than the rest of the Cloridorme Group (J. Riva, pers. comm., 1982).

Inspection of facies proportions for each member or formation (Table 5.1) reveals three distinct facies associations at this scale. The first is similar to the γ_4 Formation taken as a whole, and is interpreted as an outer fan facies associa-

Table 5.1 Facies proportions, Cloridorme Group

Member or formation	Estimated thickness (m)	Facies %							
		ARG*	DOL + LST	CS1	CS2	CW	G1	G2	G3
Facies association 1									
γ_4	1000	37.9	4.7	7.3	5.0	6.9	33.9	4.2	-
γ_2	800	41.0	0.9	4.3	12.1	0.1	37.5	4.1	-
β_7	835	44.1	0.7	6.7	9.6	0.6	31.1	7.3	-
β_5	80	46.5	0.6	4.3	5.4	-	35.8	7.5	-
β_3(est.)	43	40	-	10	25	-	25	-	-
Facies association 2									
γ_3	475	70.2	4.3	13.4	-	9.4	2.0	0.5	0.2
β_6	255	78.4	2.5	15.9	0.4	0.6	2.0	0.1	0.1
β_4	78	64.3	0.5	28.7	3.4	1.8	0.9	0.4	-
β_2	490	77.4	0.2	17.7	-	4.2	0.3	-	0.2
γ_4-IP(WCP)	-	59	4	14	8	6	4	6	-
γ_4-IP(RCT)	-	62	19	15	-	3	2	-	-
Facies association 3									
γ_1	550	83.4	3.2	3.2	-	0.8	0.3	-	9.2
β_1	1175	70.4	1.9	7.2	-	6.7	-	0.3	13.5

* - includes Dolomitic silty Argillite
WCP - wave-cut platform section
RCT - roadcut section

Table modified from Enos (1965, Table 2).

tion (Mutti and Ricci Lucchi, 1975). The second is quite similar to the interpacket units within the γ_4 Formation, and is interpreted as a fan-fringe facies association, deposited in a lobe-fringe area which was never reached by the depositional lobes (Mutti, 1977). The third type is dissimilar from any part of the γ_4 Formation, and is interpreted as a basin plain facies association.

Facies association 1 (outer fan)

Table 5.1 shows that these units have remarkably similar facies proportions. The high Dolomite and Limestone percentage in the γ_4 Formation probably results from the inclusion of some dolomitic and calcareous Argillite (see also percentages for interpacket units). The γ_4 Formation is the only one with significant amounts of Calcareous Wacke. A channel with a north-south orientation was seen on a reconnaissance survey of the γ_2 Formation at La Grande Anse. This indicates encroachment of a distributary system into the area, as suggested for the γ_4 Formation.

The β_7 member has already been discussed in terms of a depositional lobe and lobe-fringe environment (p.173). Palaeocurrent reversals in adjacent layers of Calcisiltite 2 (Bhattacharjee, 1970, p.23) can only be explained by overlapping depositional lobes, either of the same submarine fan or of separate submarine fans (Hiscott, 1980). The discontinuous layers and packet organization of the β_7 member argue against a basin plain environment, which might otherwise be considered on the basis of palaeocurrent reversals. Packets probably also

occur in the thin (43 m.) β_3 member where Enos (1965, p.55) describes Greywackes which form "groups of fairly thick beds".

Facies association 2 (fan fringe)

Comparison of this group with total facies percentages for interpacket units in the wave-cut platform and roadcut sections of the γ_4 Formation (Table 5.1) shows their broad similarity. The thick Greywacke 2 layers which occur in the wave-cut platform interpacket units (Fig. 2.11d) do not seem to be significant elsewhere. The γ_3 Formation seems particularly rich in Calcareous Wacke, a feature it shares with the γ_4 Formation. These formations yield palaeocurrent directions to the east, in contrast to the westward directions in the rest of the group. The β_4 member has a higher than usual percentage of Calcisiltite 1 and also has Calcareous Wacke layers which appear in the downcurrent direction (Enos, 1965, p.55). The latter observation is consistent with the idea that Calcareous Wacke turbidity currents bypassed lobes and only began to deposit sediment in the lobe-fringe area (p.177). It could also be accounted for by lateral spreading of turbidity currents, so that the appearances represent lateral rather than upcurrent margins of layers (Ricci Lucchi and Valmori, 1980).

Facies association 3 (basin plain)

In this facies association, the Greywacke 1 and Calci-

siltite 2 layers typical of depositional lobe areas are virtually absent. The unusual Greywacke 3 layers, which are characteristic of this association, and Calcareous Wackes show considerable downcurrent continuity and uniformity. These layers have been correlated over 12 km. in the downcurrent direction by Skipper (1971) in the β_1 member. Correlations show that the thickness of the middle pseudonoduled division of Greywacke 3 layers increases downcurrent, as does the thickness of Argillite (Skipper, 1970, p.21). Greywacke 3 layers show no consistent downcurrent change in maximum quartz grain size at the base (Skipper, 1970, p.72).

Skipper and Middleton (1975) suggested that Greywacke 3 layers were deposited from large turbidity currents flowing over relatively low slopes. The front part of the currents was turbulent and in a state close to autosuspension. This condition would explain why these flows bypassed the fan and continued to flow for long distances over the relatively flat basin plain. The presence of Calcareous Wacke layers in this association again supports the idea that they were deposited from turbidity currents close to autosuspension which had bypassed lobes.

The Greywacke 3 and Argillite of the γ_1 Formation are abruptly overlain by Greywacke 1 of the γ_2 Formation at their boundary (Enos, 1965, p.59). This is a direct superposition of facies association 1 on facies association 3, interpreted as a

depositional lobe deposited onto a basin plain. It is surprising that the two are not separated by a fan-fringe deposit.

Dispersal System Geometry

Cloridorme Group sediments are thought to have been derived from a southerly source area, yet palaeocurrent directions indicate that flow was dominantly towards the west, with flow towards the east in the γ_4 and γ_3 Formations (Table 5.2). This pattern may be explained by turning of turbidity currents through 90° on entering the longitudinal basin. This would produce asymmetric, longitudinal submarine fans rather than classically fan-shaped, transverse submarine fans.

In the Tourelle Formation, a similar westward palaeocurrent pattern was interpreted as due to a southwestward slope along the axis of the longitudinal basin (Hiscott, 1980). This slope was thought to be due to the diachronous closure of the early Palaeozoic ocean from northeast to southwest (Dallmeyer, 1977). In the Cap Enragé Formation (Cambro-Ordovician, Quebec), turbidites supplied from a source area to the northwest are thought to have turned through 90° at the base of the continental slope to flow southwestwards along a base-of-rise channel (Hein and Walker, 1982). Turbidity currents may have been forced to flow in this direction because of a submarine topographic obstruction. A similar pattern occurs in the Grosses Roches conglomerate of the Cap des Rosiers Group (Hendry, 1973, 1976).

Table 5.2 Palaeocurrent directions, Cloridorme Group

Facies association	Member/ formation	$\bar{\theta}^{o}$	s	N
1 (outer fan)	γ_4	071	22	97
	γ_2	262	26	297
	β_7	271	37	1583
	β_5	287	32	117
2 (fan fringe)	γ_3W	252	16	23
	γ_3E	071	11	83
	β_6	284	14	155
	β_4	304	25	61
	β_2	299	22	259
3 (basin plain)	γ_1	260	13	114
	β_1	282	15	553

γ_3W - west directed palaeocurrents in γ_3
γ_3E - east directed
s - standard deviation. Standard deviations are weighted averages of standard deviations for each section in the member or formation. Standard deviation for γ_4 is converted from L (see Table 4.5 for this and other symbols) using the graph of Curray (1956). γ_4 data is from sole marks only (this study), remainder from Enos (1969b).

Westward to southwestward flow in the Quebec Appalachians is therefore a continuing feature through Cambrian and Ordovician time. The diachronous closure of the ocean could account for the westward slope in part of the Cloridorme Group, but cannot explain flow in the Cap Enragé Formation, because it was deposited during opening of the ocean (Hein and Walker, 1982).

In the γ_4 and γ_3 Formations, the slope must have been locally reversed. Interlayering of beds with opposite palaeocurrents at the base of the γ_3 Formation (Enos, 1969b) indicates an almost flat area with an eastward slope on its western side (γ_4-γ_3 system) and a westward slope on its eastern side (γ_2 system). This may be interpreted as the merging of the fan-fringe areas of two oppositely-directed, asymmetric submarine fans.

Table 5.2 shows that mean palaeocurrent direction does not change systematically through the three facies associations. However, there does appear to be a broad trend of decreasing standard deviation from outer fan to basin plain facies associations. This might be explained by the greater topographic variation in the lobe area, with local slopes created by lobe topography. In the relatively flat basin plain area, flow would be controlled by the regional slope and might therefore be less variable. Such changes must occur over long distances, because Enos (1965, p.121) found no change in palaeocurrent variance downcurrent in correlated

intervals within the β_7, β_6 and β_1 members. Parkash (1970) found that the variance of sole mark directions increased downcurrent in individual layers in the β_7 member, because of meandering of currents in the downcurrent area.

Graptolite dating (Riva, 1968) suggests that the β_7 and γ_2 units are of the same age. They also have similar facies proportions, thicknesses and palaeocurrent directions (Tables 5.1, 5.2). Although the β_7 outcrops upcurrent of γ_2, γ_2 appears to have a slightly more proximal character (higher percentage of Greywacke 1 and Calcisiltite 2, lower percentage of Argillite). This need not imply that they were deposited on separate submarine fans. Proximality will vary laterally as well as downcurrent and so depends on the position of the outcrop "slice" through the fan relative to the fan axis. Eastward palaeocurrents in the β_7 member (Bhattacharjee, 1970, p.23) could then mark the beginning of the transition to eastward flow which is also seen at the base of the γ_3 Formation. Working downwards stratigraphically, the γ_1 Formation must be roughly equivalent to at least members β_3-β_6, based on thickness comparisons. In this case, facies associations for the age-equivalent units differ: γ_1 is basin plain but β_3 to β_6 are outer fan and fan fringe. Paleocurrents are westward, so that the downcurrent facies change is as expected.

The number and size of submarine fans responsible for

Cloridorme Group deposition is unclear. Opposite palaeocurrents suggest that at least two are involved. The γ_4-γ_3 system probably represents a single submarine fan, with a thickness of approximately 1500 m. (Table 5.1). Nelson and Kulm (1973) give a thickness range of 500-3000 m. for medium-sized fans (e.g. Astoria Fan, NE Pacific). The γ_4-γ_3 fan would appear to fit into this range, though it should be noted that the outer fan and fan-fringe sediments only constitute a part of the maximum fan thickness. The β sequence is more difficult to decipher because its members alternate between fan fringe and outer fan facies associations. Members β_3 to β_7 have a combined thickness of about 1300 m., which is similar to that of the γ_4-γ_3 pair. If fan size depends on regional factors, a single fan interpretation would seem most likely for this part of the β sequence.

Rotation of Rib and Furrow Structure from Sole Marks

A difficult feature to account for in the γ_4 Formation is the consistent anti-clockwise rotation of palaeocurrent directions obtained from rib and furrow structure relative to those from sole marks by an average of 47° (Table 4.5). Only units 23 and 25 show a clockwise rotation. This feature has not been reported in other studies of the Cloridorme Group.

Most of Enos's (1969b) data (Table 5.2) were taken from sole marks. Some readings were taken from rib and furrow structure, but these were not treated separately, and no mention was made of any systematic difference from sole marks. Walker (1969) noted that rib and furrow structure on Calcisiltite 2 layers in the β_7 member gave directions close to sole marks on the same layers and to the sole mark mean for the area. Bhattacharjee (1970, p.23) also noted strong parallelism between sole marks and rib and furrow structure in the β_1 and β_7 members. Parkash (1969, p.177) observed gradual changes in grain orientation and graptolite orientation from the base to the top of individual Greywacke 1 layers in the β_7 member. Changes occur in both clockwise and anti-clockwise directions relative to sole marks, even in a vertical section through a single layer. These changes are thought to be due to meandering of turbidity currents (Parkash and Middleton, 1970). The rose diagram of significant grain orientations (Parkash and Middleton, 1970, Fig. 3) shows that most orientations are close to the sole mark direction, but that secondary modes are seen in the sectors 50-60° clockwise and anti-clockwise of sole mark direction. Forty-six thin sections exhibit significant clockwise deviation from sole marks while only 30 show significant anti-clockwise deviation.

The similarity between rib and furrow structure and

grain orientation patterns is intriguing, but the differences are important. Rib and furrow structure is consistently rotated anti-clockwise from sole marks through a thick stratigraphic interval (at least 250 m.). Grain orientation is not consistently rotated even at different levels within individual layers. Also, the rotated rib and furrow direction forms the principal mode of the distribution, while rotated grain orientations only form a secondary mode.

The explanation suggested for the rotation of rib and furrow structure from sole marks involves the interplay of momentum and local slope in determining the course of an unconfined turbidity current. A turbidity current or a part of a turbidity current with high momentum will be relatively little affected by local slope; it may even flow uphill for some distance (e.g. Woodcock, 1976). In contrast, a low-momentum turbidity current will be much more affected by the slope on which it travels, and will tend to move down the line of maximum slope. Sole marks are cut by the high velocity, erosive head of the turbidity current. Ripples on or near the top of a turbidite layer are formed by the low velocity tail of the current. Ripple directions (rib and furrow structure) are therefore thought to represent the direction of maximum local slope, while sole marks indicate the direction of travel of the head of the current. Direction of movement of the head of the current must be controlled

in part by the orientation of the distributary channel mouth. The degree of lateral spreading of a turbidity current increases as its velocity decreases. Consistent anti-clockwise rotation of palaeocurrent direction requires that the outcrop area lay on one side of the depositional axis. Ripple directions could represent the direction of the lateral slopes of a depositional lobe or of the fan itself. The consistent sense of rotation and its occurrence even in lobe-fringe areas suggests the latter. It is possible that the fan was distorted in such a way that most current swings were anti-clockwise and to the NNE. The two units with clockwise rotation indicate that lobe topography may be important in some cases, as it is unlikely that the fan axis would migrate back and forth across the depositional area. However, it is difficult to see how flow direction could have been rotated 94° clockwise in unit 23 (Table 4.5).

The explanation given above is not very convincing, but seems the most likely of the available alternatives. There must have been some peculiarity in the fan shape which caused this unusual pattern. It does not explain the grain orientation patterns; these must be due to some other, unrelated cause which is unknown. Bottom current reworking cannot account for the palaeocurrent rotation. Bottom currents would most likely flow along the axis of the longitudinal basin and would therefore be parallel to sole mark direc-

tions. Bottom currents would be unlikely to produce the rates of deposition necessary for the formation of climbing ripples in Calcisiltite 2 layers, which show a northward flow direction. Meandering of turbidity currents (Parkash and Middleton, 1970) would not give a consistent sense to the palaeocurrent rotation. Deviation due to the Coriolis force would be negligible (< 3^{o}) at the 15^{o}S palaeolatitude of Cloridorme Group deposition (Bambach et al., 1980), based on parameters in Table 3.1. The swing of palaeocurrent direction through a layer due to Coriolis force would be the small difference between the Coriolis deviation acting on the part of the turbidity current which cut the sole marks and the part which formed the ripples. The difference arises because Coriolis deviation depends on the velocity and density of the current, which change during deposition.

Sedimentation Rate

Calculation of the sedimentation rate of the Cloridorme Group depends upon estimates of the absolute lengths of graptolite zones made by Carter et al. (1980). These authors calculated pure pelagic shale and chert sedimentation rates in the Ordovician and Silurian as 4 ± 1 metres of rock per million years, using known radiometric dates. Using this rate, thicknesses of graptolite zones were converted into absolute lengths in millions of years. The method requires

that rates of pelagic sedimentation were constant during this period.

The Cloridorme Group was deposited during the Dicranograptus clingani zone (Riva, 1968, 1974), and probably covers most of the length of this zone. The D. clingani zone is estimated to be at least 6.5 m.y. long (Carter et al., 1980). Its lower boundary with the Diplograptus multidens zone is uncertain; it must lie somewhere within the 7.0 m.y. "passage beds" interval of the Phi Kappa Formation, Idaho (Carter and Churkin, 1977). The "passage beds" contain a sparse fauna and cannot be divided between the two zones. J. Riva (pers. comm., 1981) has examined the graptolite collections used by Carter et al. (1980) and believes there is an unconformity or faunal gap in their sections corresponding to the D. multidens zone and part of the D. clingani zone. If this is correct, the sections obviously could not be used to estimate the length of these zones.

A further piece of evidence relating to the length of time of Cloridorme deposition comes from the L.G.P.L. core on the island of Anticosti, located about 110 km. north of the Cloridorme outcrop area. Here, the Macasty Shale includes an apparently complete Canajoharie and Lower Utica sequence (D. clingani zone) which is 85 feet (26 m.) in thickness. The contact between this black shale and the underlying Trenton limestone is sharp and is marked by a thin layer of pyrite,

indicating a disconformity. Graptolites from the base of the black shale suggest that the base is close to the beginning of the D. clingani zone (lower Canajoharie) and are similar to the oldest fauna in the Cloridorme Group (Riva, 1968). If the pelagic sedimentation rate of 4 m./m.y. is applied to this shale it gives a figure of 6.5 m.y. for the length of the zone, in agreement with the minimum estimate of Carter et al. (1980). For this reason, 6.5 m.y. is considered the best estimate of the time interval for deposition of the Cloridorme Group.

The thickness of the group may be estimated from the data in Table 5.1. The γ_2 and β_7 units are considered to be equivalent, so the thickness is taken as that of the β_3-β_6 units plus the γ_2-γ_4 units. Total thickness is 2731 m., which gives an average sedimentation rate of 420 m./m.y. This figure must be considered as a rather rough approximation, in view of the uncertainty over both the thickness and timespan of Cloridorme deposition.

Sedimentation rates for selected modern and ancient turbidite units are shown in Table 5.3. The Cloridorme sedimentation rate is seen to be similar to those in other submarine fan turbidites. It is closest to the values for the Astoria Fan and the Marnoso-Arenacea. Both of these examples are considered to have unusually high sedimentation rates. The high rate in the Astoria Fan results from the lowering

Table 5.3 Sedimentation rates of modern and ancient turbidites

Formation or fan	Environment	Age	Rate (m/m.y.)	References
Astoria Fan	Middle and lower fan	Pleistocene	360-600	Nelson, 1976
Delgada Fan	Edge of fan	Miocene-Pleistocene	10-38	Wilde et al., 1978
Monterey Fan	Suprafan	Holocene	104	Hess and Normark, 1976; Wilde et al., 1978
Nile Cone	Lower fan channel area	Pleistocene-Holocene	80->320	Maldonado and Stanley, 1978
Laga Formation	Fan average	Miocene-Pliocene	>1000	Mutti et al., 1978
Macigno Formation	Fan average	Oligocene	600	Sagri, 1975
Marnoso-Arenacea	Fan averages	Miocene	150-750	Ricci Lucchi, 1975
Ventura basin	Longitudinal basin turbidites	Pliocene-Pleistocene	1000-3000	Blackie and Yeats, 1976; Hsu et al., 1980
Cloridorme Group	Outer fan	Middle Ordovician	420	

of sea level during the Pleistocene (Nelson and Kulm, 1973); that in the Marnoso-Arenacea results from deposition in a confined basin (Ricci Lucchi, 1975). Active tectonism in the source area and confinement within a narrow basin are the most likely causes for the high rate of deposition of the Cloridorme Group.

Comparison with Tourelle Formation Submarine Fans

Similarity of source areas for the Tourelle Formation and Cloridorme Group suggests that sediment supplied to the basins should have been broadly similar. Because fan type (e.g. high-efficiency or low-efficiency) depends on grain size characteristics of sediment input (Mutti, 1979; Normark and Hess, 1980), we might expect Tourelle and Cloridorme submarine fans to be similar. However, Hiscott (1980) describes Tourelle fans as small and steep, and analogous to the modern La Jolla fan (30 by 22 km.). On the basis of Hiscott's work, Ghibaudo (1981) interprets the Tourelle Formation as having been deposited on a low-efficiency (sand-rich) fan. The γ_4 Formation of the Cloridorme Group has already been referred to a relatively high-efficiency model (p.168). Earlier in this chapter, it was suggested that the γ_4 Formation was deposited on a medium-sized submarine fan with a thickness of at least 1500 m. These interpretations imply that Cloridorme submarine fans were larger and were supplied with a higher

proportion of fine sediment (more pelite-rich) than those of the Tourelle.

Comparison of the Cloridorme and Tourelle is difficult because the Tourelle represents a more proximal fan facies than the Cloridorme and might reasonably be expected to be more "sand-rich" on this basis alone. Comparison of the more distal parts of the Tourelle Formation (facies association 3 of Hiscott, 1980) with the more proximal parts of the Cloridorme Group (γ_4 Formation) shows that they are quite similar. Both consist of an alternation of thick-bedded sandstone packets with thin-bedded siltstone-shale units, interpreted as depositional lobe and lobe-fringe deposits, respectively. If Thick Shale and Siltstone-Shale facies in the Tourelle are considered as Mutti-Ricci Lucchi facies D, the total thickness percentage of facies D in facies association 3 is about 35% (Hiscott, 1980). Facies D percentage in the γ_4 is approximately equal to the percentage of Calcareous Wacke and Calcisiltite 2 packets plus interpacket units, a total of 47%. This is of interest because the proportion of facies D in low-efficiency fans should be much less than in high-efficiency fans (Mutti, 1979). It should be added that the proportion of facies D is much less in the more proximal facies associations 1 and 2 of the Tourelle Formation (Hiscott, 1980). Sandstone packets of the Tourelle generally contain thicker layers than in the γ_4 Formation. This could indicate

a more proximal lobe environment, or reflect the larger volume of sediment carried by turbidity currents on the Tourelle fan.

No firm decision can be made on similarity or difference between Tourelle and Cloridorme submarine fans on the basis of facies comparison, because equivalent facies are not exposed. If they do represent low- and high-efficiency types, a change in grain size characteristics of sediment input is implied, despite the similar source areas. This suggests change in weathering processes and/or relief in the source area. Input of fine-grained carbonate to the Cloridorme system may also have been important.

SUMMARY

Facies and Depositional Mechanics

Most of the thickness of the measured section in the γ_4 Formation is made up of Argillite and Greywacke 1. Subsidiary facies are Calcareous Wacke, Calcisiltite 1 and 2, and Greywacke 2. With the exception of Greywacke 2 and some Argillite, all of the above are interpreted as deposits from turbidity currents of various types. These turbidites were deposited on depositional lobes and in lobe-fringe areas of a submarine fan.

Greywacke 1 layers are normally graded, medium to very coarse sandstones averaging 26 cm. in thickness. They show Bouma T_a sequences, with T_{ac} and T_{ab} sequences less common. Modelling of turbidity currents suggests that flows were supercritical (Froude number greater than 1) at the start of deposition. This appears to be incompatible with the presence of parallel lamination and cross-lamination in the upper parts of some layers, since these structures are thought to have formed beneath subcritical flows. Deposition of the lower part of a layer from a supercritical flow, followed by deposition of the upper part from a subcritical flow, is considered unlikely because there is no record of the pas-

sage of a hydraulic jump, such as a scoured surface, in the layers. Deposition of the entire layer from a subcritical flow is therefore favoured. It is concluded that a lag effect operates due to the time taken for turbidity current velocity to adjust to changes in slope, and to the time taken for sediment to fall out from suspension once conditions are right. Calculated Froude numbers therefore represent coditions some distance upstream from the outcrop area. Turbidity currents must have already gone through a hydraulic jump, perhaps at a distributary channel mouth, before reaching the area.

Greywacke 2 layers have almost 50% argillaceous matrix, and many contain large (e.g. 30 cm.) clasts of Argillite and Calcisiltite, which are most common towards the tops of layers. These layers are interpreted as deposits of laminar debris flows. Consideration of simple debris flow mechanics suggests that they came to rest on slopes of about 0.01. This slope is higher than that anticipated for the outer part of a submarine fan (0.002 to 0.006). The simple model of debris flow is considered inadequate; strength may not have been uniform throughout the flow, allowing movement along relatively weak zones while clasts were supported in stronger rigid plug areas. In this way, debris flows could have moved on lower slopes than 0.01 and still supported the observed clasts.

Calcareous Wacke layers are characterized by the

presence of traction structures, a low argillaceous matrix content, and a high proportion of carbonate cement relative to Greywacke 1. Carbonate cement is thought to be recrystallized calcareous ooze. Presence of traction structures suggests slower deposition than for Greywacke 1 layers. Slower deposition, abundant flutes on soles, and lateral persistence of layers indicate that turbidity currents were closer to autosuspension than those which deposited Greywacke 1.

Climbing ripple cross-lamination is the most distinctive feature of Calcisiltite 2 layers. Climb occurs without erosion of stoss-side laminae (Type B or depositional-stoss). Layers average 10.8 cm. in thickness and have poor lateral continuity, passing into Argillite in distances of less than a mile (1.6 km.) according to Enos (1965, p.30). Calcisiltite 1 layers are thinner, with a mean thickness of 3.2 cm., and cross-lamination is characterized by erosion of stoss-side laminae (Type A or erosional-stoss), in contrast to Calcisiltite 2. Stoss preservation suggests that Calcisiltite 2 layers were deposited more rapidly than Calcisiltite 1. Rapid deposition over a short distance may have been caused by a sudden break in slope encountered by the turbidity currents which deposited Calcisiltite 2. Calcisiltite 1 layers were deposited more slowly from turbidity currents which experienced a gradual change in slope, and which may have been close to autosuspension.

Dark-grey Argillite contains no sedimentary structures which would indicate current action during its deposition. Lateral transitions from Calcisiltite 2 to Argillite within a layer suggest that at least some Argillite was deposited by turbidity currents. Transitions from Greywacke 2 to Argillite may indicate deposition of Argillite from a fine-grained turbidity current associated with the Greywacke 2 debris flow. Most Argillite is thought to have been deposited from fine-grained, dilute turbidity currents. Some of these were associated with sandy turbidity currents, but others occurred independently.

Facies relationships and facies organization allow some conclusions to be drawn on the changes which occurred in turbidity current properties downcurrent and with time. Facies which are interpreted to have been deposited from flows with different properties may have been deposited from the same flow at different points along its course. One such downcurrent trend is that from Greywacke 1 to Greywacke 2 to Argillite, which is interpreted as a change from turbidity current to debris flow to fine-grained turbidity current deposition. Trends from Greywacke 1 to Calcisiltite 1 and from Calcareous Wacke to Calcisiltite 1 downcurrent are inferred from facies relations, though transitions are not observed. Turbidity currents which deposited Calcareous Wacke may have had different properties from those which deposited Greywacke

1 because of their higher content of fine-grained material, or because of the presence of fine-grained carbonate rather than terrigenous clay. A trend from Greywacke 1 to Calcisiltite 2 to Argillite is thought to be a lateral rather than downcurrent trend, representing the different conditions from the centre to the edges of an unconfined turbidity current.

Facies Organization and Depositional Environment

The measured section of the γ_4 Formation shows a well-developed alternation of thicker-bedded, higher sand/shale ratio units (packets) with thinner-bedded, lower sand/shale ratio units (interpacket units). Most packets consist dominantly of Greywacke 1 interbedded with Argillite, and are referred to as Greywacke 1 packets. Calcisiltite 2 and Calcareous Wacke packets are less common. Interpacket units consist of Argillite with Calcisiltite 1 layers and minor amounts of other facies. Markov analysis of the facies sequence in each unit type reveals only one preferred transition, that from Thick Shale (Argillite more than 50 cm. in thickness) to Greywacke 1 in interpacket units. This transition probably represents the boundary between underlying interpacket units and overlying Greywacke 1 packets. Analysis of the section as a whole identifies a number of additional preferred transitions, but these only reflect the facies associations in the four unit types (i.e. the non-stationarity of the seq-

uence).

Examination of layer thickness plots shows that thickening-upward sequences are more common than thinning-upward sequences in Greywacke 1 packets and interpacket units. Comparison of parts of the actual section with random sections constructed from the same layer thickness population suggests that the actual section is more ordered than would be expected under a random model. Layer thickness trends are superimposed on a layer by layer tendency for thicker and thinner layers to alternate.

Palaeocurrent means for each unit remain fairly constant through the section. Palaeocurrent variation occurs continuously through the section, and is not associated with unit organization or with layer thickness trends. Palaeocurrent directions from rib and furrow structure are generally rotated anti-clockwise from those of sole marks by an average of 47^{o}.

Characteristics of each unit type may be used to deduce the depositional environment. Greywacke 1 packets are interpreted as depositional lobe deposits on the basis of: non-channelized, gradational boundaries with underlying interpacket units; dominance of thickening-upward sequences over thinning-upward; Mutti-Ricci Lucchi facies C_1 and C_2; thicknesses of 3 to 45 m.; and sand/shale ratios averaging

2.71. Part of one Greywacke 1 packet is interpreted as a channel-fill because of its erosive base and the lateral wedging of layers within it. The channel depth is about 10 m. and it has lobe deposits above and below it. The channel has no layer thickness trend, but does terminate with a Thick Shale horizon. Calcisiltite 2 packets are also interpreted as lobe deposits, because of their similarity and possible gradation with Greywacke 1 packets. They may represent lateral margins of lobes. They differ from Greywacke 1 packets in having facies D_1 rather than C_1, and one of the two Calcisiltite 2 packets contains two thinning-upward sequences, which are difficult to explain in a lobe model. Interpacket units are mostly composed of facies D_2, with some D_1 and D_3. They are interpreted as lobe-fringe deposits rather than interchannel because of their vertical association with Greywacke 1 and Calcisiltite 2 lobe deposits. Presence of mostly thickening-upward sequences suggests a lateral relationship to Greywacke 1 packets as well. Calcareous Wacke packets are also interpreted as lobe-fringe deposits because of their facies D_1, D_2 and C_1, and sand/shale ratios close to 1. Mean layer thickness (9 cm.) is rather high for lobe-fringe facies. They do not have significant layer thickness trends.

The depositional environment is therefore characterized by an alternation of lobe and lobe-fringe environments, with a single example of a shallow channel. This alternation

is thought to result from lobe switching due to changes in channel position on a submarine fan. The environment may be described as the depositional and progradational system of a submarine fan (equivalent to outer fan or lower mid-fan). The fan is thought to be a relatively high-efficiency type, though the close association of a channel with depositional lobes suggests that a zone of bypassing was not developed.

Most lobes are of the progradational type, as indicated by their gradational bases and by their internal organization into multiple or single thickening-upward sequences. Thinning-upward sequences at the top of some lobes represent gradual lobe abandonment. More complex layer thickness trends in the thickest Greywacke 1 packets suggest aggradational lobe growth, which is consistent with their more proximal character. Evidence from the β_7 member (Enos, 1969a) suggests that Cloridorme depositional lobes are continuous for at least 10.5 km. downcurrent. Lobes are therefore much more continuous than their component layers, which die out at the rate of 50% in 4 km. Lobe continuity is comparable with that in other formations, though there is considerable variation between different examples. Continuity of individual layers in the β_7 member is less than in some other submarine fan turbidites. Comparisons of layer continuity should always be made between layers of similar thickness, because thick layers are generally much more continuous than thin ones.

Abundance of Calcisiltite 1 layers in lobe-fringe interpacket units suggests that they are the downcurrent equivalents of Greywacke 1 layers in lobes. Thick Greywacke 2 layers with clasts which occur in interpacket units are thought to be debris flow deposits originating from slumping of lobe-fringe sediments, and are not downcurrent equivalents of Greywacke 1. Calcareous Wacke packets were deposited from turbidity currents which bypassed lobes and only began to deposit in the lobe-fringe area.

Consideration of non-fan turbidite depositional environments shows that they cannot account for the observed features of the γ_4 Formation and β_7 member. Basin plain turbidites and deep-sea channel turbidites would have much more continuous layers. These environments would not produce frequent alternation of thick- and thin-bedded units. Supply of sediment from multiple source areas would normally be reflected in multimodal palaeocurrent data.

Cloridorme Group Deposition

Cloridorme Group sediments were supplied from a source land to the south of the outcrop area which included sedimentary rocks, a large ophiolite, and a volcanic arc. An adjacent shelf was an area of carbonate production and may have been cut by submarine canyons connected directly

to fluvial deltas.

Comparison of other parts of the Cloridorme Group with the γ_4 Formation allows tentative interpretation of their depositional environments. Three facies associations are recognized at the scale of members or formations. Facies association 1 is similar to the γ_4 Formation taken as a whole, and is therefore interpreted as an outer fan facies association. Facies association 2 is similar to the interpacket units of the γ_4, and is interpreted as a fan-fringe facies association. Facies association 3 is unlike any part of the γ_4, and is interpreted as a basin plain facies association. Members or formations assigned to facies association 1 are β_3, β_5, β_7, γ_2 and γ_4. Facies association 2 includes the β_2, β_4, β_6 and γ_3 units. Facies association 2 differs from interpacket units of the γ_4 Formation in that Greywacke 2 layers are extremely rare. Facies association 3 accounts for the β_1 and γ_1 units. In this association, the Greywacke 1 and Calcisiltite 2 layers ascribed to depositional lobes are virtually absent. The association is dominated by Argillite, but its most characteristic feature is the presence of the unusual Greywacke 3 facies. Greywacke 3 and Calcareous Wacke layers show considerable downcurrent continuity and uniformity in this association, and have been correlated over 12 km. downcurrent in the β_1 member (Skipper, 1971).

Cloridorme Group sediments were derived from the south, yet palaeocurrent directions are dominantly to the west, with flow to the east in the γ_3 and γ_4 Formations. This pattern may be explained by turning of turbidity currents through 90° on entering the longitudinal basin. Submarine fans were therefore asymmetric, longitudinal fans which grew along the axis of the basin rather than perpendicular to the basin margin. The γ_3 and γ_4 Formations probably represent an easterly-directed submarine fan with a thickness of at least 1500 m. The members β_3 to β_7 may have been deposited on a similar-sized, westerly-directed submarine fan. The γ_1 and γ_2 Formations are the same age as the β_3 to β_7 members and are probably related to the same submarine fan. Members β_1 and β_2 may be of a different age and are not related to the above systems.

Anti-clockwise rotation of palaeocurrent directions taken from rib and furrow structure relative to those from sole marks appears to be restricted to the γ_4 Formation. Sole mark direction is determined by the direction of the high-momentum head of the turbidity current, and so is relatively little affected by local slope. Ripples are formed by the low-momentum tail of the current, which tends to move down the local slope. Ripple directions therefore represent the local slope direction while sole marks represent the direction of flow of the head of the current, which was deter-

mined outside the depositional area. Consistent anti-clockwise rotation requires that the outcrop area lay on the northern side of the east-west fan axis.

Estimates of the absolute length of graptolite zones based on sedimentation rates of pelagic shales suggest a time interval of approximately 6.5 m.y. for deposition of the Cloridorme Group. Making allowance for age-equivalence of parts of the group, an average sedimentation rate of 420 m./m.y. is calculated. This is comparable with sedimentation rates in other submarine fan turbidites such as the Astoria Fan and Marnoso-Arenacea.

Comparison of the Cloridorme Group with the older Tourelle Formation, which is exposed west of the study area, is difficult because equivalent facies are not exposed. However, if they represent high-efficiency and low-efficiency fan types, a change in grain size characteristics of sediment input is suggested, despite the similar source areas.

BIBLIOGRAPHY

Abbreviations used for periodicals and reports are those given in "Bibliographic Guide for Editors and Authors": American Chemical Society, Washington, D.C., 362p. (1974).

Allen, J.R.L. (1970) A quantitative model of climbing ripples and their cross-laminated deposits: Sedimentology, v. 14, p.5-25.

Allen, J.R.L. (1971) A theoretical and experimental study of climbing-ripple cross-lamination, with a field application to the Uppsala Esker: Geografiska Annaler, v. 53A, p.157-187.

Anketell, J.M. and Lovell, J.P.B. (1976) Upper Llandoverian Grogal Sandstones and Aberystwyth Grits in the New Quay area, central Wales: a possible upwards transition from contourites to turbidites: Geol. J., v. 11, p.101-108.

Anketell, J.M., Cegla, J. and Dzulynski, S. (1970) On the deformational structures in systems with reversed density gradients: Ann. Soc. Geol. Pologne, v. 40, p.3-30.

Archibald, D.A. and Farrar, E. (1976) K-Ar ages of amphiboles from the Bay of Islands ophiolite and the Little Port Complex, western Newfoundland, and their geological implications: Can. J. Earth Sci., v. 13, p.520-529.

Ashley, G.M., Southard, J.B. and Boothroyd, J.C. (1982) Deposition of climbing-ripple beds: a flume simulation: Sedimentology, v. 29, p.67-80.

Bagnold, R.A. (1956) The flow of cohesionless grains in fluids: Philos. Trans. R. Soc. London, Ser. A, v. 249, p.235-297.

Bagnold, R.A. (1962) Auto-suspension of transported sediment; turbidity currents: Proc. R. Soc. London, Ser. A, v. 265, p.315-319.

Bambach, R.K., Scotese, C.R. and Ziegler, A.M. (1980) Before Pangea: the geographies of the Paleozoic world: Am. Sci., v. 68, p.26-38.

Beall, A.O. and Fischer, A.G. (1969) Sedimentology: In Initial Reports of the Deep Sea Drilling Project, Volume I, U.S. Govt. Printing Office, Washington, p.521-593.

Belt, E.S. and Bussières, L. (1981) Upper Middle Ordovician submarine fans and associated facies, northeast of Quebec City: Can. J. Earth Sci., v. 18, p.981-994.

Belt, E.S., Riva, J. and Bussières, L. (1979) Revision and correlation of late Middle Ordovician stratigraphy northeast of Quebec City: Can. J. Earth Sci., v. 16, p.1467-1483.

Berger, W.H. (1974) Deep-sea sedimentation: In Burk, C.A. and Drake, C.L., eds., The Geology of Continental Margins, Springer-Verlag, New York, 1009p.

Bergström, S., Riva, J. and Kay, M. (1974) Significance of conodonts, graptolites, and shelly faunas from the Ordovician of western and north-central Newfoundland: Can. J. Earth Sci., v. 11, p.1625-1660.

Berry, W.B.N. (1960) Graptolite faunas of the Marathon region, west Texas: Texas Univ. Publ. 6005, 179p.

Berry, W.B.N. (1971) Late Ordovician graptolites from southeastern New York: J. Paleont., v. 45, p.633-640.

Bhattacharjee, S.B. (1970) Ripple-drift cross-lamination in turbidites of the Ordovician Cloridorme Formation, Gaspé, Quebec: M.Sc. Thesis, McMaster Univ., Hamilton, Ont., 167p.

Biron, S. (1971) Géologie de la rive du St-Laurent de Cap Chat à Gros Morne: Que. Dep. Nat. Resour., Prelim. Rep., open file, 9p.

Biron, S. (1972) Géologie de la région de Ste-Anne des Monts: Que. Dep. Nat. Resour., Prelim. Rep. (+ map), open file, 7p.

Biron, S. (1973) Géologie de la région de Marsoui: Que. Dep. Nat. Resour., Prelim. Rep. (+ map), open file, 7p.

Biron, S. (1974) Géologie de la région des Méchins: Que. Dep. Nat. Resour., Prelim. Rep. (+ map), open file, 12p.

Bishop, Y.M.M., Fienberg, S.E. and Holland, P.W. (1975) Discrete Multivariate Analysis: M.I.T. Press, Cambridge, MA, 557p.

Blackie, G.W. and Yeats, R.S. (1976) Magnetic-reversal stratigraphy of Pliocene-Pleistocene producing section of Saticoy oil field, Ventura basin, California: Bull. Am. Assoc. Pet. Geol., v. 60, p.1985-1992.

Blatt, H., Middleton, G.V. and Murray, R.C. (1980) Origin of

Sedimentary Rocks, 2nd edition: Prentice-Hall, Englewood Cliffs, N.J., 782p.

Bouma, A.H. (1962) Sedimentology of some Flysch Deposits; a graphic approach to facies interpretation: Elsevier, Amsterdam, 168p.

Bouma, A.H. and Treadwell, T.K. (1975) Deep sea dune-like features: Mar. Geol., v. 19, p.M53-M59.

Brown, M.B. (1974) Identification of sources of significance in two-way contingency tables: Applied Statistics, v. 23, p.405-413.

Brown, M.B. (1981) Two-way and multiway frequency tables - measures of association and the log-linear model (complete and incomplete tables): In Dixon, W.J., chief ed., BMDP Statistical Software 1981, Univ. of California Press, Los Angeles, p.143-206.

Carr, T.R. (1982) Log-linear models, Markov chains and cyclic sedimentation: J. Sediment. Petrol., v. 52, p.905-912.

Carter, C. and Churkin, M. (1977) Ordovician and Silurian graptolite succession in the Trail Creek area, central Idaho - a graptolite zone reference section: U.S. Geol. Surv. Prof. Pap. 1020.

Carter, C., Trexler, J.H. and Churkin, M. (1980) Dating of graptolite zones by sedimentation rates: implications for rates of evolution: Lethaia, v. 13, p.279-287.

Casnedi, R., Moruzzi, G. and Mutti, E. (1978) Correlazioni elettriche di lobi deposizionali torbiditici nel Pliocene del sottosuolo abruzzese: Mem. Soc. Geol. Ital., v. 18, p.23-30.

Chough, S. and Hesse, R. (1976) Submarine meandering thalweg and turbidity currents flowing for 4000 km in the Northwest Atlantic Mid-Ocean Channel, Labrador Sea: Geology, v. 4, p.529-534.

Church, W.R. and Stevens, R.K. (1971) Early Paleozoic ophiolite complex of the Newfoundland Appalachians as mantle/oceanic crust sequences: J. Geophys. Res., v. 76, p.1460-1466.

Curray, J.R. (1956) Analysis of two-dimensional orientation data: J. Geol., v. 64, p.117-131.

Dallmeyer, R.D. (1977) Diachronous ophiolite obduction in western Newfoundland: evidence from $^{40}Ar/^{39}Ar$ ages of the Hare Bay metamorphic aureole: Am. J. Sci., v. 277, p.61-72.

Dallmeyer, R.D. and Williams, H. (1975) $^{40}Ar/^{39}Ar$ release spectra of hornblende from the Bay of Islands metamorphic aureole, western Newfoundland: their bearing on the timing of ophiolite obduction at the Ordovician continental margin: Can. J. Earth Sci., v. 12, p.1685-1690.

Doveton, J.H. and Skipper, K. (1974) Markov chain and substitutability analysis of a turbidite succession, Cloridorme Formation (Middle Ordovician), Gaspé, Quebec: Can. J. Earth Sci., v. 11, p.472-488.

Einstein, H.A. and Chien, N. (1955) Effects of heavy sediment concentration near the bed on velocity and sediment distribution: U.S. Army Corps Eng., Missouri River Division, Sediment Series 8, 76p.

Ells, R.W. (1883) Report on the geological formations of the Gaspé Peninsula: Geol. Surv. Can. Rpt. Prog., 1880-81-82, pt. D., 32p.

Elmore, R.D., Pilkey, O.H., Cleary, W.J. and Curran, H.A. (1979) Black Shell turbidite, Hatteras Abyssal Plain, western Atlantic Ocean: Geol. Soc. Am., Bull., v. 90, p.1165-1176.

Embley, R.W. (1976) New evidence for occurrence of debris flow deposits in the deep sea: Geology, v. 4, p.371-374.

Enos, P. (1965) Anatomy of a flysch - Middle Ordovician Cloridorme Formation, northern Gaspé Peninsula: Ph.D. Thesis, Yale University, 145p.

Enos, P. (1969a) Cloridorme Formation, Middle Ordovician flysch, northern Gaspé Peninsula, Quebec: Geol. Soc. Am., Spec. Pap. 117, 66p.

Enos, P. (1969b) Anatomy of a flysch: J. Sediment. Petrol., v. 39, p.680-723.

Fischer, A.G. and Arthur, M.A. (1977) Secular variations in the pelagic realm: In Cook, H.E. and Enos, P., eds., Deep-Water Carbonate Environments, Soc. Econ. Paleontol. Mineral., Spec. Publ. 25, p.19-50.

Fisher, D.W. (1977) Correlation of the Hadrynian, Cambrian and Ordovician rocks of New York State: N.Y. State Mus.

Sci. Serv., Map Chart Ser., 25.

Folk, R.L. (1959) Practical petrographic classification of limestones: Bull. Am. Assoc. Pet. Geol., v. 43, p.1-38.

Frazier, D.E. (1967) Recent deltaic deposits of the Mississippi River: their development and chronology: Trans. Gulf Coast Assoc. Geol. Soc., v. 17, p.287-315.

Ghibaudo, G. (1980) Deep-sea fan deposits in the Macigno Formation (Middle-Upper Oligocene) of the Gordana Valley, Northern Apennines, Italy: J. Sediment. Petrol., v. 50, p.723-742.

Ghibaudo, G. (1981) Deep-sea fan deposits in the Macigno Formation (Middle-Upper Oligocene) of the Gordana Valley, Northern Apennines, Italy - Reply: J. Sediment. Petrol., v. 51, p.1021-1026.

Girard, P. (1967) Région du Mont Richardson: Que. Dep. Nat. Resour., Prelim. Rep. 563.

Gonzalez-Bonorino, G. (1979) Sedimentology and stratigraphy of the Curling Group (Humber Arm Supergroup) central western Newfoundland: Ph.D. Thesis, McMaster Univ., Hamilton, Ont., 294p.

Griggs, G.B., Carey, A.G. and Kulm, L.D. (1969) Deep-sea sedimentation and sediment-fauna interaction in Cascadia Channel and on Cascadia Abyssal Plain: Deep-Sea Res., v. 16, p.157-170.

Gürich, G. (1933) Schrägschichtungsbögen und sapfenförmige Fliesswülste im "Flagstone" von Pretoria: Z. Dtsch. Geol. Ges., Bd. 85, p.652-663.

Hampton, M.A. (1972) The role of subaqueous debris flow in generating turbidity currents: J. Sediment. Petrol., v. 42, p.775-793.

Hampton, M.A. (1975) Competence of fine-grained debris flows: J. Sediment. Petrol., v. 45, p.834-844.

Hampton, M.A. (1979) Buoyancy in debris flows: J. Sediment. Petrol., v. 49, p.753-758.

Harbaugh, J.W. and Bonham-Carter, G. (1970) Computer Simulation in Geology: Wiley-Interscience, New York, 575p.

Harms, J.C., Southard, J.B., Spearing, D.R. and Walker, R.G. (1975) Depositional Environments as Interpreted from Primary Sedimentary Structures and Stratification Sequences: Soc. Econ. Paleontol. Mineral., Short Course No. 2, Dallas, 161p.

Hein, F.J. and Walker, R.G. (1982) The Cambro-Ordovician Cap Enragé Formation, Quebec, Canada: conglomeratic deposits of a braided submarine channel with terraces: Sedimentology, v. 29, p.309-329.

Hendry, H.E. (1973) Sedimentation of deep-water conglomerates in Lower Ordovician rocks of Quebec - composite bedding produced by progressive liquefaction of sediment?: J. Sediment. Petrol., v. 43, p.125-136.

Hendry, H.E. (1976) The orientation of discoidal clasts in resedimented conglomerates, Cambro-Ordovician, Gaspé, Quebec: J. Sediment. Petrol., v. 46, p.48-55.

Hess, G.R. and Normark, W.R. (1976) Holocene sedimentation history of the major fan valleys of the Monterey fan: Mar. Geol., v. 22, p.233-251.

Hesse, R. (1974) Long-distance continuity of turbidites: possible evidence for an Early Cretaceous trench-abyssal plain in the east Alps: Geol. Soc. Am., Bull., v. 85, p.859-870.

Hesse, R. and Chough, S.K. (1980) The Northwest Atlantic Mid-Ocean Channel of the Labrador Sea: II Deposition of parallel laminated levee-muds from the viscous sublayer of low density turbidity currents: Sedimentology, v. 27, p.697-711.

Hirayama, J. and Nakajima, T. (1977) Analytical study of turbidites, Otadai Formation, Boso Peninsula, Japan: Sedimentology, v. 24, p.747-779.

Hiscott, R.N. (1977) Sedimentology and regional implications of deep-water sandstones of the Tourelle Formation, Ordovician, Quebec: Ph.D. Thesis, McMaster Univ., Hamilton, Ont., 542p.

Hiscott, R.N. (1978) Provenance of Ordovician deep-water sandstones, Tourelle Formation, Quebec, and implications for initiation of the Taconic orogeny: Can. J. Earth Sci., v. 15, p.1579-1597.

Hiscott, R.N. (1980) Depositional framework of sandy mid-fan

complexes of Tourelle Formation, Ordovician, Quebec: Bull. Am. Assoc. Pet. Geol., v. 64, p.1052-1077.

Hiscott, R.N. (1981) Deep-sea fan deposits in the Macigno Formation (Middle-Upper Oligocene) of the Gordana Valley, Northern Apennines, Italy - Discussion: J. Sediment. Petrol., v. 51, p.1015-1020.

Hiscott, R.N. and Middleton, G.V. (1979) Depositional mechanics of thick-bedded sandstones at the base of a submarine slope, Tourelle Formation (Lower Ordovician), Quebec, Canada: In Doyle, L.J. and Pilkey, O.H., eds., Geology of Continental Slopes, Soc. Econ. Paleontol.Mineral., Spec. Publ. 27, p.307-326.

Hsu, K.J., Kelts, K. and Valentine, J.W. (1980) Resedimented facies in Ventura basin, California, and model of longitudinal transport of turbidity currents: Bull. Am. Assoc. Petrol. Geol., v. 64, p.1034-1051.

Islam, S. (1981) Thermal maturation patterns in Cambro-Ordovician flysch sediments of the Taconic belt, Gaspé Peninsula: M.Sc. Thesis, McGill Univ., Montreal, Que., 191p.

Islam, S., Hesse, R. and Chagnon, A. (1982) Zonation of diagenesis and low-grade metamorphism in Cambro-Ordovician flysch of Gaspé Peninsula, Quebec Appalachians: Can. Mineral., v. 20, p.155-167.

Johnson, M.A. (1966) Application of theory to an Atlantic turbidity-current path: Sedimentology, v. 7, p.117-129.

Johnson, A.M. (1970) Physical Processes in Geology: Freeman, Cooper and Co., San Francisco, 577p.

Jopling, A.V. and Walker, R.G. (1968) Morphology and origin of ripple-drift cross-lamination, with examples from the Pleistocene of Massachusetts: J. Sediment. Petrol., v. 38, p.971-984.

Kay, M. (1969) Thrust sheets and gravity slides of western Newfoundland: In Kay, M., ed., North Atlantic - Geology and Continental Drift, Am. Assoc. Pet. Geol., Memoir 12, p.665-669.

Komar, P.D. (1971) Hydraulic jumps in turbidity currents: Geol. Soc. Am., Bull., v. 81, p.2153-2160.

Komar, P.D. (1977) Computer simulation of turbidity current flow and the study of deep-sea channels and fan sedimenta-

tation: In Goldberg, E.D., McCave, I.N., O'Brien, J.J. and Steele, J.H., eds., The Sea, volume 6, p.603-621.

Laird, M.G. (1970) Vertical sheet structures - a new indicator of sedimentary fabric: J. Sediment. Petrol., v. 40, p.428-434.

Laurent, R. (1975) Occurrences and origin of the ophiolites of southern Quebec, northern Appalachians: Can. J. Earth Sci., v. 12, p.443-455.

Leggett, J.K., McKerrow, W.S., Cocks, L.R.M. and Rickards, R.B. (1981) Periodicity in the lower Palaeozoic marine realm: J. Geol. Soc. London, v. 138, p.167-176.

Logan, W.E. (1846) Sections on Chaleur Bay and the coast of Gaspé: Geol. Surv. Can. Rept. Prog., 1844, p.78-110.

Logan, W.E. (1863) Geology of Canada: Geol. Surv. Can. Rept. Prog. from commencement to 1863, 983p.

Lowe, D.R. (1975) Water escape structures in coarse-grained sediments: Sedimentology, v. 22, p.157-204.

Lowe, D.R. (1979) Sediment gravity flows: their classification and some problems of application to natural flows and deposits: In Doyle, L.J. and Pilkey, O.H., eds., Geology of Continental Slopes, Soc. Econ. Paleontol. Mineral., Spec. Publ. 27, p.75-84.

Lowe, D.R. (1982) Sediment gravity flows: II. Depositional models with special reference to the deposits of high-density turbidity currents: J. Sediment. Petrol., v. 52, p.279-298.

Maldonado, A. and Stanley, D.J. (1978) Nile Cone depositional processes and patterns in the Late Quaternary: In Stanley, D.J. and Kelling. G., eds., Sedimentation in Submarine Canyons, Fans and Trenches: Dowden, Hutchinson and Ross, Stroudsburg, PA, p.239-257.

Mattinson, C.R. (1964) Mount Logan area: Gaspé Peninsula: Que. Dep. Nat. Resour., Geol. Rep. 118, 97p.

McBride, E.F. (1962) Flysch and associated beds of the Martinsburg Formation (Ordovician), Central Appalachians: J. Sediment. Petrol., v. 32, no. 1, p.39-91.

McGerrigle, H.W. (1953) Geology of Gaspé Peninsula: Que. Dep.

Mines, Map No. 1000.

McGerrigle, H.W. and Skidmore, W.B. (1967) Geological map, Gaspé Peninsula: Que. Dep. Nat. Resour., Map No. 1642.

McIlreath, I.A. and James, N.P. (1979) Carbonate slopes: In Walker, R.G., ed., Facies Models, Geosci. Can. Reprint Ser. 1, p.133-143.

Middleton, G.V. (1966) Experiments on density and turbidity currents: II. Uniform flow of density currents: Can. J. Earth Sci., v. 3, p.627-637.

Middleton, G.V. (1967) Experiments on density and turbidity currents: III. Deposition of sediment: Can. J. Earth Sci., v. 4, p.475-505.

Middleton, G.V. and Hampton, M.A. (1973) Sediment gravity flows: mechanics of flow and deposition: In Middleton, G.V. and Bouma, A.H., eds., Turbidites and Deep-water Sedimentation, Soc. Econ. Paleontol. Mineral., Short Course, Anaheim, p.1-38.

Middleton, G.V. and Southard, J.B. (1977) Mechanics of Sediment Movement: Soc. Econ. Paleontol. Mineral., Short Course No. 3, Binghamton, New York.

Morris, R.C. (1971) Classification and interpretation of disturbed bedding types in the Jackfork flysch rocks (Upper Mississippian), Ouachita Mountains, Arkansas: J. Sediment. Petrol., v. 41, p.410-424.

Mutti, E. (1975) Remarks on the Miocene Bobbio Formation: In Examples of Turbidite Facies and Facies Associations from Selected Formations of the Northern Apennines, Field Trip Guidebook A-11, Internat. Sediment. Congr., Nice, IX, p.38-41.

Mutti, E. (1977) Distinctive thin-bedded turbidite facies and related depositional environments in the Eocene Hecho Group (South-central Pyrenees, Spain): Sedimentology, v. 24, p.107-131.

Mutti, E. (1979) Turbidites et cones sous-marins profonds: In Homewood, P., ed., Sedimentation Detritique (Fluviatile, Littorale et Marine), Institut Geol., Univ. Fribourg, Fribourg, Switzerland, p.353-419.

Mutti, E. and Ricci Lucchi, F. (1972) Le torbiditi dell'

Appennino settentrionale: introduzione all' analisi di facies: Mem. Soc. Geol. Ital., v. 11, p.161-199.

Mutti, E. and Ricci Lucchi, F. (1975) Turbidite facies and facies associations: In Examples of Turbidite Facies and Facies Associatons from Selected Formations of the Northern Apennines, Field Trip Guidebook A-11, Internat. Sediment. Congr., Nice, IX, p.21-36.

Mutti, E., Nilsen, T.H. and Ricci Lucchi, F. (1978) Outer fan depositional lobes of the Laga Formation (Upper Miocene and Lower Pliocene), East-central Italy: In Stanley, D.J. and Kelling, G., eds., Sedimentation in Submarine Canyons, Fans, and Trenches: Dowden, Hutchinson and Ross, Stroudsburg, PA, p.210-223.

Neale, E.R.W., Béland, J., Potter, R.R. and Poole, W.H. (1961) A preliminary tectonic map of the Canadian Appalachian region based on age of folding: Bull. Can. Min. Metall., v. 54, p.687-694.

Nederlof, M.H. (1959) Structure and sedimentology of the Upper Carboniferous of the upper Pisuerga valleys, Cantabrian Mountains, Spain: Leidse Geol. Meded., v. 24, p.603-703.

Nelson, C.H. (1976) Late Pleistocene and Holocene depositional trends, processes and history of Astoria deep sea fan, northeast Pacific: Mar. Geol., v. 20, p.27-40.

Nelson, C.H. and Kulm, L.D. (1973) Submarine fans and channels: In Middleton, G.V. and Bouma, A.H., eds., Turbidites and Deep-water Sedimentation, Soc. Econ. Paleontol. Mineral., Short Course, Anaheim, p.39-78.

Nelson, C.H., Carlson, P.R., Byrne, G.V. and Alpha, T.R. (1970) Development of the Astoria canyon-fan physiography and comparison with similar systems: Mar. Geol., v. 8, p.259-291.

Normark, W.R. (1970) Growth patterns of deep-sea fans: Bull. Am. Assoc. Pet. Geol., v. 54, p.2170-2195.

Normark, W.R. (1978) Fan valleys, channels, and depositional lobes on modern submarine fans: characters for recognition of sandy turbidite environments: Bull. Am. Assoc. Pet. Geol., v. 62, p.912-931.

Normark, W.R. (1980) Modern and ancient submarine fans: Reply: Bull. Am. Assoc. Pet. Geol., v. 64, p.1108-1112.

Normark, W.R. and Hess, G.R. (1980) Quaternary growth patterns of California submarine fans: In Field, M.E., Bouma, A.H., Colburn, I.P., Douglas, R.G. and Ingle, J.C., eds., Quaternary Depositional Environments of the Pacific Coast, Pacific Coast Paleogeography Symposium, pt. IV, Soc. Econ. Paleontol. Mineral., Pacific Sect., Los Angeles, p.201-210.

Normark, W.R., Piper, D.J.W. and Hess, G.R. (1979) Distributary channels, sand lobes, and mesotopography of Navy Submarine Fan, California Borderland, with applications to ancient submarine fan sediments: Sedimentology, v. 26, p.749-774.

Ollerenshaw, N.C. (1967) Cuoq-Langis area, Matane and Matapédia Co., Quebec: Que. Dep. Nat. Resour., Geol. Rep. 121, 192p.

Parkash, B. (1969) Depositional mechanism of greywackes, Cloridorme Formation (Middle Ordovician), Gaspé, Quebec: Ph.D. Thesis, McMaster Univ., Hamilton, Ont., 238p.

Parkash, B. (1970) Downcurrent changes in sedimentary structures in Ordovician turbidite greywackes: J. Sediment. Petrol., v. 40, p.572-590.

Parkash, B. and Middleton, G.V. (1970) Downcurrent textural changes in Ordovician turbidite greywackes: Sedimentology, v. 14, p.259-293.

Pett, J.W. and Walker, R.G. (1971) Relationship of flute cast morphology to internal sedimentary structures in turbidites: J. Sediment. Petrol., v. 41, p.114-128.

Pettijohn, F.J. (1975) Sedimentary Rocks, 3rd edition: Harper and Row, New York, 628p.

Pickering, K.T. (1981) Two types of outer fan lobe sequence, from the Late Pre-Cambrian Kongsfjord Formation submarine fan, Finnmark, north Norway: J. Sediment. Petrol., v. 51, p.1277-1286.

Piper, D.J.W. (1978) Turbidite muds and silts on deepsea fans and abyssal plains: In Stanley, D.J. and Kelling, G., eds., Sedimentation in Submarine Canyons, Fans, and Trenches: Dowden, Hutchinson and Ross, Stroudsburg, PA, p.163-176.

Potter, P.E. and Pettijohn, F.J. (1977) Paleocurrents and Basin Analysis, 2nd edition: Springer-Verlag, New York, 425p.

Potter, P.E., Maynard, J.B. and Pryor, W.A. (1980) Sedimentology of Shale: Springer-Verlag, New York, 303p.

Ricci Lucchi, F. (1969) Channelized deposits in the Middle Miocene Flysch of Romagna (Italy): G. Geol., S2, v. 36, p.203-282.

Ricci Lucchi, F. (1975) Depositional cycles in two turbidite formations of northern Apennines (Italy): J. Sediment. Petrol., v. 45, p.3-43.

Ricci Lucchi, F. and Valmori, E. (1980) Basin-wide turbidites in a Miocene, oversupplied deep-sea plain: a geometrical analysis: Sedimentology, v. 27, p.241-270.

Richardson, J.F. and Zaki, W.N. (1954) Sedimentation and fluidization: Trans. Inst. Chem. Eng., v. 32, p.35-53.

Riva, J. (1968) Graptolite faunas from the Middle Ordovician of the Gaspé north shore: Nat. Can., v. 95, p.1379-1400.

Riva, J. (1969) Middle and Upper Ordovician graptolite faunas of the St. Lawrence Lowlands of Quebec, and of Anticosti Island: In Kay, M., ed., North Atlantic - Geology and Continental Drift: Am. Assoc. Pet. Geol., Memoir 12, p.513-556.

Riva, J. (1972) Geology of the environs of Quebec City: XXIV Internat. Geol. Congr., Montreal, guidebook for excursion B-19, 53p.

Riva, J. (1974) A revision of some Ordovician graptolites of eastern North America: Palaeontology, v. 17, p.1-40.

Rodine, J.D. and Johnson, A.M. (1976) The ability of debris, heavily freighted with coarse clastic materials, to flow on gentle slopes: Sedimentology, v. 23, p.213-234.

Roscoe, R. (1953) Suspensions: In Hermans, J.J., ed., Flow Properties of Disperse Systems, Interscience Publ. Inc., New York, p.1-38.

Ruedemann, R. (1947) Graptolites of North America: Geol. Soc. Am., Mem. 19, 652p.

Ruitenberg, A.A., Fyffe, L.R., McCutcheon, S.R., St. Peter, C.J., Irrinki, R.R. and Venugopal, D.V. (1977) Evolution of pre-Carboniferous tectono-stratigraphic zones in the New Brunswick Appalachians: Geosci. Can., v.4, p.171-181.

Rupke, N.A. (1978) Deep clastic seas: In Reading, H.G., ed., Sedimentary Environments and Facies, Elsevier, New York, p.372-415.

Sagri, M. (1975) Sedimentation rates and lithology of the Northern Apennines turbidite basins: In Examples of Turbidite

Facies and Facies Associations from Selected Formations of the Northern Apennines, Field Trip Guidebook A-11, Internat. Sediment. Congr., Nice, IX, p.13.

St. Julien, P. and Hubert, C. (1975) Evolution of the Taconic orogen in the Quebec Appalachians: Am. J. Sci., v. 275-A, p.337-362.

St. Julien, P., Hubert, C., Skidmore, B. and Béland, J. (1972) Appalachian Structure and Stratigraphy, Quebec: XXIV Internat. Geol. Congr., Montreal, guidebook for excursion A56-C56, 99p.

Sanders, J.E. (1965) Primary sedimentary structures formed by turbidity currents and related resedimentation mechanisms: In Middleton, G.V., ed., Primary Sedimentary Structures and their Hydrodynamic Interpretation, Soc. Econ. Paleontol. Mineral., Spec. Publ. 12, p.192-219.

Schwarzacher, W. (1975) Sedimentation Models and Quantitative Stratigraphy: Elsevier, Amsterdam, 382p.

Shanmugam, G. and Moiola, R.J. (1982) Eustatic control of turbidites and winnowed turbidites: Geology, v. 10, p.231-235.

Simons, D.B., Richardson, E.V. and Nordin, C.F. (1965) Sedimentary structures generated by flow in alluvial channels: In Middleton, G.V., ed., Primary Sedimentary Structures and their Hydrodynamic Interpretation, Soc. Econ. Paleontol. Mineral., Spec. Publ. 12, p.34-52.

Skevington, D. (1969) The classification of the Ordovician System in Wales: In Wood, A., ed., The Pre-Cambrian and Lower Palaeozoic Rocks of Wales, Univ. Wales Press, Cardiff, p.161-179.

Skipper, K. (1970) Depositional mechanics of atypical turbidites, Cloridorme Formation, Gaspé, Quebec: M.Sc. Thesis, McMaster Univ., Hamilton, Ont., 137p.

Skipper, K. (1971) Antidune cross-stratification in a turbidite sequence, Cloridorme Formation, Gaspé, Quebec: Sedimentology, v. 17, p.51-68.

Skipper, K. and Middleton, G.V. (1975) The sedimentary structures and depositional mechanics of certain Ordovician turbidites, Cloridorme Formation, Gaspé Peninsula, Quebec: Can. J. Earth Sci., v. 12, p.1934-1952.

Southard, J.B., Boguchwal, L.A. and Romea, R.D. (1980) Test of scale modelling of sediment transport in steady unidirectional flow: Earth Surface Processes, v. 5, p.17-23.

Stokes, W.L. (1953) Primary sedimentary trend indicators as applied to ore findings in the Carrizo Mountains, Arizona and New Mexico: U.S. Atomic Energy Commission, RME-3043, 48p.

Stow, D.A.V. and Lovell, J.P.B. (1979) Contourites: their recognition in modern and ancient sediments: Earth Sci. Rev., v. 14, p.251-291.

Stow, D.A.V. and Bowen, A.J. (1980) A physical model for the transport and sorting of fine-grained sediment by turbidity currents: Sedimentology, v. 27, p.31-46.

Taira, A. (1976) Grain orientation and depositional processes - fabric analyses of modern and laboratory flume deposits: Ph.D. Thesis, Univ. of Texas at Dallas, p.234-309.

van Rijn, L.C. (1982) Equivalent roughness of an alluvial bed: J. Hydraulics Division, Proc. Am. Soc. Civ. Eng., v. 108, p.1215-1218.

Walker, R.G. (1969) Geometrical analysis of ripple-drift cross-lamination: Can. J. Earth Sci., v. 6, p.383-392.

Walker, R.G. (1970) Review of the geometry and facies organization of turbidites and turbidite-bearing basins: In Lajoie, J., ed., Flysch Sedimentology in North America, Geol. Assoc. Can., Spec. Pap. 7, p.219-251.

Walker, R.G. (1978) Deep-water sandstone facies and ancient submarine fans: models for exploration for stratigraphic traps: Bull. Am. Assoc. Pet. Geol., v. 62, p.932-966.

Walker, R.G. and Mutti, E. (1973) Turbidite facies and facies associations: In Middleton, G.V. and Bouma, A.H., eds., Turbidites and Deep-water Sedimentation, Soc. Econ. Paleontol. Mineral., Short Course, Anaheim, p.119-158.

Wanless, R.K, Stevens, R.D., Lachance, G.R. and Delabio, R.N. (1971) Age determinations and geological studies: K-Ar isotopic ages, Rept. 10: Geol. Surv. Can., Pap. 71-2, 96p.

Wanless, R.K. Stevens, R.D., Lachance, G.R. and Delabio, R.N. (1973) Age determinations and geological studies: K-Ar isotopic ages, Rept. 11: Geol. Surv. Can., Pap. 73-2, 139p.

Wentworth, C.K. (1922) A scale of grade and class terms for clastic sediments: J. Geol., v. 30, p.377-392.

Whittington, H.B. and Kindle, C.H. (1969) Cambrian and Ordovician stratigraphy of western Newfoundland: In Kay, M., ed., North Atlantic - Geology and Continental Drift, Am. Assoc. Pet. Geol., Memoir 12, p.655-664.

Wilde, P., Normark, W.R. and Chase, T.E. (1978) Channel sands and petroleum potential of Monterey deep-sea fan, California: Bull. Am. Assoc. Pet. Geol., v. 62, p.967-983.

Williams, H. (1969) Pre-Carboniferous development of Newfoundland Appalachians: In Kay, M., ed., North Atlantic - Geology and Continental Drift, Am. Assoc. Pet. Geol., Memoir 12, p.32-58.

Williams, H. (1975) Structural succession, nomenclature, and interpretation of transported rocks in western Newfoundland: Can. J. Earth Sci., v. 12, p.1874-1894.

Williams, H. (1978) Geological development of the northern Appalachians: its bearing on the evolution of the British Isles: In Bowes, D.R. and Leake, B.E., eds., Crustal Evolution in Northwestern Britain and Adjacent Regions, Seal House Press, Liverpool, p.1-22.

Williams, H. (1979) Appalachian orogen in Canada: Can. J. Earth Sci., v. 16, p.792-807.

Williams, H. and Smyth, W.R. (1973) Metamorphic aureoles beneath ophiolite suites and Alpine peridotites: tectonic implications with west Newfoundland examples: Am. J. Sci., v. 273, p.594-621.

Woodcock, N.H. (1976) Ludlow Series slumps and turbidites and the form of the Montgomery Trough, Powys, Wales: Proc. Geol. Assoc., v. 87, p.169-182.

Yalin, M.S. (1972) Mechanics of Sediment Transport: Pergamon Press, Oxford, 290p.

Ziegler, W., Lindström, M. and McTavish, R. (1971) Monochloroacetic acids and conodonts - a warning: Nature, v. 230, p.584-585.

APPENDIX 1

PALAEONTOLOGY

Graptolite collections

Graptolites were identified by John Riva, Laval University, 1980.

Collection 10 (Argillite, layer C95)

1. Dicranograptus nicholsoni minor Bulman
2. Orthograptus quadrimucronatus micracanthus Elles and Wood
3. Climacograptus typicalis Hall
4. Climacograptus "praetypicalis"

Collection 21 (Argillite, layer C316)

1. Climacograptus "praetypicalis"
2. Climacograptus putillus (Hall)

Collection 23 (Argillite, layer C322)

1. Dicranograptus nicholsoni minor Bulman
2. Orthograptus quadrimucronatus micracanthus Elles and Wood

Collection 26 (Argillite, layer C341)

1. Orthograptus quadrimucronatus micracanthus Elles and Wood

Collection 28 (Argillite, loose material across road from road-cut section)

1. Climacograptus cf. "praetypicalis"

Collection 38 (Greywacke 1, layer T104a)

1. Orthograptus quadrimucronatus micracanthus Elles and Wood

Conodont processing

Attempts to extract a conodont fauna from Cloridorme rocks were unsuccessful. Two Limestone samples broke down well in 15% Formic Acid over 24 hours or less, but the heavy fraction (density greater than 2.85 $g\,cm^{-3}$) lacked fossils. Samples of Greywacke 1, Dolomite and Argillite broke down poorly and all heavy fractions lacked fossils.

Greywacke 1 and Dolomite samples were broken into small pieces (e.g. 3 cm.) and placed in dilute acid. Acids used were 15% Acetic Acid, in which samples were left for up to 5 days; and 15% Formic Acid, in which they were only left for 1 day in order to avoid corrosion of conodonts (Ziegler et al., 1971). After the times stated, acid was poured off, fine material (90

microns to 850 microns) was sieved out and retained, while the remaining coarse material was placed in fresh acid. This was done several times. Argillite samples were placed in Varsol overnight. This was then poured off and water added, but little breakdown occurred. Argillite samples placed in 6% Sodium Hypochlorite solution ("Javex") for 16 days did not break down, but were bleached to a grey-green colour.

APPENDIX 2

LOCATION OF SECTIONS

Map overleaf shows the location of sections measured on the wave-cut platform between Pointe de Ruisseau à Rebours and Les Barrières (Fig. 1.2, p.5). Section begins with layer R1. Line of measurement for section R is approximate. Correlation of wave-cut platform section with roadcut section is shown. Reference points A and B refer to Fig. 1.2.

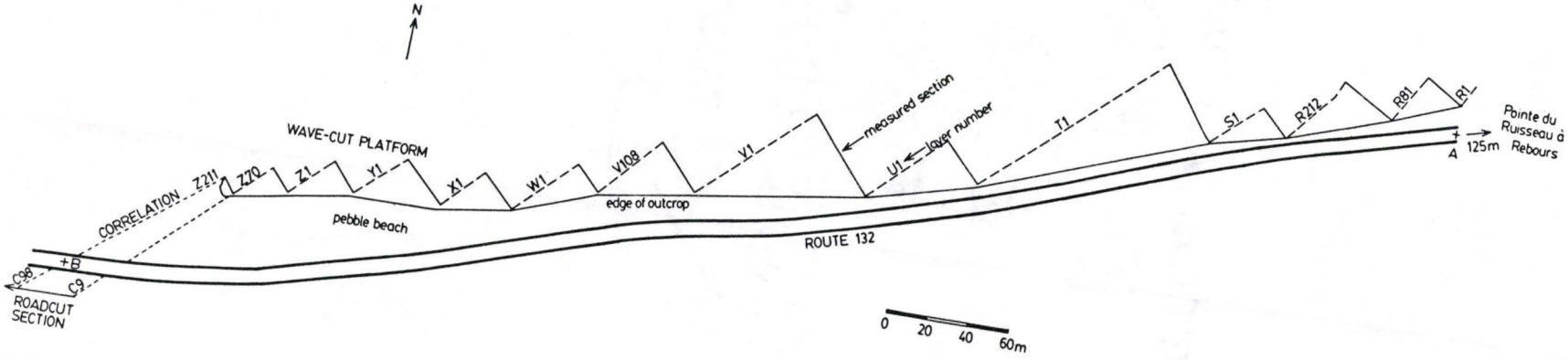
N
WAVE-CUT PLATFORM
CORRELATION
Z211
Z210
Z1
Y1
X1
W1
V108
V1
measured section
U1
layer number
T1
S1
R212
R81
R1
Pointe du Ruisseau à Rebours
125m
A
pebble beach
edge of outcrop
ROUTE 132
+B
C98
C9
ROADCUT SECTION
0
20
40
60m

APPENDIX 3

STRATIGRAPHIC SECTIONS AND LAYER THICKNESS PLOTS

Stratigraphic sections

Stratigraphic sections for the wave-cut platform and for the roadcut. Roadcut section continues stratigraphically from top of wave-cut platform section, as shown by thickness scale and unit numbers. Note that trends shown are layer thickness trends, not grain size trends. Grain size scale refers to the units and is the modal maximum size in non-lutite layers within the unit. Only layer thickness trends greater than 2 m. in thickness are shown. The full set of layer thickness trends is shown in the layer thickness plots which follow. Palaeocurrent data is shown separately for rib and furrow structure (RF) and sole marks (SOLE).

WAVE-CUT PLATFORM SECTION

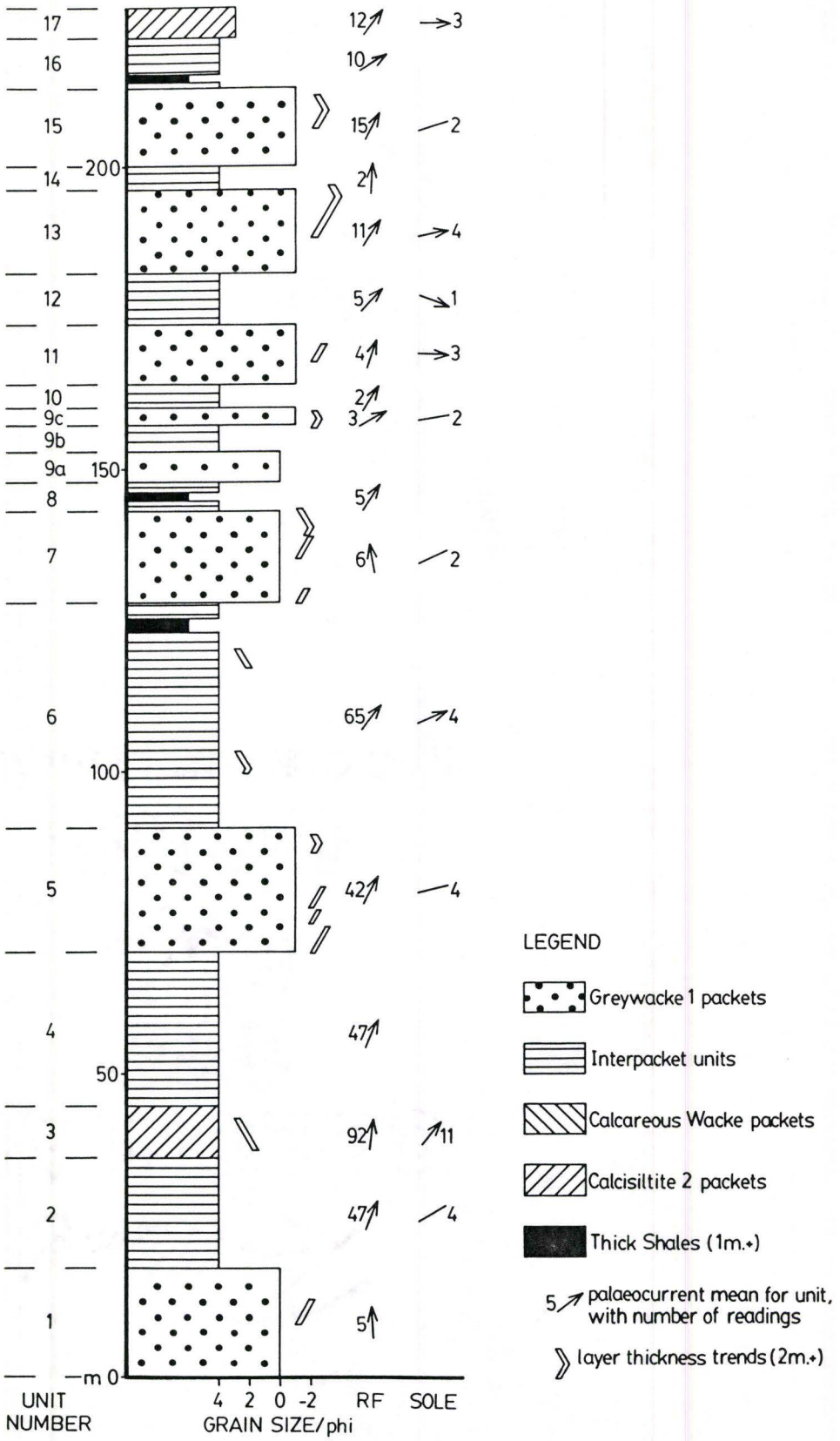

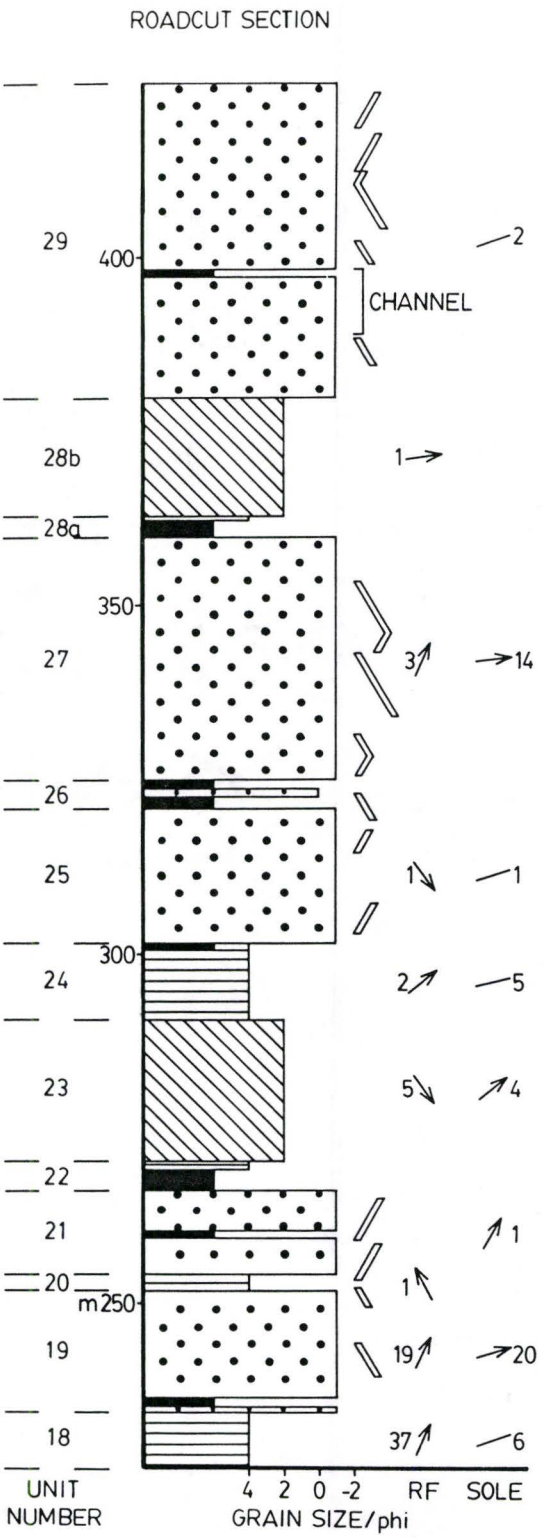
ROADCUT SECTION
29
400
CHANNEL
2
28b
1
28a
350
27
3
14
26
25
1
1
300
24
2
5
23
5
4
22
21
1
20
1
m 250
19
19
20
18
37
6
UNIT NUMBER
4 2 0 -2
GRAIN SIZE/phi
RF
SOLE

Layer thickness plots

Coarse (non-lutite) layer thickness plots for the entire section. Layer thickness trends are shown, together with their thickness in metres. Layers more than 180 cm. thick are plotted as 180 cm. thick. Parts of the section not measured in detail (i.e. facies CSA) are shown as a single point (filled circle) plotted at the approximate mean layer thickness for the horizon.

Following the plot for unit 2, there is a section produced by random superposition of the layers in unit 2 (2 pages) analogous to Fig. 4.3b (p.141). The plot for the actual section is then continued.

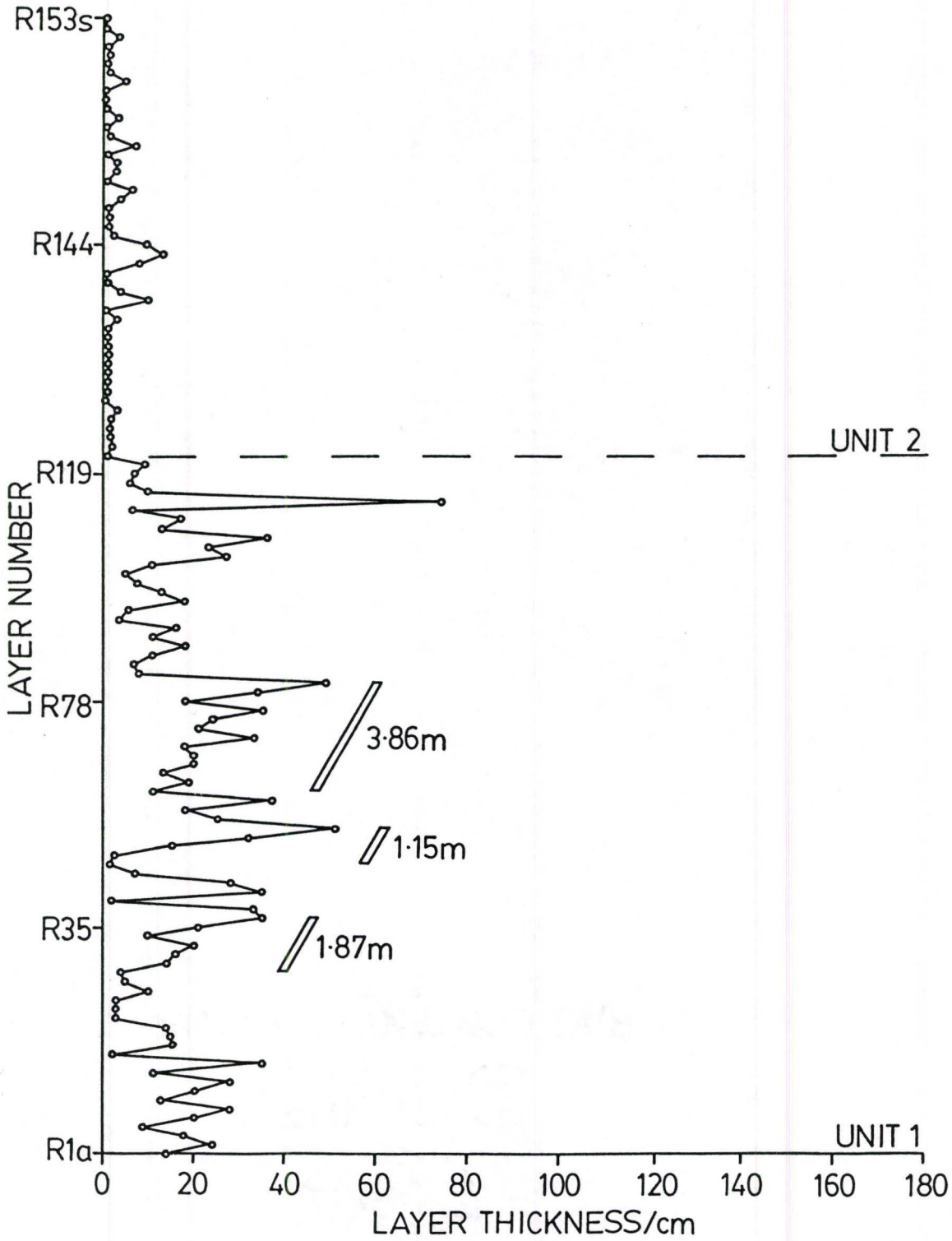
R153s
R144
R119
R78
R35
R1a
LAYER NUMBER
UNIT 2
UNIT 1
3·86m
1·15m
1·87m
0
20
40
60
80
100
120
140
160
180
LAYER THICKNESS/cm

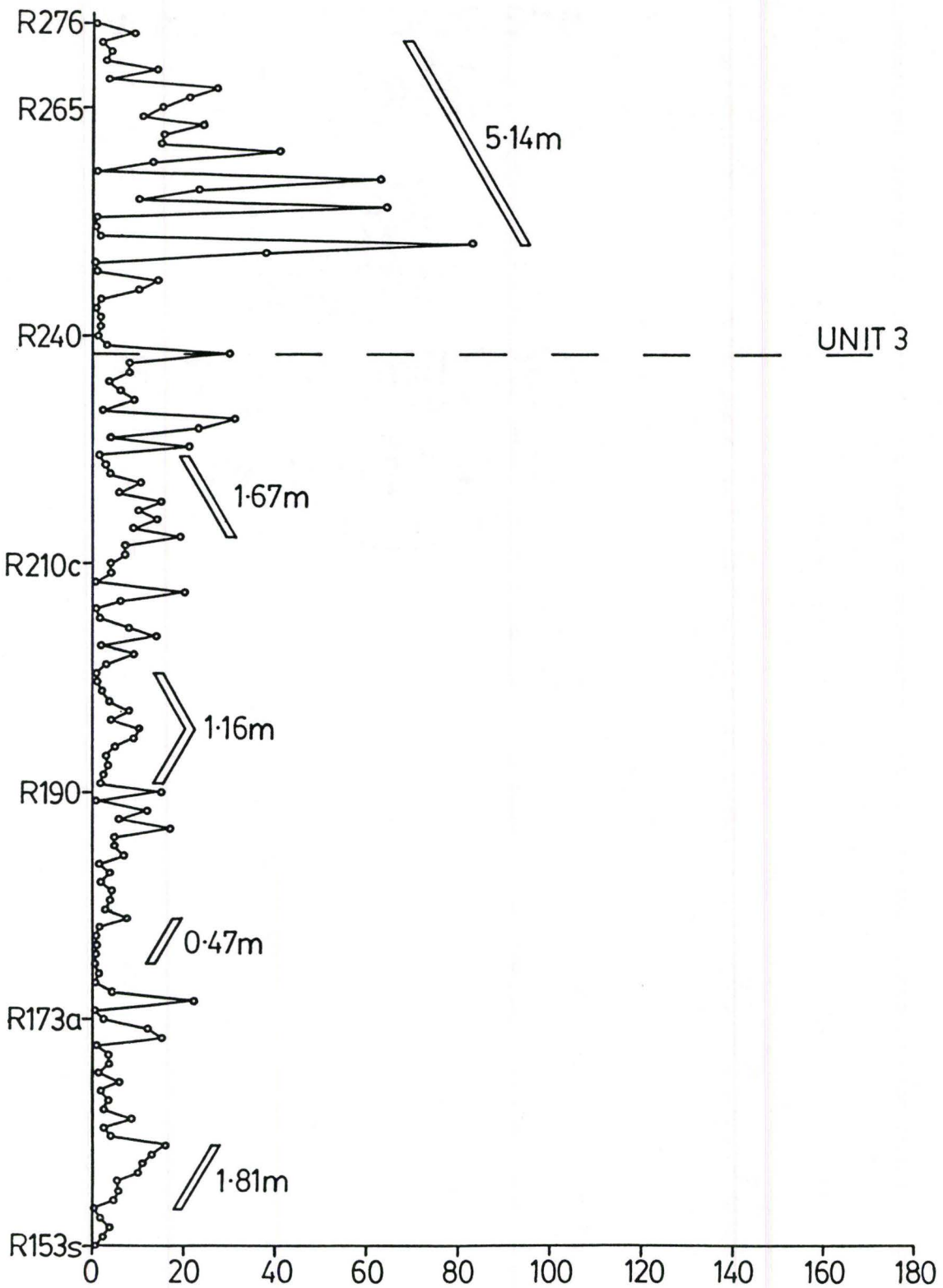
R276
R265
R240
R210c
R190
R173a
R153s
5·14m
UNIT 3
1·67m
1·16m
0·47m
1·81m
0
20
40
60
80
100
120
140
160
180

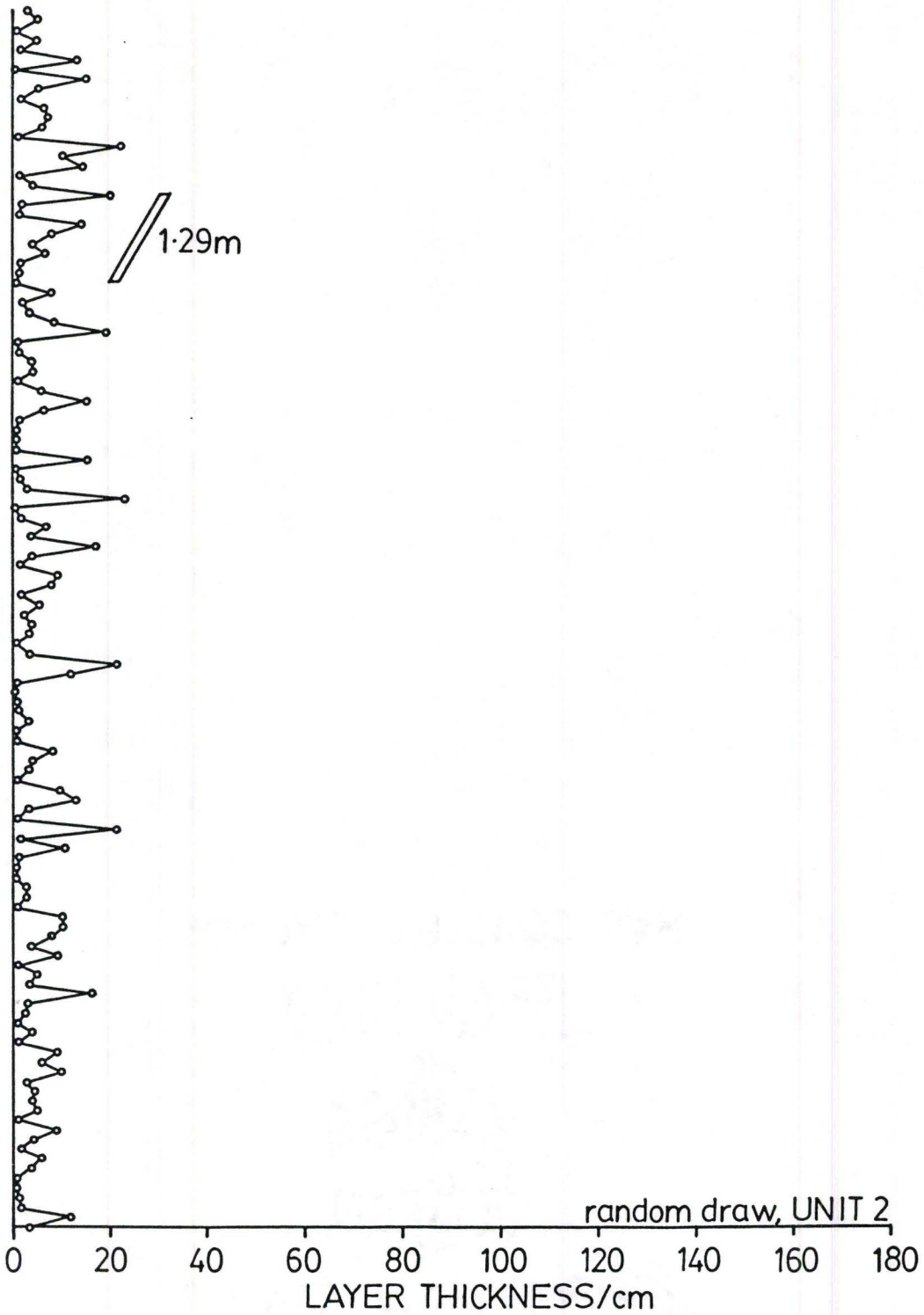
1·29m
random draw, UNIT 2
0
20
40
60
80
100
120
140
160
180
LAYER THICKNESS/cm

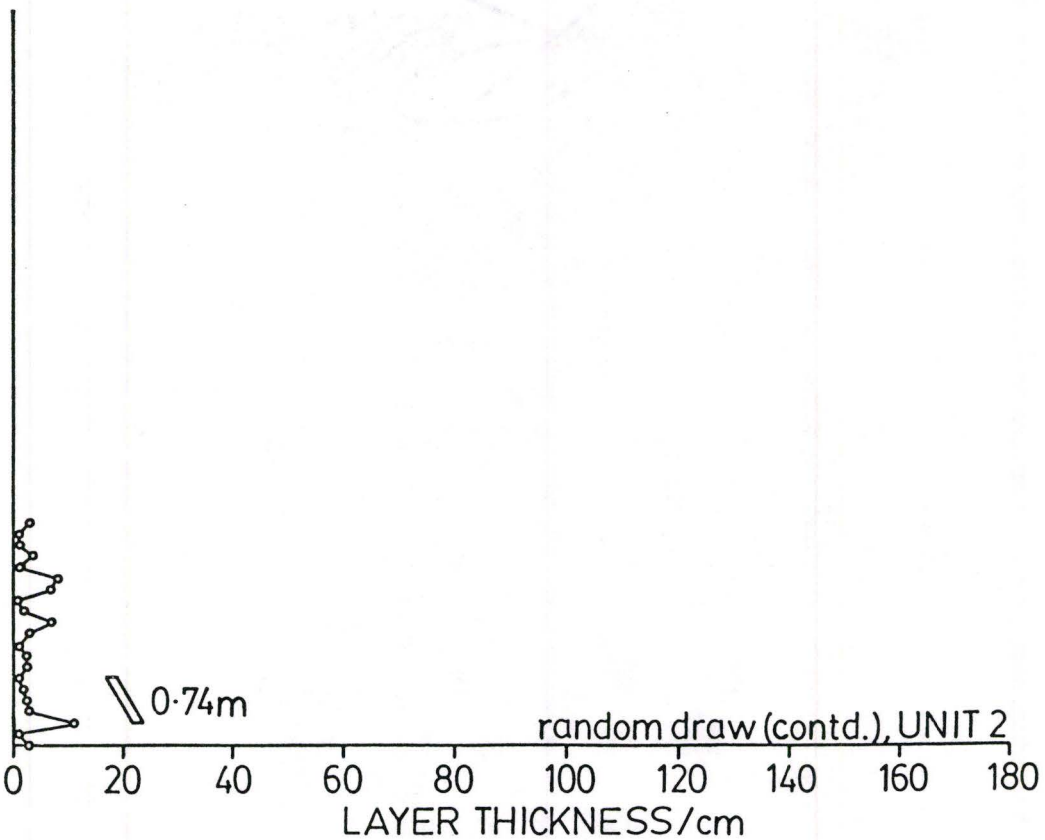
0·74m
random draw (contd.), UNIT 2
0
20
40
60
80
100
120
140
160
180
LAYER THICKNESS/cm

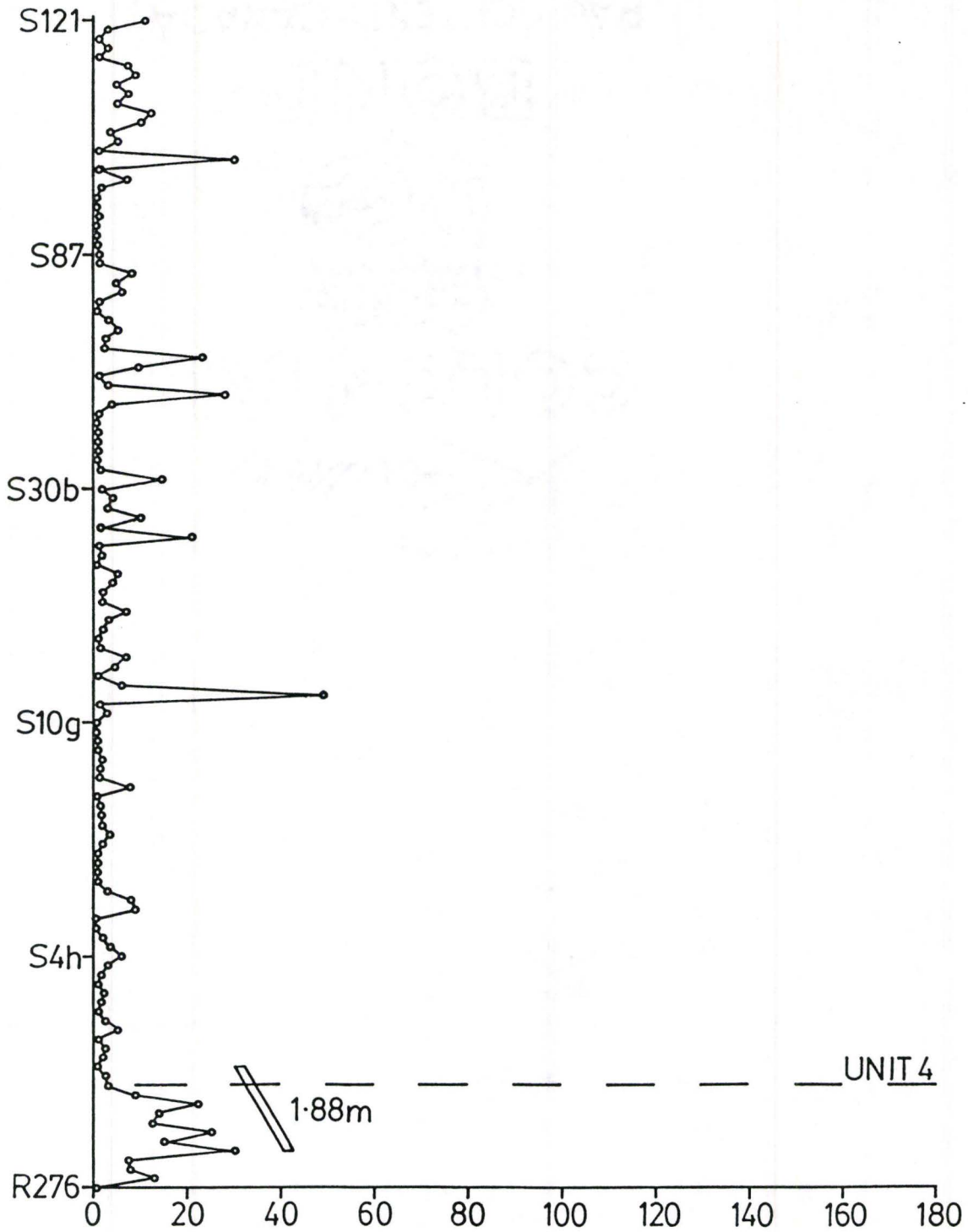
S121
S87
S30b
S10g
S4h
R276
UNIT 4
1·88m
0
20
40
60
80
100
120
140
160
180

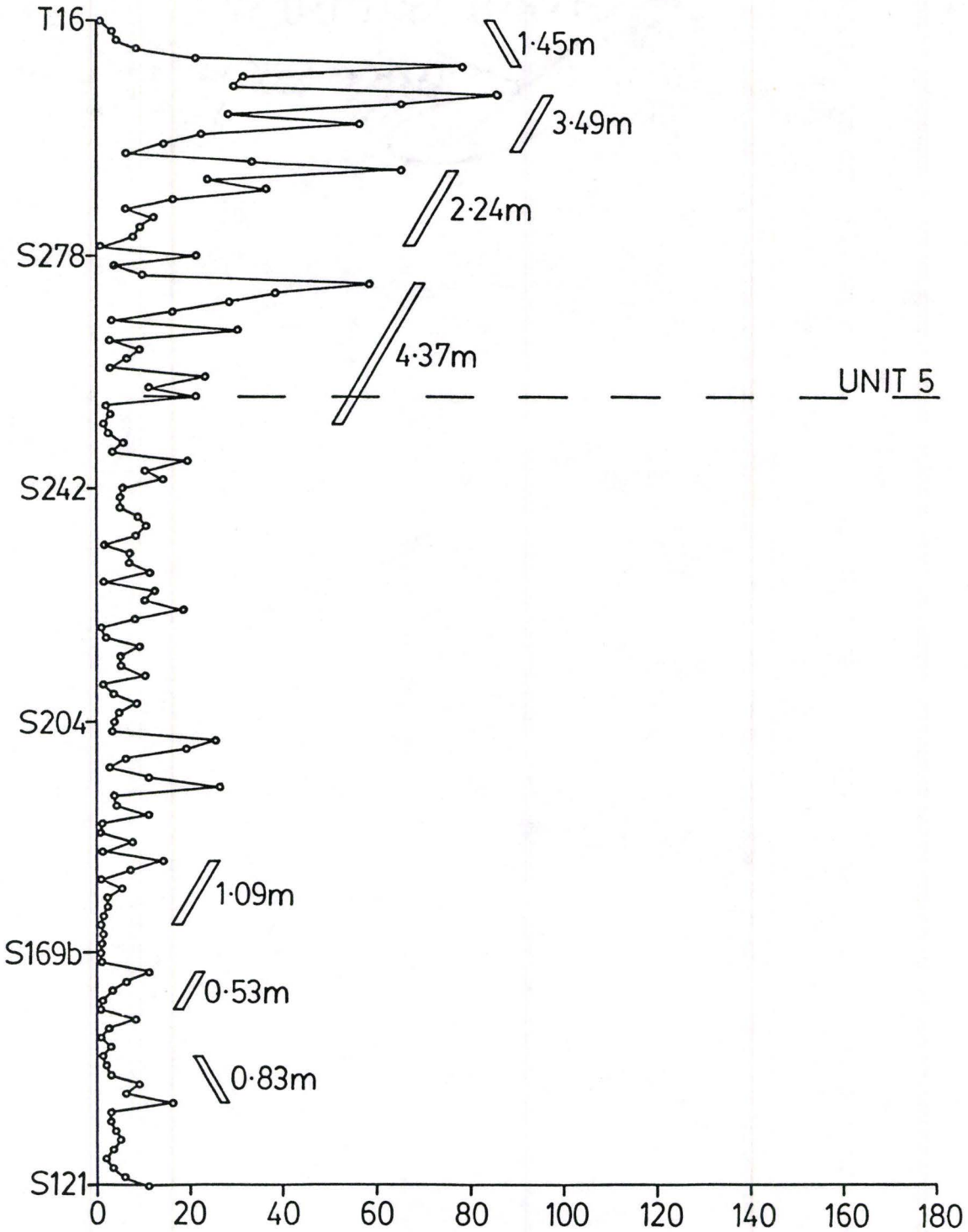
T16
S278
S242
S204
S169b
S121
1·45m
3·49m
2·24m
4·37m
UNIT 5
1·09m
0·53m
0·83m
0
20
40
60
80
100
120
140
160
180

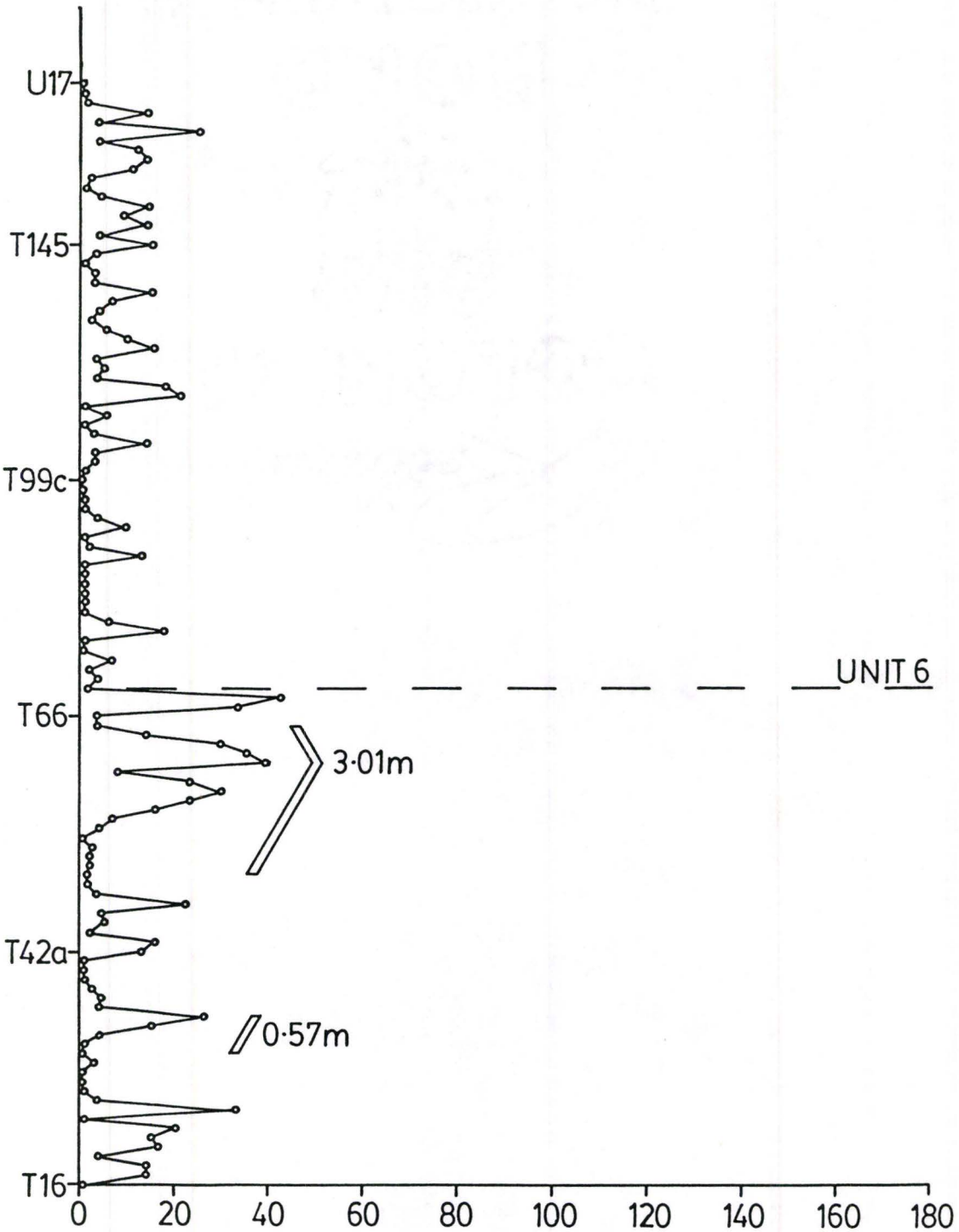
U17
T145
T99c
T66
T42a
T16
UNIT 6
3·01m
0·57m
0
20
40
60
80
100
120
140
160
180

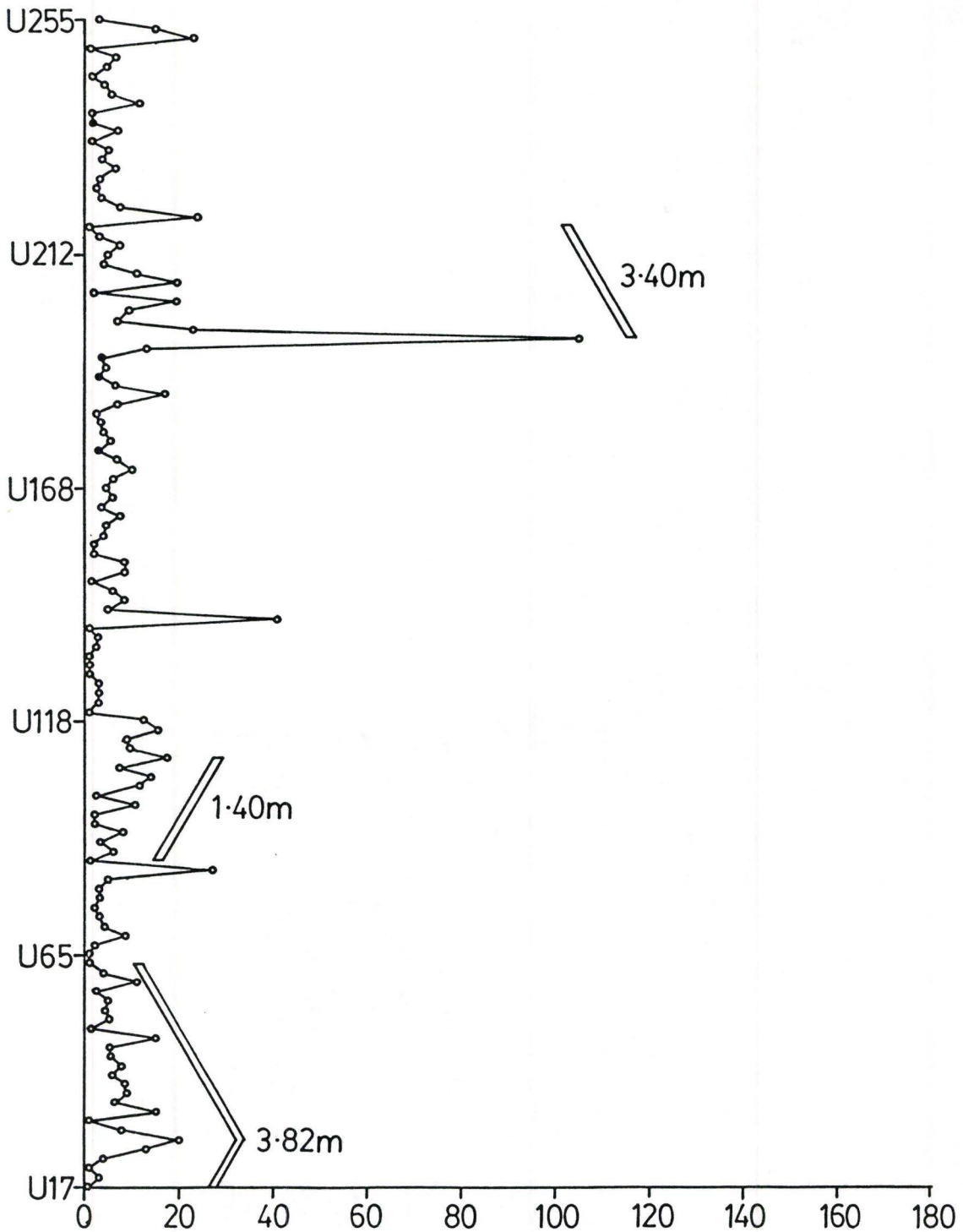
U255
U212
U168
U118
U65
U17
3·40m
1·40m
3·82m
0
20
40
60
80
100
120
140
160
180

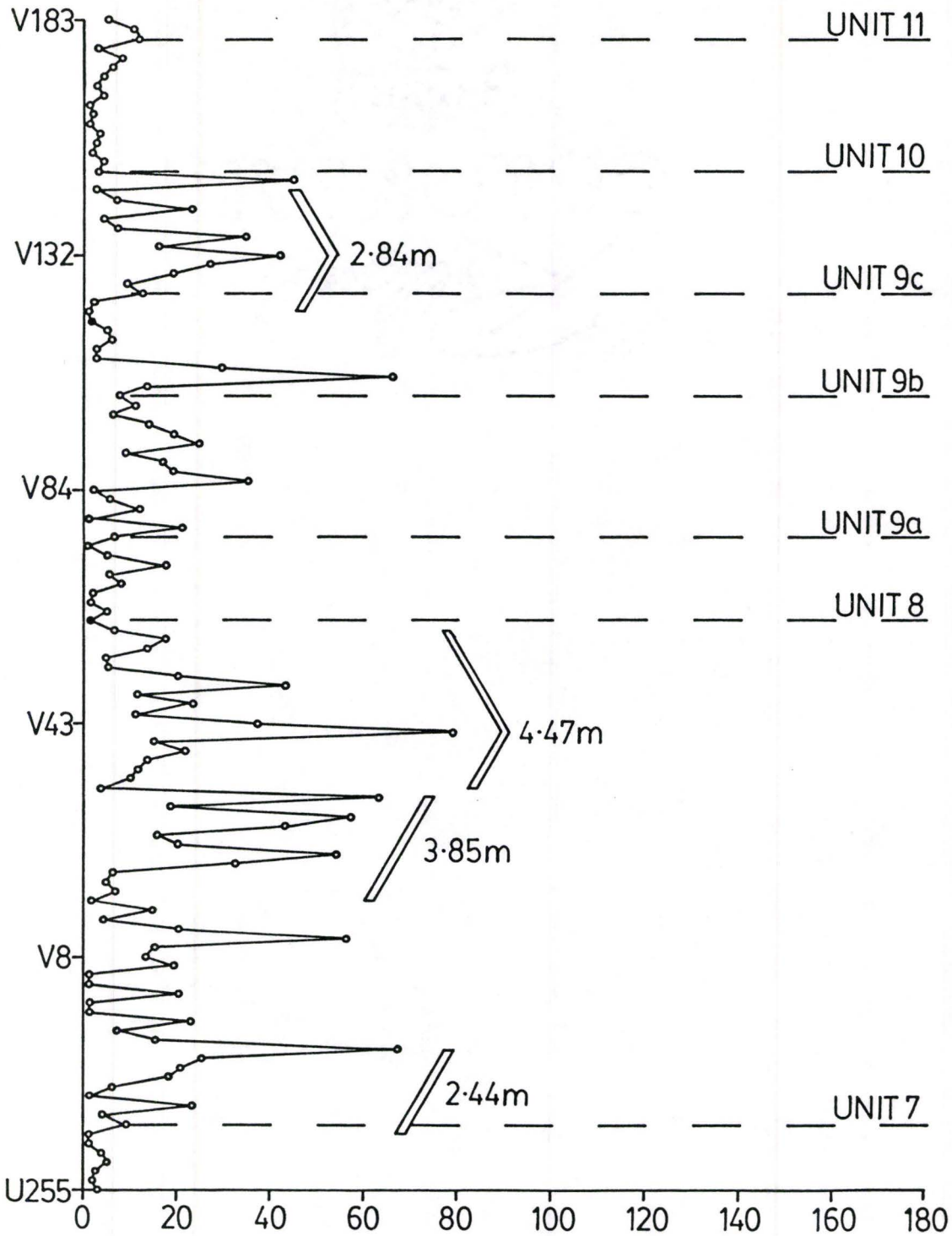
V183
V132
V84
V43
V8
U255
UNIT 11
UNIT 10
UNIT 9c
UNIT 9b
UNIT 9a
UNIT 8
UNIT 7
2·84m
4·47m
3·85m
2·44m
0
20
40
60
80
100
120
140
160
180

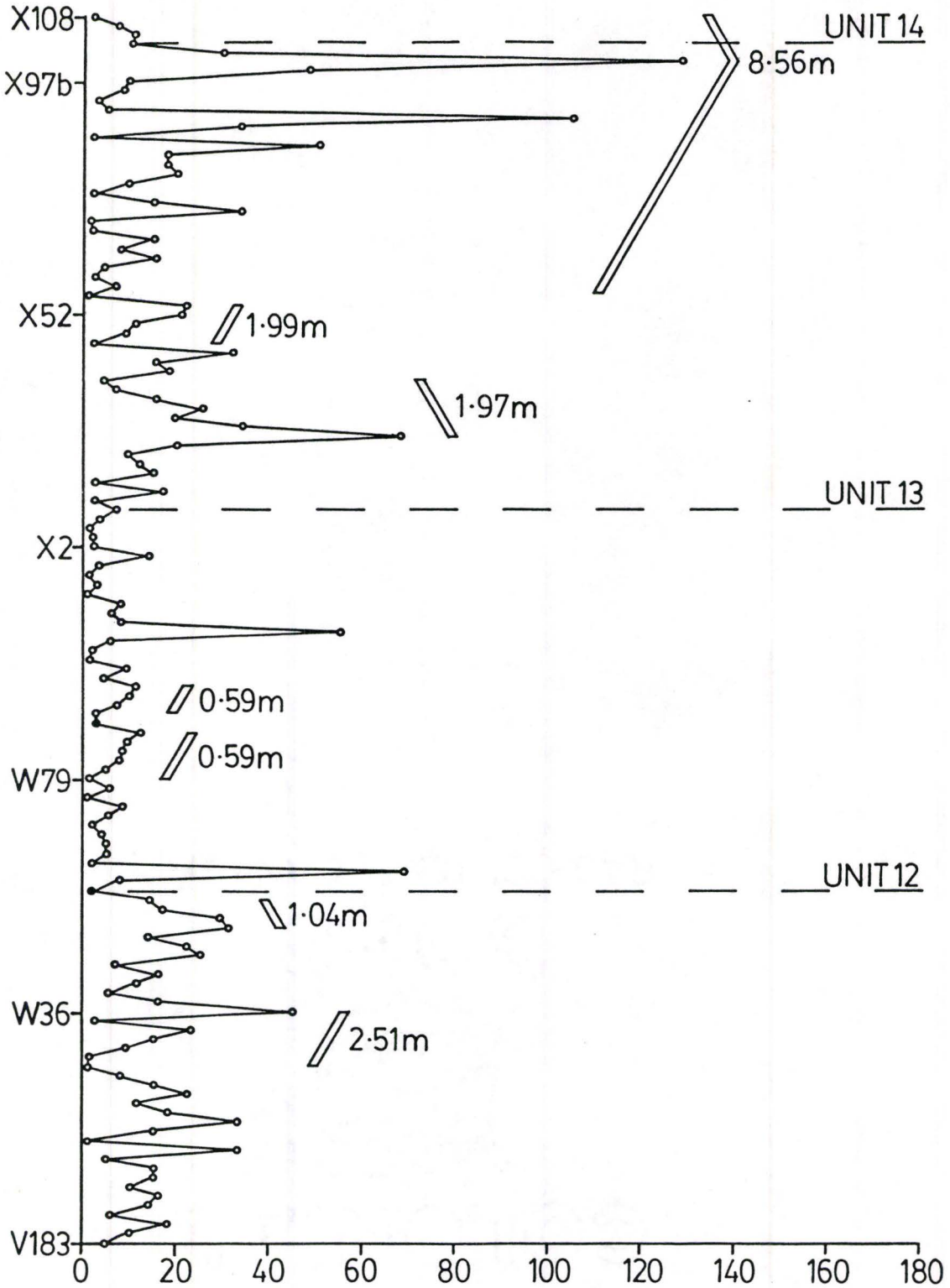
X108
X97b
X52
X2
W79
W36
V183
UNIT 14
8·56m
1·99m
1·97m
UNIT 13
0·59m
0·59m
UNIT 12
1·04m
2·51m
0
20
40
60
80
100
120
140
160
180

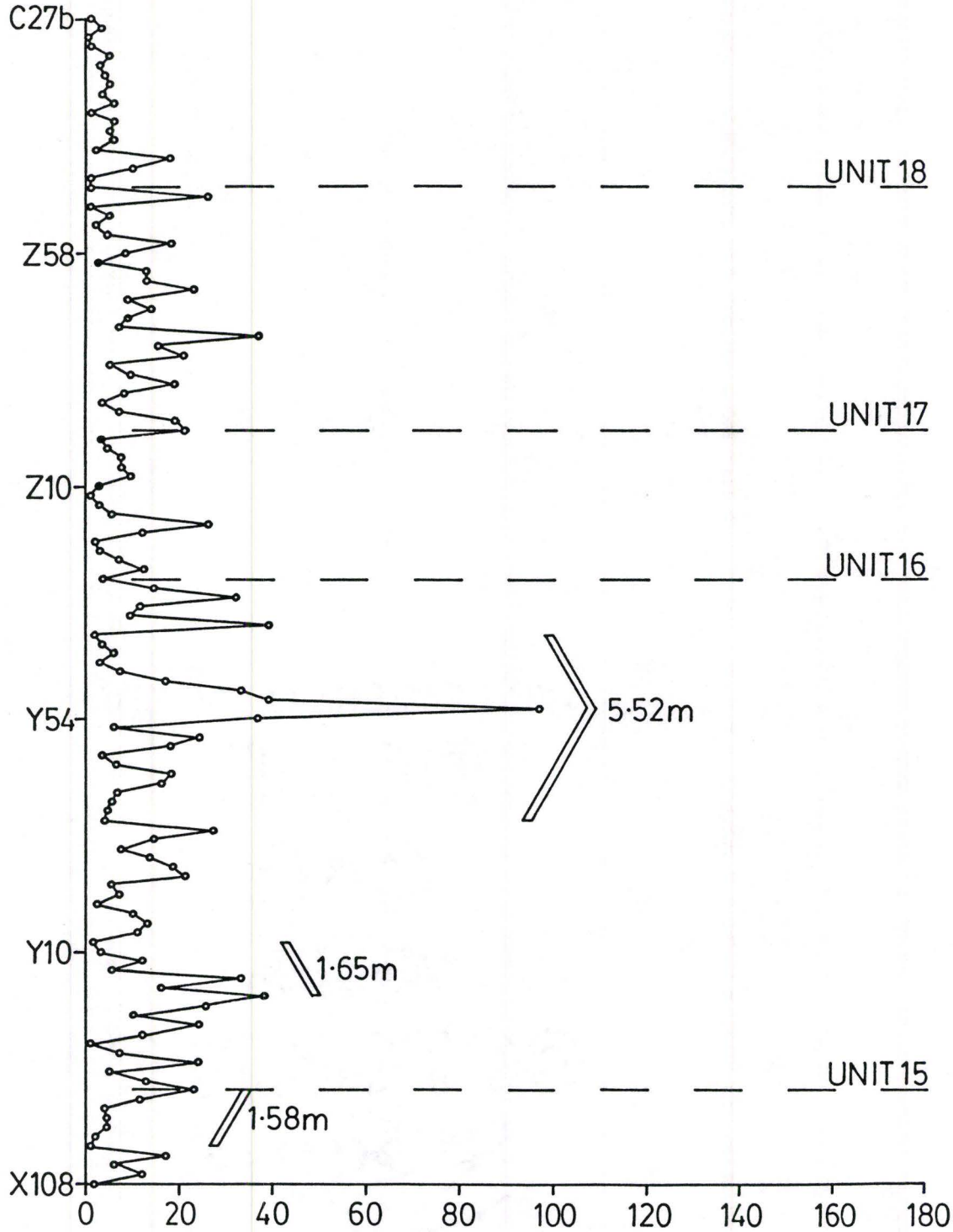
C27b
Z58
Z10
Y54
Y10
X108
UNIT 18
UNIT 17
UNIT 16
UNIT 15
5·52m
1·65m
1·58m
0
20
40
60
80
100
120
140
160
180

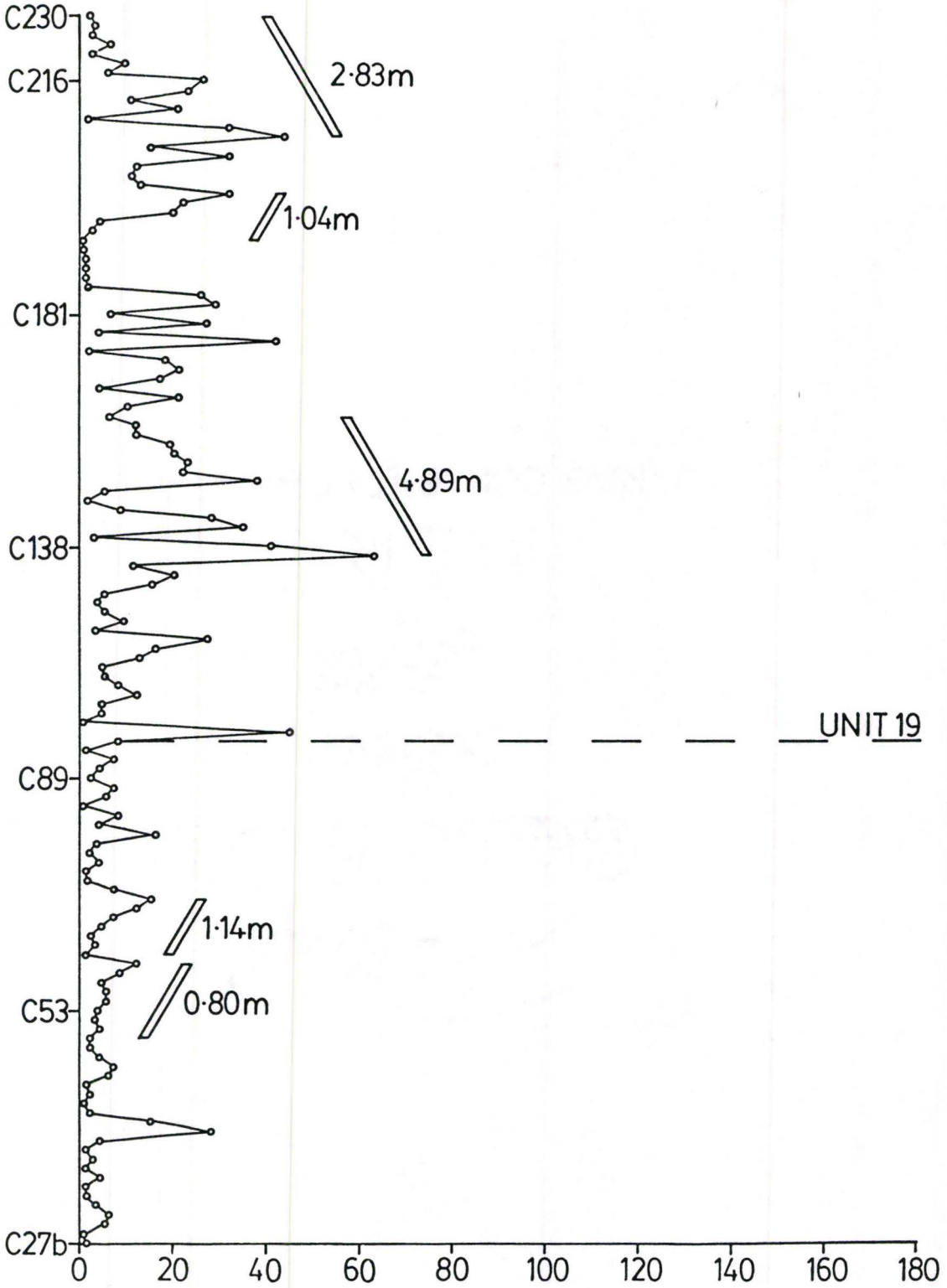
C230
C216
C181
C138
C89
C53
C27b
2·83m
1·04m
4·89m
UNIT 19
1·14m
0·80m
0
20
40
60
80
100
120
140
160
180

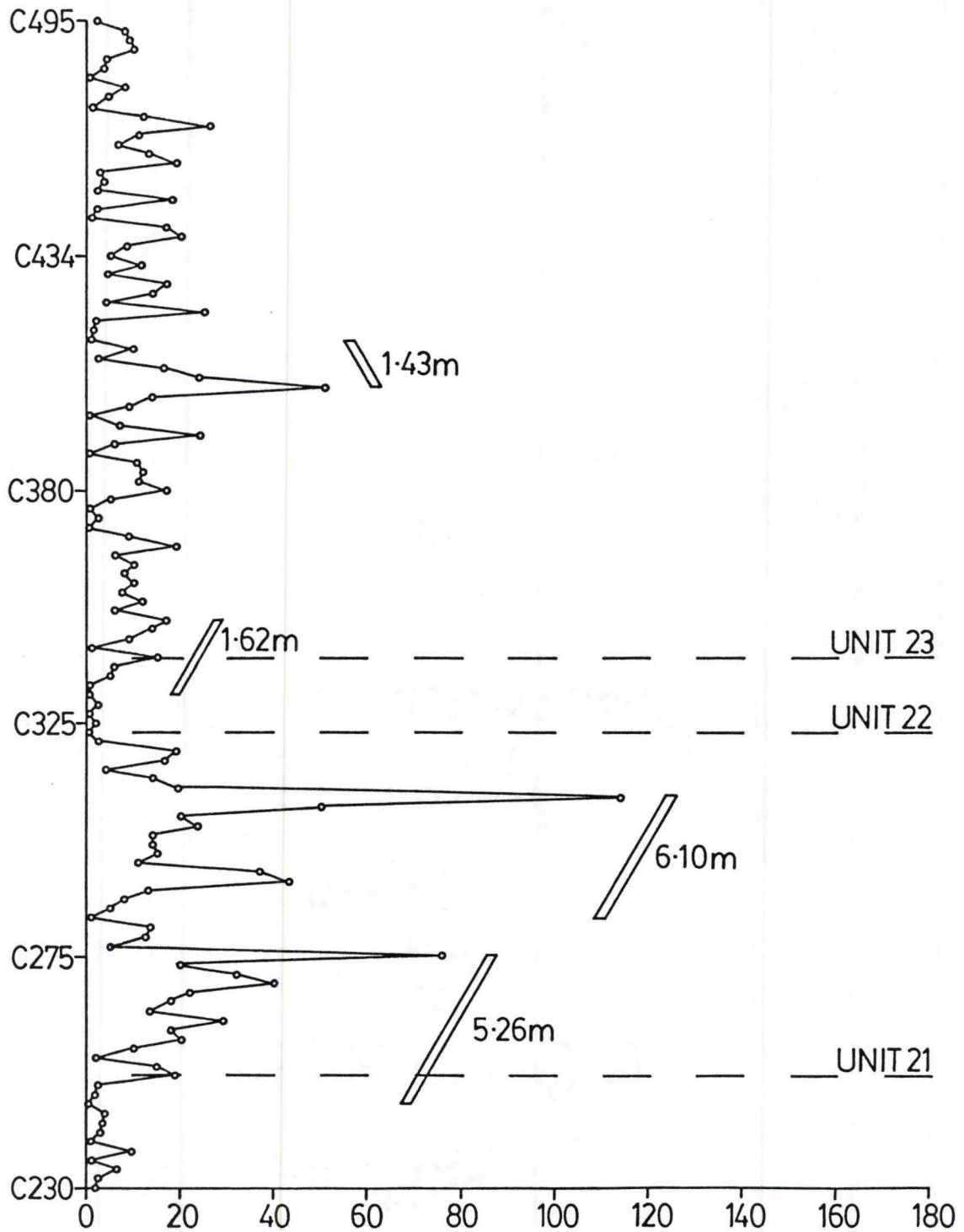
C495
C434
C380
C325
C275
C230
1·43m
1·62m
6·10m
5·26m
UNIT 23
UNIT 22
UNIT 21
0
20
40
60
80
100
120
140
160
180

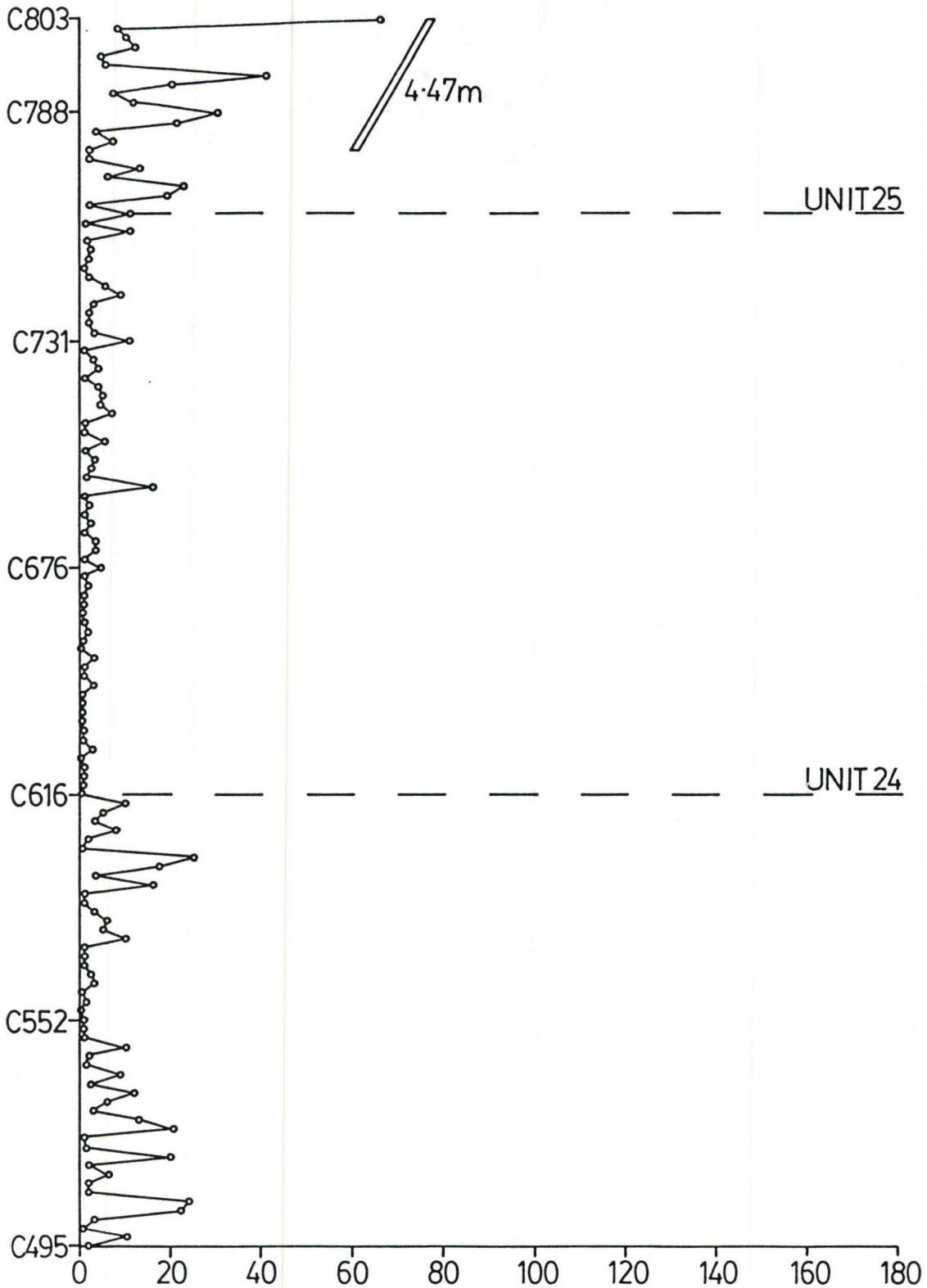
C803
C788
C731
C676
C616
C552
C495
4·47m
UNIT 25
UNIT 24
0
20
40
60
80
100
120
140
160
180

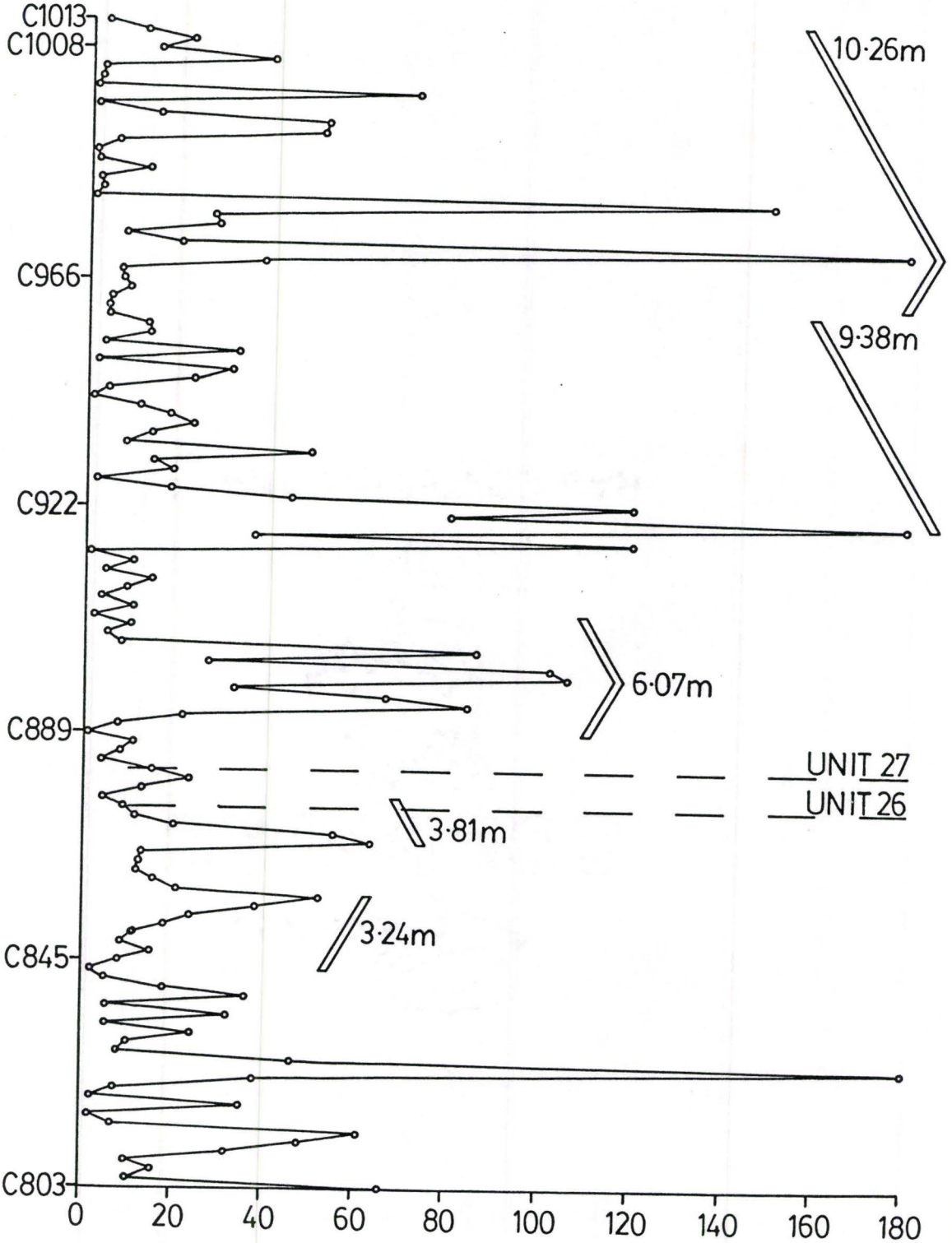
C1013
C1008
C966
C922
C889
C845
C803
10·26m
9·38m
6·07m
UNIT 27
UNIT 26
3·81m
3·24m
0
20
40
60
80
100
120
140
160
180

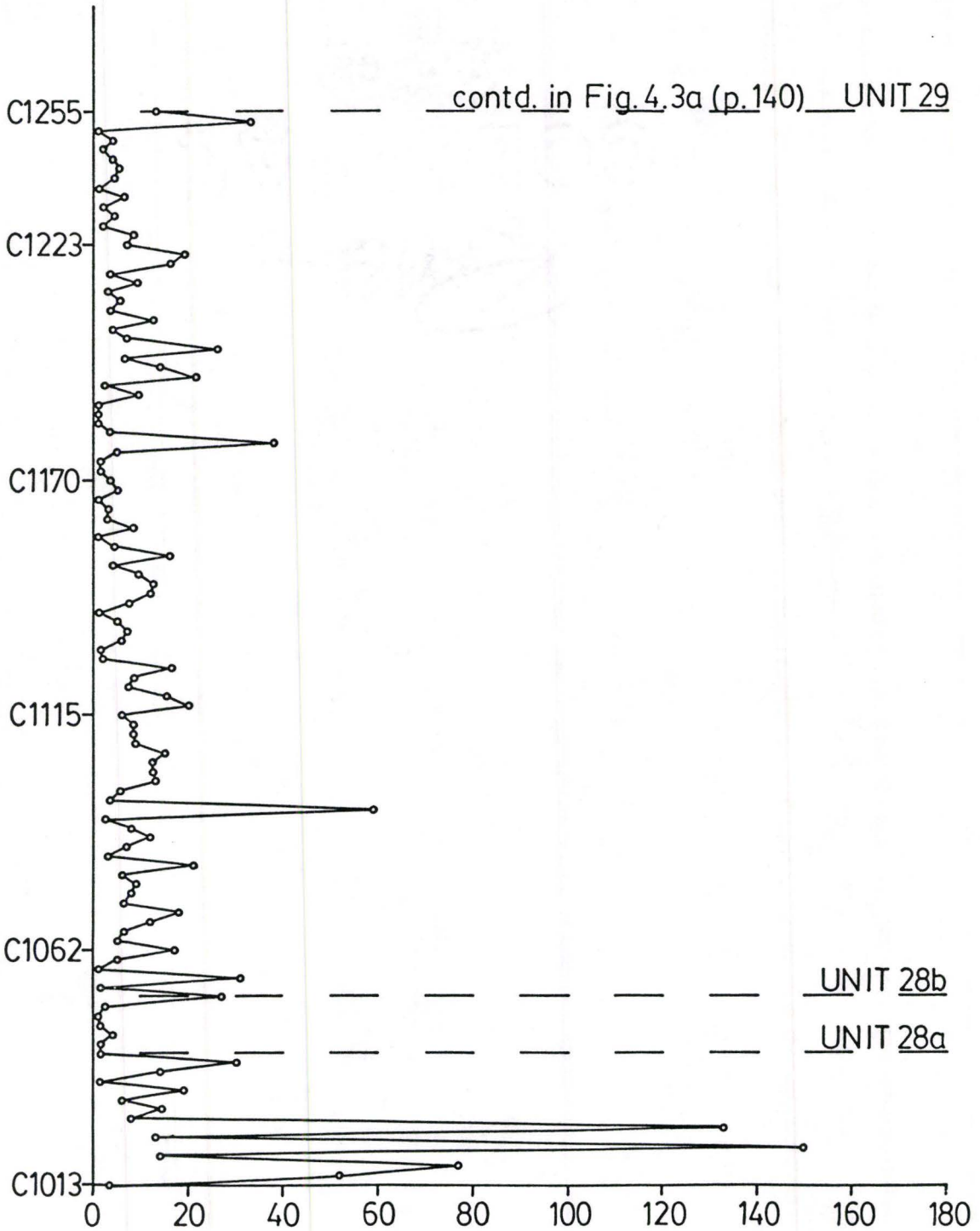
contd. in Fig. 4.3a (p. 140)
UNIT 29
C1255
C1223
C1170
C1115
C1062
C1013
UNIT 28b
UNIT 28a
0
20
40
60
80
100
120
140
160
180

APPENDIX 4

GLOSSARY OF HYDRAULICS SYMBOLS

Symbol

C - volume concentration of sediment in water.

d - depth of flow.

D - maximum grain diameter.

D_{65} - size of 65 percentile of grain size distribution.

f_o - friction factor at base of flow.

Fr - densiometric Froude number.

g - acceleration due to gravity.

h - clast thickness.

k - yield strength of a debris flow.

k_1 - k calculated from slope angle.

k_2 - k obtained from graph of k against weight percent water (Hampton, 1972).

k_s - equivalent sand roughness.

n - index with a value close to 2.4.

N - fraction of clast volume submerged in a debris flow.

Re - grain Reynolds number $(u_* k_s/\nu_e)$.

Re'_o - modified grain Reynolds number $(w_o D/\nu)$.

S - slope angle (i.e. tan α).

T - layer thickness.

u_* - shear velocity.

$\overline{U}$ - mean velocity.

$\overline{U}_c$ - critical value of $\overline{U}$ for turbulence.

w - settling velocity of a grain in a dispersion.

w_o - settling velocity of a single grain in still fluid.

α - slope angle.

κ - von Karmann's constant.

ν - clear fluid kinematic viscosity.

ν_e - effective kinematic viscosity.

ρ - flow density.

ρ_s - original clast density.

$\Delta\rho$ - density difference between flow and overlying water (i.e. $\rho-1$).

τ_c - critical shear stress for movement of clasts.